Complementary Methods and Bounds in Linear Water Waves

Richard Porter

School of Mathematics
University of Bristol

A Thesis submitted to The University of Bristol
for the degree of Doctor of Philosophy
in the Faculty of Science

November 1995

Abstract

In this thesis we use the theory of linear water waves to consider several problems concerned with the interaction of small amplitude plane waves with various structures in finite water depth with the aim of predicting important hydrodynamical coefficients such as the reflected and transmitted wave amplitudes. In particular, we choose geometries involving sharp corners such as the end of a thin barrier, or the corner of a right-angled step. The work is motivated by the absence of an accurate efficient method of predicting hydrodynamic coefficients in problems involving such geometries; previous methods are often inaccurate and sometimes unreliable as well as computationally expensive. A range of problems incorporating various degrees of complexity are considered, each of which illustrates the application of a new approach that is both accurate and efficient and has the added advantage, in most cases, of providing bounds on quantities of interest.

In chapter 1 we give a brief introduction to the thesis followed in chapter 2 by a summary of the theory of linear water waves and the framework for the methods we will use in the thesis. The approach throughout is to construct singular integral equations for either a function related to an unknown velocity or unknown pressure difference and approximate it using a Galerkin method with trial functions that accurately model the physical behaviour of these functions. Quantities of interest are given by integral properties of these functions.

The scattering of obliquely-incident plane waves by four types of vertical barriers is considered in chapter 3. In chapter 4 we extend this to two non-coplanar vertical barriers. Two wave-energy devices both having geometries involving thin vertical barriers are considered in chapter 5. In chapter 6 we consider the scattering of obliquely-incident waves by periodic arrays of thin barriers with gaps uniform in depth as a model of an offshore breakwater. Finally we adapt the method in chapter 7 to geometries involving rectangular blocks by solving the problem of scattering of waves by a step in the sea bed.

Acknowledgements

I extend my thanks to Professor David Evans for his supervison and continued help, enthusiam and motivation during this study. I would also like to thank Professor Johannes Falnes for useful discussions in the area of wave energy, my father, Dr. David Porter, for his suggestions and insight and Dr. Mark Fernyhough for many hours of contemplation. The financial support of the Engineering and Physical Sciences Research Council (MTD Ltd) under grant no. 92004667, is gratefully acknowledged.

I am grateful to my parents for their support and to everyone else who has shown concern and interest over the last three years, particularly Iggy, Sanj, Jase, Martin, John, Mark, Tim, and Dave.

Finally, this thesis owes a great deal to H for her patience, encouragement and inspiration.

Author's Declaration

The work described in this dissertation was carried out in the School of Mathematics, University of Bristol and has not been submitted for any other degree or diploma of any examining body. All the material described herein is the original work of the author, except where otherwise acknowledged.

R. Porter

Contents

1 Introduction **1**

2 Background Theory **7**

3 Wave interaction with a single line of barriers with gaps **20**

3.1 Introduction 20

3.2 Scattering by a single line of barriers with gaps 24

3.2.1 The surface-piercing barrier 29

3.2.2 The submerged bottom-mounted barrier 31

3.2.3 A barrier with a single submerged gap 33

3.2.4 The totally-submerged unmounted barrier 35

3.3 Sloshing in a rectangular tank containing a vertical baffle 37

3.4 Numerical procedure and results 39

3.5 Remarks 50

4 Wave scattering by two unequal vertical barriers **51**

4.1 Introduction 51

4.2 Formulation and solution 55

4.3 Special case of two equal barriers 65

4.4 Wide-spacing approximation 67

4.5 Approximate solution for two closely-spaced unequal barriers 68

4.6 Results 72

5 Two Oscillating-Water-Column Wave-Energy Devices 84

5.1 Introduction 84

5.2 Theory of pressure distributions 88

5.3 A two-dimensional OWC device 93

5.3.1 Velocity formulation 94

5.3.2 Pressure difference formulation 101

5.3.3 Results 108

5.4 A partially-immersed circular duct OWC device 116

5.4.1 Velocity formulation 119

5.4.2 Pressure difference formulation 127

5.4.3 Results 127

6 Scattering by periodic arrays of breakwaters 137

6.1 Introduction 137

6.2 Formulation and solution 140

6.3 Two parallel arrays of breakwaters 151

6.4 Wide-spacing approximation 155

6.5 Results 158

7 Scattering by a step in the sea bed 173

7.1 Introduction 173

7.2 Formulation and solution 175

7.3 Results 183

8 Conclusion 189

A 192

Chapter 1

Introduction

In this thesis we approximate, using semi-analytical techniques, certain important features of the solution to a variety of boundary-value problems arising from the application of linearised theory to wave scattering problems. Linear water-wave theory is a useful tool in gaining an important insight into hydrodynamic effects occuring in real 'non-linear' seas, the advantages being that analytic methods can be applied to many problems specified this way to reduce the computational effort required to a minimum as well as having the capability to reveal interesting wave phenomena. In practice we use the theory to examine the wave interactions with objects placed in the sea. In order to exploit the theory fully, these objects are usually idealised and modelled by structures having simple geometries such as infinitely thin plates, rectangular blocks, or circular cylinders. Despite this simplification, it remains a challenge to create a sound approach to approximating the resulting wave field, the difficulties arising primarily from the mixed boundary condition present on the mean free surface of the fluid.

There are, however, a small number of wave scattering problems which, when described by classical linear water-wave theory, have the property that they can be solved analytically in closed form. For instance, if the fluid motion is two dimensional and the water is of infinite depth, complex function theory may be applied to problems involving thin vertical barriers to yield, in principle, closed-form expressions for the ratio of reflected and transmitted to incident wave amplitudes (hereafter referred to as reflection and transmission coefficients and denoted by R and T). Using a so-called reduction method, the original potential is replaced by a 'reduced' potential relying on a certain combination of the original potential and its derivative and satisfying a simpler set of boundary conditions than the original one. Once found the original potential is regained as the solution of a simple first-order differential equation. Dean [8] first used this approach to solve the problem of the reflection of waves by a semi-infinite barrier extending from infinite depth to a point a below the free surface. He showed that the reflection and transmission coefficients, $|R|$ and $|T|$, could be expressed in terms of modified Bessel functions of argument ka where $k = 2\pi/\lambda$ and λ is the wavelength. Ursell [72] solved the complementary problem of the surface-piercing barrier immersed to a depth a and again found similar expressions for $|R|$, $|T|$. Subsequently much work involving thin barriers with gaps placed in a vertical plane ensued with, for example, Mei [48], Lewin [42] and Porter [63] providing analytic methods for solving the problem of a barrier with an arbitrary number of gaps. For the two simplest examples of these, other than Dean's [8] and Ursell's [72], original problems, Evans [10] and Porter [62] found closed-form expressions for the problems of the totally-submerged finite barrier and the barrier with a finite submerged gap respectively. A generalisation of the Ursell [72] surface-piercing barrier where the barrier makes an angle $\pi/2n$ to the horizontal (n an integer) was provided by John [34] where the complication of using complex function theory to find exact solutions is highlighted.

Progress can also be made in the case of two identical surface-piercing vertical barriers in infinite depth and although lacking detail, Levine & Rodemich [41] presented the method of solution. The complementary problem of the scattering of two parallel barriers extending downwards from the same depth below the mean free surface was solved by Jarvis [32], who also obtained curves of reflection and transmission coefficients as a function of wave frequency, barrier spacing and submergence, showing how for particular configurations, total wave transmission could occur.

These problems are non-trivial and are highlighted by the span in time between Dean's [8] first attempt at the submerged barrier problem in 1945 and the numerous (not all mentioned here) subsequent efforts at similar barrier problems. If oblique incidence is also to be considered, complex function theory no longer applies, the possibility of finding explicit solutions becomes even harder and some kind of approximation technique becomes a favourable option. If, in addition, the assumption of infinite depth water is replaced by a finite water depth condition, there is little or no alternative but to employ approximation procedures to the resulting boundary-value problems.

Thus, the work presented in this thesis aims to provide methods for giving extremely accurate and computationally efficient results for quantities such as reflection and transmission coefficients by considering a variety of wave scattering problems involving oblique wave incidence and finite depth water, beginning with those mentioned above. We are motivated by the absence of an accurate and reliable method for coping with problems involving geometries that include sharp corners or edges. The difficulty lies in the presence of a mild singularity in the fluid velocity at a sharp corner of a solid boundary, its strength (i.e. the exponent associated with the singularity; not the coefficient multiplying it) ascertained by a simple analysis of the flow field in the neighbourhood of the corner. In the examples above where analytic solutions are obtained, explicit account of this behaviour is incorporated into the method of solution. However when approximation methods are to be employed it is often the case that, whilst the physics requires there to be a singularity in flow at a sharp edge, it is not necessary to incorporate it explicitly in the method of solution.

Previous methods that have sought to include explicit account of this behaviour have, in general, been restricted in the accuracy of the approximation that may be achieved. In particular a popular approach used in approximating reflection and transmission coefficients for problems involving thin barriers and rectangular blocks alike is the variational approximation (otherwise known as the one-term Galerkin approximation) due to Jones [35]. The method relies on the construction of an integral equation in an unknown function, which is related to either the fluid velocity or the pressure in the fluid. This is as a direct consequence of the physical requirement that these two quantities be continuous everywhere in the fluid. The variational approach involves the substitution of an approximation to the unknown function; the better the approximation, the more accurate the results. Thus Evans & Morris [20] used this method in considering scattering of obliquely-incident waves upon a surface-piercing barrier in infinite depth and used Ursell's [72] exact solutions for the velocity under the barrier and the pressure difference across the barrier to obtain extremely accurate upper and lower bounds on the reflection and transmission coefficients. Recently, Mandal & Dolai [45] have used the same procedure to investigate reflection of obliquely-incident waves by four different barrier types in finite depth, using the variational method with the exact infinite depth expressions for the velocity through the gap in the barrier and pressure difference across the barrier. They too have been successful in obtaining extremely accurate upper and lower bounds for the modulus of the reflection and transmission coefficients.

Cruder approximations to the unknown functions in the integral equations give surprisingly good results too. In Miles's [52] treatment of the scattering of waves by a step in the ocean floor, the variational method is employed and the velocity above the corner of the step approximated by a function that has little physical significance but was chosen primarily for simplicity of algebra. It will be seen in chapter 7 that this gives three figure accuracy and outperforms other supposedly more accurate methods. The reasons for this are discussed in chapter 2.

The disadvantage of the variational approach is that in order to improve the accuracy of the results, a better description of the unknown function is required. On the other hand, methods that have been developed with the view to obtaining arbitrary accuracy which have not accomodated the singularity in the flow into the approximation have not been totally successful. In particular, many authors have opted to use a method of matching eigenfunction expansions, an early example of its use being Miles & Gilbert [54], in which physical continuity requirements lead to the solution of an infinite system of equations. As will be discussed in chapter 2, in effect this tries to model the velocity through the gap in a barrier with a set of cosine functions. Attempting to model a singularity with a truncated set of cosine functions will clearly cause convergence problems. Using a large enough truncation size can nevertheless give reasonable accuracy and this approach has been widely used with a fair amount of success. It is however computationally expensive requiring the inversion of a complex-valued matrix of typical size $O(100)$ or more for two-figure accuracy.

In this thesis we combine the ideas of incorporating the physical behaviour of the fluid with the capability of achieving arbitrary accuracy. This is done by extending the usual variational approximation (or one-term Galerkin approximation) to the use of an N-term Galerkin approximation. This is used to approximate the solution to certain integral equations involving unknown functions related to either the velocity across a gap or the pressure difference across a barrier which can are derived through the matching of eigenfunction expansions in a similar manner to that mentioned previously. By being able to express the desired hydrodynamical quantities as functionals of these unknown functions, the Galerkin method is shown to be an accurate second-order method which has the added advantage of providing bounds on the true solution provided the integral operator has certain features. The two formulations, in terms of velocity-related and pressure difference-related functions, are referred to as complementary and can furnish, in some examples, upper and lower bounds on the true solution in a similar manner to Evans & Morris [20]. By using functions in the Galerkin approximation which take into account the physical behaviour of the fluid whilst retaining simplicity in the final form it is shown how six-figure accuracy requires in general the use of fewer than eight terms. This approach forms the basis of the following work in which a variety of problems with different features are addressed. A detailed introduction to each of these problems is given at the beginning of each chapter.

The contents of chapters 3, 5, and 6 form the basis of the publications of Porter & Evans [65], Evans & Porter [22] and Porter & Evans [66] respectively, whilst Evans & Porter [23] includes material from chapters 3, 4 and 6.

Chapter 2

Background Theory

Cartesian coordinates are chosen with the x and z axes lying in the undisturbed free surface of the fluid with the y axis vertically downwards and the fluid occupying $0 < y < h$. Throughout the thesis we will use the theory of classical linear water waves; for a detailed account of the derivation of the following theory see, for example, Mei [51], Wehausen & Laitone [73]. Hence it is assumed that the fluid is inviscid and incompressible, the flow is irrotational and that the surface waves are of small amplitude. Then there exists a velocity potential $\Phi(x, y, z, t)$ satisfying

$$\nabla^2 \Phi = \frac{\partial^2 \Phi}{\partial x^2} + \frac{\partial^2 \Phi}{\partial y^2} + \frac{\partial^2 \Phi}{\partial z^2} = 0, \quad \text{in the fluid } (0 < y < h) \tag{2.1}$$

$$\frac{\partial \Phi}{\partial n} = 0, \quad \text{on solid boundaries,} \tag{2.2}$$

where n denotes the normal,

$$\frac{\partial \zeta}{\partial t} = \frac{\partial \Phi}{\partial y}, \quad \text{on } y = 0\,, \tag{2.3}$$

where $\zeta(x, z, t)$ is the elevation of the free surface measured downwards from $y = 0$, and

$$\frac{\partial \Phi}{\partial t} - g\zeta = \frac{-p_a}{\rho}, \quad \text{on } y = 0 \tag{2.4}$$

where ρ is the (constant) density of the fluid and p_a is the atmospheric pressure above the free surface of the fluid which is assumed to be constant. Hence p_a/ρ may be absorbed by Φ so that the right-hand side of (2.4) takes the value zero without loss of generality. In chapter 5 we adapt the theory presented here for time-dependent pressures above a portion of the free surface.

If we further assume that the motion is simple harmonic in time with angular frequency ω we can introduce complex-valued time-independent quantities, ϕ, η in the manner

$$\Phi(x,y,z,t) = \mathrm{Re}\{\phi(x,y,z)\mathrm{e}^{-i\omega t}\}, \tag{2.5}$$

$$\zeta(x,z,t) = \mathrm{Re}\{\eta(x,z)\mathrm{e}^{-i\omega t}\}. \tag{2.6}$$

Using these definitions in (2.1), (2.2) gives

$$\nabla^2\phi = 0, \quad \text{in the fluid}, \tag{2.7}$$

$$\frac{\partial \phi}{\partial n} = 0, \quad \text{on solid boundaries}, \tag{2.8}$$

and combining (2.3) and (2.4) gives rise to

$$K\phi + \frac{\partial \phi}{\partial y} = 0, \quad \text{on } y = 0\,, \tag{2.9}$$

the so-called 'free surface condition', where $K = \omega^2/g$. We also have the relation

$$\eta = -\frac{i\omega}{g}\phi|_{y=0}, \tag{2.10}$$

between the velocity potential and the free surface elevation.

A train of plane waves of (complex) amplitude A, making an angle θ to the $z = 0$ plane in a constant depth ocean, has a free surface elevation which may be written

$$\eta = A\mathrm{e}^{ik(x\cos\theta + z\sin\theta)}, \tag{2.11}$$

where k is the wavenumber having and is related to the wavelength, λ, by $k = 2\pi/\lambda$. A simple separation of variables procedure applied to ϕ satisfying (2.7)–(2.11) yields the solution

$$\phi = \frac{igA}{\omega}\cdot\frac{\cosh k(h-y)}{\cosh kh}\mathrm{e}^{ik(x\cos\theta + z\sin\theta)}, \tag{2.12}$$

and the wavenumber k is found to be related to the period of motion via the dispersion relation,

$$K = k \tanh kh. \tag{2.13}$$

For fixed K (2.13) has only one positive real root (this can be seen graphically) and by considering k complex it can be shown that the only other roots of this equation lie on the imaginary axis at ik_n, $n \geq 1$, say, where k_n satisfy

$$K + k_n \tan k_n h = 0. \tag{2.14}$$

By ordering k_n such that $k_1 < k_2 < \ldots$, it can be seen graphically that

$$(n - \tfrac{1}{2})\pi < k_n h < n\pi, \tag{2.15}$$

and that $k_n h \to n\pi$ as $n \to \infty$. We also find it convenient to define $k_0 = -ik$.

In the problems covered in this thesis, we will be examining the interactions of surface waves with fixed obstacles in constant, or piecewise constant, water depth h. We use this constant depth to our advantage and perform a separation of variables technique of the form $\phi(x, y, z) = f(x, z)g(y)$ in (2.7)–(2.9) to obtain a complete orthonormal set of depth eigenfunctions in $[0, h]$ (see, for example, Mei [51] pp.303-305) defined to be

$$\psi_n(y) = N_n^{-1/2} \cos k_n(h - y), \quad n \geq 0, \tag{2.16}$$

with the normalising factor

$$N_n = \frac{1}{2}\left(1 + \frac{\sin 2k_n h}{2k_n h}\right), \quad n \geq 0 \tag{2.17}$$

so that the ψ_n satisfy the following orthognality relation

$$\frac{1}{h}\int_0^h \psi_n(y)\psi_m(y)\,\mathrm{d}y = \delta_{mn}. \tag{2.18}$$

In particular, we note that

$$\psi_0(y) = N_0^{-1/2} \cosh k(h - y), \tag{2.19}$$

where

$$N_0 = \frac{1}{2}\left(1 + \frac{\sinh 2kh}{2kh}\right). \tag{2.20}$$

The remaining part of the separable solution associated with $\psi_n(y)$ will depend on the specification of the problem. If, for example, the motion is two-dimensional such that waves propagate in a direction parallel to the x-axis, we write the potential as a Fourier-type sum of all possible modes, thus

$$\phi(x,y) = (A_0 \mathrm{e}^{-ikx} + B_0 \mathrm{e}^{ikx})\psi_0(y) + \sum_{n=1}^{\infty}(A_n \mathrm{e}^{k_n x} + B_n \mathrm{e}^{-k_n x})\psi_n(y). \tag{2.21}$$

in unknown coefficients A_n, B_n, $n \geq 0$ to be determined.

In (2.21) above A_0 and B_0 are associated with the amplitues of waves propagating in the positive and negative x-directions and the terms under the sum represent decaying or *evanescent* modes. These are included to describe the fluid motion local to any body non-uniform in the vertical coordinate in the fluid domain and decay exponentially away from the body. If there is no body to interact with an incident wave, these evanescent modes are not present and the potential will be described by only propagating wave modes (as in (2.12)).

This eigenfunction expansion approach forms the starting point for solving problems in this thesis, and indeed in many problems in linear water waves involving the interaction of surface waves with obstacles in constant water depth. It is used most often where natural vertical boundaries are present due to the structure of the obstacle being considered. Other shapes of boundaries also lend themselves to the eigenfunction expansion method, in particular circular ones.

We shall now outline the basic principles behind the application of eigenfunction expansions to the solution of problems in linear water waves. The fluid domain is divided into two (or more) regions by imaginary vertical boundaries. In each of the regions an appropriate expansion of the form (2.21) for the potential is constructed satisfying all the conditions of the problem (including where neccesary a suitable radiation condition) apart from those on the vertical interface(s). The requirement that the fluid velocity and the pressure be continuous everywhere and there should be no flow across the surface of a solid body provides the remaining conditions to be satisfied. These can be enforced in different ways and it helps to have a clear idea as to what properties of the solution are required. For example, if possible schemes for offshore breakwaters are to be considered, it will be important to know how much of an incident wave is reflected from and transmitted past the structure. Thus, an approach resulting in a formulation of the problem from which such features are easily extracted is desirable.

In recent years, the so-called 'Method of matched eigenfunction expansions' has become popular, used by Miles & Gilbert [54] in the problem of scattering of surface waves by a circular dock in finite depth water. The increase in computer power has favoured this technique, which requires the solution of system of linear equations, typically of size $O(100)$. This method and its shortcomings will be discussed in more detail later in this chapter.

A subtle variation of this method, which we do not choose to examine in detail here, uses a least squares approach, but again requires the solution of a large system of equations. This scheme has recently used by Dalrymple & Martin [7] and Abul-Azim [2].

The two approaches briefly outlined above were introduced in an attempt to accurately predict the effect of wave interaction with obstacles in finite water depth and possessed, in theory, the capability of being able to achieve arbitrary accuracy for the potential everywhere in the fluid domain. This apparently superceded existing methods which had sought only to approximate certain important features of the solution with no firm certainty on their reliability. In particular, the variational approach was a simple and favoured tool for approximating desired quantities and is computationally inexpensive. It relies on using the matching conditions on the interfaces to yield a singular integral equation for a function $u(y)$ related to the unknown velocity across the interval of the interface occupied by the fluid (hereafter referred to as L_g). In its simplest form this would be

$$\mathcal{K}u = \psi_0, \quad y \in L_g, \tag{2.22}$$

and $u(y)$ is related to quantities of interest by

$$(u, \psi_0)_{L_g} = A, \tag{2.23}$$

where A has physical significance. Here, $\psi_0(y)$ is assumed given and $\mathcal{K}$ denotes a positive-definite linear self-adjoint operator. We have used the inner product notation

$$(u, v)_{L_g} = \int_{L_g} u(y)\overline{v(y)}\, \mathrm{d}y. \tag{2.24}$$

In some cases we may also use the conditions on the interface to derive a similar integral equation, this time in terms of a function related to the pressure difference, $p(y)$, across a barrier occupying an interval of the interface that we denote by L_b. This is written

$$\mathcal{M}p = \psi_0, \quad y \in L_b, \tag{2.25}$$

where, significantly, it will be seen that

$$(p, \psi_0)_{L_b} = A^{-1}. \tag{2.26}$$

Here, $\mathcal{M}$ is also positive-definite, linear and self-adjoint. The inner product in (2.26) is defined in the same manner as in (2.24) and henceforth we shall drop the subscript on the inner product on the understanding that velocity related implies L_g, whilst pressure difference related implies L_b.

The crux of this thesis lies in the derivation of complementary formulations such as those above and the subsequent approximations to them, for which Galerkin's method is employed. We now describe this method with reference to the two formulations (2.22), (2.23) and (2.25), (2.26) above by first outlining the variational principle.

Variational principles and Galerkin's method

A favoured technique for solving integral equations of the first kind such as in (2.22) where the operator, $\mathcal{K}$ is positive-definite and self-adjoint and the desired quantity is $(u, \psi_0) = A$ uses the variational principle.

We begin by defining the functional $J : L_2(L_g) \to \mathbb{R}$ by

$$J(\tilde{u}) = (\psi_0, \tilde{u}) + (\tilde{u}, \psi_0) - (\mathcal{K}\tilde{u}, \tilde{u}), \quad \text{for any } \tilde{u} \in L_2(L_g)\,. \tag{2.27}$$

Then

$$\begin{aligned} J(\tilde{u}) &= J(u + (\tilde{u} - u)) \\ &= J(u) + (\psi_0 - \mathcal{K}u, \tilde{u} - u) + (\tilde{u} - u, \psi_0 - \mathcal{K}u) - (\mathcal{K}(\tilde{u} - u), \tilde{u} - u), \end{aligned} \tag{2.28}$$

after a simple expansion where u is the solution of $\mathcal{K}u = \psi_0$. We therefore have

$$J(\tilde{u}) = J(u) - (\mathcal{K}(\tilde{u} - u), \tilde{u} - u) \leq J(u) \tag{2.29}$$

since $\mathcal{K}$ is positive with equality if and only if $\tilde{u} = u$. Now from (2.27) $J(u) = (u, \psi_0) = A$ and so

$$J(\tilde{u}) \leq A. \tag{2.30}$$

Thus $J(\tilde{u})$ is stationary at $\tilde{u} = u$ and its stationary value is A. Note that A is real and positive since $A = (u, \psi_0) = (u, \mathcal{K}u) = (\mathcal{K}u, u) = (\psi_0, u) = \overline{A}$ and we have used the fact that $\mathcal{K}$ is self-adjoint. Notice also from (2.29) that the difference between A and $J(\tilde{u})$, the approximation to A, is $O(\|\tilde{u} - u\|^2)$. Thus, if $\tilde{u}$ is a first-order approximation to u, the approximation to the stationary value will be accurate to second order.

If we now make the scaling $\tilde{u} = a_0 u_0$, say, where a_0 is a constant, and substitute into (2.27), the stationary value of $J(\tilde{u})$ will occur for a_0 such that $\partial J(\tilde{u})/\partial a_0 = 0$. This immediately gives $a_0 = (\psi_0, u_0)/(\mathcal{K}u_0, u_0)$ and the resulting variational approximation to A is then found to be

$$0 < J(\tilde{u}) = \frac{|(u_0, \psi_0)|^2}{(\mathcal{K}u_0, u_0)} \leq A, \tag{2.31}$$

and is independent of the scaling a_0. The above way of expressing the variational principle is known as the Schwinger method.

In order to improve on an approximation to A, a better description of the function u is required. This can be achieved either by a modified u_0 in (2.31), or alternatively by expanding $\tilde{u}$ as a series of test functions, written as

$$\tilde{u}(y) = \sum_{n=0}^{N} a_n u_n(y), \tag{2.32}$$

and substituting into (2.27) to obtain

$$J(\tilde{u}) = \sum_{n=0}^{N} \overline{a_n}(\psi_0, u_n) + \sum_{n=0}^{N} a_n(u_n, \psi_0) - \sum_{n=0}^{N}\sum_{m=0}^{N} \overline{a_m} a_n(\mathcal{K}u_n, u_m), \tag{2.33}$$

Forcing $J(\tilde{u})$ to be stationary with respect to a_n, for all $n = 0, \dots N$ by performing $\partial J(\tilde{u})/\partial a_n = 0$ yields the following system of equations for the coefficients a_n

$$\sum_{n=0}^{N} a_n(\mathcal{K}u_n, u_m) = (\psi_0, u_m), \quad m = 0, \dots N. \tag{2.34}$$

Note that if we were to impose, instead, that $\partial J(\tilde{u})/\partial \overline{a_n} = 0$ we would obtain the same system, (2.34). The resulting variational approximation to A is given on substitution of (2.34) back into (2.33) and yields

$$J(\tilde{u}) = \sum_{n=0}^{N} a_n(u_n, \psi_0). \tag{2.35}$$

By writing $K_{mn} = (\mathcal{K}u_n, u_m)$ and $F_{m0} = (\psi_0, u_m)$, and introducing the matrix notation $\mathbf{K} = \{K_{mn}\}$, $\mathbf{F} = (F_{00}, \dots, F_{N0})^{\mathrm{T}}$ we may eliminate the coefficients a_n by combining (2.34) and (2.35) to give the Schwinger variational form of (2.33),

$$0 < J(\tilde{u}) = \overline{\mathbf{F}}^{\mathrm{T}} \mathbf{K}^{-1} \mathbf{F} \leq A. \tag{2.36}$$

In doing so, we have shown, as in (2.31), that the Schwinger variational method is scale-invariant. Whilst not going into detail, it should be mentioned that increasing the dimension of the trial space spanned by $u_n(y)$ results in a tighter bound on A and that arbitrary accuracy can be achieved by choosing a large enough trial space. This can be achieved if the set $u_n(y)$ is complete in $L_2(L_g)$.

We now show how the approach that will be used throughout this thesis to approximate solutions to systems such as (2.22), namely Galerkin's method, is in fact equivalent to the variational principle above. Galerkin's method involves approximating u by an expansion such as (2.32) and satisfying $\mathcal{K}u = \psi_0$ in the components of the subspace spanned by the approximation. In other words, instead of satisfying $\mathcal{K}u - \psi_0 = 0$ exactly, we impose

$$(\mathcal{K}\tilde{u} - \psi_0, u_m) = 0, \quad m = 0, \dots N, \tag{2.37}$$

or

$$\sum_{n=0}^{N} a_n(\mathcal{K}u_n, u_m) = (\psi_0, u_m), \quad m = 0, \dots N, \tag{2.38}$$

which we notice, is precisely of the form given in (2.34). Likewise, the approximation to A, call it $\tilde{A}_u$, is found on substitution of (2.32) into (2.23) to be

$$\tilde{A}_u = \sum_{n=0}^{N} a_n(u_n, \psi_0), \tag{2.39}$$

and so

$$0 < \tilde{A}_u = \overline{\mathbf{F}}^{\mathrm{T}}\mathbf{K}^{-1}\mathbf{F} \leq A, \tag{2.40}$$

with the same notation as before. Thus, Galerkin's method, used in this context, is equivalent to the Schwinger variational method. A similar observation was made by Jones [35, p.271]. See also, Chambers [6], who shows that the Schwinger variational principle gives a better bound than the using the functional $J(\tilde{u})$ directly.

We also conclude that it is a second order method: if $\tilde{u}$ is an approximation to u such that $\|\tilde{u} - u\| = O(\epsilon)$ then $\|\tilde{A}_u - A\| = O(\epsilon^2)$.

In summary we have established that, in using Galerkin's method, the description of u need not be that good to achieve good accuracy for the approximation, $\tilde{A}_u$, to A. We also know that $\tilde{A}_u \leq A$ and that this bound can be made tighter by increasing the dimension of the trial space.

Thus far, only the integral equations for the velocity-related function, u, have been treated. Applying the Galerkin method to the complementary pressure difference formulation given by (2.25), (2.26) using the expansion

$$p(y) \simeq \tilde{p}(y) = \sum_{n=0}^{N} b_n p_n(y), \tag{2.41}$$

in terms of unknown coefficients b_n and known test functions $p_n(y)$, we obtain

$$\sum_{n=0}^{N} b_n(\mathcal{M}p_n, p_m) = (\psi_0, p_m), \quad m = 0, \dots, N, \tag{2.42}$$

whilst the approximation, $\tilde{A}_p^{-1}$ to A^{-1} is given by

$$\tilde{A}_p^{-1} = \sum_{n=0}^{N} b_n(p_n, \psi_0) \leq A^{-1}. \tag{2.43}$$

Using the matrix notation $\mathbf{M} = \{M_{mn}\}$ with $M_{mn} = (\mathcal{M}p_n, p_m)$, $n, m = 0, \dots N$ and $\mathbf{G} = (G_{00}, \dots, G_{N0})^{\mathrm{T}}$ where $G_{m0} = (\psi_0, p_m)$, we may eliminate the coefficients b_n from the above to give

$$0 < \tilde{A}_p^{-1} = \overline{\mathbf{G}}^{\mathrm{T}} \mathbf{M}^{-1} \mathbf{G} \leq A^{-1}. \tag{2.44}$$

Comments made with respect to the use of the Galerkin method with the velocity formulation are equally applicable here. It therefore follows immediately that

$$\tilde{A}_u \leq A \leq \tilde{A}_p, \tag{2.45}$$

and so the two formulations will provide upper and lower bounds on the quantity of interest, A.

The tightness of these bounds will depend on how well the unknown functions $u(y)$, $p(y)$ can be modelled and hence on the applicability of the series of test functions, $u_n(y)$ and $p_n(y)$. There are a number of issues that we must consider in the choice of these functions:

i. An explicit representation of the physical behaviour of the fluid must be incorporated into $u_n(y)$, $p_n(y)$.

ii. The elements of $\mathbf{K}$, $\mathbf{F}$, and $\mathbf{M}$, $\mathbf{G}$ should be easy to compute.

iii. The two sets $u_n(y)$, $p_n(y)$ should be complete over respective intervals so that convergence is assured as $N \to \infty$.

Perhaps the most important of these is condition (i) and this will motivate the choice of $u_n(y)$, $p_n(y)$, although it will be shown that (ii) and (iii) are also satisfied by the functions we choose.

Since the contents of this thesis show how the ideas expressed above can be applied to a range of well-known (and some not so well-known) problems in linear water waves it is therefore useful to make a comparison with existing methods commonly used in the solution of such problems using eigenfunction expansions as its starting point.

We pay particular attention to the so-called method of matched eigenfunction expansions, which has been briefly mentioned earlier and has seen widespread use in linear water waves.

In this, two homogeneous expressions are formed: one describes the no-flow condition across a solid portion of the matching interface, L_b, the other describing continuity of pressure across the interval occupied by the fluid, L_g. A function $F(y)$, say, defined to be zero over the whole depth, $L_g \cup L_b = [0, h]$, is consisting from of these two expressions, valid in their respective intervals. Since they are both homogenous expressions, scaling one of these by an arbitrary constant is possible in the definition of $F(y)$. The final step involves removing the y dependence by multiplying $F(y)$ by the vertical eigenfunction, $\psi_m(y)$, integrating over $[0, h]$ with use of (2.18) to give an infinite system of equations in unknown coefficients which are essentially Fourier coefficients for the expansion of the velocity across L_g. After truncating this system to a size N, say, and solving, the desired properties of the solution may then be extracted.

Let us now consider this procedure in some detail. Firstly, it is clear from above that the method of matched eigenfunction expansions seeks to find an approximation to $u(y)$, the unknown velocity across L_g, by estimating the components of a truncated Fourier series for the approximation to $u(y)$. This is somewhat awkward, since it is equivalent to an attempt at inverting the operator equation $\mathcal{K}u = \psi_0$ and since $\mathcal{K}$ is a compact operator on infinite-dimensional Hilbert space, its inverse is therefore unbounded. Thus, even though an approximation to $u(y)$ will generally converge as $N \to \infty$, it may do so slowly and since $\|\tilde{u} - u\| = \|K^{-1}(\mathcal{K}\tilde{u} - \mathcal{K}u)\| \leq \|K^{-1}\|\|\mathcal{K}\tilde{u} - \psi_0\|$ there is no way of predicting the error from the norm of the residual. Furthermore, the task of approximating $u(y)$

is made even harder if, as is found in many examples, $u(y)$ contains some singular behaviour.

This appears to be in accordance with reports of numerical difficulties associated with convergence using this method (see, for example, McIver [46]). The process of solving a truncated system of equations requires the inversion of an $N \times N$ non-symmetric, complex-valued matrix, and as such is computationally expensive if N is large. Numerical experiments carried out by the author suggest that choosing $N = 400$ is sufficient to ensure just two significant figures accuracy in many cases. An analysis of the convergence of coefficients in an application of the matching of eigenfunctions to a thin horizontal plate, consequently involving a singularity in the velocity at its edge, was given by McIver [47]. It was shown in this example, that the coefficients in the expansion of the velocity potential, A_n, decayed like $O(n^{-3/2})$. Convergence is therefore fairly slow. In order to reduce the size of N, many authors who have used this method have employed a method of linear extrapolation, based on the observation that plotting a desired quantity as a function of $1/N$ results in an approximately linear relation. Thus linear extrapolation through two points arising from 'moderate' values of N back to $1/N = 0$ ($N = \infty$) aims to provide a much better estimate at a reduced cost computationally. However, there is no mathematical basis for the method of linear extrapolation and a series of experiments by the author and M. Fernyhough suggest that it is an unreliable technique; apparently linear relations turn out to be more quadratic in nature and its use may therefore result in a significant reduction in accuracy.

Another peculiarity of the method is the presence in the final set of equations of an arbitrary (complex) parameter which we recall is introduced in the construction of $F(y)$ and reflects the 'importance' of one of the interface conditions over the other. Whatever value this parameter takes, the approximation must always approach the true solution in the limit $N \to \infty$. The question is, will convergence be altered by different choices of this parameter? Previous authors exploiting this method have suggested it does not and have taken it to be unity, but more numerical experiments by the author have shown a significant increase in convergence for fairly extreme parameter values of the order $O(10^{-3})$. Despite this, one must be suspicious of a method that relies on an arbitrary parameter that may be so easily dismissed.

In each of the problems considered in the thesis, the approach is basically the same. Firstly, we aim to provide two *complementary* formulations of the problem. Each of these is required to be in terms of linear integral operator equations of the first kind having, where possible, nice properties such as positive-definiteness and self-adjointness. Finally, if we can express the desired hydrodynamic quantities in terms of functionals of the unknown functions occuring in the integral equations then a Galerkin approximation will yield second-order accurate estimates to these quantities. Not only this, but we are also in a position to establish bounds on certain coefficients in a similar fashion to that already described earlier in this chapter. By choosing functions in the Galerkin approximation that accurately model the known physical behaviour of the fluid, we also expect there to be an accurate representation of unknown functions themselves, in addition to estimates involving functionals of them.

Although not discussed in this thesis, it is likely that other more 'local' properties of the fluid flow that rely directly on the accurate representation these functions can also be estimated accurately. Indeed, Evans & Fernyhough [16] using an extension of the ideas described in this thesis for the investigation into the existence of edge waves travelling along a periodic coastline, have been able to gain good approximations to the free surface profile, where clearly local aspects of the solution are required.

Chapter 3

Wave interaction with a single line of barriers with gaps

3.1 Introduction

This chapter is concerned with the scattering of a train of obliquely-incident plane waves by a single vertical line of thin vertical barriers in finite depth water.

Two-dimensional problems involving the scattering of a train of monochromatic surface waves by thin vertical barriers in deep water when described by linear water wave theory have the property that they can be solved analytically in closed form. Thus, Dean [8] solved the problem of the scattering of waves by a thin vertical barrier extending downwards from a point a below the mean free surface, deriving simple expressions for the ratio of reflected and transmitted wave amplitude to incident wave amplitude in terms of Bessel functions. The complementary problem to this of a vertical surface-piercing barrier immersed to a distance a below the free was treated soon after by Ursell [72], providing similar exact expressions for reflection and transmission coefficients as well as treating the problem of wave propagation due to a small amplitude rolling of the barrier.

In a complicated paper by John [34] the work of Ursell [72] was generalised to consider the effect of waves incident on a surface-piercing barrier making an angle $\pi/2n$ to the horizontal (n an integer). Subsequently, many authors have derived closed-form expressions for wave properties arising in vertical barrier schemes. For an arbitrary number of barriers with gaps between them occupying a single vertical line, Lewin [42], Mei [48], Porter [63] showed that closed form solutions were, in principle, capable of being achieved. In particular, Evans [10], solved the problem of a single finite totally-submerged vertical barrier, in terms of both scattering by an incident wave and wave radiation due to a small rolling motion of the barrier in an otherwise motionless fluid. The complementary problem to this, namely the scattering of an incident wave by a thin vertical barrier extending throughout the depth and containing a single submerged gap, was treated by Porter [62], the reflection and transmission coefficients expressible in terms of a combination of complicated integrals, similar to the case of Evans [10].

The reason for the existence of such explicit solutions to these two-dimensional infinite-depth thin barrier problems is as follows. Solutions of the two-dimensional Laplace equation can be found amongst complex analytic functions and for thin vertical barriers, the condition of no-flow across the barriers and the mixed free surface condition can together be expressed as conditions on the real and imaginary parts of a single new so-called reduced complex potential being a simple combination of the original complex potential and its derivative. The problem is thereby reduced to finding a single simpler complex function satisfying certain conditions and having certain singularities followed by solving a first-order differential for the original potential. Ursell [72] and some later authors chose to use a different approach based on an integral equation formulation requiring the application of Green's theorem to the fluid domain. In Porter [62] it is shown how these two different approaches reduce to the same Riemann-Hilbert problem.

The difficulties associated with using this complex theory and the restriction of working in two dimensions and infinite depth meant that many authors sought to adopt approximation procedures. Thus, in considering oblique wave incidence on a vertical surface-piercing barrier in infinite depth water, Evans & Morris [20] used the exact results of Ursell [72] as one-term Galerkin approximations to gain accurate upper and lower bounds on the modulus of the reflection coefficient. These bounds came from the use of two complementary formulations based on the unknown velocity under the barrier and the pressure difference across the barrier, to furnish, in the manner presented in chapter 2, maximum and minimum principles on a quantity related to the reflection coefficient. This method later became a powerful tool in showing the existence of frequencies for which total reflection occurs for the case of two identical surface-piercing barriers in infinite depth (Evans & Morris [21]).

Other efforts at approximating wave fields included the use of matched asymptotic expansions for barriers with small gaps. This method involves solving a 'near-sighted' problem close to the gap and a 'far-sighted' problem such that the gap appears as a point and then matching the outer limit of the near solution with the inner limit of the far solution. The first application of this in the context of water waves was made by Tuck [70] in considering the scattering of normally incident waves by a barrier with a small submerged gap below the free surface. Following this several applications of the method were made with respect to both thin barriers, thick barriers, and multiple barriers by most notably Tuck [71], Packham & Williams [60], Evans [11], [13] and Guiney *et al.* [30].

In an attempt to gain an accurate estimate of $|R|$, $|T|$ for the two-dimensional problem of scattering by a surface-piercing barrier in finite depth water, Smith [68] used a method of matched eigenfunction expansions. This involves expanding the potential to the left and the right of the barrier in Fourier-type series involving vertical eigenfunctions found through separation of variables and matching the potential and its derivative across the common boundary. An infinite systems of equations for unknown coefficients results, which when truncated can be solved to give estimates for $|R|$, $|T|$. The cautionary remarks made in chapter 2 over the accuracy of this method are applicable here. Nevertheless curves showing the effect of finite depth on $|R|$, $|T|$ are qualitatively accurate.

In this chapter we deal firstly with the scattering of obliquely-incident waves by four different vertical barrier configurations in water of finite depth, shown in figure

3.1: (a) the surface-piercing barrier; (b) the submerged bottom-mounted barrier; (c) the barrier with a submerged gap; and (d) the totally-submerged unmounted barrier. These are analogous to the infinite depth problems of Ursell [72], Dean [8], Porter [62] and Evans [10].

These four problems have recently been considered by Mandal & Dolai [45], concurrent with the author's own research. They used one-term Galerkin approximations based on the exact normal-incidence infinite-depth expressions for the velocity through the gaps in the barrier and pressure difference across the barrier in the complementary formulations of these problems and gained very accurate upper and lower bounds on $|R|$ and $|T|$ for a range of incident angles, barrier configurations and wave frequencies. Use of these functions clearly violates the no-flow condition on the sea-bed, but since they are only being used as trial functions in the variational principle this is not so important. We emphasize that the method we develop does respect the sea-bed condition.

We also consider the sloshing problem due to a thin vertical baffle uniformly spanning the width of a closed rectangular tank, a generalisation of Evans & McIver [19] who restricted themselves to motion parallel to the ends of the tank.

We use eigenfunction expansions as in Smith [68], but choose to proceed by constructing two integral equations, one for a function related to the unknown horizontal fluid velocity across the gap in the barrier, $u(y)$, and the other for a function proportional to the pressure difference across the barrier, $p(y)$. This follows the principle adopted by Evans & Morris [20] in infinite depth. Integral properties of $u(y)$ and $p(y)$ then supply upper and lower bounds on a real quantity, A, that translate into upper and lower bounds on $|R|$, $|T|$. By applying Galerkin's method to the resulting integral equations, with a judicious choice of test functions that correctly model the physical behaviour of the functions $u(y)$ and $p(y)$, we show how up to 6-figure accuracy can be obtained in the approximations to $|R|$, $|T|$ with only six terms in the Galerkin expansion. Note that a detailed account of the the

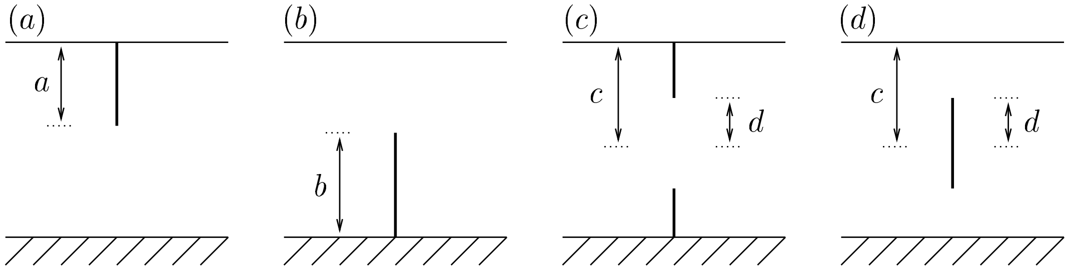

Figure 3.1: Barrier configurations: (a) A surface-piercing barrier; (b) A bottom-standing barrier; (c) A barrier with a gap; (d) A totally-submerged barrier.

Galerkin method is given in chapter 2.

In §3.2 the problem is formulated in terms of $u(y)$ and $p(y)$ for a general barrier configuration. All that remains is the specification of the test functions for the approximation to the functions $u(y)$ and $p(y)$ in the Galerkin procedure. These are introduced for each of the four barrier types being considered.

In §3.3 we formulate the sloshing problem which differs only slightly from the formulation in §3.2 due to the presence of tank walls.

Finally the results showing the accuracy of the method and some typical curves are presented in §3.4. We also make a brief comparison with the results from the eigenfunction approach of Smith [68].

3.2 Scattering by a single line of barriers with gaps

Cartesian co-ordinates are chosen with the mean-free surface $y = 0$. The fluid, of depth h, occupies $0 < y < h$, $-\infty < x, z < \infty$ and the barrier with gaps occupies the plane $x = 0$, $-\infty < z < \infty$, $0 \le y \le h$. The portion of the depth occupied by the barrier itself is denoted by L_b, whilst the gaps fill L_g so that $L_b \cup L_g$ is $[0, h]$.

It is assumed that a wave of frequency $\omega/2\pi$ is incident from $x = +\infty$ and is partially reflected at $x = 0$ and partially transmitted. The wave makes an angle θ with the plane $z = 0$. Then it follows from linear water-wave theory that there exists a velocity potential $\Phi(x, y, z, t)$ and that we may write

$$\Phi(x, y, z, t) = \mathrm{Re}\{\phi(x, y)\mathrm{e}^{ilz}\mathrm{e}^{-i\omega t}\} \tag{3.2.1}$$

where l is the wave number in the z-direction. Then $\phi(x,y)$ satisfies

$$\phi_{xx} + \phi_{yy} - l^2\phi = 0, \quad \text{in the fluid,} \tag{3.2.2}$$

$$\phi_y = 0, \quad \text{on } y = h,\ -\infty < x < \infty, \tag{3.2.3}$$

$$\phi_x = 0, \quad \text{on } x = 0,\ y \in L_b, \tag{3.2.4}$$

$$K\phi + \phi_y = 0, \quad \text{on } y = 0,\ x \neq 0, \tag{3.2.5}$$

where $K = \omega^2/g$,

$$\phi\,,\ \phi_x \text{ are continuous on } x = 0\,,\ y \in L_g\,. \tag{3.2.6}$$

The most general solutions of (3.2.2), (3.2.3), (3.2.5) which have the correct behaviour as $x \to \pm\infty$ are

$$\phi(x,y) = (\mathrm{e}^{-i\alpha x} + R\mathrm{e}^{i\alpha x})\psi_0(y) + \sum_{n=1}^{\infty} A_n \mathrm{e}^{-\alpha_n x}\psi_n(y), \quad \text{for } x > 0, \tag{3.2.7}$$

and

$$\phi(x,y) = T\mathrm{e}^{-i\alpha x}\psi_0(y) + \sum_{n=1}^{\infty} B_n \mathrm{e}^{\alpha_n x}\psi_n(y), \quad \text{for } x < 0\,. \tag{3.2.8}$$

Here $\alpha = (k^2 - l^2)^{1/2} = k\cos\theta$, $l = k\sin\theta$, and $\alpha_n = (k_n^2 + l^2)^{1/2}$ and we have used the notation introducted in chapter 2 so that k satisfies (2.13), k_n satisfies (2.14) and $\psi_n(y)$ are defined by (2.16) and satisfy the orthogonality relation (2.18).

It remains to determine R, T, (the reflection and transmission coefficients) A_n, B_n so that conditions (3.2.4) and (3.2.6) are satisfied. We define $\phi_x|_{x=0} \equiv U(y)$ and the jump in ϕ, $[\phi]_{x=0} \equiv P(y)$.

Then from (3.2.4) and (3.2.6)

$$U(y) = 0, \quad y \in L_b, \tag{3.2.9}$$

$$P(y) = 0, \quad y \in L_g. \tag{3.2.10}$$

Now from (3.2.6), (3.2.9) $U(y)$ is continuous for $y \in [0,h]$ so from (3.2.7), (3.2.8)

$$U(y) = -i\alpha(1-R)\psi_0(y) - \sum_{n=1}^{\infty} \alpha_n A_n \psi_n(y), \tag{3.2.11}$$

$$= -i\alpha T\psi_0(y) + \sum_{n=1}^{\infty} \alpha_n B_n \psi_n(y), \tag{3.2.12}$$

from which, after multiplying by $\psi_m(y)$ and integrating over $[0,h]$, we obtain

$$-i\alpha(1-R) = -i\alpha T = \frac{1}{h}\int_{L_g} U(y)\psi_0(y)\,\mathrm{d}y = U_0, \tag{3.2.13}$$

$$-\alpha_n A_n = \alpha_n B_n = \frac{1}{h}\int_{L_g} U(y)\psi_n(y)\,\mathrm{d}y = U_n, \quad n \geq 1 \tag{3.2.14}$$

where (3.2.9) has been used and

$$U(y) = \sum_{n=1}^{\infty} U_n \psi_n(y), \quad y \in [0,h]. \tag{3.2.15}$$

Application of (3.2.10) to (3.2.7), (3.2.8) now yields, after using (3.2.13), (3.2.14),

$$R\psi_0(y) = \int_{L_g} U(t)K(y,t)\,\mathrm{d}t, \quad y \in L_g, \tag{3.2.16}$$

where

$$K(y,t) = \sum_{n=1}^{\infty} (\alpha_n h)^{-1}\psi_n(y)\psi_n(t). \tag{3.2.17}$$

Defining $u(y)$ by $U(y) = Ru(y)$ and using (3.2.13) now gives

$$\mathcal{K}u \equiv \int_{L_g} u(t)K(y,t)\,\mathrm{d}t = \psi_0(y), \quad y \in L_g, \tag{3.2.18}$$

$$(u,\psi_0) \equiv \int_{L_g} u(y)\psi_0(y)\,\mathrm{d}y = A = -i\alpha h(1-R)/R. \tag{3.2.19}$$

Notice that $(u,\mathcal{K}v) = (v,\mathcal{K}u)$ and $(u,\mathcal{K}u) \geq 0$, for all $u, v \in L_2(L_g)$, using (3.2.17) to (3.2.19). The integral operator $\mathcal{K}$ is therefore self-adjoint and positive-definite and so (3.2.18) and (3.2.19) are precisely of the form (2.22), (2.23) given in chapter 2. Since from (3.2.18), (3.2.19) A is real, as is $\mathcal{K}$ and $\psi_n(y)$, then so is $u(y)$. Notice also that it follows immediately from (3.2.19) that

$$R = \alpha h/(\alpha h + iA), \tag{3.2.20}$$

whilst from (3.2.13)

$$T = iA/(\alpha h + iA), \tag{3.2.21}$$

and since A is real, $|R|^2 + |T|^2 = 1$ as expected from consideration of conservation of energy.

We now assume we have just a single gap and, following the description of the method given in chapter 2, we make the approximation

$$u(y) \simeq \tilde{u}(y) = \sum_{n=0}^{N} a_n u_n(y), \quad y \in L_g. \tag{3.2.22}$$

where we have yet to define the test functions $u_n(y)$. The Galerkin method involves substituting (3.2.22) into (3.2.18), multiplying through by $\psi_m(y)$ and integrating over L_g to give

$$\sum_{n=0}^{N} a_n K_{mn} = F_{m0}, \quad m = 0, \ldots, N, \tag{3.2.23}$$

where

$$\begin{aligned} K_{mn} = (\mathcal{K}u_n, u_m) &= \sum_{r=1}^{\infty} (\alpha_r h)^{-1} \int_{L_g} u_n(y)\psi_r(y)\,\mathrm{d}y \int_{L_g} u_m(y)\psi_r(y)\,\mathrm{d}y \\ &= \sum_{r=1}^{\infty} (\alpha_r h)^{-1} F_{mr} F_{nr}, \end{aligned} \tag{3.2.24}$$

where (3.2.17) has been used, with

$$F_{mn} = (\psi_n, u_m) = \int_{L_g} u_m(y)\psi_n(y)\,\mathrm{d}y. \tag{3.2.25}$$

Now, using (3.2.22) in (3.2.19) gives the approximation to A, thus

$$0 \leq \tilde{A}_u = \sum_{n=0}^{N} a_n F_{m0} \tag{3.2.26}$$

whence combining to eliminate the coefficients a_n, we find

$$\tilde{A}_u = \mathbf{F}^{\mathrm{T}} \mathbf{K}^{-1} \mathbf{F} \tag{3.2.27}$$

and we have used the matrix notation $\mathbf{K} = \{K_{mn}\}$ and $\mathbf{F} = (F_{00}, \ldots, F_{N0})^{\mathrm{T}}$. From chapter 2, equation (2.40) we see that $\tilde{A}_u \leq A$.

A similar integral equation for $P(y)$ can be obtained as follows. From (3.2.7), (3.2.8)

$$P(y) = 2R\psi_0(y) - 2\sum_{n=1}^{\infty} \alpha_n^{-1} U_n \psi_n(y), \quad y \in [0, h], \tag{3.2.28}$$

where (3.2.13), (3.2.14) have been used. Thus, multiplying by $\psi_m(y)$ and integrating over $[0, h]$

$$2R = \frac{1}{h} \int_{L_b} P(y)\psi_0(y)\,\mathrm{d}y = P_0, \tag{3.2.29}$$

$$-2\alpha_n^{-1}U_n = \frac{1}{h}\int_{L_b} P(y)\psi_n(y)\,\mathrm{d}y = P_n, \quad n \geq 1 \tag{3.2.30}$$

where (3.2.10) has been used, so that

$$P(y) = \sum_{n=1}^{\infty} P_n\psi_n(y), \quad y \in [0,h]. \tag{3.2.31}$$

Application of (3.2.9) to (3.2.11) now yields, for $y \in L_b$,

$$\begin{aligned} -i\alpha(1-R)\psi_0(y) &= \sum_{n=1}^{\infty} \alpha_n A_n \psi_n(y) \\ &= -\sum_{n=1}^{\infty} U_n\psi_n(y), \end{aligned}$$

from (3.2.14),

$$= \sum_{n=1}^{\infty} \psi_n(y)\frac{\alpha_n}{2h}\int_{L_b} P(t)\psi_n(t)\,\mathrm{d}t, \tag{3.2.32}$$

from (3.2.30) or, writing $P(y) = -2ih^2\alpha(1-R)p(y)$,

$$\mathcal{M}p \equiv \sum_{n=1}^{\infty} \alpha_n h \int_{L_b} p(t)\psi_n(t)\psi_n(y)\,\mathrm{d}t = \psi_0(y), \quad y \in L_b, \tag{3.2.33}$$

and from (3.2.29),

$$(p,\psi_0) \equiv \int_{L_b} p(y)\psi_0(y)\,\mathrm{d}y = A^{-1}. \tag{3.2.34}$$

which are precisely of the form given in (2.25) and (2.26) of chapter 2, with $\mathcal{M}$ real, positive-definite and self-adjoint since $(\mathcal{M}p,p) = \sum_{n=1}^{\infty}\alpha_n h|(p,\psi_n)|^2 \geq 0$, and $(\mathcal{M}p,q) = (p,\mathcal{M}q)$, $\forall p,q \in L_2(L_b)$.

Notice that, unlike in the case of the velocity $u(y)$ we cannot immediately interchange the summation and integration in (3.2.33) since the resulting infinite sum is divergent. A recent study of the numerical solution of the hypersingular integral equation obtained if the limits are interchanged has been made by Parsons & Martin [61]. We can, however, continue to apply the Galerkin method as before, and, assuming initially that there is just a single barrier, we choose an appropriate approximation to $p(y)$ of the form

$$p(y) \simeq \tilde{p}(y) = \sum_{n=0}^{N} b_n p_n(y), \quad y \in L_b \tag{3.2.35}$$

where we have yet to define the test functions $p_n(y)$. Applying the Galerkin method to (3.2.33) with (3.2.34) as in (2.41)–(2.44) gives the following approximation $\tilde{A}_p^{-1}$ to A^{-1}

$$0 < \tilde{A}_p^{-1} = \mathbf{G}^{\mathrm{T}}\mathbf{M}^{-1}\mathbf{G} \le A^{-1}. \tag{3.2.36}$$

Here we have employed the matrix and vector notation $\mathbf{M} = \{M_{mn}\}$, $\mathbf{G} = (G_{00}, \ldots, G_{N0})^{\mathrm{T}}$ where

$$M_{mn} = (\mathcal{M}p_n, p_m) = \sum_{r=1}^{\infty} \alpha_r h G_{mr} G_{nr}, \tag{3.2.37}$$

with

$$G_{mn} = (\psi_m, p_n) = \int_{L_b} p_n(y)\psi_m(y)\,\mathrm{d}y, \tag{3.2.38}$$

and we have assumed that the eventual choice of $p_n(y)$ ensures the convergence of the series defining M_{mn}. It follows that

$$0 < \tilde{A}_u \le A \le \tilde{A}_p, \tag{3.2.39}$$

with corresponding complementary bounds on $|R|$, $|T|$ apparent from (3.2.20), (3.2.21).

It remains to choose the functions $u_n(y)$, $p_n(y)$ appropriate to the particular configuration being considered.

3.2.1 The surface-piercing barrier

We assume a single surface-piercing barrier of length a so that $L_b = (0, a)$ and $L_g = (a, h)$. An analysis of the flow close to the edge of the barrier would reveal that $u(y) \sim (y-a)^{-1/2}$ as $y \to a^+$ and since $\phi_y = 0$ on $y = h$, ϕ and hence $u(y) \propto \phi_x|_{y=h}$ can be continued as an even function of y across $y = h$. Therefore the even continuous function $\{(h-a)^2 - (h-y)^2\}^{1/2}u(y)$ can be expanded in (a, h) in a *complete* set of *even* Chebychev polynomials. Thus, anticipating subsequent simplifications, we choose

$$u_m(y) = \frac{2(-1)^m}{\pi\{(h-a)^2 - (h-y)^2\}^{1/2}} T_{2m}\left(\frac{h-y}{h-a}\right), \quad y \in [a, h], \tag{3.2.40}$$

where $T_n(x) = \cos n\theta$, $x = \cos\theta$. The particular choice of $T_{2n}(x)$ as opposed to any other orthogonal function is in the desire for a simple form for F_{mn} and is motivated by the fact that the natural weighting function for the Chebychev Polynomial is an inverse square root term. It follows that

$$\begin{aligned} F_{mn} &= \int_a^h u_m(y)\psi_n(y)\,\mathrm{d}y \\ &= \frac{2N_n^{-1/2}(-1)^m}{\pi}\int_0^1 \frac{T_{2m}(t)}{(1-t^2)^{1/2}}\cos\{k_n(h-a)t\}\,\mathrm{d}t, \end{aligned}$$

after putting $h - y = (h-a)t$,

$$= N_n^{-1/2} J_{2m}\{k_n(h-a)\}, \tag{3.2.41}$$

(Erdélyi *et al.* [9], §1.10, equation 2) whilst

$$F_{m0} = (-1)^m N_0^{-1/2} I_{2m}\{k(h-a)\}, \tag{3.2.42}$$

where J_n, I_n are the Bessel function and modified Bessel function of order n respectively. Thus from (3.2.24)

$$K_{mn} = \sum_{r=1}^{\infty}(N_r\alpha_r h)^{-1} J_{2m}\{k_r(h-a)\} J_{2n}\{k_r(h-a)\}. \tag{3.2.43}$$

In choosing the functions $p_n(y)$ we bear in mind the free surface condition (3.2.5) and the behaviour $p(y) \sim (a-y)^{1/2}$ as $y \to a^-$ deduced from a consideration of the flow field in the neighbourhood of $y = a$. Thus we choose $p_n(y)$ to satisfy

$$Kp_n(y) + p_n'(y) = 0, \quad y = 0, \tag{3.2.44}$$

$$p_n(y) = 0, \quad y = a. \tag{3.2.45}$$

It is convenient to introduce a reduced function $\hat{p}_n(y)$ defined by

$$\hat{p}_n(y) = p_n(y) - K\int_y^a p_n(y)\,\mathrm{d}t, \tag{3.2.46}$$

from which it is easily verified that

$$\hat{p}_n'(y) = 0, \quad y = 0, \tag{3.2.47}$$

$$\hat{p}_n(y) = 0, \quad y = a. \tag{3.2.48}$$

Now

$$\begin{aligned} G_{mn} &= \int_0^a p_m(y)\psi_n(y)\,\mathrm{d}y \\ &= N_n^{-1/2}\int_0^a p_m(y)\cos k_n(h-y)\,\mathrm{d}y \\ &= N_n^{-1/2}\cos k_n h\int_0^a \hat{p}_m(y)\cos k_n y\,\mathrm{d}y, \end{aligned}$$

after integration by parts. Condition (3.2.47) permits the extension of $\hat{p}_n(y)$ into $(-a,0)$ as an even function of y and taking into account (3.2.48) and subsequent simplifications we write

$$\hat{p}_m(y) = \frac{2(-1)^m}{\pi(2m+1)ah}(a^2-y^2)^{1/2}U_{2m}\left(\frac{y}{a}\right), \quad y\in[0,a], \tag{3.2.49}$$

where $U_n(x)=\sin(n+1)\theta/\sin\theta$, $x=\cos\theta$ is the orthogonal Chebychev polynomial of the second kind and $U_{2m}(y)$ is even. It follows that

$$\begin{aligned} G_{mn} &= \frac{2(-1)^m N_n^{-1/2}\cos k_n h}{\pi(2m+1)ah}\int_0^a (a^2-y^2)^{1/2}U_m(y/a)\cos k_n y\,\mathrm{d}y \\ &= N_n^{-1/2}\frac{\cos k_n h}{k_n h}\,J_{2m+1}(k_n a), \end{aligned} \tag{3.2.50}$$

(Erdélyi *et al.* [9], §1.10, equation 3), whilst

$$G_{m0} = (-1)^m N_0^{-1/2}\frac{\cosh kh}{kh}\,I_{2m+1}(ka). \tag{3.2.51}$$

Note that the $k_n h$ factor in the denominator of (3.2.50) ensures that the sum in (3.2.37) converges and we have

$$M_{mn} = \sum_{r=1}^{\infty}\alpha_r h(k_r h)^{-2}N_r^{-1}\cos^2 k_r h J_{2m+1}(k_r a)J_{2n+1}(k_r a). \tag{3.2.52}$$

3.2.2 The submerged bottom-mounted barrier

We assume a submerged barrier extending upwards a distance $h-b$ from the bottom, so that $L_b=(b,h)$ whilst $L_g=(0,b)$, and use the ideas from the surface-piercing barrier arrangement.

We have

$$\begin{aligned} F_{mn} &= \int_0^b u_m(y)\cos k_n(h-y)\,\mathrm{d}y \\ &= N_n^{-1/2}\cos k_n h\int_0^b \hat{u}_m(y)\cos k_n y\,\mathrm{d}y, \end{aligned} \tag{3.2.53}$$

where we have introduced the reduced function defined by

$$\hat{u}_m(y) = u_m(y) - K\int_y^b u_m(t)\,\mathrm{d}t, \tag{3.2.54}$$

and so the condition $Ku_n(y) + u_n'(y) = 0$ on $y = 0$ becomes

$$\hat{u}_m'(y) = 0, \quad y = 0. \tag{3.2.55}$$

whilst the behaviour $u_m(y) \sim (b^2 - y^2)^{-1/2}$ as $y \to b$ is unchanged for $\hat{u}_m(y)$. Choosing

$$\hat{u}_m(y) = \frac{2(-1)^m}{\pi(b^2 - y^2)^{1/2}} T_{2m}\left(\frac{y}{b}\right), \quad y \in [0, b], \tag{3.2.56}$$

now gives

$$F_{mn} = N_n^{-1/2} \cos k_n h\; J_{2m}(k_n b), \tag{3.2.57}$$

with

$$F_{m0} = (-1)^m N_0^{-1/2} \cosh kh\; I_{2m}(kb), \tag{3.2.58}$$

whilst

$$K_{mn} = \sum_{r=1}^{\infty} (\alpha_r h N_n)^{-1} \cos^2 k_r h J_{2m}(k_r b) J_{2n}(k_r b) \tag{3.2.59}$$

For the complementary formulation,

$$G_{mn} = \int_b^h p_m(y)\psi_n(y)\,\mathrm{d}y, \tag{3.2.60}$$

where we choose

$$p_m(y) = \frac{2(-1)^m\{(h-b)^2 - (h-y)^2\}^{1/2}}{\pi(2m+1)(h-b)h} U_{2m}\left(\frac{h-y}{h-b}\right), \quad y \in [b, h], \tag{3.2.61}$$

incorporating the expected behaviour at the tip of the barrier and using the condition of $\phi_y = 0$ on $y = h$ to continue ϕ and hence $p_m(y)$ as an even function across $y = h$. Use of (3.2.61) in (3.2.60) yields

$$G_{mn} = \frac{N_n^{-1/2}}{k_n h} J_{2m+1}\{k_n(h-b)\}, \tag{3.2.62}$$

whilst

$$G_{m0} = (-1)^m \frac{N_0^{-1/2}}{kh} I_{2m+1}\{k(h-b)\}. \tag{3.2.63}$$

and

$$M_{mn} = \sum_{r=1}^{\infty} \alpha_r h (k_r h)^2 N_r^{-1} J_{2m+1}\{k_r(h-b)\} J_{2n+1}\{k_r(h-b)\} \tag{3.2.64}$$

3.2.3 A barrier with a single submerged gap

We assume L_g is (a,b) so that L_b is $(0,a) \cup (b,h)$ and two separate expansions will be needed for the pressure difference in this case.

The square-root singularities at the two edges $y = a, b$ suggest we expand the continuous function $(y-a)^{1/2}(b-y)^{1/2}u(y)$ in terms of the *complete* Chebychev polynomials T_n over $[a,b]$. Thus we write

$$u_m(y) = \frac{1}{\pi (y-a)^{1/2}(b-y)^{1/2}} T_m\left(\frac{2y-a-b}{b-a}\right), \quad y \in [a,b], \tag{3.2.65}$$

whence

$$\begin{aligned} F_{mn} &= N_n^{-1/2} \int_a^b \frac{T_m((2y-a-b)/(b-a))}{\pi (y-a)^{1/2}(b-y)^{1/2}} \cos k_n(h-y)\,\mathrm{d}y \\ &= \frac{N_n^{-1/2}}{\pi} \int_{-1}^{1} \frac{T_m(t)}{(1-t^2)^{1/2}} \cos k_n(h-c-dt)\,\mathrm{d}t, \end{aligned}$$

where $c = \frac{1}{2}(a+b)$ is the submergence depth of the centre of the gap and $d = \frac{1}{2}(b-a)$ is half the width of the gap. So

$$F_{mn} = N_n^{-1/2} \cos(k_n(h-c) - \frac{1}{2} m\pi) J_m(k_n d), \tag{3.2.66}$$

(Gradshteyn & Ryzhik [29], p.402) so that

$$F_{2m,n} = (-1)^m N_n^{-1/2} \cos k_n(h-c)\; J_{2m}(k_n d), \tag{3.2.67}$$

$$F_{2m+1,n} = (-1)^{m+1} N_n^{-1/2} \sin k_n(h-c)\; J_{2m+1}(k_n d), \tag{3.2.68}$$

whilst

$$F_{2m,0} = N_0^{-1/2} \cosh k(h-c)\; I_{2m}(kd), \tag{3.2.69}$$

$$F_{2m+1,0} = -N_0^{-1/2} \sinh k(h-c)\; I_{2m+1}(kd). \tag{3.2.70}$$

and K_{mn} is given by (3.2.24).

The integral equation for the pressure difference now involves two disjoint intervals $L_1 = (0, a)$ and $L_2 = (b, h)$ so we need to modify slightly the theory given in chapter 2. Thus we write (2.25) as

$$\mathcal{M}p \equiv \mathcal{M}_1 p + \mathcal{M}_2 p = \psi_0, \quad y \in L_1 \cup L_2, \tag{3.2.71}$$

$$(\psi_0, p) \equiv (\psi_0, p)_1 + (\psi_0, p)_2 = A^{-1}, \tag{3.2.72}$$

where the suffix i refers to the interval L_i, $i = 1, 2$. A different set of functions is appropriate to each interval so we write

$$p(y) = \begin{cases} \displaystyle\sum_{n=0}^{N} b_n p_n^{(1)}(y), & y \in L_1 \\ \displaystyle\sum_{n=0}^{N} c_n p_n^{(2)}(y), & y \in L_2, \end{cases} \tag{3.2.73}$$

where here $p_n^{(i)}(y)$, are the sets of functions chosen for the expansions of $p(y)$ in the surface-piercing ($i = 1$) and bottom-mounted ($i = 2$) problems respectively. Substitution of (3.2.73) into (3.2.71), multiplication by first $p_m^{(1)}(y)$ and then $p_m^{(2)}(y)$ and integration over L_1 and L_2 respectively, gives

$$\sum_{n=0}^{N} \{b_n M_{mn}^{(1,1)} + c_n M_{mn}^{(1,2)}\} = (p_m, \psi_0)_1 = P_{m0}^{(1)}, \tag{3.2.74}$$

$$\sum_{n=0}^{N} \{b_n M_{mn}^{(2,1)} + c_n M_{mn}^{(2,2)}\} = (q_m, \psi_0)_2 = P_{m0}^{(2)}, \tag{3.2.75}$$

both for $m = 0, \ldots, N$, whilst (3.2.73) into (3.2.72) gives the approximation to A^{-1}, namely

$$\begin{aligned} \tilde{A}_p^{-1} &= \sum_{n=0}^{N} \{b_n (p_n^{(1)}, \psi_0)_1 + c_n (p_n^{(2)}, \psi_0)_2\} \\ &= \sum_{n=0}^{N} \{b_n P_{n0}^{(1)} + c_n P_{n0}^{(2)}\}. \end{aligned} \tag{3.2.76}$$

Here

$$M_{mn}^{(i,j)} = (\mathcal{M}_j p_n^{(j)}, p_m^{(i)})_i = \sum_{r=1}^{\infty} \alpha_r h P_{mr}^{(i)} P_{nr}^{(j)}, \quad i, j = 1, 2, \tag{3.2.77}$$

whilst

$$P_{mn}^{(i)} = (p_n^{(i)}, \psi_m)_i = \int_{L_i} p_n^{(i)}(y) \psi_m(y), \quad i = 1, 2. \tag{3.2.78}$$

Note that $P_{mn}^{(i)}$, $i = 1, 2$ are identical to (3.2.50) and (3.2.62) occuring in the single surface-piercing barrier and bottom-mounted barrier problems respectively.

Eliminating the coefficients b_n, c_n from (3.2.74)–(3.2.76) allows us to write

$$\tilde{A}_p^{-1} = \begin{pmatrix} \mathbf{P}^{(1)} \\ \mathbf{P}^{(2)} \end{pmatrix}^{\mathrm{T}} \begin{pmatrix} \mathbf{M}^{(1,1)} & \mathbf{M}^{(1,2)} \\ \mathbf{M}^{(2,1)} & \mathbf{M}^{(2,2)} \end{pmatrix}^{-1} \begin{pmatrix} \mathbf{P}^{(1)} \\ \mathbf{P}^{(2)} \end{pmatrix} \leq A^{-1}, \tag{3.2.79}$$

where we define the matrices $\mathbf{M}^{(i,j)} = \{M_{mn}^{(i,j)}\}$, $i, j = 1, 2$ and the vectors $\mathbf{P}^{(i)} = (P_{00}^{(i)}, \ldots, P_{N0}^{(i)})^{\mathrm{T}}$, $i = 1, 2$. Notice also that the block matrix in (3.2.79) is real and symmetric by virtue of (3.2.77).

3.2.4 The totally-submerged unmounted barrier

We assume the barrier occupies $a < y < b$ so that $L_b = (a, b)$ and L_g is $(0, a) \cup (b, h)$ so that two separate expansions are needed for the velocity in each of the gaps; a reversal of the barrier with a submerged gap problem.

The only requirement on $p_n(y)$ on (a, b) is that $p(y) \sim (y-a)^{1/2}$ as $y \to a^+$, $p(y) \sim (b-y)^{1/2}$ as $y \to b^-$, and we need to use the full set U_n of second kind Chebychev polynomials here. Thus we choose

$$p_m(y) = \frac{(y-a)^{1/2}(b-y)^{1/2}}{\pi(m+1)dh} U_m\left(\frac{2y-a-b}{b-a}\right), \quad y \in [a, b], \tag{3.2.80}$$

whence

$$\begin{aligned} G_{mn} &= N_n^{-1/2} \int_a^b \frac{(y-a)^{1/2}(b-y)^{1/2}}{\pi(m+1)dh} U_m\left(\frac{2y-a-b}{b-a}\right) \cos k_n(h-y)\,\mathrm{d}y \\ &= \frac{dN_n^{-1/2}}{\pi(m+1)h} \int_{-1}^{1} (1-t^2)^{1/2} U_m(t) \cos k_n(h-c-dt)\,\mathrm{d}t, \end{aligned}$$

where $c = \frac{1}{2}(a+b)$, $d = \frac{1}{2}(b-a)$ as in the previous section. After some manipulation we find

$$G_{mn} = N_n^{-1/2}(k_n d)^{-1} \cos(k_n(h-c) - \tfrac{1}{2}m\pi) J_{m+1}(k_n d), \tag{3.2.81}$$

and so

$$G_{2m,n} = (-1)^m N_n^{-1/2} \frac{\cos k_n(h-c)}{k_n h} J_{2m+1}(k_n d), \tag{3.2.82}$$

$$G_{2m+1,n} = (-1)^{m+1} N_n^{-1/2} \frac{\sin k_n(h-c)}{k_n h} J_{2m+2}(k_n d), \tag{3.2.83}$$

whilst

$$G_{2m,0} = N_0^{-1/2} \frac{\cosh k(h-c)}{kh} I_{2m+1}(kd), \tag{3.2.84}$$

$$G_{2m+1,0} = -N_0^{-1/2} \frac{\sinh k(h-c)}{kh} I_{2m+2}(kd). \tag{3.2.85}$$

For the velocity formulation, we choose

$$u(y) = \begin{cases} \sum_{n=0}^{N} a_n u_n^{(1)}(y), & y \in L_1 \\ \sum_{n=0}^{N} b_n u_n^{(2)}(y), & y \in L_2, \end{cases} \tag{3.2.86}$$

where here $u_n^{(1)}(y)$, $u_n^{(2)}(y)$ are the sets of functions chosen for the expansion of $u(y)$ in the surface-piercing and bottom-mounted barrier problems respectively. Following the procedure used for the disjoint intervals in the gap between two barriers of the previous section, we finally obtain

$$\sum_{n=0}^{N} \{a_n K_{mn}^{(1,1)} + b_n K_{mn}^{(1,2)}\} = U_{m0}^{(1)}, \tag{3.2.87}$$

$$\sum_{n=0}^{N} \{a_n K_{mn}^{(2,1)} + b_n K_{mn}^{(2,2)}\} = U_{m0}^{(2)}, \tag{3.2.88}$$

with

$$\tilde{A}_u = \sum_{n=0}^{N} \{a_n U_{n0}^{(1)} + b_n U_{n0}^{(2)}\}. \tag{3.2.89}$$

Here

$$K_{mn}^{(i,j)} = \sum_{r=1}^{\infty} (\alpha_r h)^{-1} U_{mr}^{(i)} U_{nr}^{(j)}, \tag{3.2.90}$$

whilst

$$U_{mn}^{(i)} = \int_{L_i} u_n^{(i)}(y) \psi_m(y), \tag{3.2.91}$$

Note that $U_{mn}^{(i)}$, $i = 1,2$ are identical to (3.2.57) and (3.2.41) occuring in the problems of the single bottom-mounted barrier of length $(h-a)$ and surface-piercing barrier of length b respectively. Eliminating the coefficients a_n, b_n from (3.2.87)–(3.2.89) allows us to write

$$\tilde{A}_u = \begin{pmatrix} \mathbf{U}^{(1)} \\ \mathbf{U}^{(2)} \end{pmatrix}^{\mathrm{T}} \begin{pmatrix} \mathbf{K}^{(1,1)} & \mathbf{K}^{(1,2)} \\ \mathbf{K}^{(2,1)} & \mathbf{K}^{(2,2)} \end{pmatrix}^{-1} \begin{pmatrix} \mathbf{U}^{(1)} \\ \mathbf{U}^{(2)} \end{pmatrix} \leq A, \tag{3.2.92}$$

where we define the matrices $\mathbf{K}^{(i,j)} = \{K_{mn}^{(i,j)}\}$, $i,j = 1,2$ and the vectors $\mathbf{U}^{(i)} = (U_{00}^{(i)}, \ldots, U_{N0}^{(i)})^{\mathrm{T}}$, $i = 1,2$.

3.3 Sloshing in a rectangular tank containing a vertical baffle

The same technique can be applied to determine the sloshing frequencies in a rectangular tank with a baffle consisting of a thin vertical barrier with an arbitrary number of gaps. A particular case of this problem when the motion was two dimensional was considered by Evans & McIver [19] and more recently, calculations for the fully three dimensional motion using a matched eigenfunction approach have been reported in Jeyakumaran & McIver [33]. We assume that the baffle separates the tank into two regions, $-b \le x \le 0$, and $0 \le x \le c$, $b + c = d$ and the tank occupies $-b \le x \le c$, $0 \le z \le f$, $0 \le y \le h$. Again, the baffle occupies the depth $y \in L_b$ and the gap in the barrier is $y \in L_g$. Then the only changes required are that the term e^{ilz} in (3.2.1) is replaced by $\cos lz$ where $lf = m\pi$, $m = 0, 1, 2, \dots$ and that (3.2.7), (3.2.8) are replaced by

$$\phi(x, y) = A_0 \cos \alpha(x + b)\psi_0(y) + \sum_{n=1}^{\infty} A_n \cosh \alpha_n(x + b)\psi_n(y), \quad -b \le x \le 0, \tag{3.3.1}$$

and

$$\phi(x, y) = B_0 \cos \alpha(c - x)\psi_0(y) + \sum_{n=1}^{\infty} B_n \cosh \alpha_n(c - x)\psi_n(y), \quad 0 \le x \le c. \tag{3.3.2}$$

These expressions satisfy the no-flow condition on the end walls of the tank and all that remains is to match ϕ, ϕ_x across the common boundary, $x = 0$. Thus, repeating the development of §3.2 which led to (3.2.18), (3.2.19) results instead in

$$\mathcal{K}^{(s)} u^{(s)} \equiv \int_{L_g} u^{(s)}(t) K^{(s)}(y, t) \, \mathrm{d}t = \psi_0(y), \quad y \in L_g, \tag{3.3.3}$$

and

$$(u^{(s)}, \psi_0) \equiv \int_{L_g} u^{(s)}(y)\psi_0(y) \, \mathrm{d}y = A^{(s)} = \frac{\alpha h \sin \alpha b \sin \alpha c}{\sin \alpha d}, \tag{3.3.4}$$

where the s refers to the sloshing problem and

$$K^{(s)}(y, t) = \sum_{n=1}^{\infty} (\alpha_n h)^{-1} (\coth \alpha_n b + \coth \alpha_n c)\psi_n(y)\psi_n(t). \tag{3.3.5}$$

Likewise, we can repeat the process and derive a complementary formulation in terms of the pressure difference across the barrier. Thus, proceeding in the manner of §3.2 results in

$$\mathcal{M}^{(s)}p^{(s)} \equiv \int_{L_b} p^{(s)}(y)M^{(s)}(y,t)\,\mathrm{d}t = \psi_0(y), \quad y \in L_b, \tag{3.3.6}$$

with

$$(p^{(s)}, \psi_0) \equiv \int_{L_b} p^{(s)}(y)\psi_0(y)\,\mathrm{d}y = 1/A^{(s)}. \tag{3.3.7}$$

The operators $\mathcal{K}^{(s)}$, $\mathcal{M}^{(s)}$ are real, self-adjoint and positive-definite and so we have formulated the problem in the manner specified in chapter 2 by (2.22), (2.23) and (2.25), (2.26).

The problem is reduced to determining $A^{(s)}$ and hence, for given b, c, f, solving for $\alpha = \alpha^{(p)}$, $p = 1, 2, \ldots$ from (3.3.4) and determining the sloshing frequencies ω_{mp} from

$$\omega^2 = gk\tanh kh, \tag{3.3.8}$$

where $k^2 = l^2 + \alpha^2$ with $l = m\pi/f$, $m = 0, 1, 2, \ldots$.

Applying the Galerkin method to (3.2.3)–(3.2.5) with the approximation to $u^{(s)}(y)$ of $\tilde{u}^{(s)}(y) = \sum_{n=0}^{N} a_n^{(s)} u_n(y)$ (assuming that the baffle is comprised of just one gap for which the set $u_n(y)$ are appropriate test functions), now yields

$$A_u^{(s)} = \mathbf{F}^{\mathrm{T}}\mathbf{K}^{(s)^{-1}}\mathbf{F} \leq A^{(s)}, \tag{3.3.9}$$

with $\mathbf{K}^{(s)} = \{K_{mn}^{(s)}\}$ where

$$K_{mn}^{(s)} = \sum_{r=1}^{\infty} (\alpha_r h)^{-1}(\coth\alpha_r b + \coth\alpha_r c)F_{mr}F_{nr}. \tag{3.3.10}$$

and $\mathbf{F} = (F_{00}, \ldots, F_{N0})^{\mathrm{T}}$. Here, F_{mn} is defined by (3.2.41), (3.2.42) for the surface-piercing baffle or by (3.2.57), (3.2.58) for the bottom-mounted baffle.

Similarly, the Galerkin method applied to (3.3.6)–(3.3.8) with the approximation $p^{(s)}(y) \simeq \tilde{p}^{(s)}(y) = \sum_{n=0}^{N} b_n^{(s)} p_n(y)$ (assuming one barrier) yields

$$1/\tilde{A}_p^{(s)} = \mathbf{G}^{\mathrm{T}}\mathbf{M}^{(s)^{-1}}\mathbf{G} \leq 1/A^{(s)}, \tag{3.3.11}$$

where $\mathbf{M}^{(s)} = \{M_{mn}^{(s)}\}$ with

$$M_{mn}^{(s)} = \sum_{r=1}^{\infty} \alpha_r h(\coth \alpha_r b + \coth \alpha_r c)^{-1} G_{mr} G_{nr}, \tag{3.3.12}$$

and $\mathbf{G} = (G_{00}, \ldots, G_{N0})^{\mathrm{T}}$. Here, G_{mn} is given by (3.2.50), (3.2.51) for the surface-piercing baffle or by (3.2.62), (3.2.63) for the bottom-mounted baffle.

Again we have $A_u^{(s)} \leq A^{(s)} \leq A_p^{(s)}$ as upper and lower bounds for $A^{(s)}$.

Note that the methods of §3.2 for other barrier configurations than the two considered here can be used in precisely the same manner.

3.4 Numerical procedure and results

Common to all the problems in this chapter is the computation of a quantity related to global quantities for the particular problem.

Thus, for the scattering by a single line of barriers with gaps, we have

$$A = -i\alpha h(1 - R)/R, \tag{3.4.1}$$

and for the sloshing problem of a single vertical baffle with gaps

$$A^{(s)} = \frac{\alpha h \sin \alpha b \sin \alpha c}{\sin \alpha d}, \tag{3.4.2}$$

which determines the sloshing frequencies.

In both cases we have established upper and lower bounds, so that for example for A we have

$$\tilde{A}_u \leq A \leq \tilde{A}_p. \tag{3.4.3}$$

Only (3.4.1) translates into upper and lower bounds for $|R|$ (and as a consequence, for $|T|$) due to the complicated relation in (3.4.2). However we shall obtain such close bounds for $A^{(s)}$ that the resulting sloshing frequencies determined by (3.4.2) will be equally as close. It may be that for a particular set of parameters, bounds to $A^{(s)}$ are present, but in general these bounds will not occur.

The numerical procedure we use is common to all the problems considered. To fix ideas we illustrate in detail what is involved in the case of the single surface-piercing barrier. In order to solve for $\tilde{A}_u$, $\tilde{A}_p$ we must first compute K_{mn}, M_{mn} given by (3.2.43) and (3.2.52) for $m, n = 0, \ldots, N$. Each entry consists of an infinite sum which is evaluated by truncation. It is noted that, as in all the problems in this chapter, the infinite series decays like $\mathrm{O}\,(1/r^2)$ and thus many terms are needed to yield accurate entries for K_{mn}, M_{mn}. For a given truncation size M, say, it is possible to significantly increase the accuracy of these entries with little extra effort. Using the well-known fact $k_r h \sim r\pi$ as $r \to \infty$ and the asymptotic behaviour of $J_n(x)$ for large x it is readily shown that, as $r \to \infty$,

$$(\alpha_r h)^{-1} F_{mr} F_{nr} = \frac{2(-1)^{m+n}}{\pi^3(1-a/h)} s_r + \mathrm{O}(1/r^4), \tag{3.4.4}$$

and

$$\alpha_r h G_{mr} G_{nr} = \frac{2(-1)^{m+n}}{\pi^3 a/h} s_r + \mathrm{O}(1/r^4), \tag{3.4.5}$$

where

$$s_r = (1 - \sin 2r\pi a/h)/r^2. \tag{3.4.6}$$

So, in writing

$$K_{mn} = \sum_{r=1}^{M} (\alpha_r h)^{-1} F_{mr} F_{nr} + \frac{2(-1)^{m+n}}{\pi^3(1-a/h)} S, \tag{3.4.7}$$

$$M_{mn} = \sum_{r=1}^{M} \alpha_r h G_{mr} G_{nr} + \frac{2(-1)^{m+n}}{\pi^3 a/h} S, \tag{3.4.8}$$

with

$$S = \sum_{r=M+1}^{\infty} s_r, \tag{3.4.9}$$

we are including the leading order asymptotic behaviour of the original series and neglecting only terms of order $\mathrm{O}\,(1/M^4)$. This contrasts with a straightforward truncation of the series where $\mathrm{O}\,(1/M^2)$ terms are thrown away. We use 10^6 terms in the computation of S; this is a relatively quick calculation to perform due to the simplicity of s_r in (3.4.6). It is noted that S does not depend upon m, n, the wavenumber k, or the angle of incidence, θ, and thus needs only be calculated once for a particular geometry. A similar approach is used for all the problems considered in this and later chapters to improve the convergence of the infinite sums. The number of terms required to guarantee a given accuracy in the elements K_{mn} , M_{mn} varies with the geometry being considered. Thus, for typical geometries, not involving very small gaps or very small barriers where almost total reflection or total transmission occurs, the above procedure enables eight figure accuracy in K_{mn} , M_{mn} to be achieved with $M \simeq 500$ and the values obtained for $\tilde{A}_u$ and $\tilde{A}_p$ from solving (3.2.27) and (3.2.36) differ only in the seventh figure for $N \simeq 5$. Clearly, in order to claim a certain decimal place accuracy in $\tilde{A}_u$, $\tilde{A}_p$, then K_{mn} , M_{mn} must be accurate to *at least* as many decimal places. Apart from this very rough guide there appears to be no rule of thumb linking the choice of M to the choice of N or the accuracy of $\tilde{A}_u$, $\tilde{A}_p$. In the extreme cases mentioned above it is necessary to choose larger values of M and N for similar accuracy but it will turn out that in these cases one or other of the formulations, but not both, converges to the solution for values of N as low as 0 or 1 . Following extensive numerical experiments the values of $M = 500$, $N = 4$ were chosen to produce the graphs in all cases, it certainly not being possible to distinguish the curves derived from the two formulations and a value of $M = 2000$ was used in producing the numbers in the tables shown. For a discussion of the choice of N , M to ensure convergence of A in a related problem, see Wu [75].

Having determined K_{mn} , M_{mn} , for a given N , $\tilde{A}_u$ and $\tilde{A}_p$ are computed from (3.2.27) and (3.2.36). The results for the single surface-piercing barrier are summarised in table 3.1 which shows clearly the accuracy of the numerical method.

The table shows the values of $\tilde{A}_u$, $\tilde{A}_p$, respectively the lower and upper bounds on A when the barrier is submerged to depths $a/h = 0.1,\ 0.5,\ 0.9$ in normally-incident waves with non-dimensionalised wavenumber $ka = 0.5$ in each case. The truncation size, N , is increased from 0 (equivalent to a one-term variational approximation of the form given by (2.31)) until the discrepancy between the upper and lower bounds, $\tilde{A}_u$, $\tilde{A}_p$, is such that 7-figure accuracy is obtained in A . From

N	$a/h=0.1$		$a/h=0.5$		$a/h=0.9$	
	$\tilde{A}_u$ $(\leq A \leq)$ $\tilde{A}_p$		$\tilde{A}_u$ $(\leq A \leq)$ $\tilde{A}_p$		$\tilde{A}_u$ $(\leq A \leq)$ $\tilde{A}_p$	
0	2.551449	10.225129	2.6402985	2.6424255	0.7358405	0.7451010
1	10.020323	10.225129	2.6420460	2.6420502	0.7358405	0.7360358
2	10.223271	10.225129	2.6420501	2.6420502	0.7358405	0.7358475
3	10.224647	10.225129	2.6420501	2.6420502	0.7358405	0.7358407
4	10.225108	10.225129	2.6420501	2.6420502	0.7358405	0.7358405
5	10.225129	10.225129	2.6420501	2.6420502	0.7358405	0.7358405

Table 3.1: $\tilde{A}_u$, $\tilde{A}_p$ for a surface-piercing barrier with $ka = 0.5$, $\theta = 0$

N	$b/h=0.1$		$b/h=0.4$		$b/h=0.8$	
	$\tilde{A}_u$ $(\leq A \leq)$ $\tilde{A}_p$		$\tilde{A}_u$ $(\leq A \leq)$ $\tilde{A}_p$		$\tilde{A}_u$ $(\leq A \leq)$ $\tilde{A}_p$	
0	3.0956544	3.4337470	3.2771580	3.2804826	20.855972	31.981896
1	3.0956752	3.0999419	3.2798358	3.2798363	31.947507	31.981895
2	3.0956752	3.0957406	3.2798362	3.2798362	31.981683	31.981895
3	3.0956752	3.0956772	3.2798362	3.2798362	31.981894	31.981895
4	3.0956752	3.0956752	3.2798362	3.2798362	31.981895	31.981895

Table 3.2: $\tilde{A}_u$, $\tilde{A}_p$ for a bottom-mounted barrier with $kb = 0.2$, $\theta = 0$

(3.2.20), (3.2.21) this translates into complementary bounds on the reflection and transmission coefficients with the same order of accuracy in them.

It is clear from the table that $N = 5$ is sufficient to determine A to 7 significant figures at this typical wavelength for both a short barrier $(a/h = 0.1)$ or for a small gap beneath the barrier $(a/h = 0.9)$ and indeed $N = 1$, corresponding to a 2×2 system, is sufficient to give 1% accuracy in all cases. Even more remarkable is the accuracy of the one-term ($N = 0$) approximation to $\tilde{A}_u$ in the velocity formulation in the case of a small gap or the one-term approximation to $\tilde{A}_p$ in the pressure difference formulation in the case of a small barrier. This can be explained as follows. In the case of a small gap, the fluid motion is determined by a rapid flow close to the edge of the barrier which is well modelled by the square-root singularity in $u_0(y)$. Equally, in the case of a small barrier the pressure difference is dominated by its behaviour at either end, which is again correctly modelled by the choice of $p_0(y)$. Similar accuracy is achieved for $\theta \neq 0$, or obliquely-incident waves.

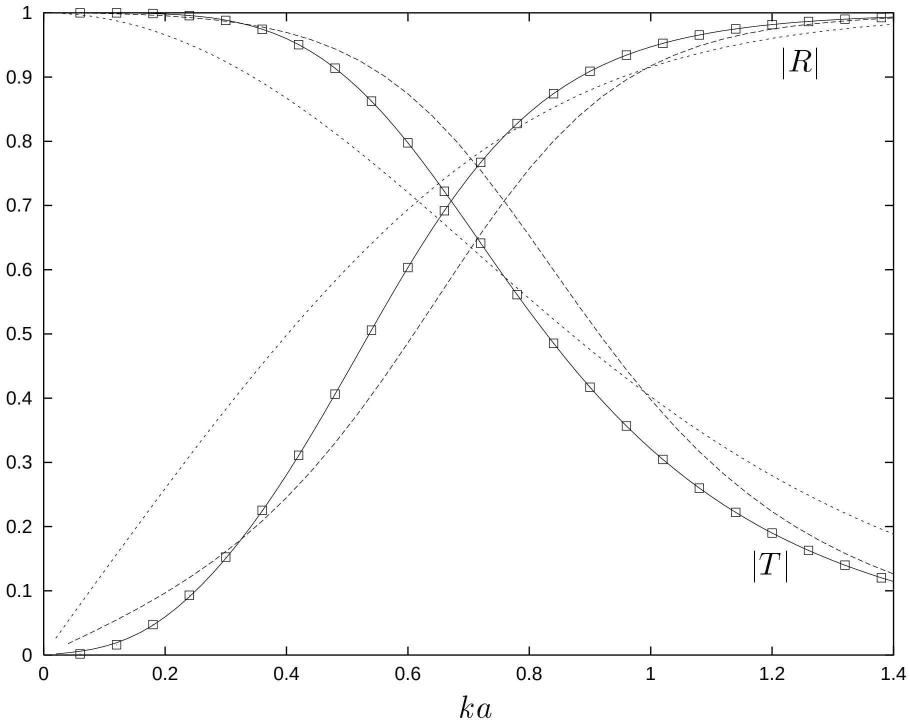

Figure 3.2: $|R|$, $|T|$ for a surface-piercing barrier in normally-incident waves: $a/h = 0.1$ (——), 0.5 (– – –), 0.9 (- - - -), infinite depth( ).

The only changes required for the bottom-mounted barrier is in the use of (3.2.57), (3.2.58) and (3.2.62), (3.2.63) for F_{mn} and G_{mn} in (3.2.24) and (3.2.37). Thus table 3.2 illustrates, for $\theta = 0$, the accuracy of the method for different gap ratios b/h above the barrier each at non-dimensionalised wavenumber $kb = 0.2$. Here $N = 4$ is sufficient to achieve 7-figure accuracy and again we see the power of a one-term approximation to $\tilde{A}_u$ in the velocity approximation in the case of small gaps ($b/h = 0.1$) and a one-term approximation to $\tilde{A}_p$ in the pressure difference formulation in the case of small barriers ($b/h = 0.8$)

The results shown in tables 3.1 and 3.2 were chosen to correspond to representative values of barrier geometry and incident wavenumber. Other values of wavenumber produce equally-accurate results for A and hence R or T and the results are illustrated in figs. 3.2 and 3.3. Figure 3.2 shows the variation of $|R|$ and $|T|$ with non-dimensionalised wavenumber ka in the case of the scattering of a normally-incident wave by a surface-piercing barrier of length a in water depth h. For long waves, corresponding to low wavenumbers, the potential behaves like a uniform horizontal flow far from the barrier and so all the wave energy is transmitted through the gap in the barrier. For short waves, or large wavenumbers, most of the wave energy is located near the free surface so that a large proportion of the wave energy is reflected by the barrier and only a small amount will 'leak' under the barrier. The exact results for the scattering by a barrier in infinite depth due to Ursell [72] are also shown in figure 3.2. It can be seen that a barrier submerged to approximately one tenth of the water depth can effectively be regarded as being in infinite depth water at all wavenumbers.

The results for the scattering of a normally-incident wave by a bottom-mounted barrier extending from the bottom to a point b beneath the free surface in water of depth h are shown in figure 3.3 where curves of $|R|$ and $|T|$ are drawn against dimensionless wavenumber kb. For kb small, as for the surface-piercing barrier the same arguments show that near total transmission occurs, but in this case in the limit of short waves, or kb large, the waves are confined to the surface and again most of the energy is transmitted. Thus for a given b/h there exists a unique value of kb at which $|T|$ is a minimum and $|R|$ is a maximum. This contrasts with the special case of a submerged barrier in infinitely deep water solved exactly by Dean [8]. In this case very long waves are confronted with a very long barrier and total reflection occurs in the limit $kb \to 0$. This difference in behaviour for long waves means that for a barrier occupying almost all the depth, i.e. $b/h = 0.1$, then good agreement with the infinite depth result only occurs for $kb > 0.5$.

The effect on $|R|$, $|T|$ of varying the angle of incidence is shown for the surface-piercing barrier in figure 3.4 and for the bottom-mounted barrier in figure 3.5. In each case $|R|$ and $|T|$ decrease and increase monotonically (respectively) with increasing incidence angle, θ.

For a barrier with a single gap the changes necessary in the velocity formulation are slight, involving the use of (3.2.66) for F_{mn}, whence $\tilde{A}_u$ is found from (3.2.27) with K_{mn} defined by (3.2.24). The pressure formulation necessitates the compu-

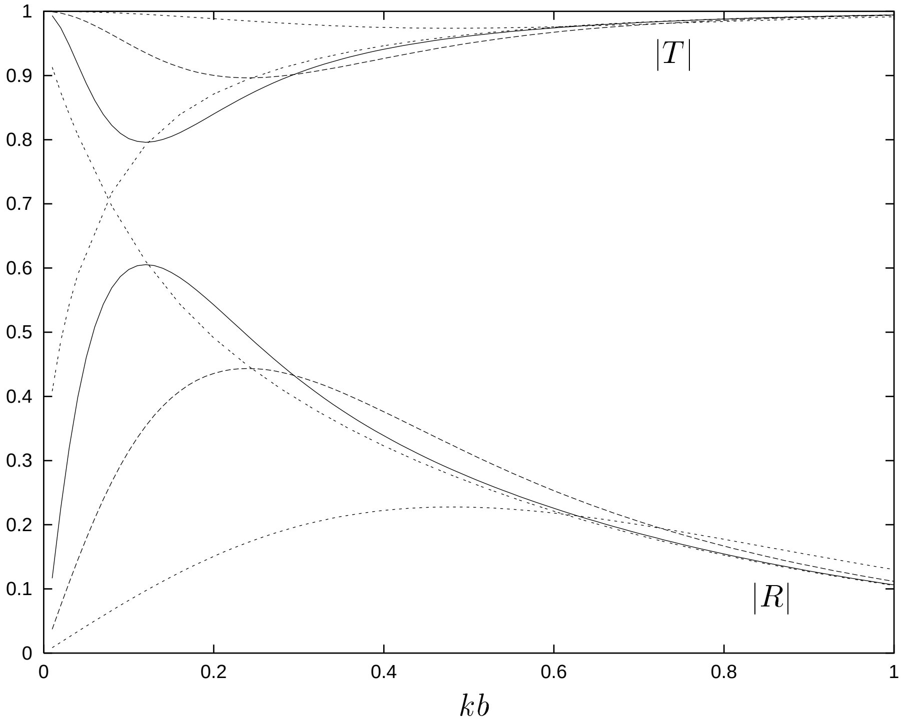

Figure 3.3: $|R|$, $|T|$ for a bottom-mounted barrier in normally-incident waves: $b/h = 0.1$ (——), 0.2 (– – –), 0.4 (- - - -), infinite depth(-- -).

tation of the slightly more complicated block matrix system (3.2.79), in obtaining $\tilde{A}_p$, but by virtue of it being a Galerkin method, this still gives an upper bound on A. The accuracy of the method is maintained and again a truncation of $N = 5$ is sufficient to assure 7-figure agreement between $\tilde{A}_u$ and $\tilde{A}_p$. The same is true for the problem of the totally-submerged barrier where G_{mn} is given by (3.2.81) and where it is the velocity formulation in which $\tilde{A}_u$ requires the solution of the block system (3.2.92). There seems little merit in presenting detailed tables of the $\tilde{A}_u$ and $\tilde{A}_p$ but it is worth emphasizing that, for small gaps and small barriers, the one-term approximations $u(y) = u_0(y)$ and $p(y) = p_0(y)$ respectively provide extremely accurate values for R and T.

The variation of $|R|$, $|T|$ with dimensionless wavenumber for a barrier with a gap in normally-incident waves $(\theta = 0)$ is shown in figure 3.6. Here the upper part of the barrier occupies $(0, a)$, the lower part (b, h) so that the centre of the gap is at depth $c = \frac{1}{2}(a + b)$ and the size of the gap is $2d = (b - a)$. Curves for various d/c are shown with fixed $c/h = 0.1$. As might be expected the curves of $|R|$,

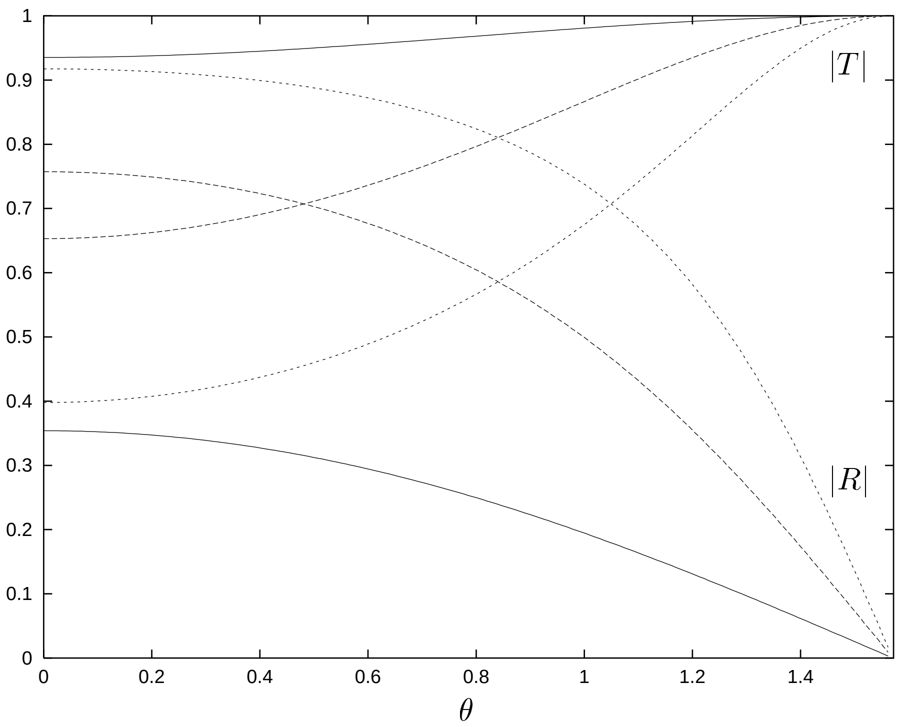

Figure 3.4: $|R|$, $|T|$ against θ for a surface-piercing barrier with $a/h = 0.5$ in obliquely-incident waves: $ka = 0.5$ (——), 0.8 (– – –), 1.0 (- - - -).

$|T|$ are now more complicated, manifesting behaviour of both bottom-mounted and surface-piercing barriers. For example, in very long waves, $kc \ll 1$, all the energy is transmitted and in very short waves, kc large, all the energy is reflected as for the surface barrier but in passing from long to short waves $|R|$ first reaches a maximum, as for the bottom-mounted barrier and then at shorter waves a minimum, before tending monotonically to unity as $kc \to \infty$.

Figure 3.7 shows the behaviour of $|R|$, $|T|$ for a totally-submerged barrier of length $2d$, centre at depth c with varying kc and fixed $c/h = 0.1$. The curves are less interesting than the gap case, with $|R| \to 0$ for both large and small kc as might be expected on physical grounds. Once again in each case the effect of increasing θ is to reduce $|R|$ and increase $|T|$.

These problems may be approached differently by using the process of matching the eigenfunctions to yield an infinite systems of equations that are truncated to a size N, say, for the solution to the problem (explained in detail in chapter 2). This requires the the inversion of an $N \times N$ complex-valued unsymmetric matrix where

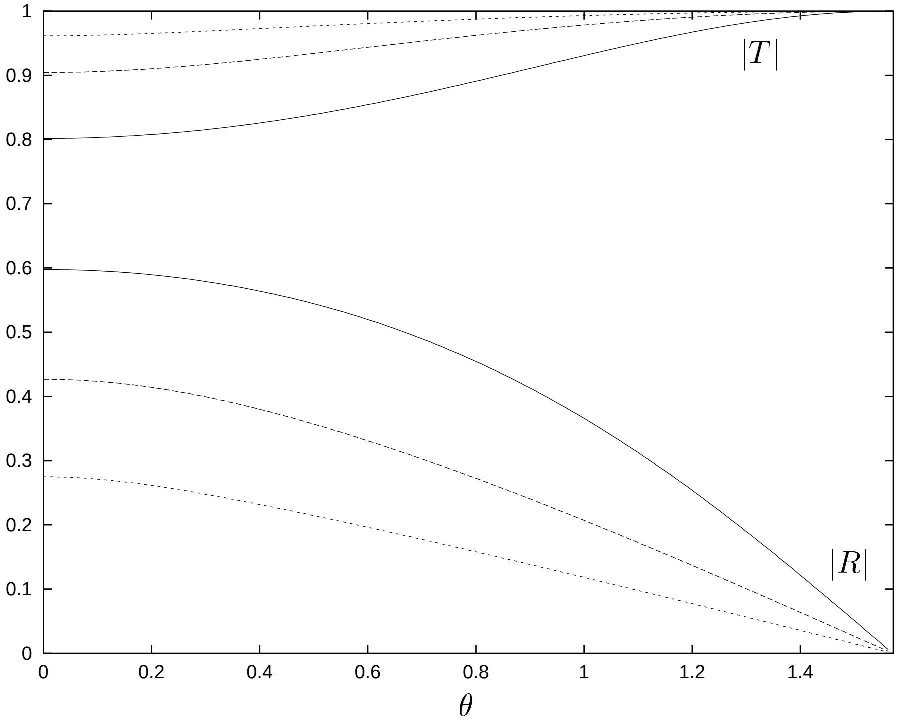

Figure 3.5: $|R|$, $|T|$ against θ for an bottom-standing barrier with $b/h = 0.1$ in obliquely-incident waves: $kb = 0.1$ (——), 0.3 (– – –), 0.5 (- - - -).

N is usually $O(100)$. Smith [68] used this approach for the surface-piercing barrier problem. Table 3.3 shows the successive estimates for $|R|$, $|T|$ with increasing N and compares with the results found from the method of §3.2 for which the heading 'Exact' means exact to the five decimal places shown (the error between the upper and lower bounds being less than 10^{-6}). These are typical results and do not highlight the worst possible cases, but are presented to illustrate the fact that whilst being accurate enough to provide qualitative behaviour they cannot be relied upon for more than two decimal place accuracy.

In order to improve the accuracy of numerical results, some authors have used the so-called method of linear extrapolation, in which $|R|$ is plotted against $1/N$ at a small number of sample points and then extrapolated back to $1/N = 0$. However, the final two columns show how convergence of $|R|$, $|T|$ cannot possibly be monotonic with increasing N and hence how linear extrapolation is an unreliable process that has no mathematical basis and should be used with extreme care. Indeed, linear extrapolation stands more chance of succeeding for the method we have

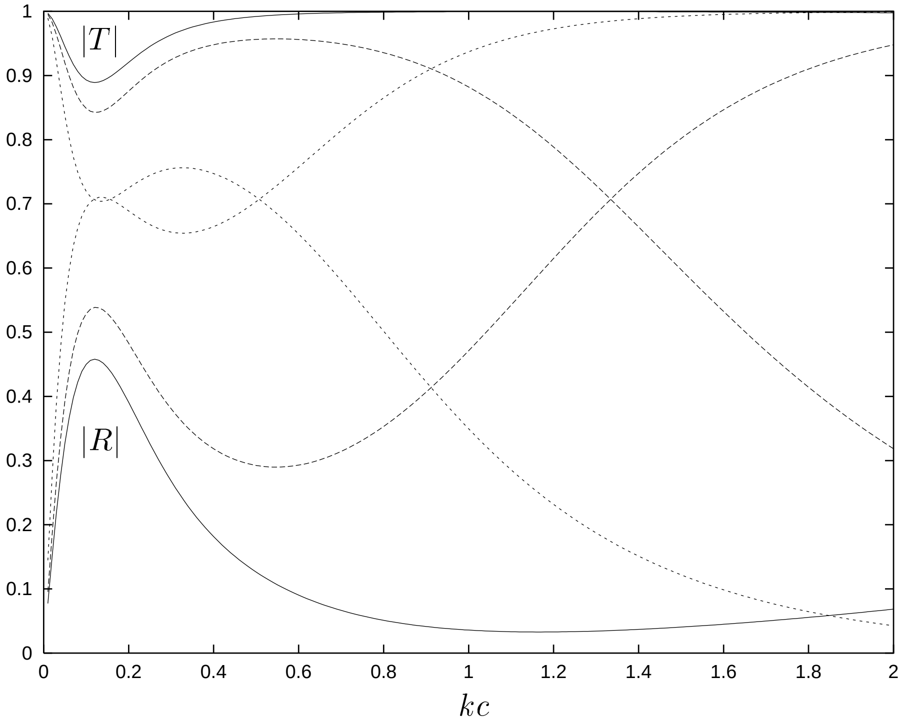

Figure 3.6: $|R|$, $|T|$ for a barrier with a gap with $c/h = 0.1$ in normally-incident waves: $d/c = 0.9$ (——), 0.5 (– – –), 0.1 (- - - -).

chosen to use in this chapter, where it has been proven that a quantity A is bounded above (or below) and that increases in the dimension of the trial space, N, for the Galerkin scheme ensures a better estimate to A.

The final example involves the sloshing of a liquid in a rectangular tank containing a baffle. The elements $K_{mn}^{(s)}$, $M_{mn}^{(s)}$ are now given by (3.3.10) and (3.3.12) and the sloshing frequencies occur at values of αd such that

$$h(\alpha d) = A^{(s)} - \frac{\alpha h \sin \alpha b \sin \alpha c}{\sin \alpha d} = 0. \tag{3.4.10}$$

	$b/h = 0.5,\ Kb = 0.5$		$b/h = 0.5,\ Kb = 0.05$		$b/h = 0.1,\ Kb = 0.1$	
N	$\lvert R\rvert$	$\lvert T\rvert$	$\lvert R\rvert$	$\lvert T\rvert$	$\lvert R\rvert$	$\lvert T\rvert$
100	0.15782	0.98747	0.07006	0.99754	0.61874	0.78560
200	0.15580	0.98779	0.06912	0.99761	0.61282	0.79022
300	0.15506	0.98791	0.06877	0.99763	0.61056	0.79197
400	0.15476	0.98797	0.06859	0.99764	0.60939	0.79287
Exact	0.15332	0.98818	0.06796	0.99768	0.61041	0.79209

Table 3.3: $|R|$, $|T|$ against increasing truncation size N using the method of matched eigenfunction expansions for a bottom-mounted barrier.

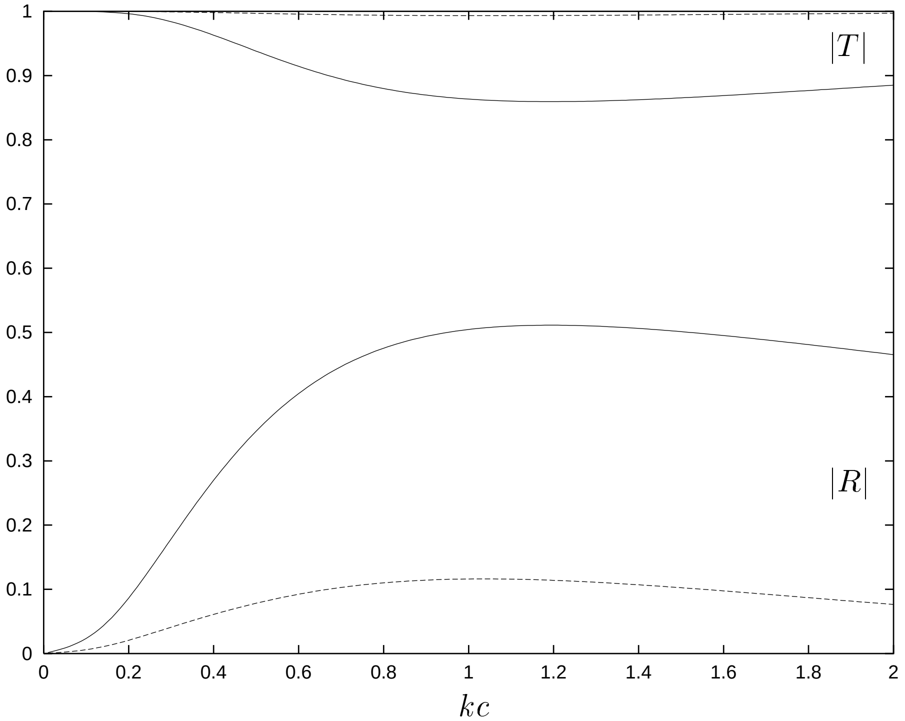

Figure 3.7: $|R|$, $|T|$ for a totally-submerged barrier with $c/h = 0.1$ in normally-incident waves: $d/c = 0.9$ (——-), 0.5 (- - - -).

Hence, a root-finding procedure must be applied to the function $h(\alpha d)$ with $\tilde{A}_u^{(s)}$ and $\tilde{A}_p^{(s)}$ in turn approximating $A^{(s)}$ in (3.4.10) to provide two approximations, associated with the velocity and the pressure difference formulations respectively, to the exact sloshing frequency. The increasing accuracy of the approximations $\tilde{A}_u^{(s)}$, $\tilde{A}_p^{(s)}$ to $A^{(s)}$ as the truncation size, N, is increased is reflected in the accuracy of the estimates to the sloshing frequencies as shown in table 3.4. Here we have examined the fundamental sloshing frequencies when the baffle is surface-piercing and close to one wall ($b/d = 0.05$, $a/h = 0.4$, $h/d = 1.0$ and no cross-tank modes ($m = 0$)). Again 6-figure accuracy is obtained for $N = 4$ in this fairly extreme case. The same is true for other configurations and for totally-submerged baffles. In all cases tested it was sufficient to choose $N = 5$ to achieve 6-figure accuracy to the sloshing frequencies given by the roots of (3.4.10).

	αd	
N	velocity	pressure
0	1.94095	2.21975
1	2.17605	2.19243
2	2.19146	2.19232
3	2.19230	2.19232
4	2.19232	2.19232

Table 3.4: Approximations to the fundamental sloshing frequencies for a surface-piercing baffle in a rectangular tank using a velocity and a pressure difference method with $a/h = 0.4$, $b/d = 0.05$, $h/d = 1.0$.

3.5 Remarks

The method of solution for the four specific barrier configurations shown in figure 3.1 were considered, and though not shown here it is possible to generalise the method to the case of an arbitrary number of barriers with gaps in a vertical plane in finite depth water, requiring a similar approach as for the two gaps in the totally submerged barrier or the two barrier segments in the case of the barrier with a submerged gap.

Chapter 4

Wave scattering by two unequal vertical barriers

4.1 Introduction

The extension of the single line of barriers with gaps of the previous chapter to two vertical planes containing barriers with gaps is considered in this chapter.

Much of the attention concerning two-barrier systems has, in the past, been concentrated on equal barrier schemes. This is because the symmetry in the geometry permits the decomposition of the total potential into symmetric and antisymmetric potentials, each of which need only be considered in a semi-infinite domain by imposing Neumann and Dirichlet conditions respectively on the line of symmetry. Thus the two-equal-barrier problem can be separated into two simpler problems involving just a single barrier with an extra boundary condition.

Levine & Rodemich [41] first studied the case of two parallel identical surface-piercing barriers in infinite depth water when the motion is two dimensional, using complex function theory and showed that an analytic solution was possible without actually providing details. Jarvis [32] later solved the complementary problem of two parallel barriers both extending indefinitely downwards from a point a below the free surface in the same analytic manner and computed results showing that for certain barrier separations and wave frequencies, zeros of reflection existed.

Using complementary formulations for both the velocity under the barriers and the pressure difference across the barriers, Evans & Morris [20] showed the existence of zeros of transmission for the two identical barrier arrangement of Levine & Rodemich [41]. This was the first instance in which two partially- or wholly-immersed bodies had been shown to reflect all the wave energy. Previously, it was a well-known fact that two bodies under certain circumstances could be capable of exhibiting total transmission, a somewhat surprising phenomemon in itself. Thus Newman [56] showed, using wide-spacing arguments, that total transmission for a two-body system was possible if the moduli of the reflection coefficients associated with two bodies are equal for some wave frequency. This is an important point and will be referred to later.

The existence of zeros of transmission and reflection for the two identical surface-piercing barriers in infinite depth was confirmed by Newman [58] who used a matched asymptotic approach for the case when the two barriers are closely spaced. The principle behind the method used is as follows. From a distance the two barriers appear as a single barrier with a pulsating source at its lowermost point due to the presence of the incident wave. This solution to this problem constitutes the so-called 'outer solution'. Close to the ends of the two barriers, the free surface appears to have a negligible effect and once the time dependence has been removed, this inner problem resembles the potential flow between two semi-infinite parallel thin plates. After satisfying the free-surface condition between the barriers an asymptotic matching of the outer solution as the source point at the barrier tip is approached with the outer limit of the inner solution finally gives the approximate solution to the whole problem.

The matched asymptotic method had first been used in the context of linear water waves by Tuck [70] although the basic ideas for this approach had been proposed by Rayleigh as far back as 1897 in work on the diffraction of sound waves through small apertures. Tuck [70] derived expressions for R and T when a plane wave is incident on a thin vertical wall with a small gap below the free surface in a fluid of infinite depth. Subsequently the method was applied to more complex geometries and problems. See, for example, Guiney *et al.* [30], Packham & Williams [60], Tuck [71], Evans [11], [13], the latter author considering the transmission through two or more thin vertical barriers each containing a small gap.

McIver [46] used a similar technique to that of Newman [58] by considering two closely-spaced barriers both extending downwards to points near the sea bed and showed that zeros of reflection are no longer possible if the barriers are unequal. The main purpose of the paper of McIver [46] was to confirm the existence of, and locate, zeros of transmission for the scattering of waves normally incident on two surface-piercing barriers in the case of finite depth water. Thus, results are given showing a discrete infinite sequence of zeros of transmission and reflection each associated with the natural modes of oscillation of the fluid between the two barriers. He decomposed the potential into symmetric and antisymmetric parts and solved the two resulting boundary-value problems using a method of matching eigenfunction expansions to obtain infinite systems of equations which are solved by truncation. The convergence of this system with increasing truncation size are poor due to the singularities at the edges of the barriers, requiring the solution of a 400×400 system to obtain results with small errors in the third decimal place.

For unequal barriers in infinite depth water, Morris [55] used complementary formulations in terms of the velocities across the gaps and the pressure differences across the barriers. The particular configuration considered consisted of one surface-piercing and one semi-infinite submerged barrier. A variational approximation is made to both the resulting coupled integral equations using the exact expressions of Ursell [72] and Dean [8] for the velocity across the gaps and the pressure difference across the barriers. Unlike the two equal surface-piercing barriers treated in a similar manner previously by Evans & Morris [20], the kernels of the integral equations for this problem are unsymmetric and there is no guarantee that the two approximations will give bounds for the exact solution. Nevertheless, Morris [55] uses an asymptotic approach to show that in theory there should exist an infinite sequence of discrete wave frequencies for which total reflection occurs only if the barriers overlap and suggests that the same is true of the phenomenon of total transmission.

In this chapter, we follow the approach of Morris [55] in the case of oblique incidence and finite water depth and formulate the problem, without specifying the barrier configuration in advance, in terms of unknown velocities and pressure differences at the two barrier interfaces. Each of these functions satisfies a coupled system of integral equations which we choose to write as a single vector integral equation. The reflection and transmission coefficients are found using a scattering matrix approach similar to that used by Miles [52], that relies on the knowledge of a 2×2 matrix $\mathbf{S}$ consisting of integral properties of the velocity related functions or alternatively a matrix $\mathbf{T}$ with entries defined as integral properties of the pressure difference functions. By applying Galerkin's method to the integral equations with the appropriate approximations already derived in chapter 3, we show how very accurate and efficient estimates to $|R|$, $|T|$ can be obtained using very few terms in the Galerkin expansion. For the same reasons as Morris [55], we cannot predict upper and lower bounds, but the agreement between results arising from the two formulations give a strong indication of their accuracy. The special case of two equal barriers is considered in §4.3, where it is shown that decoupling of the integral equations results in a system that is equivalent to decomposing the potential into symmetric and antisymmetric parts at the outset. Decoupling of the integral equations can also occur in the limit of barrier separation tending to infinity. This is shown in §4.4 to be equivalent to invoking the well-known wide-spacing approximation.

Finally, we consider a close-spacing approximation based on an upward facing/ downward facing overlapping barrier scheme using the matched asymptotic approach described earlier in this Introduction.

Results are given for various different barrier configurations in the final section, showing good accuracy with very few terms in the Galerkin expansion as in the single barrier problems of the previous chapter. Particular attention is paid to the barrier arrangements giving rise to zeros of transmission and/or reflection. Also shown are comparisons with the wide-spacing and close-spacing approximations.

4.2 Formulation and solution

Cartesian coordinates are chosen with the origin in the mean free surface of the fluid and the sea bed at $y = h$ and the geometry is uniform in the z-coordinate. For simplicity we restrict ourselves to a single barrier with a single gap on $x = b$ and on $x = -b$ denoting the interval of the depth occupied by the barriers on $x = -b$ ($+b$) by $L_b^{(1)}$ ($L_b^{(2)}$) and the interval of the depth occupied by the gap on $x = -b$ ($+b$) by $L_g^{(1)}$ ($L_g^{(2)}$). There is no inherent difficulty in extending what follows to multiple gaps or barriers on $x = \mp b$.

The incident wave of frequency $\omega/2\pi$ makes an angle θ with the plane $z = 0$ so that the potential may be expressed by (3.2.1) and then the governing equations for $\phi(x, y)$ are (3.2.2)–(3.2.6) with (3.2.4) replaced by

$$\phi_x = 0, \quad (x, y) \in L_b^{(1),(2)} \tag{4.2.1}$$

and (3.2.6) becomes

$$\phi, \phi_x \text{ continuous for } (x, y) \in L_g^{(1),(2)}\,. \tag{4.2.2}$$

The fluid domain is divided into the three regions shown in figure 4.1. Thus I, II and III denote the regions $x \leq -b$, $-b \leq x \leq b$ and $x \geq b$ respectively. We choose a general far-field behaviour and leave the consideration of the special cases of waves incident from either infinity to the end. In this way, our approach follows closely that of Morris [55].

The potential is divided up into the three regions and we use the same notation as for the single barrier in §3.2. In region I we write

$$\phi(x, y) = (A_1 \mathrm{e}^{i\alpha(x+b)} + B_1 \mathrm{e}^{-i\alpha(x+b)})\psi_0(y) + \sum_{n=1}^{\infty} \frac{U_n^{(1)} \mathrm{e}^{\alpha_n(x+b)}}{\alpha_n} \psi_n(y), \tag{4.2.3}$$

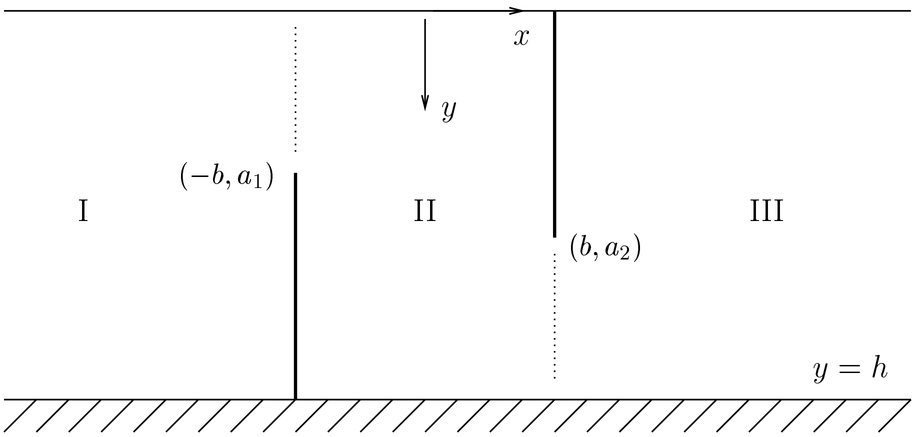

Figure 4.1: Two unequal barriers in finite water depth, h.

in II,

$$\phi(x,y) = (A_{12}\mathrm{e}^{i\alpha x} + B_{12}\mathrm{e}^{-i\alpha x})\psi_0(y) + \sum_{n=1}^{\infty} \frac{(u_n \mathrm{e}^{\alpha_n x} + v_n \mathrm{e}^{-\alpha_n x})}{\alpha_n}\psi_n(y), \qquad (4.2.4)$$

and in III

$$\phi(x,y) = -(A_2\mathrm{e}^{-i\alpha(x-b)} + B_2\mathrm{e}^{i\alpha(x-b)})\psi_0(y) - \sum_{n=1}^{\infty} \frac{U_n^{(2)}\mathrm{e}^{-\alpha_n(x-b)}}{\alpha_n}\psi_n(y). \qquad (4.2.5)$$

If we denote by R_+ (R_-) and T_+ (T_-) the reflection coefficients for waves incident from $x > 0$ (< 0) then we have

$$R_+ = B_2\mathrm{e}^{-2i\alpha b}/A_2, \quad T_+ = -B_1\mathrm{e}^{-2i\alpha b}/A_2, \quad A_1 = 0 \qquad (4.2.6)$$

$$\text{and} \quad R_- = B_1\mathrm{e}^{-2i\alpha b}/A_1, \quad T_- = -B_2\mathrm{e}^{-2i\alpha b}/A_1, \quad A_2 = 0 \qquad (4.2.7)$$

which may be written as

$$\begin{pmatrix} B_1 \\ B_2 \end{pmatrix} = \begin{pmatrix} R_- & -T_+ \\ -T_- & R_+ \end{pmatrix} \begin{pmatrix} A_1 \\ A_2 \end{pmatrix} \mathrm{e}^{2i\alpha b}. \qquad (4.2.8)$$

Recently, Porter & Chamberlain [64] have shown that by expressing the problem in terms of a scattering matrix, relating the outgoing and incoming amplitudes as above, the well-known relations between the scattering coefficients are in fact satisfied identically. The formulation we will adopt here does indeed construct a solution in terms of a scattering matrix.

Let the components of velocity in the x-direction at $x=-b$ $(+b)$ be given by $U^{(1)}(y)$ $(U^{(2)}(y))$. Then from (4.2.3), (4.2.4)

$$U^{(1)}(y) = i\alpha(A_1 - B_1)\psi_0(y) + \sum_{n=1}^{\infty} U_n^{(1)}\psi_n(y) \tag{4.2.9}$$

$$= i\alpha(A_{12}\mathrm{e}^{-i\alpha b} - B_{12}\mathrm{e}^{i\alpha b})\psi_0(y) + \sum_{n=1}^{\infty}(u_n\mathrm{e}^{-\alpha_n b} - v_n\mathrm{e}^{\alpha_n b})\psi_n(y), \tag{4.2.10}$$

whilst from (4.2.4), (4.2.5)

$$U^{(2)}(y) = i\alpha(A_{12}\mathrm{e}^{i\alpha b} - B_{12}\mathrm{e}^{-i\alpha b})\psi_0(y) + \sum_{n=1}^{\infty}(u_n\mathrm{e}^{\alpha_n b} - v_n\mathrm{e}^{-\alpha_n b})\psi_n(y) \tag{4.2.11}$$

$$= i\alpha(A_2 - B_2)\psi_0(y) + \sum_{n=1}^{\infty} U_n^{(2)}\psi_n(y). \tag{4.2.12}$$

Multiplying by $\psi_0(y)$ and integrating over $[0,h]$ gives

$$A_{12}\mathrm{e}^{-i\alpha b} - B_{12}\mathrm{e}^{i\alpha b} = A_1 - B_1$$

$$A_{12}\mathrm{e}^{i\alpha b} - B_{12}\mathrm{e}^{-i\alpha b} = A_2 - B_2,$$

whence

$$\begin{aligned} A_{12} &= \tfrac{1}{2}i\mathrm{cosec}\,2\alpha b\left\{(A_1 - B_1)\mathrm{e}^{-i\alpha b} - (A_2 - B_2)\mathrm{e}^{i\alpha b}\right\} \\ B_{12} &= \tfrac{1}{2}i\mathrm{cosec}\,2\alpha b\left\{(A_1 - B_1)\mathrm{e}^{i\alpha b} - (A_2 - B_2)\mathrm{e}^{-i\alpha b}\right\}. \end{aligned} \tag{4.2.13}$$

Similarly, we are able to use the orthogonality of the $\psi_n(y)$'s to express the coefficients u_n, v_n in terms of $U_n^{(1)}$, $U_n^{(2)}$

$$\begin{aligned} u_n &= \frac{U_n^{(2)}\mathrm{e}^{\alpha_n b} - U_n^{(1)}\mathrm{e}^{-\alpha_n b}}{2\sinh 2\alpha_n b} \\ v_n &= \frac{U_n^{(2)}\mathrm{e}^{-\alpha_n b} - U_n^{(1)}\mathrm{e}^{\alpha_n b}}{2\sinh 2\alpha_n b}. \end{aligned} \tag{4.2.14}$$

Thus, the potential in region II can be expressed solely in terms of the solution to the potential in the two outer regions. Also

$$i\alpha(A_i - B_i) = \frac{1}{h}\int_{L_g^{(i)}} U^{(i)}(y)\psi_0(y)\,\mathrm{d}y = U_0^{(i)}, \quad i = 1,2 \tag{4.2.15}$$

and

$$U_n^{(i)} = \frac{1}{h}\int_{L_g^{(i)}} U^{(i)}(y)\psi_n(y)\,\mathrm{d}y, \quad n \geq 1, \quad i = 1,2, \tag{4.2.16}$$

where we have used (4.2.1). With these definitions we have

$$U^{(i)}(y) = \sum_{n=0}^{\infty} U_n^{(i)} \psi_n(y), \quad i = 1, 2. \tag{4.2.17}$$

Defining $P^{(1)}(y)$ ($P^{(2)}(y)$) to be the jump in potential across the interface at $x = -b$ ($+b$) gives us after use of (4.2.13), (4.2.14)

$$P^{(i)}(y) = i\mathrm{cosec}\, 2\alpha b \left\{ A_i \mathrm{e}^{2i\alpha b} - B_i \mathrm{e}^{-2i\alpha b} - A_{3-i} + B_{3-i} \right\} \psi_0(y)$$
$$- \sum_{n=1}^{\infty} \frac{U_n^{(i)}(1 + \coth 2\alpha_n b)}{\alpha_n} \psi_n(y) + \sum_{n=1}^{\infty} \frac{U_n^{(3-i)} \mathrm{cosech}\, 2\alpha_n b}{\alpha_n} \psi_n(y), \quad i = 1, 2, \tag{4.2.18}$$

where the equations for $P^{(1)}(y)$, $P^{(2)}(y)$ have been combined for compactness, the purpose of the $3 - i$ being to give an entry of 2 for $i = 1$ and vice versa.

The requirement that the pressure be continuous across the gaps at $x = \mp b$ gives us $P^{(i)}(y) = 0$ for $y \in L_g^{(i)}$, $i = 1, 2$ respectively. Using this in (4.2.18) after substitution of $U_n^{(i)}$ from (4.2.16) yields the following coupled system of integral equations for the unknowns $U^{(i)}(y)$.

$$\int_{L_g^{(i)}} U^{(i)}(t) K^{(1)}(y,t)\, \mathrm{d}t - \int_{L_g^{(3-i)}} U^{(3-i)}(t) K^{(2)}(y,t)\, \mathrm{d}t$$
$$= i\mathrm{cosec}\, 2\alpha b \left\{ A_i \mathrm{e}^{2i\alpha b} - B_i \mathrm{e}^{-2i\alpha b} - A_{3-i} + B_{3-i} \right\} \psi_0(y), \quad y \in L_g^{(i)}, \tag{4.2.19}$$

$i = 1, 2$, where the kernels $K^{(1)}(y,t)$ and $K^{(2)}(y,t)$ are given by

$$K^{(1)}(y,t) = \sum_{n=1}^{\infty} \frac{(1 + \coth 2\alpha_n b)}{\alpha_n h} \psi_n(y) \psi_n(t) \tag{4.2.20}$$

and

$$K^{(2)}(y,t) = \sum_{n=1}^{\infty} \frac{\mathrm{cosech}\, 2\alpha_n b}{\alpha_n h} \psi_n(y) \psi_n(t). \tag{4.2.21}$$

We note that the two equations given by choosing $i = 1, 2$ in (4.2.19) are valid over different intervals. We would like to be able to combine them into a single vector equation, and in order to do this we follow the method of Morris [55] by introducing the unit step functions

$$H_i(y) = \begin{cases} 1, & y \in L_g^{(i)} \\ 0, & y \in L_b^{(i)} \end{cases} \quad i = 1, 2. \tag{4.2.22}$$

Since $U^{(i)}(y)$ is zero on $L_b^{(i)}$ for $i = 1, 2$ (the barriers at $x = \mp b$ respectively) we can write $U^{(i)}(y) = H_i(y)U^{(i)}(y)$ for $y \in L = [0, h]$. Hence, the two coupled equations can be combined, both now being valid over the interval L by writing

$$\int_L H_i(y)\left[K^{(1)}(y,t)H_i(t)U^{(i)}(y) - K^{(2)}(y,t)H_{3-i}(t)U^{(3-i)}(t)\right]\,\mathrm{d}t$$
$$= i\mathrm{cosec}\,2\alpha b\left\{A_i\mathrm{e}^{2i\alpha b} - B_i\mathrm{e}^{-2i\alpha b} - A_{3-i} + B_{3-i}\right\}H_i(y)\psi_0(y), \quad y \in L. \tag{4.2.23}$$

These two equations ($i = 1, 2$) can now be combined using a convenient matrix notation as follows

$$\int_L \mathbf{H}(y)\mathbf{K}(y,t)\mathbf{H}(t)\mathbf{U}(t)\,\mathrm{d}t = i\mathrm{cosec}\,2\alpha b\,\mathbf{H}(y)(\mathbf{DA} - \overline{\mathbf{D}}\mathbf{B})\psi_0(y), \quad y \in L \tag{4.2.24}$$

where we have defined matrices $\mathbf{H}(y) = \mathrm{diag}\{H_i(y)\}_{i=1,2}$,

$$\mathbf{K}(y,t) = \begin{pmatrix} K^{(1)}(y,t) & -K^{(2)}(y,t) \\ -K^{(2)}(y,t) & K^{(1)}(y,t) \end{pmatrix}, \quad \mathbf{D} = \begin{pmatrix} \mathrm{e}^{2i\alpha b} & -1 \\ -1 & \mathrm{e}^{2i\alpha b} \end{pmatrix}$$

and vectors $\mathbf{U}(y) = (U_1(y), U_2(y))^{\mathrm{T}}$, $\mathbf{A} = (A_1, A_2)^{\mathrm{T}}$, $\mathbf{B} = (B_1, B_2)^{\mathrm{T}}$. The bar denotes complex conjugate. Now let the 2×2 matrix $\mathbf{u}(y) = \{u_{mn}(y)\}$ be the solution of

$$\int_L \mathbf{H}(y)\mathbf{K}(y,t)\mathbf{H}(t)\mathbf{u}(t)\,\mathrm{d}t = \mathbf{H}(y)\psi_0(y), \quad y \in L. \tag{4.2.25}$$

Then

$$\mathbf{U}(y) = i\mathrm{cosec}\,2\alpha b\,\mathbf{u}(y)(\mathbf{DA} - \overline{\mathbf{D}}\mathbf{B}) \tag{4.2.26}$$

will satisfy (4.2.24). We may also write (4.2.15) in matrix form by first using the definition of the step functions to unify the interval of integration

$$i\alpha h(\mathbf{A} - \mathbf{B}) = \int_L \mathbf{H}(y)\mathbf{U}(y)\psi_0(y)\,\mathrm{d}y, \tag{4.2.27}$$

and use of (4.2.26) in the above gives

$$\alpha h \sin 2\alpha b\,(\mathbf{A} - \mathbf{B}) = \mathbf{S}(\mathbf{DA} - \overline{\mathbf{D}}\mathbf{B}), \tag{4.2.28}$$

where the 2×2 matrix $\mathbf{S} = \{S_{mn}\}$ is defined by

$$\mathbf{S} = \int_L \mathbf{H}(y)\mathbf{u}(y)\psi_0(y)\,\mathrm{d}y. \tag{4.2.29}$$

Rearrangement of (4.2.28) gives the relation between the incoming and outgoing wave amplitudes to be

$$\mathbf{B} = \mathbf{X}\mathbf{A}, \tag{4.2.30}$$

where

$$\mathbf{X} = (\alpha h \sin 2\alpha b\, \mathbf{I} - \mathbf{S}\overline{\mathbf{D}})^{-1}(\alpha h \sin 2\alpha b\, \mathbf{I} - \mathbf{S}\mathbf{D}), \tag{4.2.31}$$

and $\mathbf{I}$ is the 2×2 identity. Here, $\mathbf{X}$ is a scattering matrix converting two incident waves of arbitrary amplitude from $x = \pm\infty$ into two outgoing waves. The reflection and transmission coefficients, R_1, T_1, R_2 and T_1 are found from comparison of (4.2.30) with (4.2.8).

As in the previous chapter, it is possible to construct an alternative formulation by considering the jump in pressure across each barrier. For this, we use the fact that $U^{(i)}(y) = 0$ for $y \in L_b^{(i)}$, $i = 1, 2$ (i.e. no-flow across the barriers at $x = \mp b$ respectively) in (4.2.17) with (4.2.15) to give

$$-i\alpha(A_i - B_i)\psi_0(y) = \sum_{n=1}^{\infty} U_n^{(i)}\psi_n(y), \quad y \in L_b^{(i)}. \tag{4.2.32}$$

Multiplying (4.2.18) by $\psi_m(y)$ and integrating over $[0, h]$ gives, for $n = 0$

$$\int_{L_b^{(i)}} P^{(i)}(y)\psi_0(y)\,\mathrm{d}y = ih\mathrm{cosec}\, 2\alpha b \left\{ A_i \mathrm{e}^{2i\alpha b} - B_i \mathrm{e}^{-2i\alpha b} - A_{3-i} + B_{3-i} \right\}, \tag{4.2.33}$$

and for $n \geq 1$

$$\alpha_n \int_{L_b^{(i)}} P^{(i)}(y)\psi_n(y)\,\mathrm{d}y = -hU_n^{(i)}(1 + \coth 2\alpha_n b) + hU_n^{(3-i)}\mathrm{cosech}\, 2\alpha_n b, \tag{4.2.34}$$

where (4.2.2) has been used. Eliminating $U_n^{(1)}$ and $U_n^{(2)}$ in turn from the above with $i = 1, 2$ now gives

$$-\frac{2h}{\alpha_n}U_n^{(i)} = \int_{L_b^{(i)}} P^{(i)}(y)\psi_n(y)\,\mathrm{d}y + \mathrm{e}^{-2\alpha_n b}\int_{L_b^{(3-i)}} P^{(3-i)}(y)\psi_n(y)\,\mathrm{d}y, \quad n \geq 1$$

and substituting these into (4.2.32) gives the following integral equations for the unknown functions $P^{(i)}(y)$

$$\int_{L_b^{(i)}} P^{(i)}(t)M^{(1)}(y,t)\,\mathrm{d}t + \int_{L_b^{(3-i)}} P^{(3-i)}(t)M^{(2)}(y,t)\,\mathrm{d}t$$
$$= i\alpha h^2(A_i - B_i)\psi_0(y), \quad y \in L_b^{(i)}, \quad i = 1, 2 \tag{4.2.35}$$

where the kernels are given by

$$M^{(1)}(y,t) = \frac{1}{2}\sum_{n=1}^{\infty} \alpha_n h \psi_n(y)\psi_n(t), \tag{4.2.36}$$

and

$$M^{(2)}(y,t) = \frac{1}{2}\sum_{n=1}^{\infty} \alpha_n h \mathrm{e}^{-2\alpha_n b}\psi_n(y)\psi_n(t). \tag{4.2.37}$$

(We have interchanged the order of summation and integration illegally in (4.2.35) for convenience of notation only; retaining the original order leads to the same result in what is to follow).

The two coupled integral equations in (4.2.35) are valid over different intervals and we now employ the same technique as in the velocity formulation of the previous section to unify these two equations into a single vector equation. Hence, we define

$$H_i^c(y) = 1 - H_i(y) = \begin{cases} 0, & y \in L_g^{(i)} \\ 1, & y \in L_b^{(i)} \end{cases} \quad i = 1,2, \tag{4.2.38}$$

reversing the effect of the unit step function, $H_i(y)$ in (4.2.22). We may now write (4.2.35) as

$$\begin{aligned}\int_L H_i^c(y)\left[M^{(1)}(y,t)H_i^c(t)P^{(i)}(t) + M^{(2)}(y,t)H_{3-i}^c(t)P^{(3-i)}(t)\right]\mathrm{d}t \\ = i\alpha h^2(A_i - B_i)H_i^c(y)\psi_0(y), \quad y \in L, \quad i = 1,2,\end{aligned}$$

and in matrix notation this is

$$\int_L \mathbf{H}^c(y)\mathbf{M}(y,t)\mathbf{H}^c(t)\mathbf{P}(t)\,\mathrm{d}t = i\alpha h^2\mathbf{H}^c(y)(\mathbf{A} - \mathbf{B})\psi_0(y), \quad y \in L, \tag{4.2.39}$$

where the previous notation has been used with $\mathbf{H}^c(y) = \mathrm{diag}\{H_i^c(y)\}_{i=1,2}$

$$\mathbf{M}(y,t) = \begin{pmatrix} M^{(1)}(y,t) & M^{(2)}(y,t) \\ M^{(2)}(y,t) & M^{(1)}(y,t) \end{pmatrix},$$

and $\mathbf{P}(y) = (P^{(1)}(y), P^{(2)}(y))^{\mathrm{T}}$. Now, if the 2×2 matrix $\mathbf{p}(y) = \{p_{mn}\}$ is the solution to

$$\int_L \mathbf{H}^c(y)\mathbf{M}(y,t)\mathbf{H}^c(t)\mathbf{p}(t)\,\mathrm{d}t = \mathbf{H}^c(y)\psi_0(y), \quad y \in L, \tag{4.2.40}$$

then

$$\mathbf{P}(y) = i\alpha h^2\mathbf{p}(y)(\mathbf{A} - \mathbf{B}), \tag{4.2.41}$$

satisfies (4.2.39). Also, writing (4.2.33) in vector notation after using the definition of $H_i^c(y)$ to unify the integration range we find

$$\int_L \mathbf{H}^c(y)\mathbf{P}(y)\psi_0(y)\,\mathrm{d}y = ih\mathrm{cosec}\,2\alpha b\,(\mathbf{DA}-\overline{\mathbf{D}}\mathbf{B}), \tag{4.2.42}$$

and susbtitution of (4.2.41) now yields

$$\alpha h\sin 2\alpha b\,\mathbf{T}(\mathbf{A}-\mathbf{B}) = \mathbf{DA}-\overline{\mathbf{D}}\mathbf{B}, \tag{4.2.43}$$

where we have defined the 2×2 matrix $\mathbf{T}=\{T_{mn}\}$ to be

$$\mathbf{T} = \int_L \mathbf{H}^c(y)\mathbf{p}(y)\psi_0(y)\,\mathrm{d}y. \tag{4.2.44}$$

Rearrangement of (4.2.43) leads us to the relation $\mathbf{B}=\mathbf{XA}$ as in (4.2.30) but with

$$\mathbf{X} = (\alpha h\sin 2\alpha b\,\mathbf{T}-\overline{\mathbf{D}})^{-1}(\alpha h\sin 2\alpha b\,\mathbf{T}-\mathbf{D}), \tag{4.2.45}$$

whence it can be seen from (4.2.45), (4.2.31) that $\mathbf{S}=\mathbf{T}^{-1}$.

The solution to the problem is in terms of a 2×2 matrix $\mathbf{S}$, related to the matrix $\mathbf{u}(y)$ by (4.2.29), where $\mathbf{u}(y)$ is the solution of the set of integral operator equations (4.2.24) *or* in terms of a 2×2 matrix $\mathbf{T}$, related to the matrix $\mathbf{p}(y)$ by (4.2.44), where $\mathbf{p}(y)$ is the solution of (4.2.40).

In the remainder of this section, we apply a Galerkin approach to the two complementary formulations to gain approximations to the two matrices $\mathbf{S}$, $\mathbf{T}$.

From (4.2.26) we note that the functions $u_{1j}(y)$, $j=1,2$ are related to $U_1(y)$ and hence to the horizontal component of velocity of the fluid across the gap at $x=-b$, whilst $u_{2j}(y)$, $j=1,2$ are related to the velocity across $x=+b$. We expand these unknowns in terms of unknown coefficients $a_n^{(ij)}$ such that

$$u_{ij}(y) \simeq \tilde{u}_{ij}(y) = \sum_{n=0}^{N} a_n^{(ij)} v_n^{(j)}(y), \quad i,j=1,2, \tag{4.2.46}$$

where $\{v_n^{(j)}(y)\}$, $j=1$ (2) are sets of test functions for the velocity at $x=-b$ $(+b)$ to be defined later. Inserting this into (4.2.25) and using the definition of

$H_i(y)$ to restrict the range of integration yields

$$\sum_{n=0}^{N} a_n^{(1j)} \int_{L_g^{(1)}} H_1(y)K^{(1)}(y,t)v_n^{(1)}(t)\,\mathrm{d}t - \sum_{n=0}^{N} a_n^{(2j)} \int_{L_g^{(2)}} H_1(y)K^{(2)}(y,t)v_n^{(2)}(t)\,\mathrm{d}t$$
$$= \delta_{1j}H_1(y)\psi_0(y), \quad j=1,2$$
$$-\sum_{n=0}^{N} a_n^{(1j)} \int_{L_g^{(1)}} H_2(y)K^{(2)}(y,t)v_n^{(1)}(t)\,\mathrm{d}t + \sum_{n=0}^{N} a_n^{(2j)} \int_{L_g^{(2)}} H_2(y)K^{(1)}(y,t)v_n^{(2)}(t)\,\mathrm{d}t$$
$$= \delta_{2j}H_2(y)\psi_0(y), \quad j=1,2.$$

We now multiply the above two equations by $v_m^{(i)}(y)$, $i=1,2$ respectively and integrate over L to obtain

$$\left.\begin{aligned} \sum_{n=0}^{N} a_n^{(1j)}K_{mn}^{(1,1)} - \sum_{n=0}^{N} a_n^{(2j)}K_{mn}^{(1,2)} &= \delta_{1j}F_{m0}^{(1)} \\ -\sum_{n=0}^{N} a_n^{(1j)}K_{mn}^{(2,1)} + \sum_{n=0}^{N} a_n^{(2j)}K_{mn}^{(2,2)} &= \delta_{2j}F_{m0}^{(2)} \end{aligned}\right\}, \quad \left\{\begin{array}{l} m=0,\ldots,N \\ j=1,2 \end{array}\right., \tag{4.2.47}$$

where

$$K_{mn}^{(i,i)} = \sum_{r=1}^{\infty}(\alpha_r h)^{-1}(1+\coth 2\alpha_r b)F_{mr}^{(i)}F_{nr}^{(i)}, \quad i=1,2 \tag{4.2.48}$$

$$K_{mn}^{(i,3-i)} = \sum_{r=1}^{\infty}(\alpha_r h)^{-1}\mathrm{cosech}\, 2\alpha_r b F_{mr}^{(i)}F_{nr}^{(3-i)}, \quad i=1,2, \tag{4.2.49}$$

after use of (4.2.20), (4.2.21) and where

$$F_{mn}^{(i)} = \int_{L_g^{(i)}} v_m^{(i)}(y)\psi_n(y)\,\mathrm{d}y, \quad i=1,2, \tag{4.2.50}$$

are defined by either (3.2.41), (3.2.42) or (3.2.57), (3.2.58) depending on whether the barrier at $x=\mp b$ ($i=1,2$ respectively) is surface-piercing or bottom-mounted. We notice that the two coupled systems, (4.2.47) may be written in terms of a block-structured matrix equation for the unknown coefficients thus

$$\begin{pmatrix} \mathbf{K}^{(1,1)} & -\mathbf{K}^{(1,2)} \\ -\mathbf{K}^{(2,1)} & \mathbf{K}^{(2,2)} \end{pmatrix} \begin{pmatrix} \mathbf{a}^{(11)} & \mathbf{a}^{(12)} \\ \mathbf{a}^{(21)} & \mathbf{a}^{(22)} \end{pmatrix} = \begin{pmatrix} \mathbf{F}^{(1)} & \mathbf{0} \\ \mathbf{0} & \mathbf{F}^{(2)} \end{pmatrix} \tag{4.2.51}$$

where we define $\mathbf{K}^{(i,j)} = \{K_{mn}^{(i,j)}\}$, $i,j=1,2$ and $\mathbf{a}^{(ij)} = (a_0^{(ij)},\ldots,a_N^{(ij)})^{\mathrm{T}}$, $i,j=1,2$ and $\mathbf{F}^{(i)} = (F_{00}^{(i)},\ldots,F_{N0}^{(i)})^{\mathrm{T}}$, $i=1,2$ whilst $\mathbf{0}$ is the null vector of length $N+1$. It is clear from (4.2.48), (4.2.49) that the block matrix in (4.2.51) with entries $\mathbf{K}^{(i,j)}$ is in fact symmetric.

Returning to (4.2.29), we find that the approximation, $\tilde{\mathbf{S}}$ to $\mathbf{S}$ after substitution of (4.2.46) in (4.2.29) is

$$S_{ij} \simeq \tilde{S}_{ij} = \sum_{n=0}^{N} a_n^{(ij)} F_{n0}^{(i)}, \quad i, j = 1, 2 \tag{4.2.52}$$

which can be written

$$\begin{aligned}\tilde{\mathbf{S}} &= \begin{pmatrix} \mathbf{F}^{(1)} & \mathbf{0} \\ \mathbf{0} & \mathbf{F}^{(2)} \end{pmatrix}^{\mathrm{T}} \begin{pmatrix} \mathbf{a}^{(11)} & \mathbf{a}^{(12)} \\ \mathbf{a}^{(21)} & \mathbf{a}^{(22)} \end{pmatrix} \\ &= \begin{pmatrix} \mathbf{F}^{(1)} & \mathbf{0} \\ \mathbf{0} & \mathbf{F}^{(2)} \end{pmatrix}^{\mathrm{T}} \begin{pmatrix} \mathbf{K}^{(1,1)} & -\mathbf{K}^{(1,2)} \\ -\mathbf{K}^{(2,1)} & \mathbf{K}^{(2,2)} \end{pmatrix}^{-1} \begin{pmatrix} \mathbf{F}^{(1)} & \mathbf{0} \\ \mathbf{0} & \mathbf{F}^{(2)} \end{pmatrix},\end{aligned} \tag{4.2.53}$$

using (4.2.51). Hence, we have an expression for the approximation to the entries of the 2×2 matrix $\mathbf{S}$, and so we can find $\mathbf{X}$ from (4.2.31) and the reflection and transmission coefficients arising from an incident wave from $x = \pm\infty$ are computed from (4.2.8).

Notice that the Galerkin method has given an expression for the approximation to $\mathbf{S}$ which has the quadratic form of (2.44) and is again scale-invariant.

A Galerkin approximation to the integral equations, (4.2.40), arising in the pressure difference formulation can be found in a similar manner to that shown above by introducing the expansions

$$p_{ij}(y) = \sum_{n=0}^{N} b_n^{(ij)} w_n^{(j)}(y), \quad y \in L_b^{(j)}, \quad i, j = 1, 2, \tag{4.2.54}$$

for the entries of the matrix $\mathbf{p}(y)$. Here, the two sets of functions $\{w_n^{(j)}(y)\}$ are test functions for the jump in potential across the barrier at $x = -b$ $(+b)$, $j = 1$ (2). Applying the Galerkin procedure leads eventually to the following approximation $\tilde{\mathbf{T}}$ to $\mathbf{T}$, defined by (4.2.44),

$$\tilde{\mathbf{T}} = \begin{pmatrix} \mathbf{G}^{(1)} & \mathbf{0} \\ \mathbf{0} & \mathbf{G}^{(2)} \end{pmatrix}^{\mathrm{T}} \begin{pmatrix} \mathbf{M}^{(1,1)} & \mathbf{M}^{(1,2)} \\ \mathbf{M}^{(2,1)} & \mathbf{M}^{(2,2)} \end{pmatrix}^{-1} \begin{pmatrix} \mathbf{G}^{(1)} & \mathbf{0} \\ \mathbf{0} & \mathbf{G}^{(2)} \end{pmatrix}, \tag{4.2.55}$$

where $\mathbf{G}^{(i)} = (G_{00}^{(i)}, \dots, G_{N0}^{(i)})^{\mathrm{T}}$, $\mathbf{M}^{(i,j)} = \{M_{mn}^{(i,j)}\}$ and

$$M_{mn}^{(i,i)} = \frac{1}{2} \sum_{r=1}^{\infty} \alpha_r h G_{mr}^{(i)} G_{nr}^{(i)}, \quad i = 1, 2, \tag{4.2.56}$$

$$M_{mn}^{(i,3-i)} = \frac{1}{2}\sum_{r=1}^{\infty} \alpha_r h \, \mathrm{e}^{-2\alpha_r b} G_{mr}^{(i)} G_{nr}^{(3-i)}, \quad i = 1, 2, \tag{4.2.57}$$

from (4.2.36), (4.2.37) and where

$$G_{mn}^{(i)} = \int_{L_b^{(i)}} w_m^{(i)}(y)\psi_n(y)\,\mathrm{d}y, \quad i = 1, 2 \tag{4.2.58}$$

are given by (3.2.50), (3.2.51) or (3.2.62), (3.2.63) depending on whether the barriers at $x = \mp b$, ($i = 1, 2$ in (4.2.58)) are surface-piercing or bottom-mounted, respectively.

4.3 Special case of two equal barriers

By choosing the two barriers at $x = \mp b$ to be identical, either both surface-piercing or both bottom-mounted of equal length, we are able to simplify the above analysis. The case of two identical surface-piercing barriers has been addressed in detail by McIver [46] and by Porter & Evans [65], both of whom used the symmetry of the geometry to decompose the potential into symmetric and antisymmetric parts each satisfying an appropriate boundary condition on $x = 0$.

The complication in §4.2 arose due to the two integral equations in (4.2.19) being valid over different intervals. We notice that by choosing $L_{g,b}^{(1)} = L_{g,b}^{(2)}$, we may add/subtract (4.2.19), $i = 1$ to/from $i = 2$ to obtain

$$\int_{L_g^{(1)}} (U^{(1)} \pm U^{(2)})(t)(K^{(1)} \mp K^{(2)})(y,t)\,\mathrm{d}t = \\ \frac{i}{\sin 2\alpha b}\left\{(A_1 \pm A_2)(\mathrm{e}^{2i\alpha b} \mp 1) - (B_1 \pm B_2)(\mathrm{e}^{-2i\alpha b} \mp 1)\right\}\psi_0(y). \tag{4.3.1}$$

We now choose to call the two unknown functions above $U^s(y) = \frac{1}{2}(U^{(1)}(y) - U^{(2)}(y))$ and $U^a(y) = \frac{1}{2}(U^{(1)}(y) + U^{(2)}(y))$ and accordingly define the two new kernels in (4.3.1) to be

$$K^s(y,t) \equiv (K^{(1)} + K^{(2)})(y,t) = \sum_{n=1}^{\infty} \frac{(1 + \coth \alpha_n b)}{\alpha_n h}\psi_n(y)\psi_n(t) \tag{4.3.2}$$

and

$$K^a(y,t) \equiv (K^{(1)} - K^{(2)})(y,t) = \sum_{n=1}^{\infty} \frac{(1 + \tanh \alpha_n b)}{\alpha_n h}\psi_n(y)\psi_n(t), \tag{4.3.3}$$

where we have used (4.2.20), (4.2.21). Thus, (4.3.1) becomes

$$\int_{L_g^{(1)}} U^{a,s}(t) K^{a,s}(y,t)\,\mathrm{d}t = \frac{i}{2\sin 2\alpha b}\left\{(A_1 \pm A_2)(\mathrm{e}^{2i\alpha b} \mp 1) - (B_1 \pm B_2)(\mathrm{e}^{-2i\alpha b} \mp 1)\right\}\psi_0(y), \qquad (4.3.4)$$

where the superscripts a and s refer to the top and bottom signs respectively. Also, from (4.2.15) adding and subtracting $i = 1, 2$ we have

$$\int_{L_g^{(1)}} U^{a,s}(y)\psi_0(y)\,\mathrm{d}y = i\alpha h\{(A_1 \pm A_2) - (B_1 \pm B_2)\}. \qquad (4.3.5)$$

A rescaling of the unknowns $U^{a,s}(y)$ by the factor multiplying $\psi_0(y)$ in (4.3.4) leads to the system

$$\int_{L_g^{(1)}} U^{a,s}(t) K^{a,s}(y,t)\,\mathrm{d}t = \psi_0(y), \quad y \in L_g^{(1)}, \qquad (4.3.6)$$

$$\int_{L_g^{(1)}} U^{a,s}(y)\psi_0(y)\,\mathrm{d}y = A^{a,s}, \qquad (4.3.7)$$

where

$$A^{a,s} = \frac{\alpha h \sin 2\alpha b\{(A_1 \pm A_2) - (B_1 \pm B_2)\}}{(A_1 \pm A_2)(\mathrm{e}^{2i\alpha b} \mp 1) - (B_1 \pm B_2)(\mathrm{e}^{-2i\alpha b} \mp 1)}. \qquad (4.3.8)$$

Since the geometry of the problem is now symmetric about $x = 0$, we may choose the only incident wave to come from $x = +\infty$ with unit amplitude without loss of generality, whence $A_1 = 0$, $A_2 = 1$, and so $B_1 = -T$, $B_2 = R$ are the reflection and transmission coefficients. By choosing $B_1 + B_2 = R - T = R^a$, and $B_1 - B_2 = -R - T = -R^s$, say, then it can easily be shown after careful manipulation that

$$A^a = \frac{i\alpha h(R^a - 1)}{(R^a + 1) - i\tan\alpha b(R^a - 1)}, \qquad (4.3.9)$$

$$A^s = \frac{i\alpha h(R^s - 1)}{(R^s + 1) + i\cot\alpha b(R^s - 1)}, \qquad (4.3.10)$$

where the reflection and transmission coefficients may be recovered from $R = \frac{1}{2}(R^s + R^a)$, $T = \frac{1}{2}(R^s - R^a)$. The equations (4.3.6), (4.3.7) with (4.3.9), (4.3.10) are precisely those found from a decomposition of the potential into antisymmetric and symmetric potentials at the outset and $R^{a,s}$ are the reflection coefficients arising from the solution of the two resulting boundary-value problems.

A similar analysis of the pressure difference formulation gives

$$\int_{L_b^{(1)}} P^{a,s}(t) M^{a,s}(y,t)\,\mathrm{d}t = \psi_0(y), \quad y \in L_b^{(1)}, \tag{4.3.11}$$

$$\int_{L_b^{(1)}} P^{a,s}(y)\psi_0(y)\,\mathrm{d}y = 1/A^{a,s}, \tag{4.3.12}$$

where

$$M^a(y,t) = \sum_{n=1}^{\infty} \frac{\alpha_n h \psi_n(y)\psi_n(t)}{(1+\tanh\alpha_n b)}, \qquad M^s(y,t) = \sum_{n=1}^{\infty} \frac{\alpha_n h \psi_n(y)\psi_n(t)}{(1+\coth\alpha_n b)}. \tag{4.3.13}$$

The occurence of the $A^{a,s}$, $1/A^{a,s}$ in (4.3.7), (4.3.12) implies that a Galerkin approximation will furnish upper and lower bounds on $A^{a,s}$. See chapter 2 for details.

4.4 Wide-spacing approximation

In the previous section a simplification to the coupled integral equations (4.2.19) and (4.2.35) was given under the condition that the two barriers were identical. Another situation in which simplification can occur is in the limit of $b \to \infty$. Then we find from (4.2.20), (4.2.21)

$$K^{(1)}(y,t) \to 2\sum_{n=1}^{\infty} (\alpha_n h)^{-1}\psi_n(y)\psi_n(t), \quad \text{and} \quad K^{(2)}(y,t) \to 0, \tag{4.4.1}$$

and from (4.2.38), (4.2.39)

$$M^{(1)}(y,t) \to \frac{1}{2}\sum_{n=1}^{\infty} \alpha_n h\; \psi_n(y)\psi_n(t), \quad \text{and} \quad M^{(2)}(y,t) \to 0, \tag{4.4.2}$$

and so the matrices occuring in (4.2.24), (4.2.39) become diagonal yielding distinct integral equations for $u_{ii}(y)$, $p_{ii}(y)$ equivalent to those for a single barrier in isolation, cf. (3.2.18), (3.2.33). The resulting values of the matrix $\mathbf{S}$ are then

$$S_{11} = -i\alpha h\frac{(1-r_1)}{2r_1}, \quad S_{22} = -i\alpha h\frac{(1-r_2)}{2r_2}, \quad S_{12} = S_{21} = 0, \tag{4.4.3}$$

by analogy with the single barrier problem equation (3.2.19), where r_i, t_i, $i = 1,2$ are the reflection and transmission coefficients for the barriers at $x = \mp b$ each placed in isolation at $x = 0$. Notice that since $\mathbf{S}$ is diagonal and $\mathbf{S} = \mathbf{T}^{-1}$ as stated earlier, $T_{ii} = 1/S_{ii}$ as expected from comparison of (3.2.19) with (3.2.34).

Note also that the extra factor of 2 in (4.4.3) has come from the factor of 2 present in (4.4.1) but absent in (3.2.17).

Substituting (4.4.3) into the scattering matrix $\mathbf{X}$ in (4.2.31) gives, after considerable algebra, the well-known wide-spacing expressions to the reflection and transmission coefficients for a two-body system. For example, we find

$$R_- = X_{11}\mathrm{e}^{-2i\alpha b} = r_1\mathrm{e}^{-2i\alpha b} + \frac{r_2 t_1^2 \mathrm{e}^{2i\alpha b}}{1 - r_1 r_2 \mathrm{e}^{4i\alpha b}} \tag{4.4.4}$$

$$T_- = -X_{21}\mathrm{e}^{-2i\alpha b} = \frac{t_1 t_2}{1 - r_1 r_2 \mathrm{e}^{4i\alpha b}}. \tag{4.4.5}$$

This outcome is not surprising since the effect of letting the spacing tend to infinity is to ignore the influence of the evanescent modes emanating from the neighbouring barrier and this forms the basis of the wide-spacing approximation. The usual procedure for applying the wide-spacing procedure is to consider the interactions of just the propagating wave modes at each of the two barriers with a fixed finite spacing b.

We can use the wide-spacing approximation to check the numerical results for the full solution of §4.2 when the barrier spacing is large enough.

4.5 Approximate solution for two closely-spaced unequal barriers

Another approximate solution can be obtained in the case of two closely-spaced overlapping barriers, one surface-piercing and one bottom-standing. Under the assumptions that compared to the average depth of submergence of the two barrier tips the separation distance, $2b$, and the overlap, $a_2 - a_1$ are small and that these horizontal and vertical separations are small compared to the depth and that the wavelength and the depth are the same order of magnitude, a method of matched asymptotic expansions can be applied to yield approximate expressions for the reflection and transmission coefficients.

The idea behind the method of matched asymptotic expansions is simple. Far

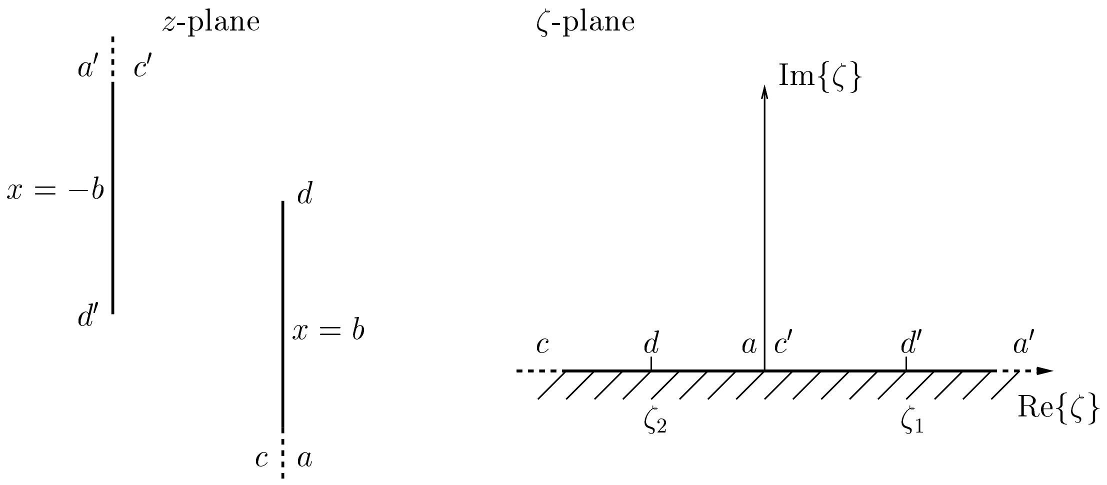

Figure 4.2: Mapping of the two semi-infinite plates from z-plane to the upper-half ζ-plane

away from the structure, the assumptions imposed that various length scales are small compared to others allows the structure to be regarded as being of a simpler form, small gaps in the structure appearing as source points in the fluid. Thus in our problem the two barriers appear, at a distance, to merge into a vertical wall extending throughout the depth with a source point at $y = a_2$ when viewed from $x > 0$ and at $y = a_1$ when viewed from $x < 0$. If we now take a magnified view of the small gaps and the surrounding geometry, we are not aware of the boundaries far away. Thus in our case, close to the overlap it appears that we are looking at a flow in an infinite fluid past two overlapping semi-infinite plates.

Matching the outer limit of the near solution with the inner limit of the far-away solution in an asymptotic manner completes the solution to the whole problem. This not only provides a check on the method of the previous section, but also provides a means by which we can compute accurately results for geometries that are out of bounds to our previous method.

We first examine the solution to the inner problem shown in figure 4.2. An application of the Schwarz-Christoffel transformation for two semi-infinite plates gives

$$\frac{j\pi z}{b} = A + \zeta + \frac{\gamma^2}{\zeta} + 2\log\zeta, \tag{4.5.1}$$

(Kober [38], p. 153) where $z = x + j(y - \frac{1}{2}(a_1 + a_2))$, $j = \sqrt{-1}$ so that the origin is located mid-way between the ends of the plates and the critical points are given by

$$\zeta_1 = -1 + (\gamma^2 + 1)^{1/2} > 0, \quad \text{and} \quad \zeta_2 = -1 - (\gamma^2 + 1)^{1/2} < 0, \tag{4.5.2}$$

with γ real and positive, which must correspond to the plate end points d' and d respectively. The imaginary unit j does not interact with i used already for time variation. The transformation in (4.5.1) maps the plates at $x = -b$ (b) to the positive (negative) real axis in the ζ-plane as shown in figure 4.2, this mapping determining the unknowns γ and A. Thus substituting $(x, y) = (-b, a_1)$ when $\zeta = \zeta_1$ and $(x, y) = (b, a_2)$ when $\zeta = \zeta_2$ gives after manipulation

$$A = -2 \log \gamma - \pi j, \tag{4.5.3}$$

and

$$\frac{\pi(a_2 - a_1)}{b} = 2(\gamma^2 + 1)^{1/2} + \log \left[\frac{(\gamma^2 + 1)^{1/2} - 1}{(\gamma^2 + 1)^{1/2} + 1} \right], \tag{4.5.4}$$

relating γ to the barrier overlap, $(a_2 - a_1)$. Hence, the mapping from the z-plane to the ζ-plane is

$$\frac{j\pi z}{b} = -\pi j + \zeta + \frac{\gamma^2}{\zeta} + 2 \log(\zeta/\gamma), \tag{4.5.5}$$

with γ being determined from (4.5.4). We now impose a potential flow on the ζ-plane by placing a sink at $\zeta = 0$. This is equivalent to imposing a flow through the barriers in the z-plane from the region $x < -b$ into $x > b$. Such a sink is written as

$$w(\zeta) = -\frac{m}{2\pi} \log \zeta + C + jD, \tag{4.5.6}$$

where C, D are real constants and m is the strength of the sink. We are interested in the solution to the potential flow problem far away from the barriers, and so we need only consider the limiting cases of $\zeta \to 0$ and $|\zeta| \to \infty$. Using $\zeta \to 0$ in (4.5.5) gives

$$\zeta \simeq -\frac{j\gamma^2 b}{\pi(z - \frac{1}{2}j(a_2 - a_1))}, \tag{4.5.7}$$

which, when substituted into (4.5.6) gives

$$\phi(x,y) \simeq -\frac{m}{2\pi}\log\left(\frac{\gamma^2 b}{\pi r_2}\right) + C, \tag{4.5.8}$$

as $r_2 \to \infty$, $r_2^2 = x^2 + (y-a_2)^2$, corresponding to the region $x > 0$. Similarly, as $|\zeta| \to \infty$

$$\zeta \simeq \frac{j\pi(z + \frac{1}{2}j(a_2 - a_1))}{b}, \tag{4.5.9}$$

and so we find

$$\phi(x,y) \simeq -\frac{m}{2\pi}\log\left(\frac{\pi r_1}{b}\right) + C, \tag{4.5.10}$$

as $r_1 \to \infty$, $r_1^2 = x^2 + (y-a_1)^2$, corresponding to the region $x < 0$.

We now turn our attention to the outer solution. Far away from the barriers in $x > 0$, the flow appears to be generated by a wave incident on a solid vertical wall with a pulsating source at $(x,y) = (0,a_2)$, whilst in $x < 0$, the flow appears to be due, by continuity, to a sink of equal strength at $(x,y) = (0,a_1)$ in a wall in an otherwise motionless fluid. Thus we write

$$\phi(x,y) = (\mathrm{e}^{-ikx} + \mathrm{e}^{ikx})\psi_0(y) + m_1 G(x,y;0,a_2), \quad x > 0, \tag{4.5.11}$$

$$\phi(x,y) = -m_1 G(x,y;0,a_1), \quad x < 0, \tag{4.5.12}$$

where $G(x,y;0,a_i)$, $i = 1,2$ is the two-dimensional Green function due to a source of unit strength at the point $(x,y) = (0,a_i)$ in a fluid of depth h. This has a simple form (see for example Mei [51, p.380]) and can be written

$$G(x,y;0,a_i) = -\frac{i}{2kh}\psi_0(a_i)\psi_0(y)\mathrm{e}^{ik|x|} - \sum_{n=1}^{\infty}\frac{1}{2k_n h}\psi_n(a_i)\psi_n(y)\mathrm{e}^{-k_n|x|}. \tag{4.5.13}$$

For large n, $k_n h \sim n\pi$ and $N_n \sim \frac{1}{2}$ so that at the source point the n^{th} term in the above sum behaves like $1/n$ and the series diverges. In order to obtain the behaviour of G as the source point is approached, see Appendix A. Hence, from (A.11)

$$G(x,y;0,a_i) = R(a_i) - G_i, \quad \text{as } r_i \to 0, \tag{4.5.14}$$

where $R(a_i)$, G_i are defined by (A.12) and (A.10) respectively.

We are now in a position to match the solution in the inner region with the two solutions in the outer regions, $x < 0$ and $x > 0$. Thus matching the appropriate limiting form in (4.5.8), (4.5.11) yields

$$-\frac{m}{2\pi}\log\left(\frac{\gamma^2 b}{\pi r_2}\right)+C=2\psi_0(a_2)+\frac{m_1}{2\pi}\log\left\{\frac{2\pi r_2}{h}\sin\left(\frac{\pi a_2}{h}\right)\right\}+m_1 R(a_2), \quad (4.5.15)$$

from which we must have $m = m_1$, and so cancelling the r_2 terms gives

$$-\frac{m}{2\pi}\log\left\{\frac{2\gamma^2 b}{h}\sin\left(\frac{\pi a_2}{h}\right)\right\}-mR(a_2)+C=2N_0^{-1/2}\cosh k(h-a_2), \qquad (4.5.16)$$

whilst for $x < 0$ we find in a similar manner

$$\frac{m}{2\pi}\log\left\{\frac{2b}{h}\sin\left(\frac{\pi a_1}{h}\right)\right\}+mR(a_1)+C=0. \qquad (4.5.17)$$

The two unknowns, m and C, in the two equations can be solved for and the solution is complete. Hence

$$m=\frac{-2N_0^{1/2}\cosh k(h-a_2)}{\frac{1}{2\pi}\log\left\{\left(\frac{2b\gamma}{h}\right)^2\sin\left(\frac{\pi a_1}{h}\right)\sin\left(\frac{\pi a_2}{h}\right)\right\}+R(a_1)+R(a_2)}. \qquad (4.5.18)$$

All that remains is to write down the expressions for the reflection and transmission coefficients, R and T from the far field forms of (4.5.11), (4.5.12) using (A.13):

$$R=1-\frac{imN_0^{-1/2}\cosh k(h-a_2)}{2kh}, \qquad (4.5.19)$$

and

$$T=\frac{imN_0^{-1/2}\cosh k(h-a_1)}{2kh}. \qquad (4.5.20)$$

4.6 Results

As in the previous two sections we first give an indication of the accuracy of the method by presenting a table of results showing the convergence of the two approximations to $\mathbf{S}$ and $\mathbf{T}(=\mathbf{S}^{-1})$ for a typical set of parameters. Thus table 4.1 shows values of the elements of the symmetric matrices $\tilde{\mathbf{S}}$ and $\tilde{\mathbf{T}}$ as the truncation size N is increased in the case of an overlapping arrangement consisting of a bottom-mounted barrier at $x = -b$ with $a_1/h = 0.2$ and a surface-piercing barrier at $x = b$

N	$\tilde{S}_{11}$	$\tilde{S}_{12}=\tilde{S}_{21}$	$\tilde{S}_{22}$	$\tilde{T}_{11}$	$\tilde{T}_{12}=\tilde{T}_{21}$	$\tilde{T}_{22}$
0	2.222324	-1.411611	1.278297	0.602626	0.467398	1.016030
1	2.403372	-1.265936	1.434987	0.722509	0.610344	1.186925
2	2.430338	-1.251491	1.442730	0.730981	0.621184	1.205751
3	2.430778	-1.250659	1.444324	0.739356	0.637745	1.239544
4	2.430793	-1.250630	1.444380	0.741338	0.641206	1.245776
5	2.430794	-1.250632	1.444382	0.741407	0.641296	1.246075
6	2.430795	-1.250633	1.444385	0.741729	0.642044	1.247829
7	2.430795	-1.250633	1.444386	0.741838	0.642260	1.248270
8	2.430795	-1.250633	1.444386	0.741839	0.642264	1.248289

Table 4.1: Convergence of the elements of the 2×2 matrices $\tilde{\mathbf{S}}$ and $\tilde{\mathbf{T}}$ with increasing N for parameter values $a_1/h = 0.2$ (bottom-mounted), $a_2/h = 0.3$ (surface-piercing), $2b/h = 0.05$, $kh = 2$.

with $a_2/h = 0.3$. A close spacing of $2b/h = 0.05$ was chosen in order to test the method. It can be seen that good accuracy is again achieved with very few terms, although a value of $N = 8$ is required to gain an accuracy comparable to the single barrier results of §3.4. Corresponding accuracy is also achieved in the reflection and transmission coefficients. It should be mentioned that the calculation of the infinite series in (4.2.48), (4.2.49) and (4.2.57), (4.2.58) is performed by truncation to a size M, say, and that the leading order asymptotic behaviour of the terms in the series are used to calculate a correction term to increase accuracy in the manner described in §3.4 of the previous chapter.

In the cases when the barriers at $x \pm b$ are equal, we have shown in §4.3 that simplification to the coupled system occurs. Thus, it is no longer necessary to determine approximations to $\mathbf{S}$ and $\mathbf{T}$ which involve the computation and inversion of the block matrices with entries $\mathbf{K}^{(i,j)}$ (or $\mathbf{M}^{(i,j)}$). Instead, the reflection and transmission coefficients are expressible in terms of $A^{s,a}$ by equations (4.3.9), (4.3.10) which are bounded above and below once a Galerkin approximation has been made to (4.3.6), (4.3.7) and (4.3.11), (4.3.12). The bounds occur by virtue of the term $A^{a,s}$ in the velocity formulation, which in the pressure difference formulation is replaced by $1/A^{a,s}$. The resulting approximations to $A^{a,s}$ are therefore very similar to those occuring in the single barrier problems of the previous chapter and follow

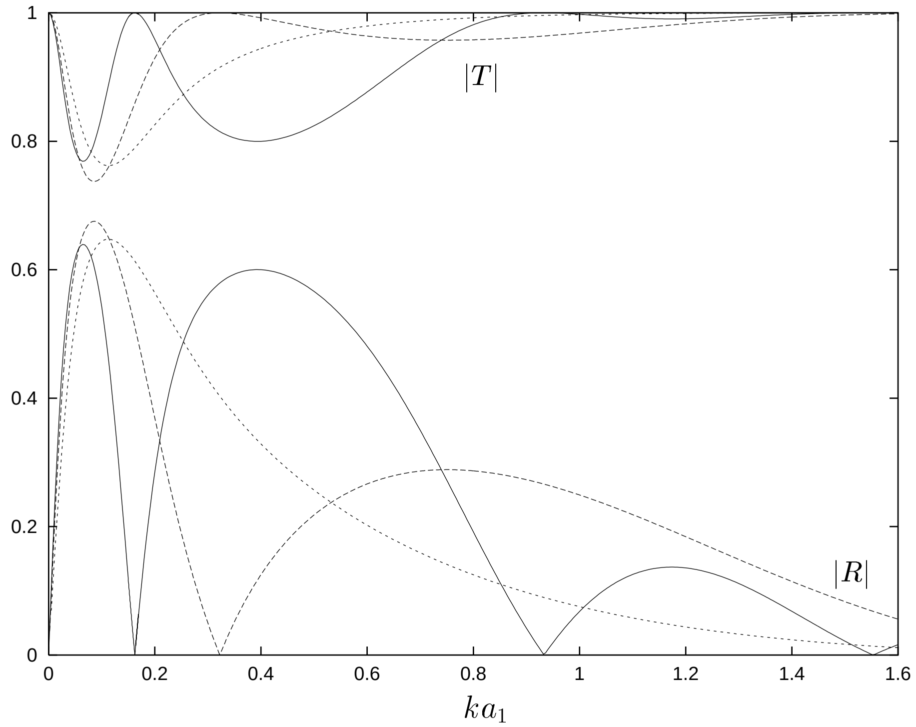

Figure 4.3: $|R|$, $|T|$ varying with ka_1 for two equal bottom-mounted barriers: $a_1/h = a_2/h = 0.1$; $2b/h = 0.5$ (——), 0.25 (– – –), 0.05 (- - - -).

the theory described in chapter 2. In fact it is easily shown that the modifications from the single to the two identical surface-piercing barriers involves simple factors of $(1 + \tanh \alpha_r h)$ and $(1 + \coth \alpha_r h)$ in the infinite series defining the elements of the matrices.

A wide range of different results and phenomena can be extracted in this problem due to the flexibility allowed in the choice of geometry. For example, if both barriers are chosen to be bottom-mounted and of equal length we confirm the existence of zeros of reflection discovered in the infinite depth version of this problem by Jarvis [32]. Curves demonstrating this are given in figure 4.3 where the barriers occupy nine-tenths of the depth and three different barrier separations are chosen. If the length of one of the barriers is altered slightly, these zeros vanish and are replaced by a minimum in $|R|$. In fact total reflection appears only to occur if the barriers are equal.

For two surface-piercing barriers we are able to reproduce the results of McIver [46] and confirm that zeros of transmission exist for any configuration of two surface-

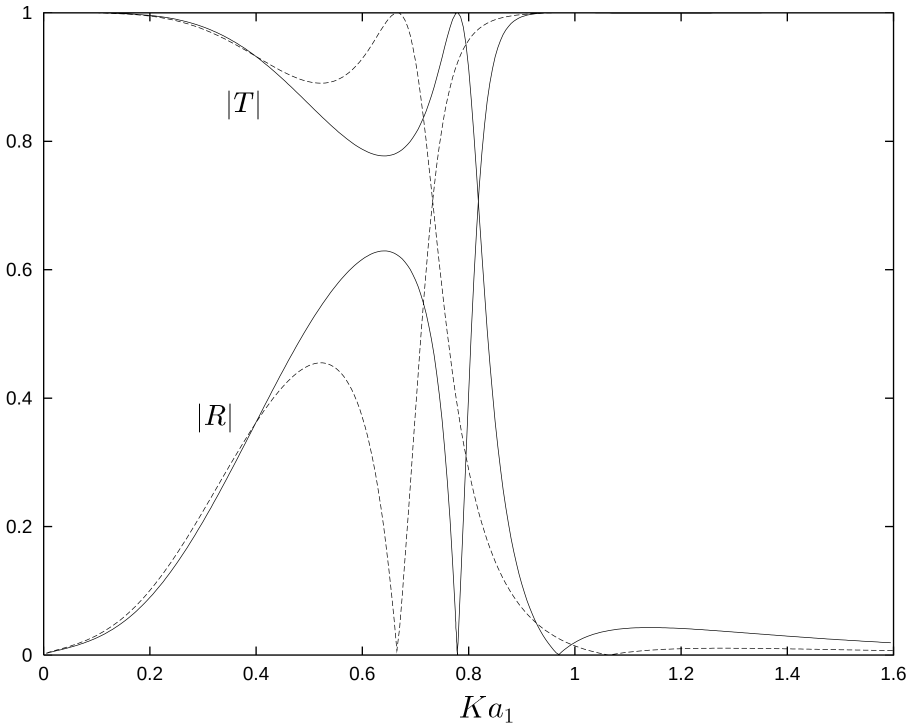

Figure 4.4: $|R|$, $|T|$ varying with Ka_1 for two equal surface-piercing barriers: $a_1/h = a_2/h = 0.1$; $2b/h = 0.1$ (——), 0.2 (– – –).

piercing barriers, whilst zeros of reflection appear only to occur if the barriers are equal. Typical curves showing the variation of $|R|$ and $|T|$ with Ka_1 where $a_1/h = a_2/h = 0.1$ due to normally-incident waves are given in figure 4.4 from which zeros of $|R|$, $|T|$ are clearly visible. When the waves are obliquely-incident upon equal surface-piercing barrier arrangements these zeros are still present. Figure 4.5 shows the variation of $|R|$, $|T|$ with θ, the angle of incidence for three different wavenumbers. Thus, for $ka_1 = 1$, the incident wave first undergoes total reflection then total transmission as θ is increased.

McIver [46] used matched eigenfunction expansions to obtain an infinite system of equations for the unknown coefficients in the expansions of the potential and, as he pointed out, the square root singularity at the tip of each barrier necessitated the use of large values of N, the truncation parameter, together with extrapolation, to achieve reasonable accuracy for R, T. To locate zeros in R or T he examined the phase of these complex coefficients, looking for values of dimensionless frequency at which the phase changes discontinuously by π radians as indicating a zero in R

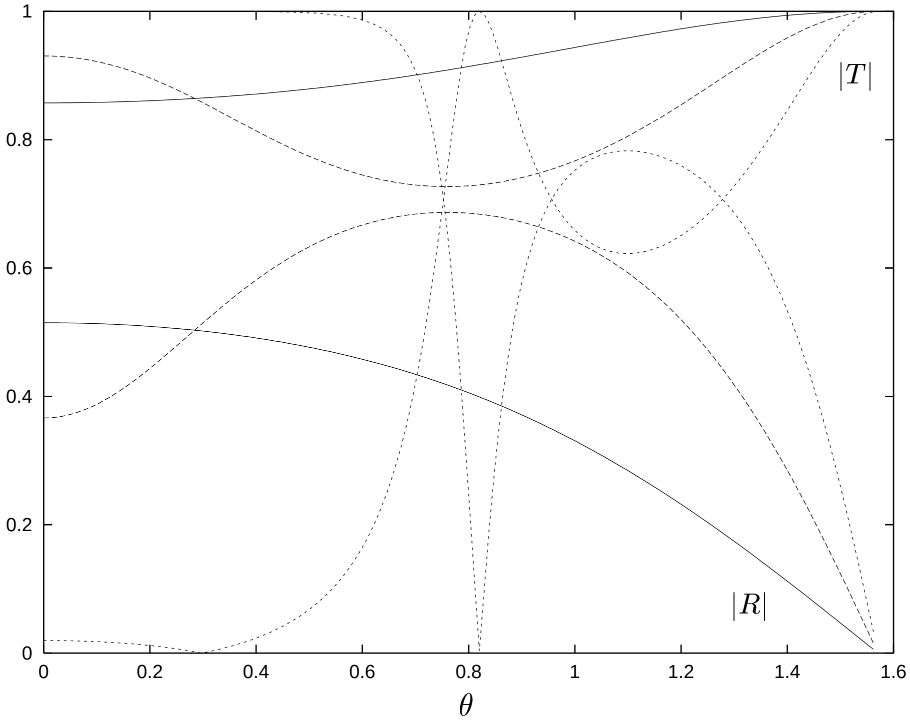

Figure 4.5: $|R|$, $|T|$ varying with incidence angle θ in the case of two equal surface-piercing barriers, $a_1/h = a_2/h = 0.1$, $2b/h = 0.1$: $ka_1 = 0.5$ (——), 0.75 (– – –), 1.0 (- - - -).

and T. He estimated that the frequencies so obtained had small errors in the third significant figure for the fundamental frequencies and in the fourth significant figure for the higher frequencies by choosing $N = 400$ and using extrapolation.

An alternative approach is used here in which the condition for a zero of R and T is expressed as an equation involving A^s and A^a each of which can be determined extremely accurately. Thus it is straightforward to show that the condition for $T = 0$, or $R^s = R^a$, reduces, using (4.3.9) and (4.3.10) to

$$f(\alpha b) = 2\mathrm{cosec} 2\alpha b - \alpha h((A^s)^{-1} - (A^a)^{-1}) = 0, \qquad (4.6.1)$$

whilst the condition for $R = 0$, or $R^s = -R^a$, reduces to

$$g(\alpha b) = A^s \cot \alpha b - A^a \tan \alpha b - \alpha h = 0. \qquad (4.6.2)$$

It is clear from the simplicity of the equations (4.6.1) and (4.6.2) that accurate estimates of the zeros of R, T, just as for the values of R, T themselves, depend purely on the accuracy with which A^s, A^a can be determined.

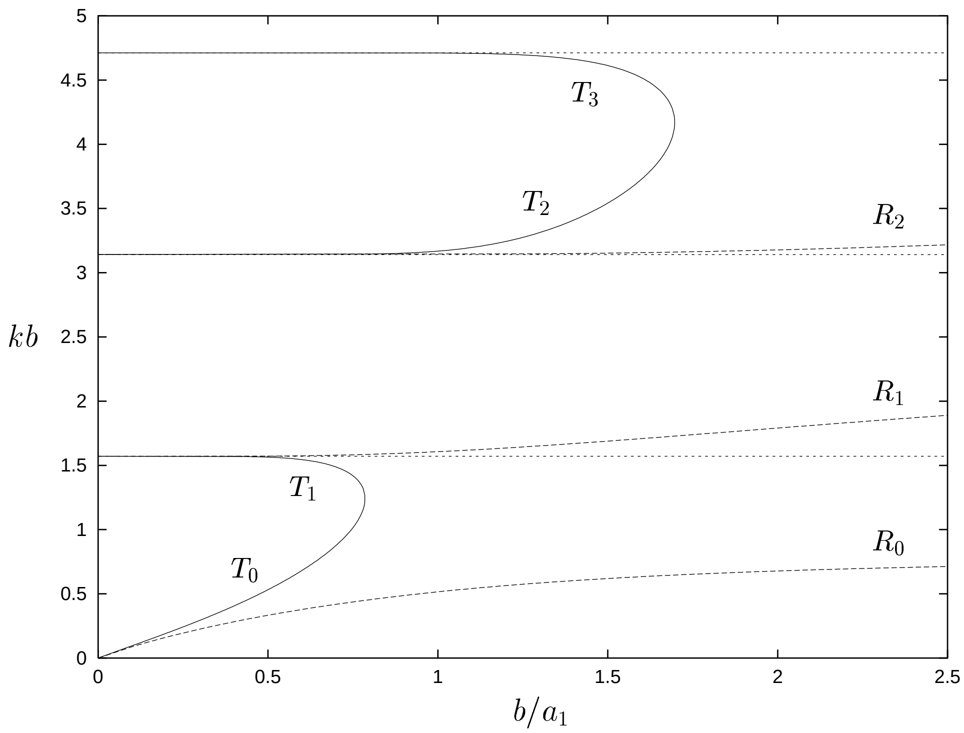

Figure 4.6: The variation of the frequencies associated with the zeros of transmission and reflection with the barrier spacing, b/a_1 for the case of two equal surface-piercing barriers, $a_1/h = a_2/h = 0.1$

The location of zeros of transmission and reflection in normally incident waves are shown in figure 4.6 in a reproduction of the curves of McIver [46]. Difficulties associated with convergence of the truncated system of equations arising from McIver's [46] matching of eigenfunctions hindered the computation of the curves in the area around the coalition of zeros of T. The accuracy of the method described in this chapter has permitted the completion of the curves in these regions. As already discussed in detail in McIver [46], there are an infinite sequence of zeros of both reflection and transmission, denoted in figure 4.6 by R_n and T_n occuring at increasing frequencies and each associated with natural modes of oscillation of the fluid between the barriers.

The least investigated of the possible barrier configurations consists of one barrier bottom-mounted and the other surface-piercing. Morris [55] considered this arrangement in the case of infinite depth qualitatively, and suggested that an infinite set of zeros of both transmission and reflection exist when there is an overlap.

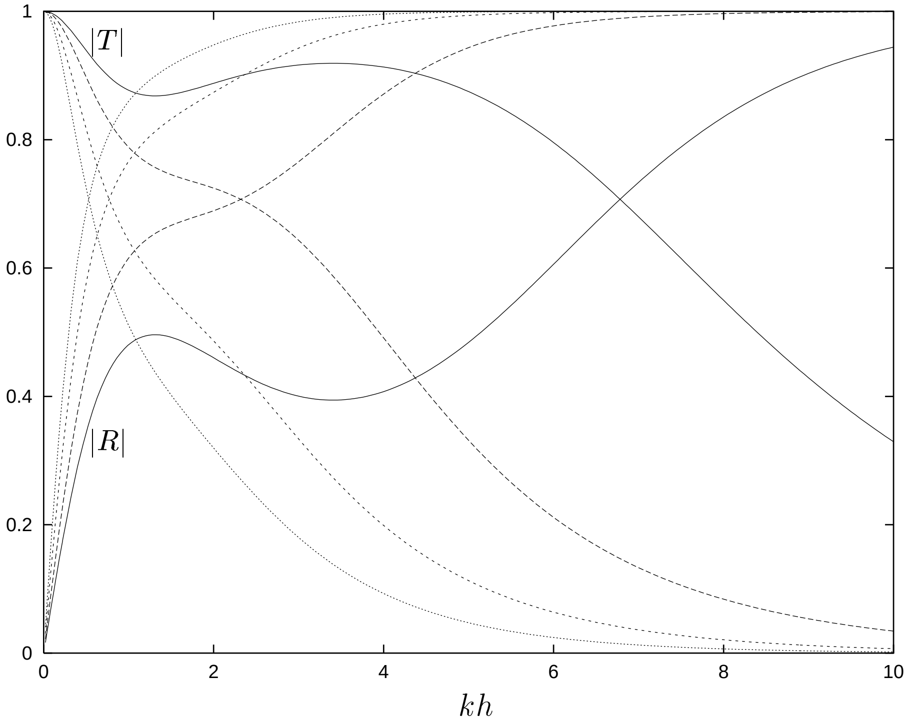

Figure 4.7: $|R|$, $|T|$ varying with kh for an unsymmetric barrier arrangement: $a_1/h = 0.2$ (upward); $2b/h = 0.1$; $a_2/h = 0.1$ (——), 0.2 (– – –), 0.3 (- - - -), 0.4 ($\cdots\cdots$) (all downward).

However, no quantitative results reinforcing this prediction were computed. Numerical experiments performed using our method confirm that zeros of transmission do indeed occur for an overlapping arrangement but suggest that zeros of reflection do not, in general, exist. Before considering this aspect of the problem we first discuss curves of $|R|$, $|T|$.

Figure 4.7 shows the behaviour of the reflection and transmission coefficients in an upward/downward-facing barrier configuration as the non-dimensionalised wavenumber kh is varied. Here, the bottom-mounted barrier and barrier separation are fixed at values of $a_1/h = 0.2$ and $b/h = 0.1$ whilst the submergence of the surface-piercing barrier is varied from 0.1 to 0.4. Thus, when $a_2/h = 0.1$, the barriers do not overlap and the curves exhibit a similar behaviour as in the problem of a single barrier with a gap (see figure 3.6). As the barrier is immersed further, increased reflection occurs at all values of kh. Although zeros of transmission are present in the curves of $a_2/h = 0.3$ and 0.4, they occur at large values of kh when

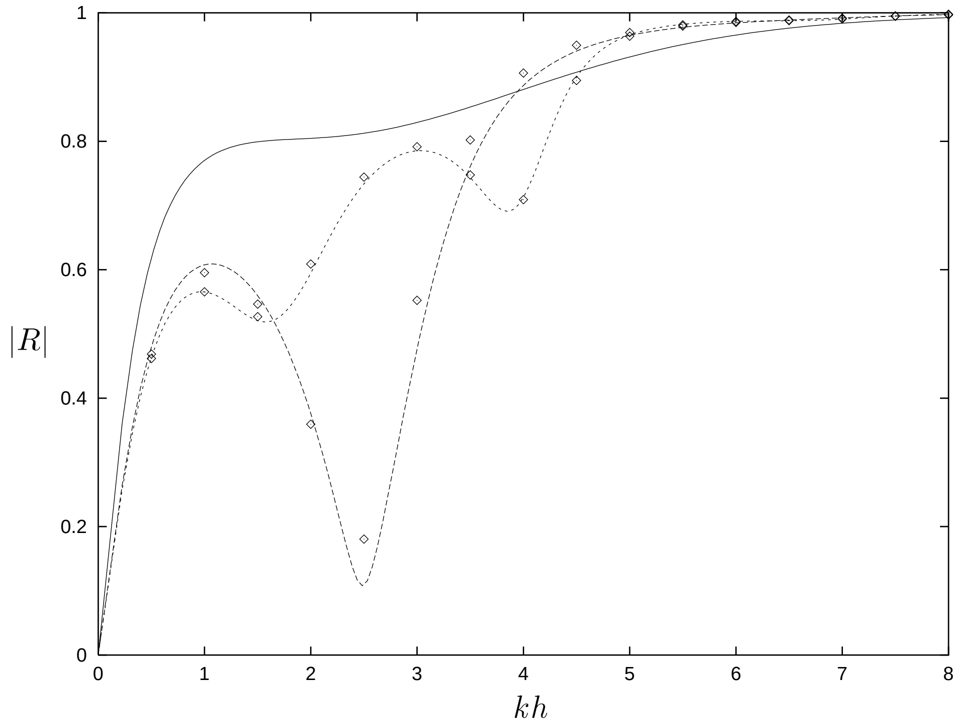

Figure 4.8: $|R|$ varying with kh for an unsymmetric barrier arrangement with $a_1/h = 0.2$ (upward), $a_2/h = 0.2$ (downward); $2b/h = 0.1$ (——), 0.5 (– – –), 1.0 (- - - -), wide-spacing(⋄).

the transmission is negligible and are not visible in figure 4.7.

Fixing the barrier lengths for an overlapping barrier arrangement and altering the separation gives the curves presented in figure 4.8. A comparison is made with the wide-spacing approximation using the expressions (4.4.4), (4.4.5) which require the reflection and transmission coefficients for each of the two barriers in isolation on the line $x = 0$. These are determined accurately using the methods of chapter 3. Good agreement between the results from the wide-spacing approximation and the full treatment of the problem is found for the spacing $2b/h = 1$, though for barrier separations smaller than this value significant discrepancies begin to creep in.

In figures 4.9 and 4.10 we compare the results from the full theory with those from the close-spacing approximation for an upward/downward overlapping configuration developed in §4.5. In figure 4.9 the dimensions of the upward-facing barrier and the separation are fixed with respect to the depth and the submergence of the surface-piercing barrier is varied from an overlapping arrangement to a scheme where there is

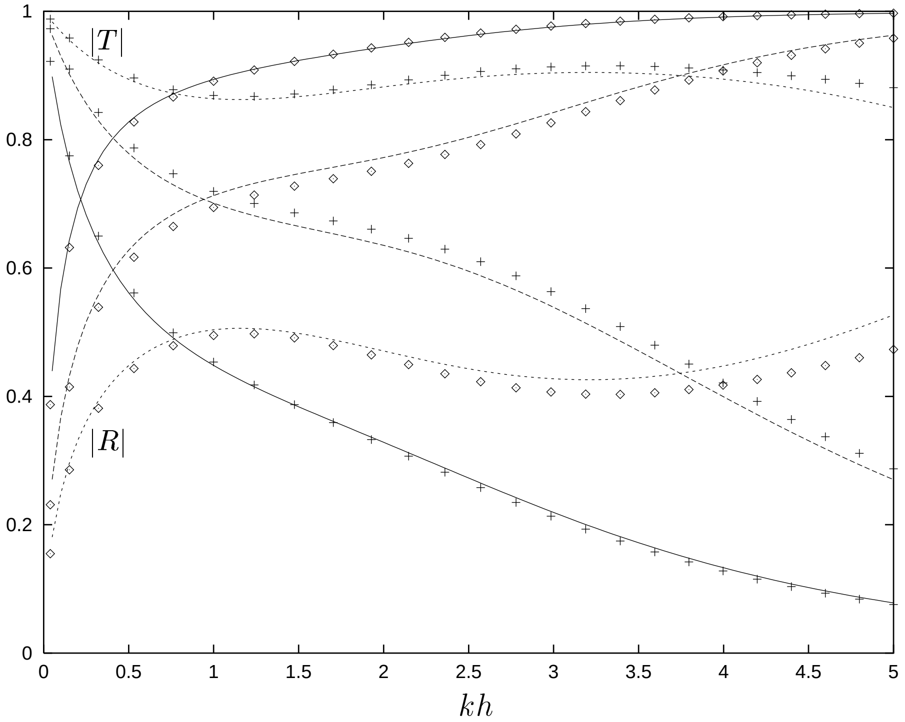

Figure 4.9: Comparison of full solution with close-spacing approximation for $2b/h = 0.05$, $a_1/h = 0.2$ (bottom-mounted): $a_2/h = 0.3$ (——), 0.2 (– – –), 0.1 (- - - -) (all surface-piercing); close-spacing ($+$, $\diamond$).

a gap between the upper edge of the upward-facing barrier and the lower edge of the downward-facing barrier. If there is an overlap agreement is good over all frequencies as expected. For no overlap, agreement is still good within the restrictions placed on the use of the method of matched asymptotic expansions, that is, when $k|a_2 - a_1|, kb << 1$.

In figure 4.10 the barrier lengths have been fixed with an overlap given by $(a_2 - a_1)/h = 0.1$ and the barrier separation varied. Thus, for a very close separation the curves from the two theories are almost indistinguishable. As the spacing increases, the close-spacing approximation becomes less effective, but is within 2% of the results from the full theory for $2b/h < 0.1$.

As mentioned earlier, it is possible to find zeros of transmission for the overlapping scheme whilst zeros of reflection do not appear to exist. The condition to be satisfied for zero transmission is found from consideration of (4.2.8), (4.2.31) to

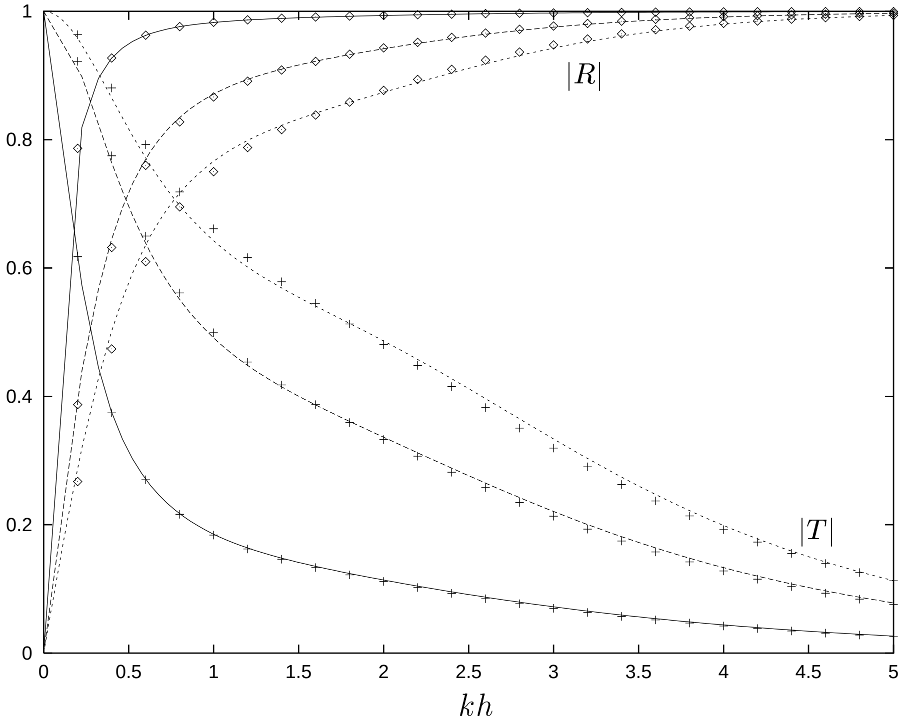

Figure 4.10: Comparison of full solution with close-spacing approximation for $a_1/h = 0.2$ (bottom-mounted), $a_2/h = 0.3$ (surface-piercing): $2b/h = 0.01$ (——), 0.05 (– – –), 0.1 (- - - -), close-spacing($+$, $\diamond$).

simply be

$$f(\alpha b) = S_{12}\alpha h \sin 2\alpha b - \Delta = T_{12}\alpha h \sin 2\alpha b + 1 = 0, \qquad (4.6.3)$$

where $\Delta = S_{11}S_{22} - S_{12}S_{21}$, in terms of both velocity and pressure difference formulations where we have used $\mathbf{S} = \mathbf{T}^{-1}$. In order to locate the zeros, a root-finding procedure is applied f. Figures 4.11 and 4.12 show the variation of non-dimensional wavenumber, kb, at which zeros of transmission occur first with barrier separation, and then in figure 4.12 with barrier overlap. As in the two surface-piercing barrier problem, for closely-spaced barriers the zeros are closely associated with the standing wave modes in a tank of width $2b$ with vertical sides. Since only one barrier intersects the free surface in this opposing barrier scheme, it is not intuitively clear why this should be. Figure 4.11 is incomplete due to numerical difficulties in finding zeros when the barriers only just overlap. Whilst not conclusive, the form of figures 4.11 and 4.12 adds weight to Morris's [55] conviction that an infinite set of zeros of transmission will exist if there is an overlap for any separation, whilst no

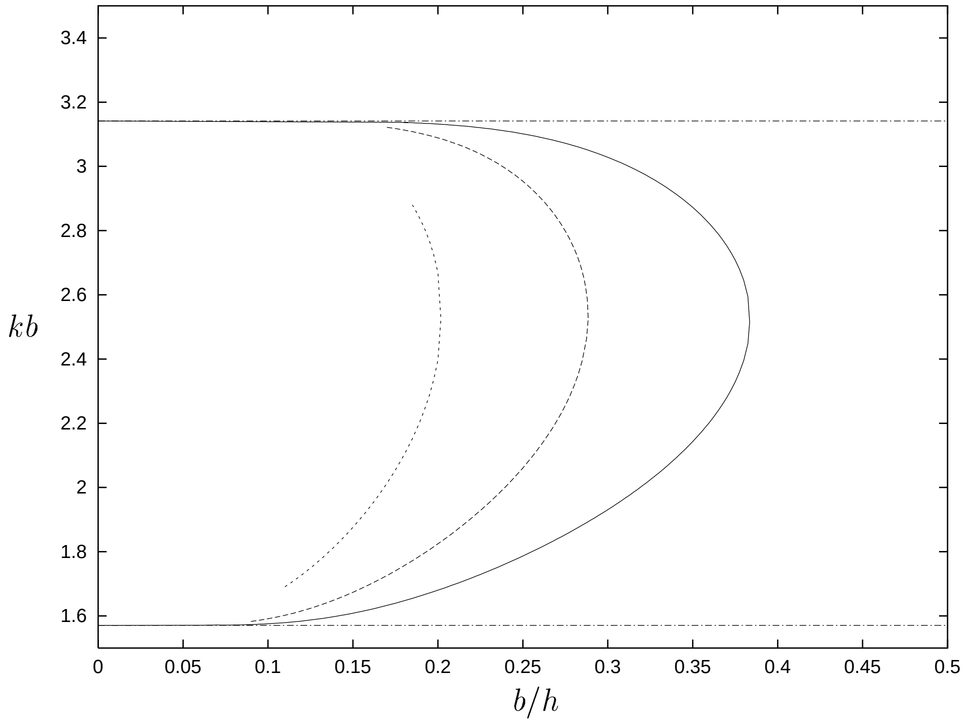

Figure 4.11: The variation of the wavenumbers associated with the zeros of transmission with barrier separation, b/h, with $a_1/h = 0.2$ (upward); 0.5 (——), 0.4 (– – –), 0.3 (- - - -) (all downward).

overlap implies no zeros. The close-spacing approximation can give no information in this aspect of the problem since from (4.5.20), the source strength m would have to be zero for $|T| = 0$ and this would be equivalent to no flow through the barriers. Inspection of (4.5.18) reveals that the numerator is always strictly negative whilst the denominator can never be infinite since all the terms contributing to the denominator are bounded.

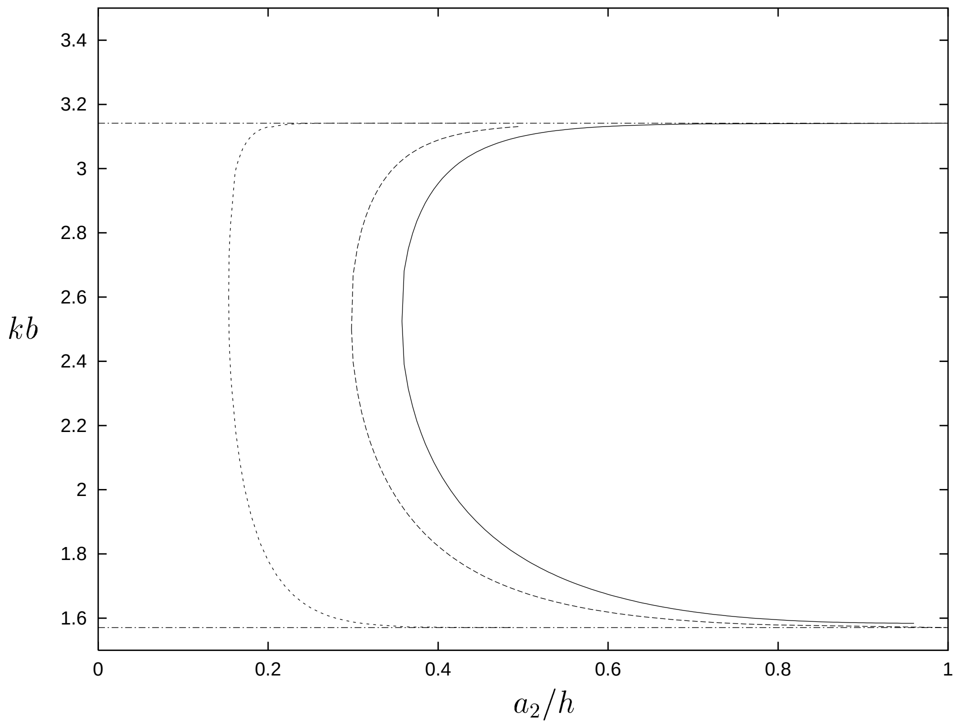

Figure 4.12: The variation of the wavenumbers associated with the zeros of transmission with barrier submergence, a_2/h, with $a_1/h = 0.1$ (upward); $2b/h = 0.5$ (——), 0.4 (– – –), 0.1 (- - - -) (all downward).

Chapter 5

Two Oscillating-Water-Column Wave-Energy Devices

5.1 Introduction

During the 1970's and the early 1980's there was considerable worldwide interest in harnessing energy from natural renewable sources, brought about by fears of rapidly decreasing oil and gas reserves and climaxing in the oil crisis of 1973. An obvious source of natural reliable energy is provided by the motion of the seas and has resulted in the development of many ingenious devices for the extraction of power from the waves. In this chapter we consider two such devices, both based on the principle of the oscillating water column (OWC) in which the oscillatory motion of the fluid inside an open-ended duct due to an incident wave is used as the 'piston' for producing power. Many variations of wave-energy device using the OWC principle have been proposed, some totally submerged and some partially immersed. The classic design of OWC wave-energy device, and the type we consider here, has one end of the duct piercing the water and the other open to the atmosphere. It does not rely on contact of the surface of the water with a rigid piston for power take-off, but uses the oscillatory motion of the water inside the device to pump the volume of air above the free surface through a constriction containing a uni-directional air turbine of the Wells-type.

The theme of thin barriers is continued in this chapter by a choice of devices both of which involve thin vertical surface-piercing walls. Whereas in previous chapters the aim of the problem has been to provide expressions for the far-field scattered wave amplitudes, the performance prediction of an OWC additionally requires a means of calculating accurately the induced volume flow rate across the internal mean free surface of the device. The two devices we choose to model in this chapter have previously been investigated in some detail by Smith [68] and Thomas [69]. The novelty in the work that follows is in the adaptation of the methods of the previous chapters in determining all the hydrodynamic coefficients necessary to predict to performance of the OWC. This is discussed in more detail later.

The first designs for wave energy converters relied on the relative motion of large rigid bodies, the coupling between the bodies being exploited to extract the energy. A theory to predict characteristics of rigid-body motion was developed as a result of work by Evans [12], Mei [50], Newman [59], and Budal & Falnes [5], aiding the design elements and performance prediction of wave-energy devices such as the Salter duck, the Cockerell articulated raft and the Bristol submerged cylinder.

Clearly, the OWC does not come under the regime of rigid-body theory but in the absence of a better theory, attempts at applying it were nevertheless made. Thus, an application of the rigid-body theory to a simple OWC model was provided by Evans [14]. More generally it was argued that in long waves at least the internal fluid motion could indeed be regarded as a solid mass with the free surface acting as a light rigid piston. This required attributing a value to the 'added mass' of this body of fluid. Falcão & Sarmento [26] sought to improve on this model of an OWC by allowing for the increased pressure on the free surface and for the possibility of a non-plane wave surface. This work was generalised by Evans [15] who provided a general theory for any number of fixed rigid bodies each enclosing an internal free surface experiencing a variable pressure. He showed that there existed a parallel with the rigid-body motion provided the ideas of exciting force on fixed bodies and the given velocities of moving bodies were replaced by the ideas of volume flux across the internal free surfaces open to the atmosphere and the given forcing pressures on those free surfaces respectively. A further generalisation was provided by Falnes & McIver [25] who, in addition to the internal pressure distribution, allowed the possibility of motion of the rigid bodies also.

Two applications of these ideas to OWC models were made by Smith [68] and Thomas [69]. The latter investigated the performance aspects of an OWC device consisting of an open-ended thin-walled circular cylinder partially immersed in an ocean of finite depth. Smith [68] considered a two-dimensional model with the internal free surface contained between a vertical wall and a partially immersed vertical barrier also in finite depth water. Both authors used a method of matching eigenfunction expansions to solve the boundary-value problems which occur.

Being able to solve such problems both accurately and efficiently is clearly important in itself. If, in addition, a more accurate model of the non-linear aspects of the energy conversion such as the power take-off mechanism (for which the theory of Evans [15] assumes the turbine has linear characteristics) is required or if an optimal control is to be applied to the overall system, it is necessary to operate in the time-domain rather than the frequency-domain. Crucial to such time-domain modelling is a convolution-type integral which represents the 'memory' of the fluid and which contains a kernel function which is essentially a sine or cosine transform of a function in the frequency-domain. This function, which in a rigid-body model would just be the radiation damping, and which in a pressure distribution model is related to the induced volume flux across the internal free surface, needs to be computed accurately *at all frequencies* from the steady-state frequency-domain problem. Furthermore, in any systematic optimisation procedure involving a variation in geometric and power take-off parameters, it will be important to have an accurate and efficient method for repeated calculation of this function. Also required in the time-domain model is the high-frequency behaviour of the rigid-body equivalent of the added mass coefficient, again related to the induced volume flux in the pressure distribution model.

In section 5.2 the general theory of oscillating pressure distributions due to Evans [15] is simplified to just one internal free surface showing how the total solution can be found in terms of a *scattering* problem where the internal free surface of the device suffers no increased pressure and a *radiation* problem that includes the increased pressure but omits any incoming waves.

The two-dimensional OWC device is treated in section 5.3. It consists of a thin vertical lip a distance b from a wall extending vertically to the sea bottom. We derive two 'complementary' formulations of the problem, each requiring the solution of both scattering and radiation problems and the subsequent application of a Galerkin approximation to the resulting integral equations. The first formulation constructs singular integral equations for functions related to the unknown horizontal fluid velocity across the gap under the barrier. It can then be shown that all the necessary hydrodynamic coefficients arising from the problem can be expressed in terms of a 2×2 matrix, $\mathbf{S}$, with entries being weighted integrals involving the unknown velocity functions. As was shown in chapter 2, Galerkin's method lends itself to approximating such systems and we use the functions introduced in §3.2 for the scattering by a single surface-piercing barrier. Another formulation based on the pressure difference across the barrier is also described and, whilst being slightly more difficult to implement, results in a similar outcome to the velocity formulation, the information for the problem now contained within a 2×2 matrix, $\mathbf{T}$. It is shown how the various reciprocal relations known to exist between the hydrodynamic coefficients are in fact satisfied identically by this matrix development whereas in the method of matching eigenfunction expansions described in Thomas [69] and Smith [68] they are used as a check on numerics. Results are given showing the rapid convergence of the approximation to the entries of the matrices $\mathbf{S}$ and $\mathbf{T}$ as the truncation size N is increased. They also confirm that the approximations are bounded above, a fact we are able to prove, although this will not in general result in bounds on the important hydrodynamic coefficients. Some typical curves are also presented agreeing with those given in Smith [68].

The second half of this chapter is concerned with a fully three-dimensional problem of the performance of an OWC device consisting of a partially-immersed thin-walled circular cylinder excited by a train of parallel-crested waves. Once again, the problem is decomposed into scattering and radiation problems. Despite the inclusion of an extra dimension, the resulting formulation is just as simple as the two-dimensional OWC model and all comments concerning the previous problem are equally applicable to this model. To avoid unnecessary complication we omit the rather tricky development of the pressure difference formulation although here too it turns out that it can be successfully implemented. Results show good accuracy even for small N and curves are presented agreeing with Thomas [69].

5.2 Theory of pressure distributions

The general theory of chapter 2 assumes a constant atmospheric pressure, p_a, across the entire free surface of the fluid. For an oscillating water column wave-energy device such as those described in the introduction we expect the internal free surface of the device to be subjected to an oscillating pressure having the same period, ω, as the incident wave. In a rather complicated paper by Evans [15], the general theory is constructed for the problem of an arbitrary number of such oscillating pressure distributions and the interactions between them with a view to wave-energy absorption from multiple OWC wave-energy devices. In this section his theory is simplified for the case of just one device and subsequently developed for the specific examples dealt with in this chapter.

The device consists of walls enclosing an internal free surface (denoted by S_i) which is subjected to an oscillating pressure distribution of $p_a + P(t)$, where $P(t)$ has the same frequency, ω, as the incident wave and we assume that the horizontal pressure variation across S_i is negligible. There is a constant atmospheric pressure, p_a, above the external free surface, denoted by S_e. Once again we will be working in constant water depth h and much of the theory of chapter 2 is relevant in what follows.

Under the assumptions of linear water-wave theory there exists a velocity potential, $\Phi(x,y,z,t)$ satisfying

$$\nabla^2\Phi = 0, \quad \text{in the fluid,} \tag{5.2.1}$$

$$\Phi_n = 0, \quad \text{on solid boundaries,} \tag{5.2.2}$$

where the suffix n denotes the normal derivative, whilst the linearised free-surface condition becomes

$$g\zeta - \frac{\partial\Phi}{\partial t} = \begin{cases} (p_a + P(t))/\rho, & \text{on } S_i, \\ p_a/\rho, & \text{on } S_e, \end{cases} \tag{5.2.3}$$

where ρ is the density of the fluid and where $\zeta(x,z,t)$ is the surface elevation measured downwards and is related to the velocity potential through

$$\frac{\partial\zeta}{\partial t} = \frac{\partial\Phi}{\partial y}, \quad \text{on } y = 0\,. \tag{5.2.4}$$

It is assumed that the motion is time-harmonic with angular frequency ω and so we introduce the time-independent quantities ϕ, p, η by

$$\Phi(x,y,z,t) = \mathrm{Re}\{\phi(x,y,z)\mathrm{e}^{-i\omega t}\},\ P(t) = \mathrm{Re}\{p\mathrm{e}^{-i\omega t}\},\ \zeta(x,z,t) = \mathrm{Re}\{\eta(x,z)\mathrm{e}^{-i\omega t}\}. \tag{5.2.5}$$

On combining (5.2.1)–(5.2.5) above in much the same manner as in chapter 2, we find that the problem can now be expressed in terms of the time-independent velocity potential, ϕ, satisfying the following:

$$\nabla^2\phi = 0, \quad \text{in the fluid,} \tag{5.2.6}$$

$$\phi_n = 0, \quad \text{on solid boundaries,} \tag{5.2.7}$$

with

$$K\phi + \frac{\partial\phi}{\partial y} = \begin{cases} -i\omega p/\rho g, & \text{on } S_i, \\ 0, & \text{on } S_e, \end{cases} \tag{5.2.8}$$

where $K = \omega^2/g$. A suitable radiation condition must also be enforced.

Following the method of Evans [15] we decompose the potential into two parts such that

$$\phi = \phi^S - \frac{i\omega p}{\rho g}\phi^R, \tag{5.2.9}$$

where ϕ^S is the potential associated with the scattering of an incident wave of unit amplitude from infinity in the absence of a pressure variation on S_i and satisfies (5.2.6)–(5.2.8) with $p = 0$. Here, ϕ^R is the potential describing the flow due to an oscillating pressure on S_i in the absence of an incident wave and satisfies (5.2.6), (5.2.7) with (5.2.8) replaced by

$$K\phi^R + \frac{\partial \phi^R}{\partial y} = \begin{cases} 1, & \text{on } S_i, \\ 0, & \text{on } S_e. \end{cases} \tag{5.2.10}$$

We call the boundary-value problem defined by (5.2.6), (5.2.7) and (5.2.10) the radiation problem.

We expect that the amount of power that may be extracted by the device to depend on the induced volume flux across the internal free surface of the device, S_i. We call this quantity $Q(t)$ and the time dependence can be removed by writing $Q(t) = \mathrm{Re}\{q\mathrm{e}^{-i\omega t}\}$. Then

$$\begin{aligned} q &= -\int_{S_i} \frac{\partial \phi}{\partial y}\,\mathrm{d}S \\ &= q^S - \frac{i\omega p}{\rho g} q^R, \quad \text{say,} \end{aligned} \tag{5.2.11}$$

where q^S, q^R are the induced volume fluxes across S_i in the scattering and radiation problems respectively and are defined by

$$q^{S,R} = -\int_{S_i} \frac{\partial \phi^{S,R}}{\partial y}\mathrm{d}S. \tag{5.2.12}$$

Following Evans [15] we make the convenient but arbitrary decomposition of the volume flux due to the radiation potential, thus

$$-\frac{i\omega p}{\rho g} q^R = -(\tilde{B} - i\tilde{A})p, \tag{5.2.13}$$

where $\tilde{A}$ and $\tilde{B}$ are real and directly analogous to the added mass and radiation damping coefficients in a rigid-body system. By analogy with electric circuit theory, and following Falnes & McIver [25], we shall call the complex quantity $\tilde{B} - i\tilde{A}$ the radiation admittance with $\tilde{B}$ the radiation conductance and $\tilde{A}$ the radiation susceptance. Clearly

$$\tilde{A} = -\frac{\omega}{\rho g}\mathrm{Re}\{q^R\} \tag{5.2.14}$$

$$\tilde{B} = -\frac{\omega}{\rho g}\mathrm{Im}\{q^R\}. \tag{5.2.15}$$

The mean rate of working of the pressure force, or the mean power absorbed per unit area of the pressure distribution on S_i, W, is the time average of the pressure and the volume flux over a period of oscillation. In other words, we write

$$\begin{aligned} W &= \tfrac{1}{2}\mathrm{Re}\{\overline{p}q\} \\ &= \tfrac{1}{2}\mathrm{Re}\{\overline{p}q^S\} - \tfrac{1}{2}|p|^2\tilde{B} \\ &= \frac{|q^S|^2}{8\tilde{B}} - \frac{\tilde{B}}{2}\left|p - \frac{q^S}{2\tilde{B}}\right|^2, \end{aligned} \tag{5.2.16}$$

where the bar denotes the complex conjugate. This takes a maximum value of

$$W_{max} = \frac{|q^S|^2}{8\tilde{B}}, \tag{5.2.17}$$

when

$$p = \frac{q^S}{2\tilde{B}}. \tag{5.2.18}$$

The proportion of available power per unit frontage of the incident wave which extracted from the device, which we call the maximum efficiency of power absorption, is

$$\eta_{max} = \frac{W_{max}}{P_w}, \tag{5.2.19}$$

where P_w is the power per unit frontage of the incident wave (that is, the mean energy flux per unit length across a vertical plane normal to the wave direction) and is given by

$$P_w = \rho g K k h / 2\omega, \tag{5.2.20}$$

when the incident wave is represented by $\phi_{inc}(x, y) = \mathrm{e}^{\pm ikx}\psi_0(y)$.

The maximum efficiency can only occur under the condition (5.2.18). In practice it is difficult to control the pressure drop across the turbine, but it may be easier to control the volume flow rate across through the turbine. If we assume that these two quantities are related linearly and that the turbine characteristics do not allow a phase lag between the pressure and the volume flux to develop, then we may write

$$q = \Lambda p, \tag{5.2.21}$$

where Λ is a real positive control parameter. Hence, $[\Lambda + (\tilde{B} + i\tilde{A})]p = q^S$ and so

$$W = \frac{|q^S|^2}{8\tilde{B}} \left\{ 1 - \frac{|\Lambda - (\tilde{B} + i\tilde{A})|^2}{|\Lambda + (\tilde{B} + i\tilde{A})|^2} \right\}, \tag{5.2.22}$$

which has a maximum value of

$$W_{max} = \frac{|q^S|^2}{8\tilde{B}} \left\{ 1 - \frac{\Lambda_{opt} - \tilde{B}}{\Lambda_{opt} + \tilde{B}} \right\} \tag{5.2.23}$$

when $\Lambda = \Lambda_{opt}$ where

$$\Lambda_{opt} = (\tilde{B}^2 + \tilde{A}^2)^{1/2}. \tag{5.2.24}$$

The resulting maximum efficiency is then given by

$$\eta_{max} = \frac{|q^S|^2}{4P_w} \cdot \frac{1}{\Lambda_{opt} + \tilde{B}}. \tag{5.2.25}$$

Details of the derivation of the above theory can also be found in Evans [15] or Smith [68].

Before proceding to the solution to the two OWC problems that form the remainder of this chapter, we will use the specific geometry of the problem to derive important reciprocal relations between the various hydrodynamical coefficients arising from each problem. These are again basic results derived in Evans [15], which we tailor in accordance with our chosen specification of each of the two problems. The basis for these relations stems from the use of certain choices for harmonic functions ϕ, ψ in Green's second identity which states that

$$\int_{S_c} \phi \frac{\partial \psi}{\partial n} - \psi \frac{\partial \phi}{\partial n} \, \mathrm{d}S = 0, \tag{5.2.26}$$

where S_c is a closed contour in two dimensions or a closed surface in three dimensions and n denotes the *inward* normal.

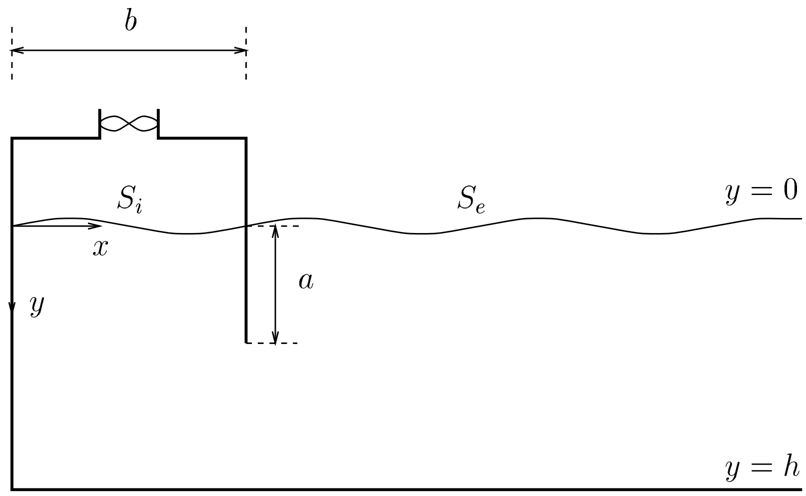

Figure 5.1: Definition sketch.

5.3 A two-dimensional OWC device

Cartesian co-ordinates are chosen with the mean free surface $y = 0$. The fluid occupies $0 < y < h$, $0 < x < \infty$ and the OWC device consists of a thin vertical barrier immersed to a depth a below the free surface a distance b from the wall at $x = 0$, as shown in figure 5.1. The internal and external free surfaces are given by $S_i = \{x, y : \ y = 0, \ 0 < x < b\}$ and $S_e = \{x, y : \ y = 0, \ b < x < \infty\}$ respectively and we denote the barrier by $L_b = [0, a]$ and the gap under the barrier by $L_g = [a, h]$.

The far field behaviour of the radiation and scattering potentials may be written as

$$\left.\begin{aligned} \phi^R(x,y) &\sim A^R \mathrm{e}^{ik(x-b)} \psi_0(y) \\ \phi^S(x,y) &\sim (\mathrm{e}^{-ik(x-b)} + R^S \mathrm{e}^{ik(x-b)}) \psi_0(y) \end{aligned}\right\} \quad \text{as } x \to \infty, \tag{5.3.27}$$

where A^R and R^S are the outgoing wave amplitudes in each problem. Using the functions ϕ^R and $\overline{\phi^R}$ (the conjugate of ϕ^R) in Green's second identity, (5.2.26), with the closed contour $S_c = S_i \cup S_e \cup S_b \cup S_\infty$ where S_b denotes rigid boundaries (including the barrier) and $S_\infty = \{x, y : \ y \in [0, h], \ x \to \infty\}$, we find that

$$\begin{aligned} \frac{1}{K} \int_{S_i} \overline{\frac{\partial \phi^R}{\partial y}} - \frac{\partial \phi^R}{\partial y} \ \mathrm{d}S &= \lim_{x \to \infty} \int_0^h \phi^R \overline{\frac{\partial \phi^R}{\partial x}} - \overline{\phi^R} \frac{\partial \phi^S}{\partial x} \ \mathrm{d}y \\ &= -2ikh|A^R|^2, \end{aligned} \tag{5.3.28}$$

the only contributions to the integral having come from the line segments S_i and S_∞. From (5.2.12), (5.2.15) the relationship between the radiation conductance and the far-field radiated amplitude can easily be verified to be

$$\tilde{B} = \frac{\omega}{\rho g} kKh|A^R|^2. \tag{5.3.29}$$

If we now use the functions ϕ^S and ϕ^R in (5.2.26) with S_c as above, it appears that

$$-\frac{1}{K}\int_{S_i} \frac{\partial \phi^S}{\partial y}\,\mathrm{d}S = 2ikhA^R, \tag{5.3.30}$$

where the contributions to S_c have come from S_i and S_∞ as before. Thus

$$q^S = 2ikKhA^R, \tag{5.3.31}$$

provides a simple relation between quantities arising from the scattering and radiation problems. This can be compared with a similar relation, due to Haskind, which exists between the exciting force on a fixed body in waves and the amplitude of the waves radiated by the corresponding forced motion of the same body. See, for example, Newman [59]. Combining (5.3.29) and (5.3.31) gives

$$\tilde{B} = \frac{\omega}{4\rho g kKh}|q^S|^2 = \frac{|q^S|^2}{8P_w}, \tag{5.3.32}$$

from (5.2.20) so that

$$\eta_{max} = \frac{2\tilde{B}}{\Lambda_{opt} + \tilde{B}}. \tag{5.3.33}$$

Using ϕ^S and $\overline{\phi^S}$ gives the expected result of $|R^S| = 1$ since all incident wave energy must be reflected in the scattering problem.

5.3.1 Velocity formulation

We first examine a method of solution based on the formulation of a pair of integral equations for functions relating to the fluid velocity under the barrier at $x = b$. In a later section, the problem is reformulated in terms of a different pair of integral equations in unknown functions that are proportional to the pressure difference across the barrier. The former approach is, however, the more natural way to solve the problem since we notice that the induced volume flux is related to the horizontal component of velocity under the barrier by

$$q^{S,R} = -\int_{S_i} \frac{\partial \phi^{S,R}}{\partial y} \mathrm{d}S = -\int_{L_g} \left.\frac{\partial \phi^{S,R}}{\partial x}\right|_{x=b} \mathrm{d}S, \tag{5.3.34}$$

using continuity of flux arguments. There is no such natural way of expressing the volume flux in terms of the pressure difference across the barrier, but as we will find later, there is an artificial way round this.

The radiation problem

With $\psi_n(y)$, k_n defined by (2.16), (2.14) we may write the radiation potential in $0 < x < b$ as

$$\phi^R(x,y) = B_0^R \cos kx\psi_0(y) + \sum_{n=1}^{\infty} B_n^R \cosh k_n x\psi_n(y) + K^{-1}, \tag{5.3.35}$$

and in $x > b$

$$\phi^R(x,y) = A^R \mathrm{e}^{ik(x-b)}\psi_0(y) + \sum_{n=1}^{\infty} A_n^R \mathrm{e}^{-k_n(x-b)}\psi_n(y), \tag{5.3.36}$$

such that (5.2.6), (5.2.7), and (5.3.27) are satisfied and where the term K^{-1} in (5.3.35) is included to satisfy (5.2.10), the free surface condition. The continuity of the potential and velocity across L_g and the no-flow condition on L_b still need to be imposed. Let

$$U^R(y) \equiv \left.\frac{\partial \phi^R}{\partial x}\right|_{x=b} = ikA^R\psi_0(y) - \sum_{n=1}^{\infty} k_n A_n^R \psi_n(y) \tag{5.3.37}$$

$$= -kB_0^R \sin kb\psi_0(y) + \sum_{n=1}^{\infty} k_n B_n^R \sinh k_n b\psi_n(y). \tag{5.3.38}$$

Using the orthogonality of the ψ_n 's we obtain

$$ikA^R = -kB_0^R \sin kb = \frac{1}{h}\int_{L_g} U^R(y)\psi_0(y)\,\mathrm{d}y = U_0^R, \tag{5.3.39}$$

$$-k_n A_n^R = k_n B_n^R \sinh k_n b = \frac{1}{h}\int_{L_g} U^R(y)\psi_n(y)\,\mathrm{d}y = U_n^R, \quad n \geq 1, \tag{5.3.40}$$

where the fact that $U^R(y) = 0$, $y = L_b$ has been used, so that

$$U^R(y) = \sum_{n=0}^{\infty} U_n^R \psi_n(y). \tag{5.3.41}$$

Let the jump in potential across $x = b$ be defined by $P^R(y) \equiv [\phi]_{x=b}$. Then

$$\begin{aligned} P^R(y) &= (A^R - B_0^R \cos kb)\psi_0(y) - K^{-1} + \sum_{n=1}^{\infty}(A_n^R - B_n^R \cosh k_n b)\psi_n(y) \\ &= A^R(1 + i\cot kb)\psi_0(y) - K^{-1} - \sum_{n=1}^{\infty} \frac{U_n^R}{k_n}(1 + \coth k_n b)\psi_n(y). \end{aligned} \tag{5.3.42}$$

Using continuity of potential, $P^R(y) = 0$ for $y \in L_g$, and (5.3.40) in (5.3.42) we obtain

$$\int_{L_g} U^R(t)K(y,t)\,\mathrm{d}t = -K^{-1} + A^R(1 + i\cot kb)\psi_0(y), \tag{5.3.43}$$

where

$$K(y,t) = \sum_{n=1}^{\infty} \frac{(1 + \coth k_n b)}{k_n h}\psi_n(y)\psi_n(t). \tag{5.3.44}$$

We now write $U^R(t)$ as the combination of two functions $u_1(t)$, $u_2(t)$ in the form

$$U^R(t) = -K^{-1}u_1(t) + A^R(1 + i\cot kb)u_2(t). \tag{5.3.45}$$

Hence, if $u_1(t)$, $u_2(t)$ satisfy

$$\int_{L_g} u_1(t)K(y,t)\,\mathrm{d}t = 1, \quad y \in L_g, \tag{5.3.46}$$

$$\int_{L_g} u_2(t)K(y,t)\,\mathrm{d}t = \psi_0(y), \quad y \in L_g, \tag{5.3.47}$$

then $U^R(t)$ defined by (5.3.45) will satisfy (5.3.43). We write the above as

$$\int_{L_g} u_i(t)K(y,t)\mathrm{d}t = d_i(y), \quad i = 1,2, \quad \text{with } d_i(y) = \begin{cases} 1, & i = 1, \\ \psi_0(y), & i = 2, \end{cases} \tag{5.3.48}$$

and define the 2×2 matrix $\mathbf{S}$ by

$$S_{ij} = \int_{L_g} u_i(t)d_j(t)\,\mathrm{d}t, \quad i,j = 1,2. \tag{5.3.49}$$

Now from (5.3.39)

$$ikhA^R = \int_{L_g} U^R(y)\psi_0(y)\,\mathrm{d}y = -K^{-1}S_{12} + A^R(1 + i\cot kb)S_{22}, \tag{5.3.50}$$

after use of (5.3.45) and (5.3.49), yielding

$$A^R = \frac{K^{-1}S_{12}}{(1 + i\cot kb)S_{22} - ikh}, \tag{5.3.51}$$

on rearrangement. Also, from (5.3.34)

$$q^R = -\int_{L_g} U^R(y)\,\mathrm{d}y = K^{-1}S_{11} - A^R(1 + i\cot kb)S_{21}, \tag{5.3.52}$$

where (5.3.45), (5.3.49) have been used. Substituting from (5.3.51) and simplifying gives

$$q^R = \frac{K^{-1}\{(1 + i\cot kb)\Delta - ikhS_{11}\}}{(1 + i\cot kb)S_{22} - ikh}, \tag{5.3.53}$$

where $\Delta = S_{11}S_{22} - S_{12}S_{21}$.

The scattering problem

This problem is identical to the symmetric part of the problem of the scattering of waves by two equally-submerged surface-piercing barriers in finite depth covered briefly in chapter 4.

The general scattering potential can be written in $0 < x < b$ as

$$\phi^S(x, y) = B_0^S \cos kx\psi_0(y) + \sum_{n=1}^{\infty} B_n^S \cosh k_n x\psi_n(y), \tag{5.3.54}$$

and in $x > b$ as

$$\phi^S(x, y) = (\mathrm{e}^{-ik(x-b)} + R^S\mathrm{e}^{ik(x-b)})\psi_0(y) + \sum_{n=1}^{\infty} A_n^S\mathrm{e}^{-k_n(x-b)}\psi_n(y), \tag{5.3.55}$$

whereby all that remains to be satisfied are the conditions on $x = b$. This leads to the following integral equation for the unknown horizontal velocity, $U^S(y)$, across the gap under the barrier

$$\int_{L_g} U^S(t)K(y,t)\,\mathrm{d}t = \{(R^S + 1) + i\cot kb(R^S - 1)\}\psi_0(y), \quad y \in L_g, \tag{5.3.56}$$

where $K(y, t)$ is defined by (5.3.44), and so if $u_2(t)$ is the solution of (5.3.47) then $U^S(y)$ defined by

$$U^S(y) = \{(R^S + 1) + i\cot kb(R^S - 1)\}u_2(y), \tag{5.3.57}$$

will satisfy (5.3.56). It can also be shown that

$$\int_{L_g} U^S(y)\psi_0(y)\,\mathrm{d}y = -ikh(1 - R^S), \tag{5.3.58}$$

$$= \{(R^S + 1) + i\cot kb(R^S - 1)\}S_{22}, \tag{5.3.59}$$

from (5.3.57), (5.3.49). Rearranging the above gives

$$R^S = -\frac{(1 - i\cot kb)S_{22} + ikh}{(1 + i\cot kb)S_{22} - ikh}, \tag{5.3.60}$$

and clearly $|R^S| = 1$, as expected. From (5.3.34) we have

$$q^S = -\int_{L_g} U^S(y)\,\mathrm{d}y = -\{(R^S + 1) + i\cot kb(R^S - 1)\}S_{21}, \tag{5.3.61}$$

after use of equations (5.3.57) and (5.3.49). Substituting (5.3.60) in the above gives

$$q^S = \frac{2ikhS_{21}}{(1 + i\cot kb)S_{22} - ikh}. \tag{5.3.62}$$

Combining (5.3.48), (5.3.49) gives

$$S_{ij} = \int_{L_g}\int_{L_g} u_j(t)K(y,t)u_i(y)\,\mathrm{d}t\,\mathrm{d}y = S_{ji}, \tag{5.3.63}$$

since $K(y,t) = K(t,y)$ and so the matrix $\mathbf{S}$ is symmetric.

We have shown how the quantities q^R (and hence $\tilde{A}$, $\tilde{B}$), q^S, A^R and R^S can all be determined in terms of the real 2×2 matrix S_{ij}, $i,j = 1,2$ with $S_{21} = S_{12}$. In the next section we shall provide an accurate Galerkin approximation to the system (5.3.48) from which the S_{ij} can be determined easily and accurately. However we first show how the various reciprocal relations which exist for these problem can be shown to be satisfied identically. For example, it is a simple matter to verify (5.3.31) using (5.3.51) and (5.3.62), whilst using (5.3.53) in (5.2.15) confirms (5.3.29) once (5.3.51) is used and shows that

$$\tilde{B} = \frac{\omega b}{\rho g}\cdot\frac{kh(Kb)^{-1}S_{12}^2}{(\cot kbS_{22} - kh)^2 + S_{22}^2}. \tag{5.3.64}$$

In the treatment of this problem by Smith [68], the particular matching of eigenfunction expansions leads to the solution of an infinite systems of equations. Consequently it is not evident that these relations are satisfied identically.

Galerkin approximation

In operator notation (5.3.48), (5.3.49) can be written

$$\mathcal{K}u_i = d_i, \quad i = 1,2, \quad \text{with} \begin{cases} d_1 = 1, \\ d_2 = \psi_0, \end{cases} \tag{5.3.65}$$

$$(u_i, d_j) = S_{ij}, \tag{5.3.66}$$

where $(\cdot,\cdot)$ denotes the inner product. Once the matrix $\mathbf{S}$ has been found through a suitable approximation to u_i in (5.3.65) all the important properties of the problem are easily obtained. Applying Galerkin's method to (5.3.65) involves approximating $u_i(y)$ by an expansion in terms of unknown coefficients and a series of test functions such that

$$u_i(y) \simeq \tilde{u}_i(y) = \sum_{n=0}^{N} a_n^{(i)} v_n(y), \quad i = 1, 2. \tag{5.3.67}$$

Substituting this expression into (5.3.65), multiplying through by $v_m(y)$, $m = 0, \ldots, N$ and integrating over L_g gives

$$\sum_{n=0}^{N} a_n^{(i)} K_{mn} = L_m^{(i)}, \quad m = 0, \ldots, N, \tag{5.3.68}$$

where $K_{mn} = (v_m, \mathcal{K} v_n)$ and $L_m^{(i)} = (v_m, d_i)$. Also the approximation $\tilde{S}_{ij}$ to S_{ij} is found on insertion of (5.3.67) into (5.3.66) to be

$$S_{ij} \simeq \tilde{S}_{ij} = \sum_{n=0}^{N} a_n^{(i)} L_n^{(j)}. \tag{5.3.69}$$

and elimination of the unknown coefficients from (5.3.68) and (5.3.69) gives, in matrix notation

$$\tilde{\mathbf{S}} = \mathbf{L}^{\mathrm{T}} \mathbf{K}^{-1} \mathbf{L} \tag{5.3.70}$$

where $\mathbf{K} = \{K_{mn}\}$, and $\mathbf{L} = \{L_{mn}\}$ where $L_{mn} = L_m^{(n)}$ is of size $(N+1) \times 2$. The absence of the coefficients $a_n^{(i)}$ in the final form for $\mathbf{S}$ is a direct consequence of the use of Galerkin's method, shown in chapter 2 to be equivalent to the Schwinger variational principle.

Now

$$K_{mn} = (v_m, \mathcal{K} v_n) = \sum_{r=1}^{\infty} \frac{(1 + \coth k_r b)}{k_r h} F_{mr} F_{nr}, \tag{5.3.71}$$

say, where (5.3.43) has been used, and where $F_{mn} = (v_m, \psi_n)$. Note that

$$F_{m0} = (v_m, \psi_0) = (v_m, d_2) = L_m^{(2)}. \tag{5.3.72}$$

Since $u^{(i)}(y)$ is proportional to the velocity under a surface-piercing barrier we use the definition in (3.2.40) for the set $\{v_m(y)\}$. This choice results in (3.2.41), namely

$$F_{mn} = N_n^{-1/2} J_{2m}\left\{k_n(h-a)\right\}. \tag{5.3.73}$$

For a detailed discussion of the choice of the test functions, $v_m(y)$, see §3.2. From (5.3.71) we now have

$$K_{mn} = \sum_{r=1}^{\infty}(N_r k_r h)^{-1}(1+\coth k_r b)J_{2m}\{k_r(h-a)\}J_{2n}\{k_r(h-a)\}, \tag{5.3.74}$$

whilst

$$L_m^{(2)} = F_{m0} = (-1)^m N_0^{-1/2} I_{2m}\{k(h-a)\}, \tag{5.3.75}$$

from (3.2.42) and

$$\begin{aligned} L_m^{(1)} = (v_m, 1) &= \int_a^h \frac{2(-1)^m}{\pi\left\{(h-a)^2-(h-y)^2\right\}^{1/2}} T_{2m}\left(\frac{h-y}{h-a}\right) \mathrm{d}y \\ &= \frac{2(-1)^m}{\pi}\int_0^1 \frac{T_{2m}(t)}{(1-t^2)^{1/2}}\,\mathrm{d}t \\ &= \frac{2(-1)^m}{\pi}\int_0^{\pi/2} \cos 2m\theta\,\mathrm{d}\theta \\ &= \delta_{m0}. \end{aligned} \tag{5.3.76}$$

Furthermore, we can show that the modulus of each $\tilde{S}_{ij}$ is bounded above by its true value, S_{ij}. This can be shown as follows. Consider S_{ii}, $i = 1, 2$ first. Thus, $S_{ii} = (u_i, d_i)$ where u_i satisfies $\mathcal{K}u_i = d_i$ and this is precisely the type of situation described in chapter 2 where we were able to show that

$$0 < \tilde{S}_{ii} \leq S_{ii} \tag{5.3.77}$$

since $\mathcal{K}$ is positive-definite and self-adjoint. To show that $|\tilde{S}_{ij}| \leq |S_{ij}|$, $i \neq j$, where $|\cdot|$ denotes the absolute value (recall that S_{ij} are real), we consider the inequality

$$0 \leq (\tilde{u}_{ij}, \mathcal{K}\tilde{u}_{ij}) \leq (u_{ij}, \mathcal{K}u_{ij}), \tag{5.3.78}$$

arising directly from (5.3.77) and we now choose $\tilde{u}_{ij} = \tilde{u}_i \pm \tilde{u}_j$ as an approximation to $u_{ij} = u_i \pm u_j$ to give

$$0 \leq (\tilde{u}_i \pm \tilde{u}_j, \mathcal{K}(\tilde{u}_i \pm \tilde{u}_j)) \leq (u_i \pm u_j, \mathcal{K}(u_i \pm u_j)).$$

Expanding both sides and subtracting the two inequalities gives

$$|\tilde{S}_{ij}| \leq |S_{ij}|, \quad i \neq j. \tag{5.3.79}$$

5.3.2 Pressure difference formulation

The complementary formulation to the velocity formulation of the previous section is now derived in which the quantities q^R, A^R, q^S and R^S are found to be expressible in terms of combinations of integral properties of functions related to the pressure difference across the barrier at $x = b$.

The radiation problem

From the velocity formulation of the previous section we have already found that

$$U^R(y) = \sum_{n=0}^{\infty} U_n^R \psi_n(y), \tag{5.3.80}$$

and

$$P^R(y) = A^R(1 + i\cot kb)\psi_0(y) - K^{-1} - \sum_{n=1}^{\infty} \frac{U_n^R}{k_n}(1 + \coth k_n b)\psi_n(y). \tag{5.3.81}$$

Expanding the K^{-1} term in the above in a fourier series as

$$K^{-1} = \sum_{n=0}^{\infty} c_n h \psi_n(y), \quad y \in [0, h] \tag{5.3.82}$$

and using orthogonality gives

$$c_n = -\frac{N_n^{-1/2}\cos k_n h}{(k_n h)^2} \sim \frac{2^{1/2}(-1)^{n+1}}{n^2\pi^2}, \quad \text{as } n \to \infty \tag{5.3.83}$$

and in particular $c_0 = N_0^{-1/2}\cosh kh/(kh)^2$. Using this expansion in (5.3.81), multiplying through by $\psi_m(y)$ and integrating over the depth gives

$$\frac{1}{h}\int_{L_b} P^R(y)\psi_n(y)\,\mathrm{d}y = -c_n h - \frac{U_n^R}{k_n}(1 + \coth k_n b), \quad \text{for } n \geq 1 \tag{5.3.84}$$

where we have used $P^R(y) = 0$ for $y \in L_g$. Rearranging and summing over all $n \geq 1$ yields, after use of $U^R(y) = 0$, $y \in L_b$ in (5.3.80),

$$\sum_{n=1}^{\infty} \frac{k_n h}{(1 + \coth k_n b)} \int_{L_b} P^R(t)\psi_n(y)\psi_n(t)\,\mathrm{d}t = -h^2 \sum_{n=1}^{\infty} \frac{k_n h c_n \psi_n(y)}{(1 + \coth k_n b)} + h^2 U_0^R \psi_0(y),$$
$$y \in L_b, \tag{5.3.85}$$

or

$$\int_{L_b} P^R(t)M(y,t)\,\mathrm{d}t = -h^2\chi(y) + ikh^2A^R\psi_0(y), \quad y \in L_b \tag{5.3.86}$$

where we have defined

$$M(y,t) = \sum_{n=1}^{\infty} \frac{k_n h\psi_n(y)\psi_n(t)}{(1+\coth k_n b)}, \tag{5.3.87}$$

and

$$\chi(y) = \sum_{n=1}^{\infty} \frac{k_n h c_n \psi_n(y)}{(1+\coth k_n b)}. \tag{5.3.88}$$

Now if $p_1(t)$ and $p_2(t)$ are solutions of

$$\int_{L_b} p_i(t)M(y,t)\,\mathrm{d}t = f_i(y), \quad i=1,2, \quad \text{where} \left\{ \begin{array}{l} f_1(y) = \chi(t) \\ f_2(y) = \psi_0(t) \end{array} \right. \tag{5.3.89}$$

then $P^R(y)$ defined by

$$P^R(y) = -h^2 p_1(y) + ikh^2A^R p_2(y), \tag{5.3.90}$$

will satisfy (5.3.86). As in §2 the 2×2 matrix $\mathbf{T} = \{T_{ij}\}$ is introduced by

$$\int_{L_b} p_i(y)f_j(y)\,\mathrm{d}y = T_{ij}, \quad i,j=1,2. \tag{5.3.91}$$

We now ask ourselves how we can relate the pressure difference, $P^R(y)$ across the barrier, to the internal volume flux, q^R, given by (5.2.12). In the velocity formulation the relation between the internal flux and the horizontal velocity under the barrier is a simple one, obtained using physical arguments. There are no such obvious physical arguments that can be used here and instead we choose an alternative route. We would like to be able to express the hydrodynamic coefficients A^R, q^R in terms of T_{ij}. Thus, multiplying by $\psi_0(y)$ in (5.3.81) and integrating over $(0,h)$ gives the relation

$$\int_{L_b} P^R(y)\psi_0(y)\,\mathrm{d}y = hA^R(1+i\cot kb) - c_0h^2, \tag{5.3.92}$$

between the pressure difference and the far-field radiated amplitude. Also, multiplying (5.3.84) by $c_nk_n/(1+\coth k_nb)$ and summing over $n=1,\ldots,\infty$ gives

$$\int_{L_b} P^R(y)\chi(y)\,\mathrm{d}y = -h^2\sum_{n=1}^{\infty}\frac{k_nhc_n^2}{(1+\coth k_nb)} - h^2\sum_{n=1}^{\infty}c_nU_n^R. \tag{5.3.93}$$

Now from (5.3.34), (5.3.37), (5.3.40) we find

$$q^R = -\int_0^b \left.\frac{\partial \phi^R}{\partial y}\right|_{y=0} \mathrm{d}x = -iKhkhc_0A^R - Kh^2\sum_{n=1}^{\infty} c_n U_n^R, \tag{5.3.94}$$

where we have used the result

$$Kh^2 c_n = \int_0^h \psi_n(y)\,\mathrm{d}y, \tag{5.3.95}$$

from (5.3.67). Substitution of (5.3.93) into the above gives

$$q^R = -iKhkhc_0A^R + K\int_{L_b} P^R(y)\chi(y)\,\mathrm{d}y + Kh^2\sum_{n=1}^{\infty}\frac{k_n h c_n^2}{(1+\coth k_n b)} \tag{5.3.96}$$

providing a relation between the induced volume flux across the internal free surface and integral properties of the pressure difference across the barrier once (5.3.92) has been used in (5.3.96).

The occurrence of the term $\sum\limits_{n=1}^{\infty} c_n U_n^R$ in both (5.3.93) and (5.3.94) may appear rather fortuitous. However, there is further motivation for the derivation of the results above. It comes from the use of Green's identity with certain judicious choices of harmonic functions to be used in conjunction with ϕ^R, the radiation potential. Bearing in mind that it is desirable to generate integral properties of the pressure difference across the barrier at $x = b$, $P^R(y)$, we choose the two functions $\overline{\phi^I}$ and $\overline{\phi^P}$. Here, ϕ^I is simply the potential due to an incident wave in the absence of the barrier at $x = b$ and any increased pressure on S_i, and may be written explicitly as $\phi^I = 2\cos kx\psi_0(y)$. The potential ϕ^P is due to a forcing pressure on S_i, once again in the absence of the barrier at $x = b$ and also has an explicit solution, namely

$$\phi^P = -c_0 \mathrm{e}^{ikb}\cos kx\psi_0(y) + K^{-1} - \sum_{n=1}^{\infty}\frac{c_n\cosh k_n x}{\sinh k_n b(1+\coth k_n b)}\psi_n(y), \tag{5.3.97}$$

in $0 \le x \le b$ and

$$\phi^P = -ic_0\sin kb\mathrm{e}^{ikx}\psi_0(y) + \sum_{n=1}^{\infty}\frac{c_n \mathrm{e}^{-k_n(x-b)}}{(1+\coth k_n b)}\psi_n(y), \tag{5.3.98}$$

in $b \le x$, where c_n are defined by (5.3.83) and have arisen due to the expansion for K^{-1} given in (5.3.82). Thus using Green's identity, (5.2.26), with ϕ^R and $\overline{\phi^I}$ gives

(5.3.92) whilst use of ϕ^R with $\overline{\phi^P}$ in (5.2.26) gives the relation (5.3.96) between q^R, A^R and a weighted integral of $P^R(y)$.

Substituting (5.3.90) into (5.3.92) using the definitions for T_{ij} in (5.3.91) gives

$$-hT_{12} + ikhA^R T_{22} = A^R(1 + i\cot kb) - c_0 h, \tag{5.3.99}$$

or, rearranging,

$$A^R = \frac{h(c_0 - T_{12})}{(1 + i\cot kb) - ikhT_{22}}. \tag{5.3.100}$$

Similarily, for (5.3.96) we find

$$q^R = -iKhkhc_0 A^R + Kh^2 \sum_{n=1}^{\infty} \frac{k_n h c_n^2}{(1 + \coth k_n b)} - Kh^2 T_{11} + iKhkhA^R T_{21}, \tag{5.3.101}$$

which, on rearrangement, is

$$q^R = -\frac{iKh^2kh(c_0 - T_{21})(c_0 - T_{12})}{(1 + i\cot kb) - ikhT_{22}} - Kh^2(T_{11} - X), \tag{5.3.102}$$

where

$$X = \sum_{n=1}^{\infty} \frac{k_n h c_n^2}{(1 + \coth k_n b)}. \tag{5.3.103}$$

It is found, as in the velocity formulation, that the various reciprocal relations are satisfied identically. For example, substitution of either (5.3.100) into (5.2.15) or (5.3.102) into (5.3.29) in the determination of $\tilde{B}$ gives

$$\tilde{B} = \frac{\omega b}{\rho g} \cdot \frac{Kb^{-1}h^2kh(c_0 - T_{12})^2}{(\cot kb - khT_{22})^2 + 1}, \tag{5.3.104}$$

where we have used the symmetry $T_{21} = T_{12}$, an identity which is clear from (5.3.89), (5.3.91)

The scattering problem

The pressure difference formulation of the scattering problem is needed to find q^S and R^S. Using the expansions for the potential given in (5.3.54), (5.3.55) and proceeding in the standard manner leads to

$$P^S(y) = \{(R^S + 1) + i\cot kb(R^S - 1)\}\psi_0(y) - \sum_{n=1}^{\infty} \frac{U_n^S}{k_n}(1 + \coth k_n b)\psi_n(y), \tag{5.3.105}$$

for the pressure difference, and use of orthogonality gives rise to

$$\int_{L_b} P^S(t)\psi_n(t)\,\mathrm{d}t = -\frac{hU_n^S}{k_n}(1+\coth k_n b), \quad n \geq 1, \tag{5.3.106}$$

and then, after use of $U^S(y) = 0\,,\ y \in L_b\,,$

$$\int_{L_b} P^S(t)M(y,t)\,\mathrm{d}t = ikh^2(R^S-1)\psi_0(y), \quad y \in L_b, \tag{5.3.107}$$

where $M(y,t)$ is defined by (5.3.87), whilst orthogonality in (5.3.105) immediately gives us

$$\int_{L_b} P^S(y)\psi_0(y)\,\mathrm{d}y = h\{(R^S+1) + i\cot kb(R^S-1)\}. \tag{5.3.108}$$

Now if $p_2(t)$ is the solution of (5.3.89) with $i=2$ then $P^S(y)$ defined by

$$P^S(y) = ikh^2(R^S-1)p_2(y), \tag{5.3.109}$$

will satisfy (5.3.107). Substituting this definition into (5.3.108) and rearranging gives

$$R^S = -\frac{1-i(\cot kb - khT_{22})}{1+i(\cot kb - khT_{22})}, \tag{5.3.110}$$

and $|R^S| = 1$ as expected.

In order to derive an expression for the induced volume flux we first multiply (5.3.108) by $k_n h c_n/(1+\coth k_n b)$ and sum over $n = 1,\ldots,\infty$ to obtain

$$\int_{L_b} P^S(y)\chi(y)\,\mathrm{d}y = -h^2\sum_{n=1}^{\infty} c_n U_n^s. \tag{5.3.111}$$

Also, it can be shown from (5.3.54) after some algebra, that

$$q^S = -\int_0^b \left.\frac{\partial\phi^S}{\partial y}\right|_{y=0}\mathrm{d}x = iKhkhc_0(1-R^S) - Kh^2\sum_{n=1}^{\infty} c_n U_n^S, \tag{5.3.112}$$

and so using (5.3.111) and then (5.3.109) in the above gives

$$q^S = iKhkh(1-R^S)(c_0 - T_{21}), \tag{5.3.113}$$

which when simplified using (5.3.110) is

$$q^S = \frac{2iKhkh(c_0 - T_{21})}{1+i(\cot kb - khT_{22})}, \tag{5.3.114}$$

and it is clear that the relation (5.3.31) is satisfied identically on substitution of (5.3.102) and (5.3.114).

We have therefore provided an alternative formulation to the problem in terms of the pressure difference across the barrier, and as in the velocity formulation all important hydrodynamic coefficients may easily be expressed in terms of the elements of a 2×2 matrix. It is unclear what relation, if any, holds between $\mathbf{S}$ and $\mathbf{T}$ derived from velocity and pressure difference formulations respectively. In the other water-wave problems considered in this thesis and set up in this way it is usual to expect an inverse relation to hold, but this does not appear to be the case here.

Galerkin approximation

The approximate solution of the integral equations follows in a manner identical to the velocity formulation, the only major difference being in the replacement of the function $d_1(t) = 1$ by $f_1(t) = \chi(t)$ in the right hand side functions. This will not cause any difficulties. So, in operator notation, we write (5.3.89), (5.3.91) as

$$\mathcal{M}p_i = f_i, \quad i = 1, 2, \quad \text{with} \quad \left\{ \begin{array}{l} f_1 = \chi, \\ f_2 = \psi_0 \end{array} \right. \tag{5.3.115}$$

$$(p_i, f_j) = T_{ij}, \quad i, j = 1, 2. \tag{5.3.116}$$

Let

$$p_i(y) \simeq \tilde{p}_i(y) = \sum_{n=0}^{N} b_n^{(i)} w_n(y), \quad i = 1, 2. \tag{5.3.117}$$

Substitution of this approximation into (5.3.115), multiplying through by $w_m(y)$, $m = 0, \ldots, N$ and integrating over L_b gives the Galerkin approximation

$$\sum_{n=0}^{N} b_n^{(i)} M_{mn} = Q_m^{(i)}, \quad m = 0, \ldots, N, \tag{5.3.118}$$

where $M_{mn} = (w_m, \mathcal{M}w_n)$ and $Q_m^{(i)} = (w_m, f_i)$. Also, from (5.3.116)

$$T_{ij} \simeq \tilde{T}_{ij} = \sum_{n=0}^{N} b_n^{(i)} Q_m^{(j)}. \tag{5.3.119}$$

or, in matrix notation

$$\tilde{\mathbf{T}} = \mathbf{Q}^{\mathrm{T}}\mathbf{M}^{-1}\mathbf{Q}, \tag{5.3.120}$$

where $\mathbf{M} = \{M_{mn}\}$, and $\mathbf{Q} = \{Q_{mn}\}$, $Q_{mn} = Q_m^{(n)}$ is of size $(N+1)\times 2$.

Now,

$$M_{mn} = (w_m, \mathcal{M}w_n) = \sum_{r=1}^{\infty} \frac{k_r h}{(1+\coth k_r b)} G_{mr}G_{nr} \tag{5.3.121}$$

from (5.3.87) where $G_{mn} = (w_m, \psi_n)$ and so $Q_m^{(2)} = G_{m0}$, whilst

$$Q_m^{(1)} = \sum_{r=1}^{\infty} \frac{k_r h c_r G_{mr}}{(1+\coth k_r b)}. \tag{5.3.122}$$

We now need to determine

$$G_{mn} = (w_m, \psi_n) = N_n^{-1/2}\int_0^a w_m(t)\cos k_n(h-t)\,\mathrm{d}t. \tag{5.3.123}$$

Choosing the approach of §3.2, equations (3.2.44)–(3.2.51) for the surface-piercing barrier scattering problem gives us

$$G_{mn} = N_n^{-1/2}\frac{\cos k_n h}{k_n h} J_{2m+1}(k_n a), \tag{5.3.124}$$

whilst

$$Q_m^{(2)} = G_{m0} = N_0^{-1/2}(-1)^m \frac{\cosh kh}{kh} I_{2m+1}(ka), \tag{5.3.125}$$

and so

$$Q_m^{(1)} = \sum_{r=1}^{\infty} \frac{-\cos^2 k_r h}{N_r (k_r h)^2 (1+\coth k_r b)} J_{2m+1}(k_r a), \tag{5.3.126}$$

after use of (5.3.122) with (5.3.83), (5.3.124). From (5.3.121), we have

$$M_{mn} = \sum_{r=1}^{\infty} \frac{\cos^2 k_r h}{N_r k_r h (1+\coth k_r b)} J_{2m+1}(k_r a) J_{2n+1}(k_r a). \tag{5.3.127}$$

Notice that $0 < \tilde{T}_{ii} \leq T_{ii}$ and $|\tilde{T}_{ij}| \leq |T_{ij}|$ following identically the process for showing bounds on the elements of $\mathbf{S}$ in the velocity formulation (see (5.3.77)–(5.3.79)).

N	$\tilde{S}_{11}$	$\tilde{S}_{12}=\tilde{S}_{21}$	$\tilde{S}_{22}$	$\tilde{T}_{11}$	$\tilde{T}_{12}=\tilde{T}_{21}$	$\tilde{T}_{22}$
0	0.360999	0.264645	0.194008	0.015956	−0.202279	2.564405
1	0.412472	0.319606	0.252694	0.022295	−0.216861	2.597946
2	0.414681	0.321857	0.254988	0.023598	−0.216927	2.597949
3	0.414719	0.321895	0.255027	0.024064	−0.216873	2.597955
4	0.414720	0.321896	0.255027	0.024285	−0.216877	2.597955
5	0.414720	0.321896	0.255027	0.024405	−0.216877	2.597955

Table 5.1: Convergence of the elements of $\mathbf{S}$, $\mathbf{T}$ with increasing N in the case $a/h=1/2$, $b/h=1/8$ and $Kh=1.55$.

5.3.3 Results

We introduce non-dimensionalised quantities μ, ν to represent the radiation susceptance and radiation conductance coefficients through

$$\mu = \frac{\rho g}{\omega b}\tilde{A}, \tag{5.3.128}$$

and

$$\nu = \frac{\rho g}{\omega b}\tilde{B}. \tag{5.3.129}$$

where $\tilde{A}$, $\tilde{B}$ are given by (5.2.14), (5.2.15). The efficiency η_{max} is then given by

$$\eta_{max} = \frac{2\nu}{(\nu^2+\mu^2)^{1/2}+\nu}, \tag{5.3.130}$$

from (5.3.33).

One of the quantities of interest, $|q^S|$, is non-dimensionalised by the volume flux across the internal free surface of a mass of fluid oscillating as a solid body with amplitude and frequency of the incident wave, $|q^I|$ say, giving rise to

$$\frac{|q^S|}{|q^I|} = \frac{N_0^{1/2}|q^S|}{kb\sinh kh}, \tag{5.3.131}$$

where q^S is defined by (5.3.62).

All of the quantities above have been shown to be expressible in terms of the elements of either the 2×2 matrix $\mathbf{S}$ or the 2×2 matrix $\mathbf{T}$. Estimates to these matrices are given by (5.3.70) or (5.3.120), the only significant numerical effort required in the determination and inversion of the $N\times N$ matrix $\mathbf{K}$ or $\mathbf{M}$. Since N will be small in general, the inversion operation is relatively straightforward.

It is noted that the K_{mn}, the elements of $\mathbf{K}$, given by (5.3.74) require the evaluation of an infinite sum. This is done numerically by truncating the series at a value of M, say. The asymptotic form of the series is used to approximate the remainder, as in §3.4, in order to provide increased accuracy. The same procedure is adopted for the M_{mn}, given by (5.3.127) and for $Q_m^{(1)}$ in (5.3.126) which is also defined by an infinite series and is required in the definition of $\tilde{\mathbf{T}}$ in (5.3.120).

Table 5.1 illustrates the rapid convergence of the method for a set of parameters Kh, a/h, b/h. The series was truncated at $M = 1500$. It can be seen that convergence is extremely rapid, the elements $\tilde{S}_{ij}$ approaching S_{ij} from below with six-figure accuracy for N as low as 4. The complementary pressure difference formulation requires the calculation of the $\tilde{T}_{ij}$. Although convergence of $\tilde{T}_{12}$, $\tilde{T}_{21}$ and $\tilde{T}_{22}$ is as impressive as the $\tilde{S}_{ij}$ arising from the velocity formulation, $\tilde{T}_{11}$ is somewhat less convergent. This can be explained as follows. Since from (5.3.120), $\tilde{T}_{11} = (Q_0^{(1)}, \ldots, Q_N^{(1)})^{\mathrm{T}}\mathbf{M}^{-1}(Q_0^{(1)}, \ldots, Q_N^{(1)})$ is the only element of $\mathbf{T}$ that is quadratic in the vector $(Q_0^{(1)}, \ldots, Q_N^{(1)})$, the cumulative effect of errors due to truncation of the infinite series defining $Q_m^{(1)}$ may lead to decreased accuracy. However, μ is the only coefficient defined in terms of $\tilde{T}_{11}$ and approximations to all other coefficients resulting from the two different formulations are in six-figure agreement for $N = 5$. Notice also from table 5.1 how $|\tilde{T}_{ij}| \leq |T_{ij}|$ as predicted. Different sets of parameters give equally satisfactory results although larger values of M, N are needed when a/h is *very* small in the velocity formulation whilst the pressure difference formulation improves in accuracy in this case.

In the graphs which follow truncation parameters of $N = 4$, $M = 500$ give at least five-figure accuracy in all cases. Figures 5.2–5.5 are all for the case of a fixed barrier to depth ratio of $a/h = 1/2$, and barrier to back-wall spacing, b/h, varying from $\frac{1}{8}$ to 1, whilst figures 5.6–5.9 are all for fixed barrier to back-wall spacing of $b/h = 1$ and barrier to depths ratios a/h varying from $\frac{1}{8}$ to $\frac{3}{4}$. The figures show how μ, ν, $|q^S|$, θ_{q^S} (the phase of q^S), and η_{max} computed from (5.3.130) all vary with dimensionless frequency Kh.

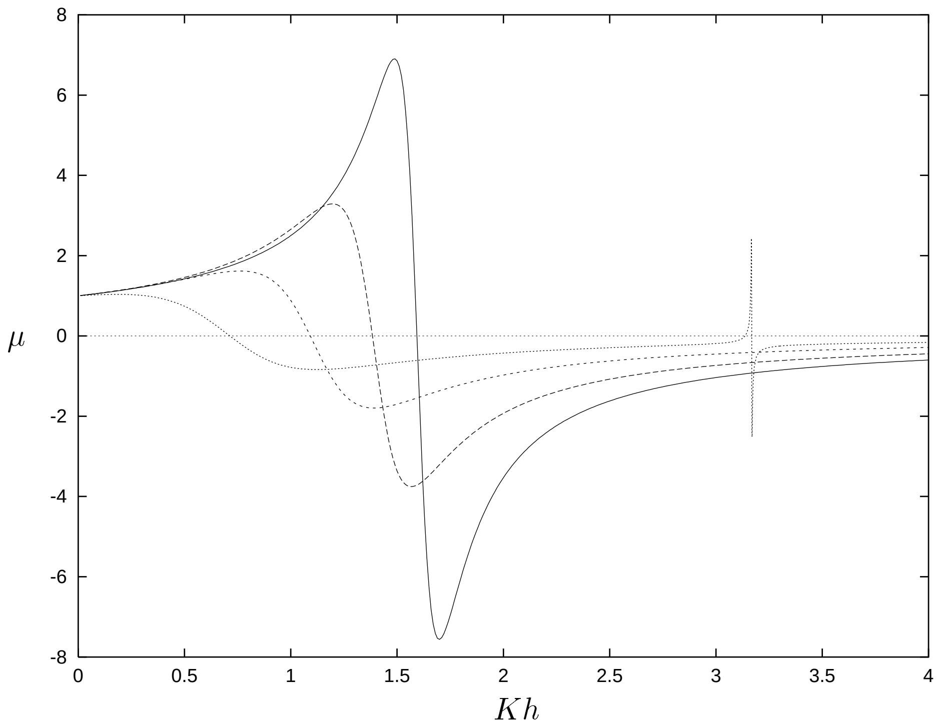

Figure 5.2: The radiation susceptance coefficient against Kh in the case of $a/h = 1/2$ for various barrier to wall spacings: $b/h = \frac{1}{8}$ (———), $\frac{1}{4}$ (– – –), $\frac{1}{2}$ (- - - -), 1 (· · · · · ·).

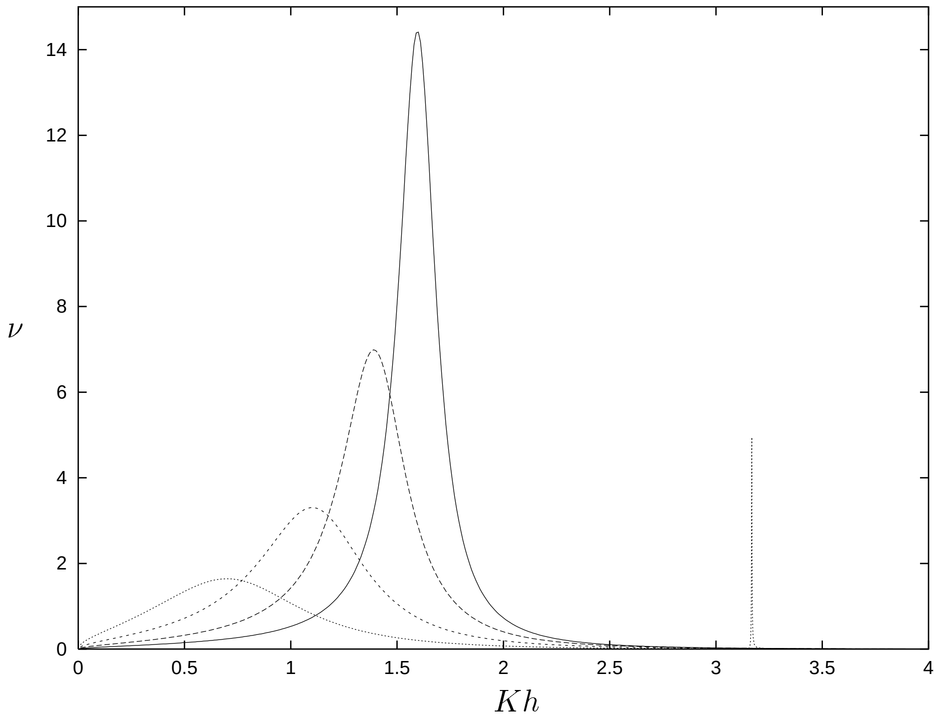

Figure 5.3: The radiation conductance coefficient against Kh in the case of $a/h = 1/2$ for various barrier to wall spacings: $b/h = \frac{1}{8}$ (———), $\frac{1}{4}$ (– – –), $\frac{1}{2}$ (- - - -), 1 (· · · · · ·).

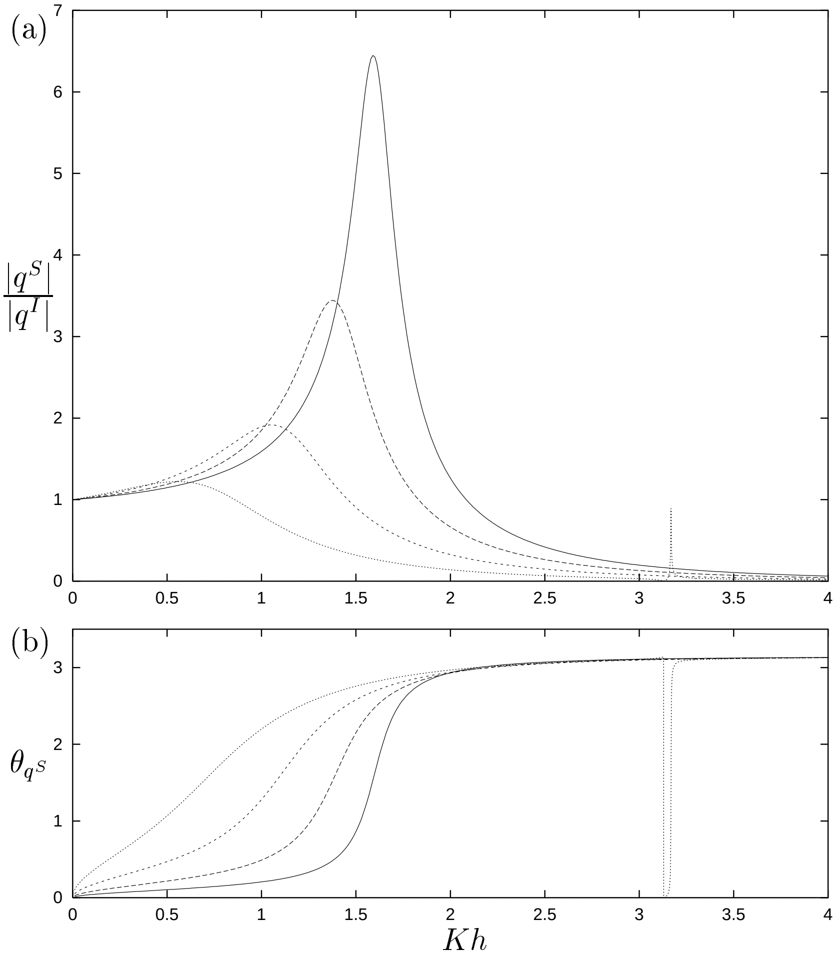

Figure 5.4: The (a) magnitude and (b) phase of induced volume flux due to the scattering potential against Kh in the case $a/h = 1/2$ for various barrier to wall spacings: $b/h = \frac{1}{8}$ (———), $\frac{1}{4}$ (– – –), $\frac{1}{2}$ (- - - -), 1 (· · · · · ·).

There are two situations in which large motions can arise inside the OWC. The more dominant of these, and therefore the one we are more interested in capturing in terms of wave energy, occurs when the fluid between the barrier and the back wall is excited by the incident wave into a resonant piston-like motion inside the OWC. An approximation to this natural frequency of oscillation can be obtained under the assumption that b/a is small and so the fluid in between the walls can be regarded as a solid body. A simple hydrostatic modelling of this situation gives rise to the condition $Ka \approx 1$ for resonance. Thus it can be seen from figure 5.3 that expected resonance at $Kh = 2$, corresponding to $Ka = 1$, is approached for smaller values of b/h, whilst the effect of a larger spacing is to decrease the frequency at which

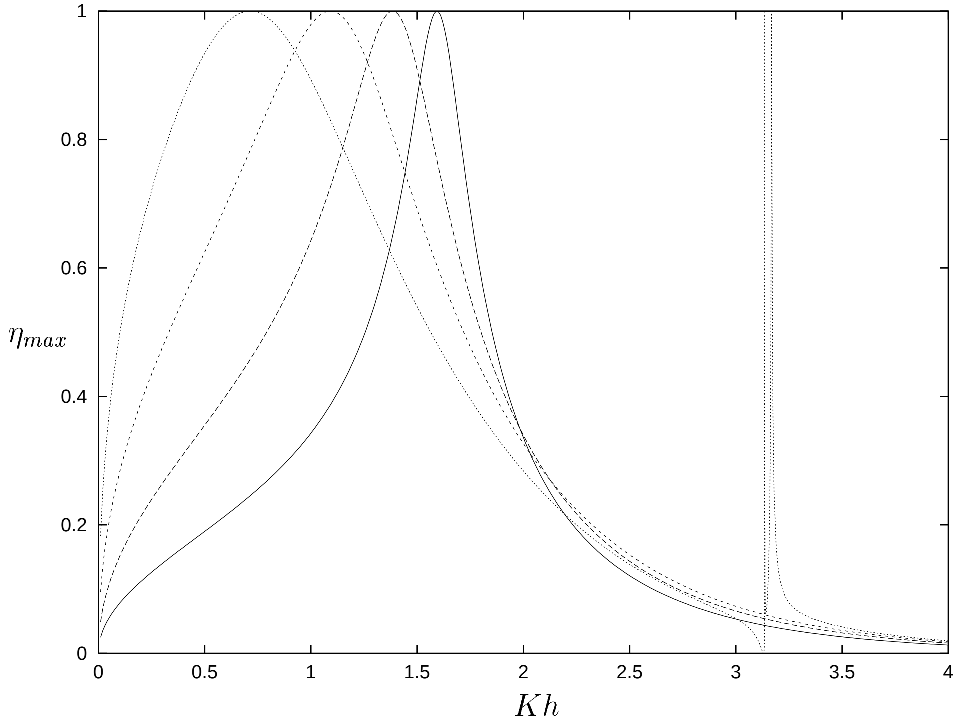

Figure 5.5: Efficiency against Kh in the case of $a/h = 1/2$ for various barrier to wall spacings: $b/h = \frac{1}{8}$ (———), $\frac{1}{4}$ (– – –), $\frac{1}{2}$ (- - - -), 1 (· · · · · ·).

this resonance occurs. Clearly an increase in b/h allows more local fluid motion inside the OWC and thus a breakdown in the solid-body model of resonance, the amplitude of oscillation is decreased.

Large motions inside the OWC can also occur when the incident wave frequency is such that the fluid is excited into a sloshing mode, as though it were in a closed tank with parallel sides. Such a resonance will become more prominent the further the barrier is submerged. In a closed tank, it is straightforward to show that the sloshing frequencies occur at values of the dimensionless wavenumber $kb = n\pi$ and this explains the spikey behaviour in figures 5.2–5.5 for the curve corresponding to $b/h = 1$, the first sloshing mode occuring at $Kh \approx \pi$ in this case. For larger values of Kh, all geometries will give rise to varying degrees of this behaviour and this is shown clearly in figures 5.6–5.9, where b/h is fixed and the depth of submergence of the barrier is allowed to vary. Here, it is seen that for a barrier immersed to only a small proportion of the depth, the resonant effect of the sloshing frequency is small and relatively far away from $kb = \pi$. Increasing the immersion of the barrier moves

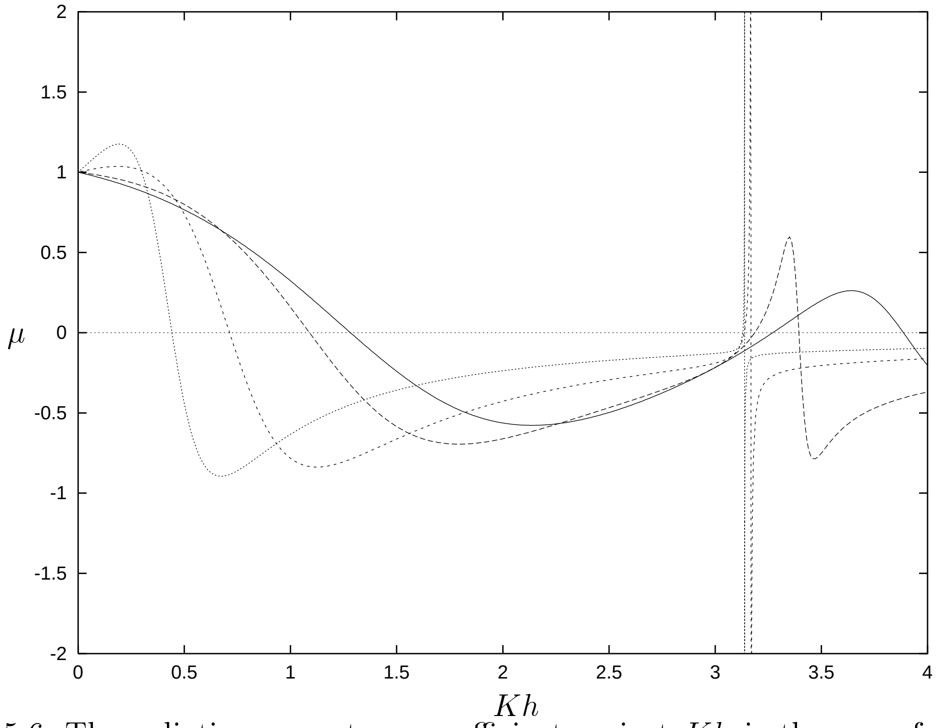

Figure 5.6: The radiation susceptance coefficient against Kh in the case of $b/h = 1$ for various barrier submergence depths: $a/h = \frac{1}{8}$ (———), $\frac{1}{4}$ (– – –), $\frac{1}{2}$ (- - - -), $\frac{3}{4}$ ($\cdots\cdots$).

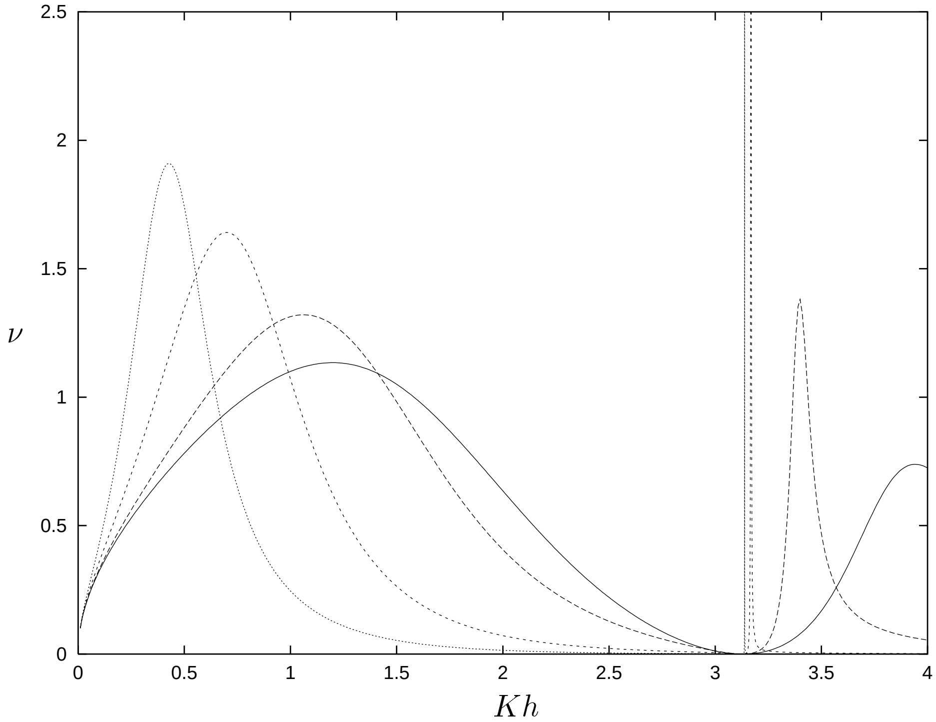

Figure 5.7: The radiation conductance coefficient against Kh in the case of $b/h = 1$ for various barrier submergence depth: $a/h = \frac{1}{8}$ (———), $\frac{1}{4}$ (– – –), $\frac{1}{2}$ (- - - -), $\frac{3}{4}$ ($\cdots\cdots$).

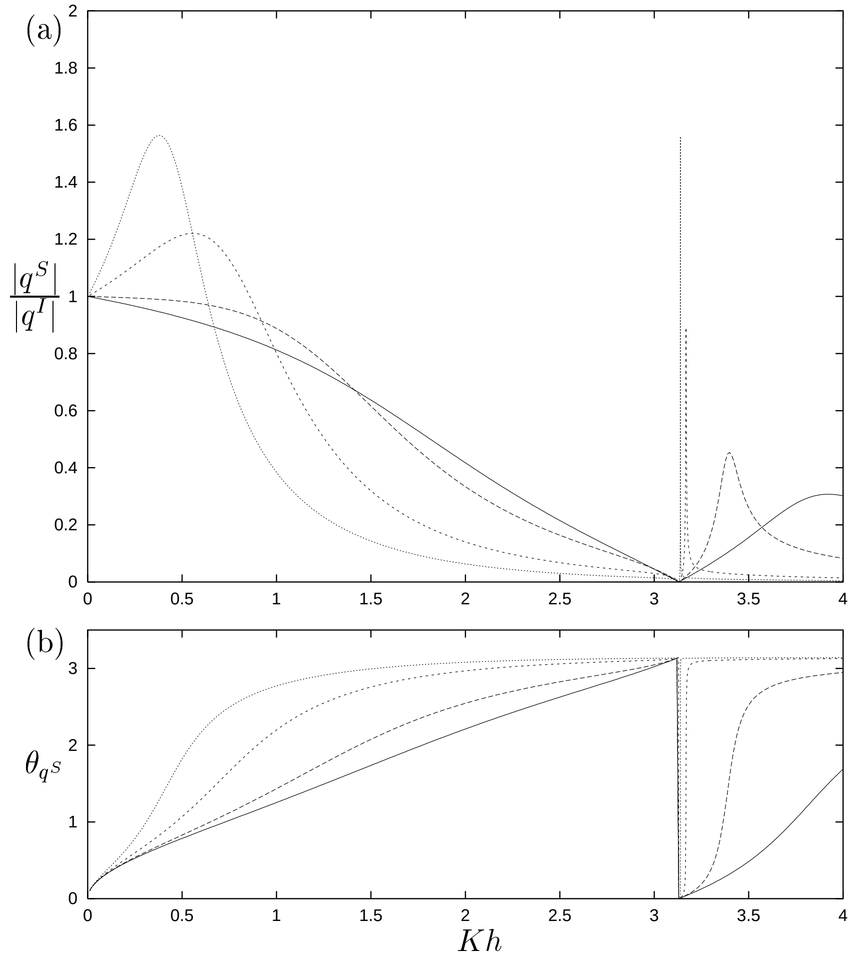

Figure 5.8: The (a) magnitude and (b) phase of induced volume flux due to the scattering potential against Kh in the case of $b/h = 1$ for various barrier submergence depths: $a/h = \frac{1}{8}$ (———), $\frac{1}{4}$ (– – –), $\frac{1}{2}$ (- - - -), $\frac{3}{4}$ ($\cdots\cdots$).

the resonant frequency nearer to the sloshing frequency in a closed tank, whilst the peak becomes much larger and spiked.

Associated with every zero of μ is a maximum in η_{max}, the maximum efficiency, yielding two peaks in the curves for η_{max} for every resonance where the curve of μ passes through zero twice.

Finally, figure 5.10 shows the behaviour of the radiation susceptance, μ, as $Kh \to \infty$. The knowledge of this asymptotic behaviour is important in modelling of time-domain approaches and it can be seen from the gradient of the curves in figure 5.10 that $\mu \propto \omega^{-2}$ as $Kh \to \infty$. This is very different from the solid-body equivalent to μ, the so-called added mass, which has been shown to tend to a non-

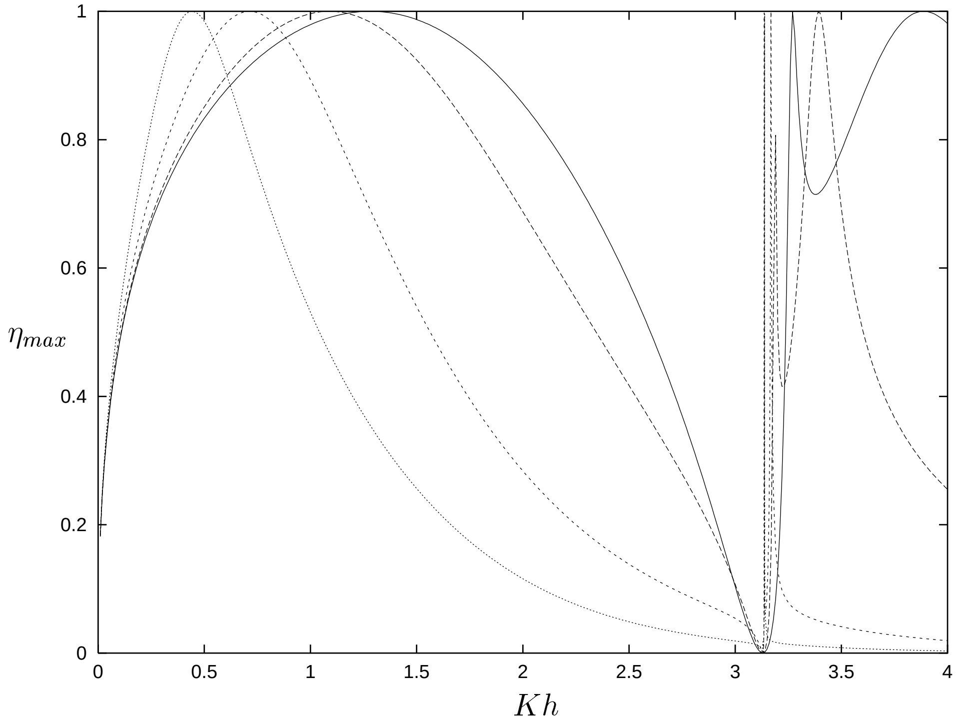

Figure 5.9: Efficiency against Kh in the case of $b/h = 1$ for various barrier submergence depths: $a/h = \frac{1}{8}$ (———), $\frac{1}{4}$ (– – –), $\frac{1}{2}$ (- - - -), $\frac{3}{4}$ ($\cdots\cdots$).

zero constant at high frequencies. The spikes in figure 5.10 are due to resonances at sloshing frequencies.

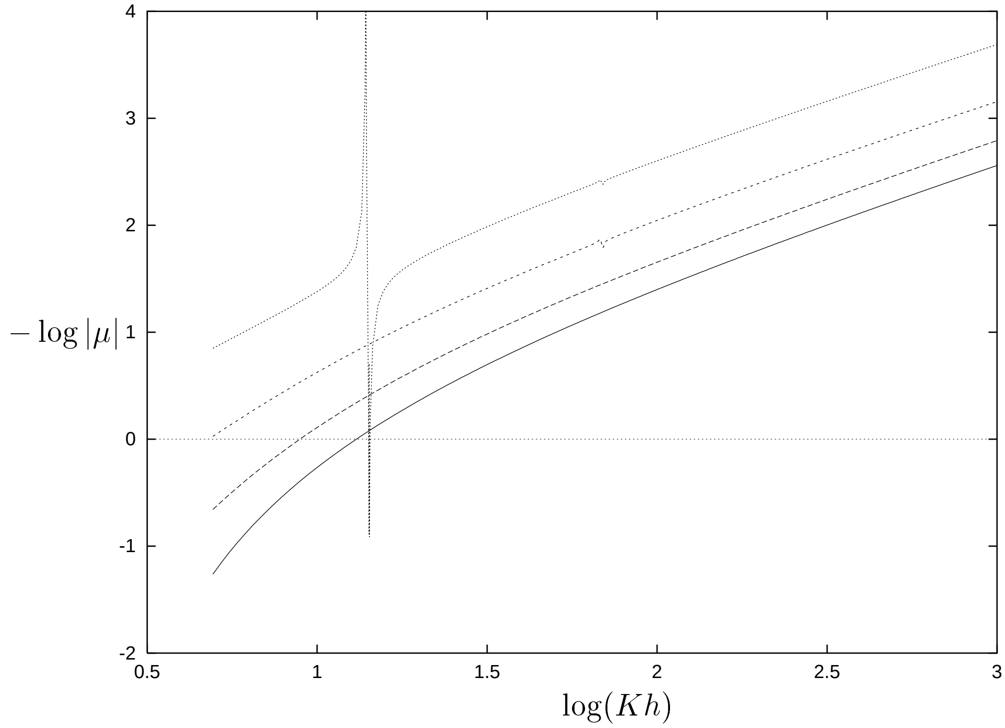

Figure 5.10: Asymptotic behaviour of μ, the radiation susceptance, as $Kh \to \infty$, corresponding to the curves in Figure 4.2

5.4 A partially-immersed circular duct OWC device

Figure 5.11 shows the oscillating-water-column wave-energy device being considered in the remainder of this chapter. The x and z axes are chosen to lie horizontally in the mean free surface with the y-axis vertically downwards with the sea-bed at $y = h$. A plane parallel-crested wave of unit amplitude travelling in the positive x-direction is incident on the OWC device which consists of a thin open-ended circular cylinder, or duct, of radius b is immersed to a depth a below the free surface, its centre coinciding with the y-axis.

Cylindrical polars will be used in this section and so the time dependence is removed from the velocity potential by

$$\Phi(x, y, z, t) = \mathrm{Re}\{\phi(r, \theta, y)\mathrm{e}^{-i\omega t}\}, \tag{5.4.1}$$

where we define

$$r = (x^2 + z^2)^{1/2}, \quad \text{and} \quad \theta = \tan^{-1}(z/x). \tag{5.4.2}$$

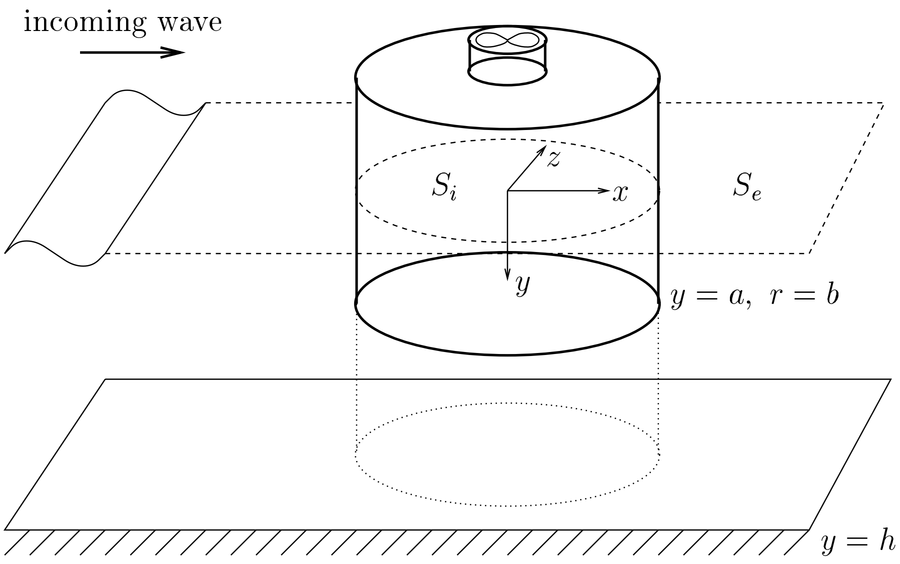

Figure 5.11: Situation of the OWC duct device.

The potential, ϕ, is divided into radiation and scattering potentials, ϕ^S and ϕ^R, using (5.2.8). A description of the boundary-value problems that these potentials must satisfy is given in §5.2 where the Laplacian operator in cylindrical coordinates is

$$\nabla^2 \equiv \frac{1}{r}\frac{\partial}{\partial r}\left(r\frac{\partial}{\partial r}\right) + \frac{1}{r^2}\frac{\partial^2}{\partial \theta^2} + \frac{\partial^2}{\partial y^2}. \tag{5.4.3}$$

Applying a separation of variables procedure of the form $\phi(r,\theta,y) = \phi_n(r,\theta)\psi_n(y)$ to (5.2.6)–(5.2.8, p=0) with (5.4.3) gives, as expected, the depth eigenfunctions, $\psi_n(y)$, defined in chapter 2 by (2.16) with k_n as the roots of (2.14). Possible solutions for $\phi_n(r,\theta)$ include

$$\phi_n(r,\theta) = \begin{cases} J_q(kr)\cos q\theta \\ H_q(kr)\cos q\theta \\ \left.\begin{array}{l} I_q(k_n r)\cos q\theta \\ K_q(k_n r)\cos q\theta \end{array}\right\} \quad n \geq 1, \end{cases} \tag{5.4.4}$$

for all $q \geq 0$, where J_q, Y_q, I_q and K_q are Bessel functions in the usual notation and $H_q(x) \equiv H_q^{(1)}(x) = J_q(x) + iY_q(x)$ is the Hankel function of the first kind, chosen to ensure an outgoing potential. Note that since there is symmetry about the plane $z = 0$, we neglect solutions where $\cos q\theta$ is replaced by $\sin q\theta$ in (5.4.4).

In three-dimensional problems, the wave field away from the body is written

$$\left.\begin{aligned} \phi^R(x,y) &\sim \mathcal{A}^R \left(\frac{2}{\pi k r}\right)^{1/2} \mathrm{e}^{ikr - i\pi/4}\psi_0(y) \\ \phi^S(x,y) &\sim (\mathrm{e}^{ikx} + \mathcal{R}^S(\theta)\left(\frac{2}{\pi k r}\right)^{1/2} \mathrm{e}^{ikr - i\pi/4})\psi_0(y) \end{aligned}\right\} \quad \text{as } r \to \infty\,, \tag{5.4.5}$$

(see Mei [51], p307) where $\mathcal{A}^R$ and $\mathcal{R}^S(\theta)$ are the outgoing wave amplitudes, the former a constant due to the angular symmetry in the radiation problem.

Relations equivalent to (5.3.29) and (5.3.31) occuring in the two-dimensional OWC problem can be derived for this axisymmetric three-dimensional configuration using Green's second identity with S_c chosen to be the closed surface comprised of S_i , S_e , S_b (solid boundaries) and S_∞ (an infinitely large circular cylinder extending throughout the depth). Using the functions ϕ^R and $\overline{\phi^R}$ in (5.2.26) gives

$$\begin{aligned} \frac{1}{K}\int_{S_i} \frac{\overline{\partial \phi^R}}{\partial y} - \frac{\partial \phi^R}{\partial y}\,\mathrm{d}S &= \lim_{r\to\infty}\int_0^h\int_0^{2\pi}\left\{\phi^R\frac{\overline{\partial\phi^R}}{\partial r} - \overline{\phi^R}\frac{\partial\phi^S}{\partial r}\right\} r\,\mathrm{d}\theta\,\mathrm{d}y \\ &= -8iKh|\mathcal{A}^R|^2, \end{aligned} \tag{5.4.6}$$

on use of (5.4.5), (5.2.10) and after some manipulation. This immediately leads to the three-dimensional equivalent of (5.3.29) being

$$\tilde{B} = \frac{\omega}{\rho g} 4Kh|\mathcal{A}^R|^2. \tag{5.4.7}$$

The other relation that can be found here comes from the use of ϕ^S with ϕ^R in (5.2.26). We eventually arrive at

$$-\frac{1}{K}\int_{S_i}\frac{\partial\phi^S}{\partial y}\,\mathrm{d}S = \lim_{r\to\infty} \mathrm{e}^{i\pi/4}\mathcal{A}^R h\left(\frac{2kr}{\pi}\right)^{1/2}\int_0^{2\pi}(1-\cos\theta)\mathrm{e}^{ikr(1+\cos\theta)}\,\mathrm{d}\theta. \tag{5.4.8}$$

The integral in the above equation can be evaluated using the method of stationary phase, the right-hand side taking the value $4ih\mathcal{A}^R$. Thus

$$q^S = 4iKh\mathcal{A}^R. \tag{5.4.9}$$

Also, we can combine (5.4.7) with (5.4.9) to obtain

$$\tilde{B} = \frac{\omega}{4\rho g K h}|q^S|^2 = \frac{k|q^S|^2}{8P_w}, \tag{5.4.10}$$

using (5.2.20) whence the maximum efficiency, or *capture width*, defined by (5.2.25) becomes

$$\eta_{max} = \frac{2\tilde{B}}{k(\Lambda_{opt} + \tilde{B})}. \tag{5.4.11}$$

Evans [15] showed that the difference between the two-dimensional and axisymmetric three-dimensional relations connecting B and q^S is a simple factor of $2\pi/\lambda$ ($= k$), and this factor can be confirmed from a comparison of (5.3.32) with (5.4.10).

5.4.1 Velocity formulation

In what follows the radiation and scattering problems are formulated in terms of functions related to the radial velocity across the gap under the circular duct and solved using Galerkin's method.

The radiation problem

We divide the fluid domain into the two regions inside and outside the cylinder $r = b$. Using the set of possible solutions given by (5.4.4) we construct general expansions satisfying all conditions of the problem apart from those on the cylinder $r = b$. Hence, in $r \geq b$ we write

$$\phi^R = \alpha_0^R H_0(kr)\psi_0(y) + \sum_{n=1}^{\infty} \alpha_n^R K_0(k_n r)\psi_n(y), \tag{5.4.12}$$

and in $r \leq b$

$$\phi^R = \beta_0^R J_0(kr)\psi_0(y) + \sum_{n=1}^{\infty} \beta_n^R I_0(k_n r)\psi_n(y) + K^{-1}. \tag{5.4.13}$$

The term K^{-1} ensures that (5.2.10) is satisfied. We note that since the forcing of the internal free surface is independent of θ, there can be no angular variation in the potential and so (5.4.12), (5.4.13) include only the $q = 0$ modes from (5.4.4). We also note that, in the expansion for $r \geq b$, the first term represents the outgoing radiated wave, whilst the terms under the sum are all exponentially decaying modes. Defining $U^R(y)$ to be the outward radial velocity on $r = b$, we have

$$U^R(y) = \left.\frac{\partial \phi^R}{\partial r}\right|_{r=b} = \alpha_0^R k H_0'(kb)\psi_0(y) + \sum_{n=1}^{\infty} \alpha_n^R k_n K_0'(k_n b)\psi_n(y) \tag{5.4.14}$$

$$= \beta_0^R k J_0'(kb)\psi_0(y) + \sum_{n=1}^{\infty} \beta_n^R k_n I_0'(k_n b)\psi_n(y), \qquad (5.4.15)$$

and matching terms from (5.4.14) and (5.4.15) gives us

$$\alpha_0^R k H_0'(kb) = \beta_0^R k J_0'(kb) = \frac{1}{h}\int_{L_g} U^R(y)\psi_0(y)\,\mathrm{d}y = U_0^R, \qquad (5.4.16)$$

$$\alpha_n^R k_n K_0'(k_n b) = \beta_n^R k_n I_0'(k_n b) = \frac{1}{h}\int_{L_g} U^R(y)\psi_n(y)\,\mathrm{d}y = U_n^R, \quad n \geq 1, \qquad (5.4.17)$$

where $U^R(y) = 0$, $y \in L_b$ has been used so that we may write

$$U^R(y) = \sum_{n=0}^{\infty} U_n^R \psi_n(y). \qquad (5.4.18)$$

The jump in pressure across $r = b$, $P^R(y) = \phi^R|_{r=b^+} - \phi^R|_{r=b^-}$, is given by

$$\begin{aligned} P^R(y) = {} & \alpha_0^R \left[H_0(kb) - \frac{H_0'(kb)}{J_0'(kb)} J_0(kb) \right] \psi_0(y) \\ & -K^{-1} + \sum_{n=1}^{\infty} U_n^R \left[\frac{K_0(k_n b)}{k_n K_0'(k_n b)} - \frac{I_0(k_n b)}{k_n I_0'(k_n b)} \right] \psi_n(y), \end{aligned} \qquad (5.4.19)$$

where (5.4.16), (5.4.17) have been used. Simplification to the above equation can be achieved by employing the following Wronksian identities for Bessel functions (see Abramowitz & Stegun [1], equations (9.1.16) & (9.6.15))

$$J_n'(x)H_n(x) - H_n'(x)J_n(x) = -2i/\pi x \qquad (5.4.20)$$

$$I_n'(x)K_n(x) - K_n'(x)I_n(x) = 1/x. \qquad (5.4.21)$$

Thus (5.4.19) becomes

$$P^R(y) = \frac{-2i\alpha_0^R}{\pi kb J_0'(kb)}\psi_0(y) - K^{-1} + \sum_{n=1}^{\infty} \frac{U_n^R}{k_n^2 b I_0'(k_n b) K_0'(k_n b)}\psi_n(y). \qquad (5.4.22)$$

Hereafter we will make use of the following relations for derivatives of Bessel functions

$$\{H_0', J_0', K_0', I_0'\}(x) = \{-H_1, -J_1, -K_1, I_1\}(x).$$

The pressure is continuous across the gap under the duct and so $P^R(y) = 0$, for $y \in L_g$. Using this in the above equation and substituting from (5.4.17) gives

$$\int_{L_g} U^R(y) L(y,t)\,\mathrm{d}y = -K^{-1} + \frac{2i\alpha_0^R}{\pi kb J_1(kb)}\psi_0(t), \quad t \in L_g, \qquad (5.4.23)$$

where the kernel is defined to be

$$L(y,t) = \sum_{n=1}^{\infty} \frac{\psi_n(y)\psi_n(t)}{k_n^2 hb\, I_1(k_n b)K_1(k_n b)}, \tag{5.4.24}$$

and we note the behaviour

$$I_1(x)K_1(x) \sim \frac{1}{2x}\left(1 - \frac{3}{8x^2} + \ldots\right), \quad \text{as } x \to \infty\,. \tag{5.4.25}$$

Following the method of the §5.3, we introduce the functions $u_i(y)$ satisfying

$$\int_{L_g} u_i(y)L(y,t)\,\mathrm{d}y = d_i(t), \quad t \in L_g, \quad i = 1,2, \tag{5.4.26}$$

where

$$d_1(t) = 1, \quad \text{and} \quad d_2(t) = \psi_0(t). \tag{5.4.27}$$

Then the combination

$$U^R(y) = -K^{-1}u_1(y) + \frac{2i\alpha_0^R}{\pi kbJ_1(kb)}u_2(y), \tag{5.4.28}$$

satisfies (5.4.23). As in the §5.3, let the 2×2 matrix $\mathbf{S} = \{S_{ij}\}$ be defined by

$$S_{ij} = \int_{L_g} u_i(y)d_j(y)\,\mathrm{d}y. \tag{5.4.29}$$

We are interested in the induced volume flux, q^R and the far-field radiated wave amplitude $\mathcal{A}^R$. From (5.4.13) we note that, as $kr \to \infty$

$$\begin{aligned}\phi^R &\sim \alpha_0^R H_0(kr)\psi_0(y)\\ &\sim \alpha_0^R\left(\frac{2}{\pi kr}\right)^{1/2} \mathrm{e}^{ikr - i\pi/4}\psi_0(y),\end{aligned} \tag{5.4.30}$$

so that, on comparison with (5.3.27), the far-field radiated wave amplitude is given by $\mathcal{A}^R = \alpha_0^R$. From (5.4.16)

$$-\alpha_0^R khH_1(kb) = \int_{L_g} U^R(y)\psi_0(y)\,\mathrm{d}y = -K^{-1}S_{12} + \frac{2i\alpha_0^R S_{22}}{\pi kbJ_1(kb)}, \tag{5.4.31}$$

and on rearrangement we obtain

$$\mathcal{A}^R = \alpha_0^R = \frac{K^{-1}\pi kbJ_1(kb)S_{12}}{\gamma H_1(kb) + 2iS_{22}}, \tag{5.4.32}$$

where $\gamma = \pi kb\, khJ_1(kb)$ is real. The induced volume flux is given by

$$q^R = -\int_{S_i} \frac{\partial \phi^R}{\partial y}\,\mathrm{d}S = -\int_{L_g}\int_0^{2\pi} U^R(y) b\,\mathrm{d}\theta\,\mathrm{d}y, \tag{5.4.33}$$

using continuity of flux arguments in $r < b$, $0 < y < h$. Substituting (5.4.28) into the above and using (5.4.29) gives

$$\begin{aligned} q^R &= 2\pi b\left[K^{-1}S_{11} - \frac{2i\alpha_0^R S_{21}}{\pi kbJ_1(kb)}\right] \\ &= \frac{2\pi K^{-1}b(\gamma H_1(kb)S_{11} + 2i\Delta)}{\gamma H_1(kb) + 2iS_{22}}, \end{aligned} \tag{5.4.34}$$

where $\Delta = S_{11}S_{22} - S_{12}S_{21}$.

Using this in (5.2.15) gives

$$\tilde{B} = \frac{\omega}{\rho g}\cdot\frac{4\pi K^{-1}b\gamma J_1(kb)S_{12}^2}{\gamma^2 J_1^2(kb) + (\gamma Y_1(kb) + 2S_{22})^2}. \tag{5.4.35}$$

It is a simple matter to show that the relation derived earlier between $\mathcal{A}^R$ and $\tilde{B}$ and given by (5.4.7) is in fact satisfied identically by comparison of (5.4.32) with (5.4.35). Previously Thomas [69], using a method of matched eigenfunction expansions, had used the relation (5.4.7) as a numerical check.

The scattering problem

In this section we consider the problem of the scattering of an incident wave travelling in the positive x-direction in the absence of pressure variations on the internal free surface of the duct. We recall that the potential of the incident wave is given by $\phi_{inc} = \mathrm{e}^{ikx}\psi_0(y)$. From Abramowitz & Stegun [1], equation (9.1.41), we have

$$\mathrm{e}^{ikx} = \sum_{q=0}^{\infty} \epsilon_q i^q J_q(kr)\cos q\theta, \quad \begin{cases} \epsilon_0 = 1, \\ \epsilon_n = 2, \quad n \geq 1. \end{cases} \tag{5.4.36}$$

The presence of the incident wave destroys the angular symmetry enjoyed in the radiation problem and as a result, the expansions for the scattering potential must include all $\cos q\theta$ modes. Bearing in mind the incident wave potential, the most general expansions for the scattering potential are, in $r \geq b$

$$\phi^S = \sum_{q=0}^{\infty} \epsilon_q i^q \cos q\theta\left[\left(J_q(kr) + \alpha_{q,0}^S H_q(kr)\right)\psi_0(y) + \sum_{n=1}^{\infty}\alpha_{q,n}^S K_q(k_n r)\psi_n(y)\right], \tag{5.4.37}$$

and in $r \leq b$

$$\phi^S = \sum_{q=0}^{\infty} \epsilon_q i^q \cos q\theta \left[\beta_{q,0}^S J_q(kr)\psi_0(y) + \sum_{n=1}^{\infty} \beta_{q,n}^S I_q(k_n r)\psi_n(y) \right], \tag{5.4.38}$$

where it is noted that $\alpha_{q,0}^S$ are associated with the outgoing progressive waves, and $\beta_{q,0}^S$ represent the amplitudes of the standing wave modes inside the cylinder, whereas the terms under the sum over n are exponentially decaying disturbances.

We combine the above two expansions such that

$$\phi^S = \sum_{q=0}^{\infty} \epsilon_q i^q \cos q\theta \chi_q^S(r,y), \tag{5.4.39}$$

where $\chi_q^S(r,y)$ represents the terms in the square brackets in (5.4.37), (5.4.38) for $r \geq b$, $r \leq b$, respectively. Defining $U_q^S(y)$ to be the velocity across $r = b$ associated with the q th angular mode, we have

$$U_q^S(y) = \left. \frac{\partial \chi_q^S}{\partial r} \right|_{r=b} = \Big(kJ_q'(kb) + \alpha_{q,0}^S kH_q'(kb) \Big) \psi_0(y) + \sum_{n=1}^{\infty} \alpha_{q,n}^S k_n K_q'(k_n b)\psi_n(y) \tag{5.4.40}$$

$$= \beta_{q,0}^S kJ_q'(kb)\psi_0(y) + \sum_{n=1}^{\infty} \beta_{q,n}^S k_n I_q'(k_n b)\psi_n(y). \tag{5.4.41}$$

Multiplying (5.4.40), (5.4.41) by $\psi_m(y)$ and integrating over $[0,h]$ gives

$$kJ_q'(kb) + \alpha_{q,0}^S kH_q'(kb) = \beta_{q,0}^S kJ_q'(kb) = \frac{1}{h}\int_{L_g} U_q^S(y)\psi_0(y)\,\mathrm{d}y = U_{q,0}^S \tag{5.4.42}$$

$$\alpha_{q,n}^S k_n K_q'(k_n b) = \beta_{q,n}^S k_n I_q'(k_n b) = \frac{1}{h}\int_{L_g} U_q^S(y)\psi_n(y)\,\mathrm{d}y = U_{q,n}^S, \quad n \geq 1, \tag{5.4.43}$$

where we have used the fact that $U_q^S(y) = 0$ for $y \in L_b$ and so

$$U_q^S(y) = \sum_{n=0}^{\infty} U_{q,n}^S \psi_n(y). \tag{5.4.44}$$

In what has become the standard procedure by now, we let $P_q^S(y)$ be the jump in pressure at $r = b$ associated with the q th angular mode, defined as

$$\begin{aligned} P_q^S(y) &= \chi_q^S|_{r=b^+} - \chi_q^S|_{r=b^-} \\ &= \Big(J_q(kb) + \alpha_{q,0}^S H_q(kb) - \beta_{q,0}^S J_q(kb) \Big)\psi_0(y) \\ &\quad + \sum_{n=1}^{\infty} \Big(\alpha_{q,n}^S K_q(k_n b) - \beta_{q,n}^S I_q(k_n b) \Big)\psi_n(y) \\ &= \frac{-2i\alpha_{q,0}^S}{\pi kb J_q'(kb)}\psi_0(y) + \sum_{n=1}^{\infty} \frac{U_{q,n}^S}{k_n^2 b K_q'(k_n b) I_q'(k_n b)}\psi_n(y), \end{aligned} \tag{5.4.45}$$

where (5.4.42), (5.4.43) and the Wronksian identities for the Bessel functions have been used. Using (5.4.43) in the above with $P_q^S(y) = 0$ for $y \in L_g$ gives

$$\int_{L_g} U_q^S(t) L_q(y,t)\,\mathrm{d}t = \frac{-2i\alpha_{q,0}^S}{\pi k b J_q'(kb)}\psi_0(y), \quad y \in L_g, \tag{5.4.46}$$

where

$$L_q(y,t) = -\sum_{n=1}^{\infty} \frac{\psi_n(y)\psi_n(t)}{k_n^2 hb\, I_q'(k_n b) K_q'(k_n b)}, \tag{5.4.47}$$

and $L_0(y,t)$ is equivalent to the $L(y,t)$ defined in (5.4.24).

The induced volume flux across S_i, the internal free surface of the device is

$$q^S = -\int_{S_i} \frac{\partial \phi^S}{\partial y}\,\mathrm{d}S = -\int_{L_g}\int_0^{2\pi} \left.\frac{\partial \phi^S}{\partial r}\right|_{r=b} b\,\mathrm{d}\theta\,\mathrm{d}y = -b\sum_{q=0}^{\infty} \epsilon_q i^q \int_0^{2\pi}\int_{L_g} U_q^S(y)\cos q\theta\,\mathrm{d}y\,\mathrm{d}\theta$$
$$= -2\pi b\int_{L_g} U_0^S(y)\,\mathrm{d}y, \tag{5.4.48}$$

where the first step comes from continuity of flux. Hence, the only contribution to q^S comes from the $q = 0$ mode as in the radiation problem of the previous section. This is expected due to averaging of $\cos q\theta$ over S_i being zero. However, the scattered wave field cannot be determined from the $q = 0$ mode alone. This is clearly because the scattered wave amplitude is a function of θ and thus requires a knowledge of all $\alpha_{q,0}^S$ coefficients.

In terms of assessing the hydrodynamic properties of the duct OWC, we are only really interested in q^S and hence the value $q = 0$ throughout the preceding analysis. We therefore notice that $U_0^S(y)$ satisfies (5.4.46) with $q = 0$ by defining

$$U_0^S(y) = \frac{2i\alpha_{0,0}^S}{\pi k b J_1(kb)} u_2(y), \tag{5.4.49}$$

where $u_2(y)$ satisfies (5.4.26). Then from (5.4.42) we have

$$-khJ_1(kb) - \alpha_{0,0}^S khH_1(kb) = \frac{2i\alpha_{0,0}^S}{\pi k b J_1(kb)}\int_{L_g} u_2(y)\psi_0(y)\mathrm{d}y = \frac{2i\alpha_{0,0}^S}{\pi k b J_1(kb)} S_{22}, \tag{5.4.50}$$

where we have used (5.4.29). Rearranging gives

$$\alpha_{0,0}^S = \frac{-\gamma J_1(kb)}{\gamma H_1(kb) + 2iS_{22}}, \tag{5.4.51}$$

with $\gamma = \pi kb\, khJ_1(kb)$ as before. Also, from (5.4.48) we have

$$\begin{aligned} q^S &= \frac{-4ib\alpha_{0,0}^S}{kbJ_1(kb)} \int_{L_g} u_2(y)\,\mathrm{d}y \\ &= \frac{4\pi ikbhJ_1(kb)S_{21}}{\gamma H_1(kb) + 2iS_{22}}. \end{aligned} \tag{5.4.52}$$

Again, it is clear that one of the relations derived in §5.2 using Green's identity, namely (5.4.9), is satisfied identically on substitution of (5.4.52) and (5.4.32).

The far-field amplitude due to the scattering potential is given by

$$\begin{aligned} \phi^S &\sim \sum_{q=0}^{\infty} \epsilon_q i^q \cos q\theta \alpha_{q,0}^S H_q(kr)\psi_0(y) \\ &\sim \mathcal{R}^S(\theta)\left(\frac{2}{\pi kr}\right)^{1/2} \mathrm{e}^{ikr - i\pi/4}\psi_0(y), \end{aligned} \tag{5.4.53}$$

where

$$\mathcal{R}^S(\theta) = \sum_{q=0}^{\infty} \epsilon_q \alpha_{q,0}^S \cos q\theta \tag{5.4.54}$$

requires knowledge of the coefficients $\alpha_{q,0}^S$, for all q. This is, in principle, possible and the method of determining $\alpha_{q,0}^S$ for any $q \geq 0$ apparent from equations (5.4.42) and (5.4.46) using the standard techniques employed throughout this thesis.

Returning to (5.4.46) and rescaling $U_q^S(y)$ by

$$U_q^S(y) = \frac{-2i\alpha_{q,0}^S}{\pi kbJ_q'(kb)} u_q^S(y), \tag{5.4.55}$$

then $u_q^S(y)$ satisfies

$$\int_{L_g} u_q^S(t) L_q(y,t)\,\mathrm{d}t = \psi_0(y), \quad y \in L_g, \tag{5.4.56}$$

with the kernel $L_q(y,t)$ defined by (5.4.47) whilst (5.4.42) becomes

$$khJ_q'(kb) + \alpha_{q,0}^S khH_q'(kb) = \frac{-2i\alpha_{q,0}^S}{\pi kbJ_q'(kb)} \int_{L_g} u_q^S(y)\psi_0(y)\,\mathrm{d}y, \tag{5.4.57}$$

whence

$$\alpha_{q,0}^S = \frac{-\gamma_q J_q'(kb)}{\gamma_q H_q'(kb) + 2iA_q^S}, \tag{5.4.58}$$

where $\gamma_q = \pi kbkhJ_q'(kb)$ and

$$A_q^S = \int_{L_g} u_q^S(y)\psi_0(y)\,\mathrm{d}y. \tag{5.4.59}$$

Galerkin approximation

No extra complication has arisen in the three-dimensional OWC model and the problem can be expressed in operator notation as

$$\mathcal{L}u_i = d_i, \quad y \in L_g, \qquad \text{where} \begin{cases} d_1(y) = 1, \\ d_2(y) = \psi_0(y), \end{cases} \tag{5.4.60}$$

$$(u_i, d_j) = S_{ij}, \quad i, j = 1, 2, \tag{5.4.61}$$

from (5.4.26), (5.4.29). Once S_{ij} is known, q^S, $\mathcal{A}^R$, q^R and hence $\tilde{A}$, $\tilde{B}$ can all be determined. The only difference between the two-dimensional OWC problem of §5.3 and this problem is the kernel of the integral operator. The subsequent outcome of making the Galerkin approximation involves only slight changes and gives

$$\tilde{\mathbf{S}} = \mathbf{L}^{\mathrm{T}}\mathbf{K}^{-1}\mathbf{L}, \tag{5.4.62}$$

with the $(N+1) \times 2$ matrix $\mathbf{L} = \{L_{mn}\}$, $L_{mn} = L_m^{(n)}$ where $L_m^{(1)}$ and $L_m^{(2)}$ given by (5.3.76), (5.3.75) respectively. Here $\mathbf{K} = \{K_{mn}\}$ is an $(N+1) \times (N+1)$ matrix and

$$K_{mn} = \sum_{r=1}^{\infty} \frac{J_{2m}\{k_r(h-a)\} J_{2n}\{k_r(h-a)\}}{N_r k_r h \, k_r b \, I_1(k_r b) K_1(k_r b)}. \tag{5.4.63}$$

See §5.3 for more details.

Equations (5.4.56) and (5.4.59) with the positive-definite symmetric kernel defined by (5.4.47) constitute, for each q, a system similar to that defined by (2.22), (2.23) in chapter 2. The result of making a Galerkin approximation to $u_q^s(y)$, $q = 0, 1, 2, \ldots$ with trial functions consisting of the set defined for the velocity across the gap under the surface-piercing barrier described in §3.2, will result in an approximation $\tilde{A}_q^S$ to A_q^S such that, for each q,

$$0 < \tilde{A}_q^S = \mathbf{F}^{\mathrm{T}} \mathbf{K}^{(q)^{-1}} \mathbf{F} \le A_q^S, \tag{5.4.64}$$

where $\mathbf{F} = (F_{00}, \ldots, F_{N0})^{\mathrm{T}}$ and F_{m0} is given by (3.2.42) and $\mathbf{K}^{(q)} = \{K_{mn}^{(q)}\}$ where

$$K_{mn}^{(q)} = -\sum_{r=1}^{\infty} \frac{J_{2m}\{k_r(h-a)\} J_{2n}\{k_r(h-a)\}}{N_r k_r h \, k_r b \, I_q'(k_r b) K_q'(k_r b)}. \tag{5.4.65}$$

The coefficients $\alpha_{q,0}^S$ are then found from (5.4.58) and the amplitude of the scattered wave field is given by (5.4.54).

Notice that $K_{mn}^{(0)}$ in (5.4.65) is identical to K_{mn} in (5.4.63) and $\mathbf{F}$ is equivalent to $\mathbf{L}^{(2)}$ so that $A_0^S = S_{22}$.

5.4.2 Pressure difference formulation

The method of solution for the three-dimensional duct OWC above was based on a velocity formulation, the natural way of expressing the problem due to the link between the induced volume flux and the radial velocity of the fluid across the gap under the circular wall of the duct.

Without giving a full mathematical account of the process of formulating the duct OWC problem in terms of functions relating to the pressure difference across the wall of the duct, it should be mentioned that this complementary formulation is possible and can be achieved in a manner similar to that given in §5.3.

5.4.3 Results

We introduce non-dimensionalised quantities μ and ν to represent the radiation susceptance and radiation conductance coefficients through

$$\mu = \frac{\rho g}{\omega \pi b^2} \tilde{A}, \tag{5.4.66}$$

and

$$\nu = \frac{\rho g}{\omega \pi b^2} \tilde{B}, \tag{5.4.67}$$

so that the non-dimensionalised capture width, $\eta_{max}/2b$, is given by

$$\eta_{max} = \frac{\nu}{kb((\nu^2 + \mu^2)^{1/2} + \nu)}. \tag{5.4.68}$$

As in the two-dimensional OWC example, we choose to non-dimensionalise the induced volume flux due to the scattering potential, $|q^S|$, by the volume flux across S_i due to a solid mass of fluid oscillating with the frequency and amplitude of the

N	$\tilde{S}_{11}$	$\tilde{S}_{12} = \tilde{S}_{21}$	$\tilde{S}_{22}$
0	0.356038	0.248080	0.172856
1	0.407823	0.303642	0.232472
2	0.409336	0.305232	0.234144
3	0.409350	0.305247	0.234159
4	0.409350	0.305247	0.234159

Table 5.2: Convergence of the elements of $\mathbf{S}$, with increasing N in the case $a/h = 1/2$, $b/h = 1/8$ and $Kh = 1.7$.

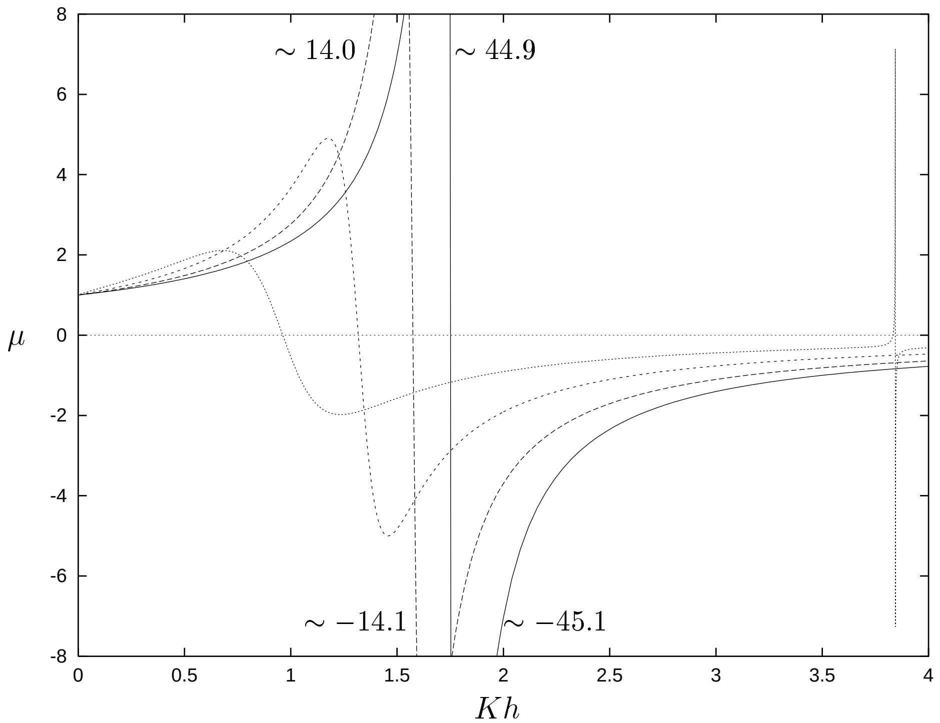

Figure 5.12: The radiation susceptance coefficient against Kh in the case of $a/h = 1/2$ for various duct radii: $b/h = \frac{1}{8}$ (———), $\frac{1}{4}$ (– – –), $\frac{1}{2}$ (- - - -), 1 (· · · · · ·).

incident wave, $|q^I|$ say, giving rise to

$$\frac{|q^S|}{|q^I|} = \frac{N_0^{1/2}|q^S|}{\pi k b^2 \sinh kh}. \tag{5.4.69}$$

These hydrodynamic coefficients are all expressible in terms of a 2×2 matrix $\mathbf{S}$ which is approximated by (5.4.62), the only changes required to the numerical procedure employed in the two-dimensional OWC model being the definition of the elements K_{mn} given by (5.4.63) in the symmetric $(N+1) \times (N+1)$ matrix $\mathbf{K}$. The test functions used for the expansion in the Galerkin approximation and related to the unknown velocity under the wall of the duct, have been chosen to incorporate

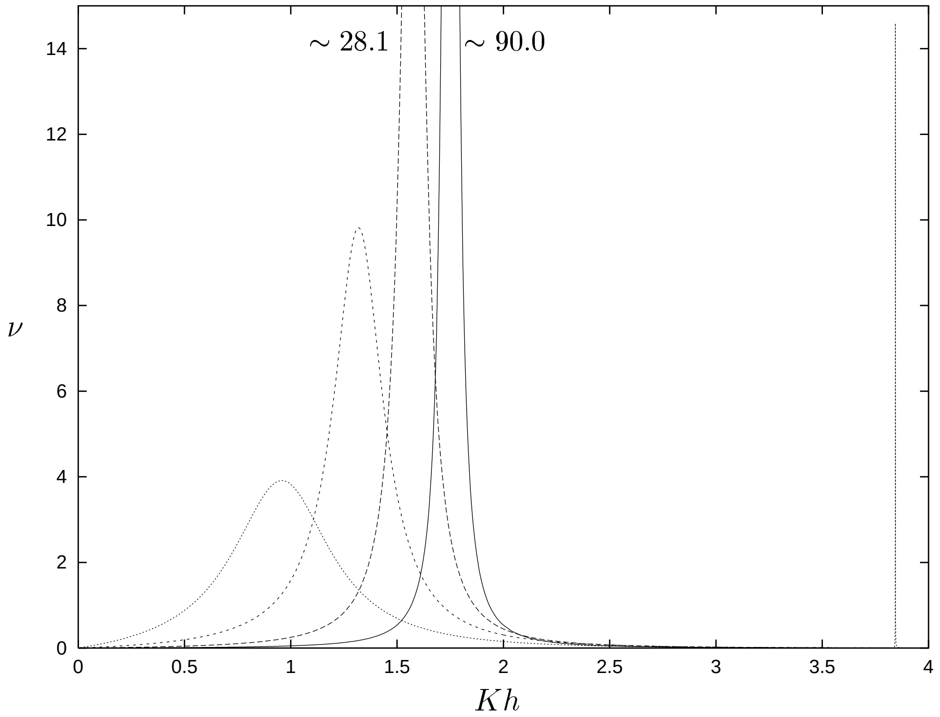

Figure 5.13: The radiation conductance coefficient against Kh in the case of $a/h = 1/2$ for various duct radii: $b/h = \frac{1}{8}$ (———), $\frac{1}{4}$ (– – –), $\frac{1}{2}$ (- - - -), 1 (· · · · · ·).

the correct singular behaviour at the lower edge of the duct. The convergence of the Galerkin approximation is shown in table 5.2. The estimates to S_{ij} for increasing values of truncation size, N, are all bounded above by their true values and six-figure accuracy is attained for N as low as 3 for the example chosen. In all cases, apart from a/h *very* small, choosing $N = 5$ assures six-figure accuracy in S_{ij} which translates into similar accuracy in the hydrodynamic coefficients. The infinite series defining the elements K_{mn} are truncated at a value of $M = 1500$ for the figures in table 5.2 and a leading order asymptotic correction similar to that described in §3.4 is used to improve accuracy in K_{mn}. For the figures that follow, $N, M = 5, 500$ is used.

We will not dwell on a detailed discussion of the results for this problem for two reasons. Firstly, Thomas [69] provides a comprehensive set of curves showing certain performance features for the duct OWC. Also, the results for the three-dimensional OWC closely match the behaviour of those for the two-dimensional model considered previously in §5.3.

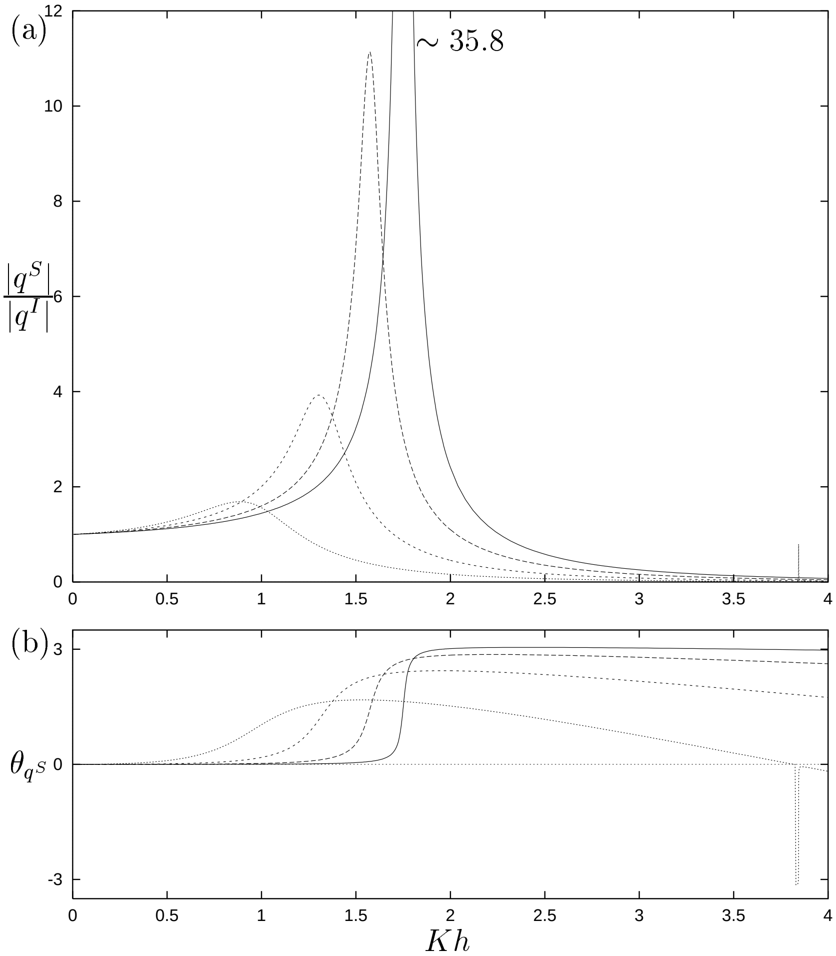

Figure 5.14: The (a) magnitude and (b) phase of induced volume flux due to the scattering potential against Kh in the case $a/h = 1/2$ for various duct radii: $b/h = \frac{1}{8}$ (———), $\frac{1}{4}$ (– – –), $\frac{1}{2}$ (- - - -), 1 (· · · · · ·).

However, two sets of figures are presented each showing the variation of μ, ν and the modulus and phase of q^S with dimensionless parameter Kh for certain arrangements. The first set, including figures 5.12–5.14, are for a fixed submergence depth of $a/h = \frac{1}{2}$ and shows curves for b/h, the ratio of the duct radius to water depth, varying between $\frac{1}{8}$ and 1. The curves exhibit the behavioural patterns seen in the two-dimensional OWC model. The large peaks in figures 5.12–5.14 are associated with the fundamental resonance in inside the duct. This resonance, already discussed in detail for the two-dimensional OWC case, is associated with the approximate solid-body motion of the fluid in a narrow (b/a small) duct when excited by an incident wave, which, using simple hydrostatic arguments, is shown

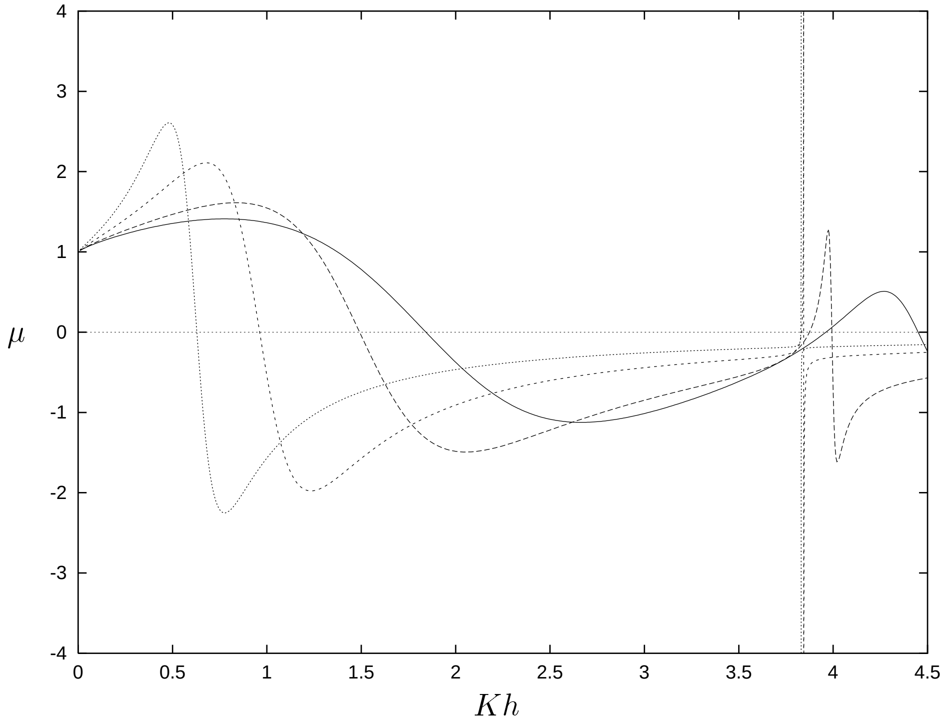

Figure 5.15: The radiation susceptance coefficient against Kh in the case of $b/h = 1$ for various duct radii: $a/h = \frac{1}{8}$ (———), $\frac{1}{4}$ (– – –), $\frac{1}{2}$ (- - - -), $\frac{3}{4}$ ($\cdots\cdots$).

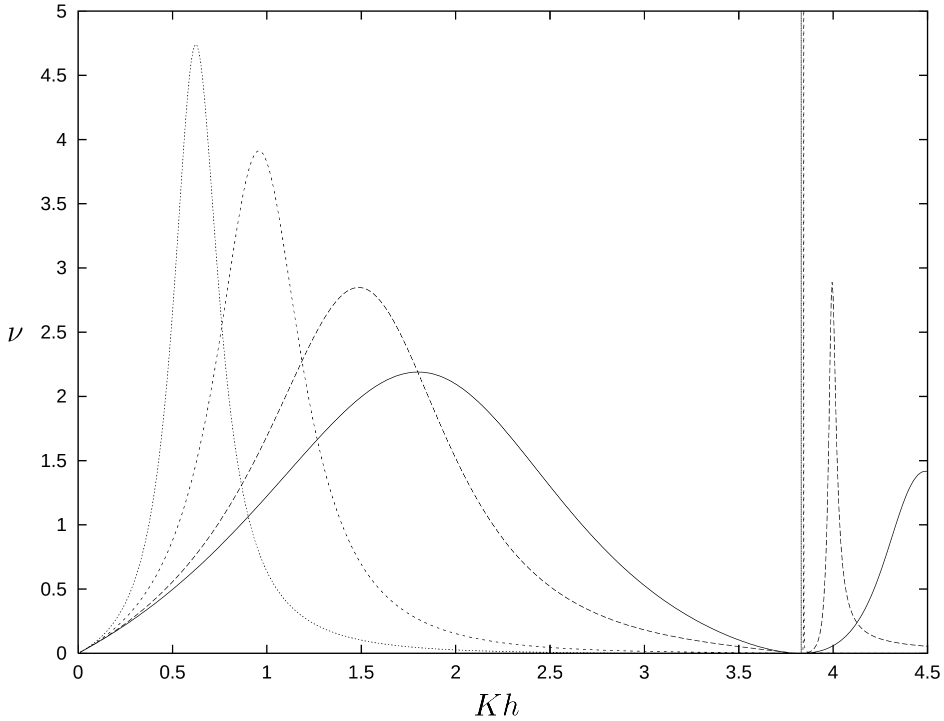

Figure 5.16: The radiation conductance coefficient against Kh in the case of $b/h = 1$ for various duct radii: $a/h = \frac{1}{8}$ (———), $\frac{1}{4}$ (– – –), $\frac{1}{2}$ (- - - -), $\frac{3}{4}$ ($\cdots\cdots$).

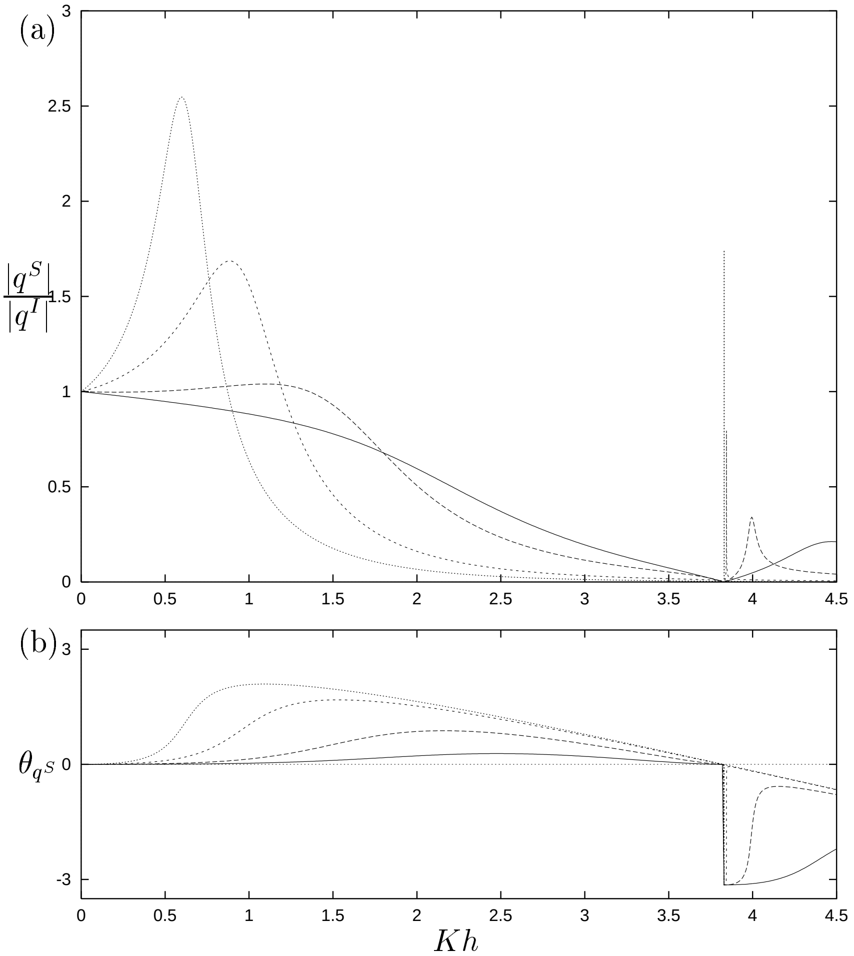

Figure 5.17: The (a) magnitude and (b) phase of induced volume flux due to the scattering potential against Kh in the case of $b/h = 1$ for various duct radii: $a/h = \frac{1}{8}$ (———), $\frac{1}{4}$ (– – –), $\frac{1}{2}$ (- - - -), $\frac{3}{4}$ (······).

to occur at $Ka \approx 1$. Thus we see that for a relatively narrow duct ($b/a = \frac{1}{4}$) the induced volume flux amplification factor, $|q^S/q^I|$, is very large (35.8).

At higher frequencies, further resonances occur each associated with the natural sloshing frequencies inside a duct whose walls extend throughout the depth. In the two-dimensional OWC model, this is equivalent to the sloshing modes in a two-dimensional tank which occur at $kb = n\pi$. In the duct OWC case resonances occur at zeros of $J_0'(kb)$ (or $J_1(kb)$) which are associated with the natural sloshing modes of fluid inside a vertical circular cylinder in finite depth. Note the first zero of $J_0'(kb)$ is at $kb = 3.831$. Other standing wave freqencies do not generate a net volume flux in the duct due to the averaging of $\cos q\theta$. Garrett [28] investigated these oscillations

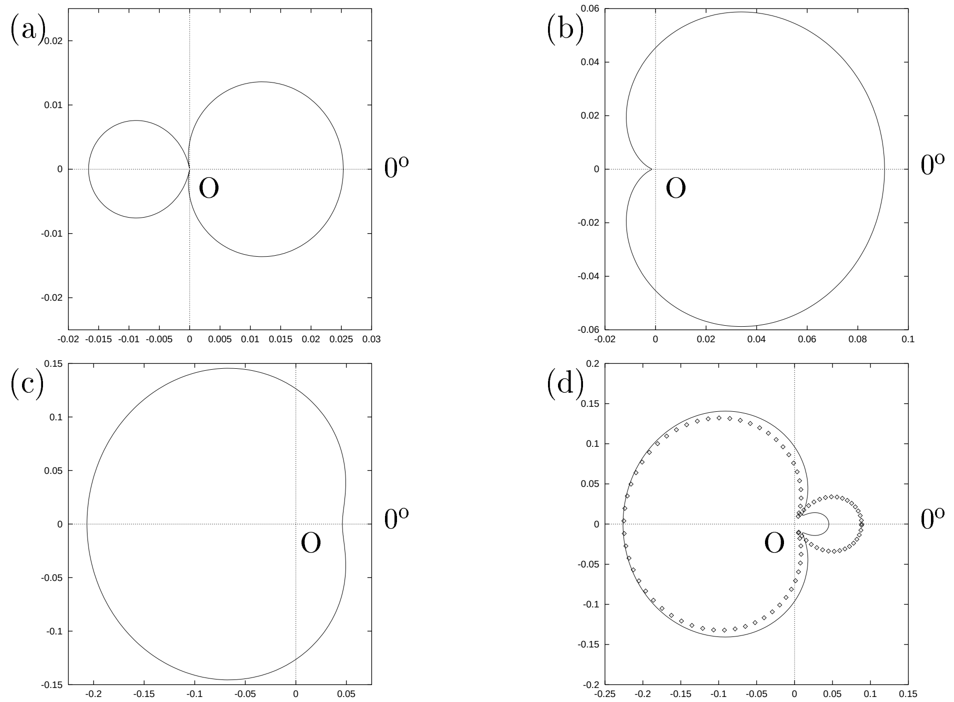

Figure 5.18: $|\mathcal{R}^S(\theta)|$, the modulus of the scattered wave amplitude, measured from O as θ varies: $a/h = \frac{1}{2}$, $b/h = \frac{1}{8}$; (a) $Kh = 1$, (b) $Kh = 1.5$, (c) $Kh = 2$, (d) $Kh = 2.5$, $\diamond$ are results for a cylinder extending to the bottom.

and also showed that large motions inside the duct due to an incident wave occur at small values beyond these resonant frequencies, a phenomenon which can be seen more clearly in the second set of figures. Thus, figures 5.15–5.17 show results for the case of a fixed duct radius of $b/h = 1.0$ where the depth of submergence of the circular lip is varied from $\frac{1}{8}$ to $\frac{3}{4}$. The closer the duct becomes to being a closed vertical cylinder, the more pronounced the resonance in the duct.

Notice also how the height of the maxima in the graphs of radiation susecptance is equal to the total jump from positive to negative in the graphs of radiation conductance. An explanation of this is given in, for example, Linton & Evans [43] and is due basically to the occurence of a pole close to the real axis of the complex plane $\nu + i\mu$.

Finally, in figures 5.18–5.20 we show curves of the scattered wave field when a train of parallel-crested waves are incident on the partially-immersed circular cylinder. This is presented diagramatically as in Miles & Gilbert [54] in the following way.

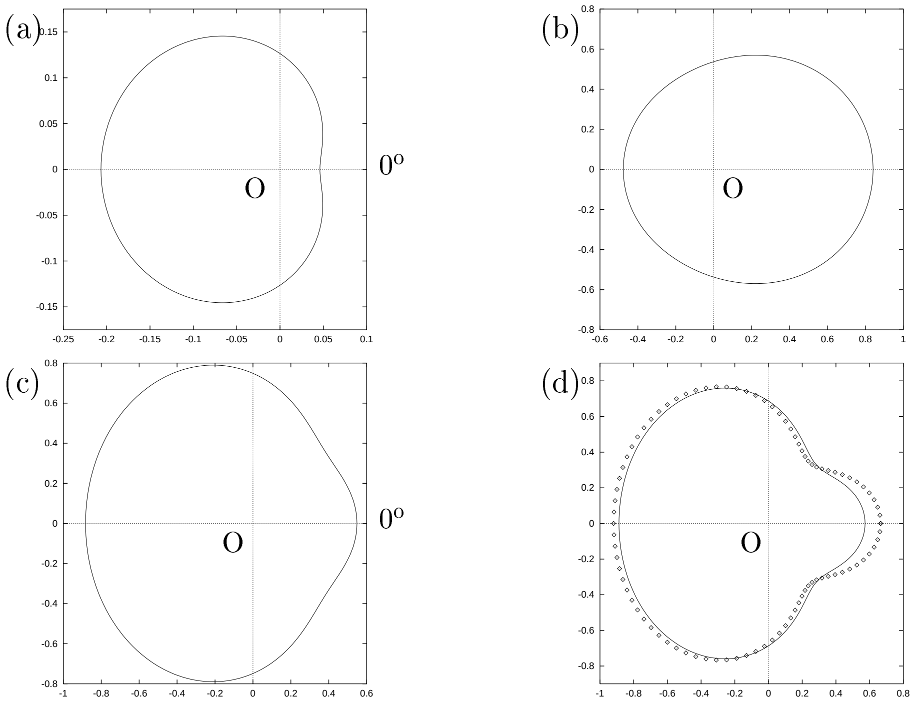

Figure 5.19: $|\mathcal{R}^S(\theta)|$, the modulus of the scattered wave amplitude, measured from O as θ varies: $b/h = \frac{1}{2}$, $Kh = 2$; (a) $a/h = \frac{1}{8}$, (b) $a/h = \frac{1}{4}$, (c) $a/h = \frac{1}{2}$, (d) $a/h = \frac{3}{4}$, $\diamond$ are results for a cylinder extending to the bottom.

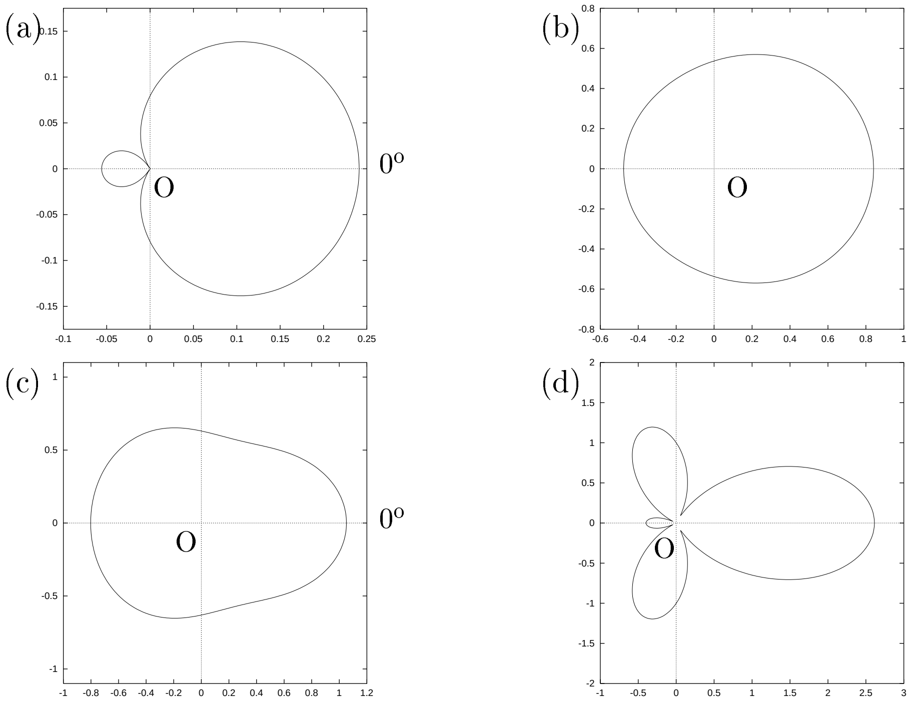

Figure 5.20: $|\mathcal{R}^S(\theta)|$, the modulus of the scattered wave amplitude, measured from O as θ varies: $a/h = \frac{1}{4}$, $Kh = 2$; (a) $b/h = \frac{1}{4}$, (b) $b/h = \frac{1}{2}$, (c) $b/h = 1$, (d) $b/h = 2$.

The distance of a point P on the curve from the origin, O, represents the modulus of the scattered wave amplitude in the direction θ, $|\mathcal{R}^S(\theta)|$, where θ is the angle between the line OP and the positive x-axis and where the incident wave comes from $\theta = \pi$ (the negative x-axis). So, for example, in figure 5.18(b) the amplitude of the waves scattered 'behind' the duct are large compared to those being reflected back in the direction of the oncoming waves. The strange cusps in figure 5.18(a) suggest that there is little or no waves scattered out towards $\theta \approx \pm 100^{\mathrm{o}}$ in this particular case.

The expression for $|\mathcal{R}^S(\theta)|$ in (5.4.54) is defined in terms of the coefficients $\alpha_{q,0}^S$, $q \geq 0$. Each $\alpha_{q,0}^S$ is related to A_q^S by (5.4.58) which is approximated by the lower bound $\tilde{A}_q^S$ in (5.4.64) as a result of a Galerkin approximation to the integral equations (5.4.56), (5.4.59). The infinite series defining $|\mathcal{R}^S(\theta)|$ in (5.4.54) requires truncation for some value of q. Numerically, we find that $|\alpha_{q,0}^S|$ are rapidly decreasing coefficients as q increases and using the criterion $|\alpha_{q,0}^S| \leq 10^{-6}$ for truncation of the series, never more than 15 azimuthal modes are required. In most cases only 5 modes are necessary for convergence.

Fixing two of the three flexible parameters of the problem, Kh, a/h and b/h in turn and choosing four values for the remaining parameter gives figures 5.18–5.20, (a)–(d), respectively. In figure 5.18, we choose $a/h = \frac{1}{2}$, $b/h = \frac{1}{8}$ and vary Kh from 1 to 2.5 in steps of 0.5. Beyond the largest of these values, the influence of the gap under the duct is small and the scattering resembles that of a vertical cylinder extending throughout the depth. The scattering of waves by such a geometry has a simple analytic solution (see Mei [51], p.313) and the scattered wave amplitude is found to be

$$\mathcal{R}^S(\theta) = \sum_{q=0}^{\infty} \epsilon_q \frac{J_q'(kb)}{H_q'(kb)} \cos q\theta. \tag{5.4.70}$$

Figure 5.18(d) compares results for the duct with the full cylinder.

In figure 5.19, the immersion of the duct is varied from $a/h = \frac{1}{8}$ to $\frac{3}{4}$ with $b/h = \frac{1}{2}$ and $Kh = 2$. The results for a duct immersed to three-quarters of the depth agree well with those for a cylinder extending throughout the depth.

Figure 5.20 shows the variation of $|\mathcal{R}^S(\theta)|$ with duct radius, b/h. Here, Kh and a/h have fixed values of 2 and $\frac{1}{4}$ respectively.

A variety of scattering problems can be achieved by varying the parameters of the problem. Those shown in figures 5.18–5.20 are just typical of the variety of shapes which can occur. In all cases considered the power of the numerical technique has been confirmed and the method can be used with confidence to explore any particular aspect of scattering by partially-immersed ducts.

The adaption of the methods presented in this chapter to a duct wave-energy device mounted on the sea-bed with a rigid-piston power take-off mechanism in the depths of the duct such as that considered by Simon [67] is trivial, as is the problem of scattering by a wholly-immersed duct either mounted on the sea bed or raised from the sea bed using the functions introduced in chapter 2 for the scattering of waves by different barrier configurations.

Chapter 6

Scattering by periodic arrays of breakwaters

6.1 Introduction

In chapters 3 & 4 we investigated the reflection properties of a number of thin vertical barrier configurations which were non-uniform in depth, but infinite and uniform in length. In terms of modelling an offshore breakwater scheme to protect a coastline or harbour from ocean waves, it may be advantageous to include gaps along the structure to enable vessels to pass through. In this chapter we model such a breakwater design by a periodic in-line array of thin-walled vertical barriers with gaps extending throughout the depth uniformly. The scattering of an incident wave by such an arrangement has received attention from a number of authors not only in the context of water waves. Due to the uniformity in depth, the equations describing the flow field are analogous to those in the the scattering of two-dimensional sound waves by an array of identical hard screens in linear acoustic theory. There are also analogies in other research areas and the equations describe, for example, the diffraction of monochromatic light by a thin grating or the scattering of electromagnetic waves by an array of thin dielectrics.

Amongst authors who have recently considered this problem are Dalrymple & Martin [7] who consider normal incidence only and Williams & Crull [74] who exploit a technique used by Achenbach & Li [3] for a general orientation of the barriers.

These latter two authors use a suitable Green's function to obtain a singular integral equation for the jump in the potential across just one of the barriers which is then reduced to an infinite system of equations by expanding the potential in a series of Chebychev polynomials. By considering normal incidence only, the problem becomes analogous to the scattering of waves by a thin baffle with a gap in a uniform two-dimensional waveguide. This problem has the property that an analytic solution exists for the case of equal screen and gap size. This was first shown by Baldwin & Heins [4] using a Wiener-Hopf technique to solve the resulting boundary-value problem exactly. Karp & Williams [36] showed by direct arguments the equivalence of this problem to the boundary-value problem of the scattering of plane waves by a thin semi-infinite plate lying on the centreline of a two-dimensional waveguide, a problem for which the Wiener-Hopf technique also provides an analytic solution. Dalrymple & Martin [7] investigate this normal-incidence problem for arbitrary barrier to gap sizes by expanding the potential on both sides of the barrier in terms of appropriate eigenfunctions and matching across the common boundary. This matching process can be performed in several different ways and Dalrymple & Martin [7] compare three approaches to approximate the reflection and transmission coefficients: the so-called method of matched eigenfunction expansions where two homogeneous equations expressing continuity of pressure and velocity across the gap are combined to yield an infinite system of equations (see chapter 2); a least squares method ; and a variational method using a trial function that incorporates the singular behaviour of the velocity at the edge of the barrier.

The number of propagating modes arising from the scattering of a given incident wave by the periodic array is dictated by the angle of incidence of the incoming wave and the ratio of its wavelength to the periodicity of the array. Thus, for a small enough wavenumber (a long enough wavelength) there exists only one reflected and one transmitted wave. As the wavenumber increases beyond each so-called cut-off frequency, an extra reflected and transmitted wave is generated. Thus, in general, for a given set of parameters, the reflection and transmission coefficients are given by R_n , T_n . The formulation of Dalrymple & Martin [7] allows a description of just the fundamental mode R_0 , T_0 .

We extend the approach of Dalrymple & Martin [7] by considering a train of monochromatic waves obliquely-incident upon the array by extracting the periodicity and constructing appropriate eigenfunction expansions either side of the in-line array. We match across the common boundary in such a way that two singular integral equations are obtained, one for the horizontal fluid velocity through a typical gap in the array, the other for the jump across a typical barrier (as described in a related problem by Wu [75]).

By separating out the propagating modes it is shown how the reflection and transmission coefficients R_n , T_n can be determined in terms of either a matrix $\mathbf{S}$ whose elements S_{mn} are defined as integrals of functions $u_n(y)$ related to the velocity across the gap between adjacent barriers, or a matrix $\mathbf{P}$ whose elements P_{mn} are defined as integrals of functions $p_n(y)$ related to the difference in pressure across a barrier. Here u_n , p_n satisfy singular integral equations each with the same Hermitian positive definite kernel but different inhomogenous functions. A simple Galerkin approximation incorporating the expected behaviour of either the velocity or the pressure difference provides accurate lower bounds to S_{mn} and P_{mn} . For sufficiently long waves, only one wave is reflected or transmitted and accurate upper and lower bounds for $|R_0|$, $|T_0|$, the fundamental reflection or transmission coefficients, are obtained from S_{00} and P_{00} . However, for more than one mode the lower bounds on S_{mn} and P_{mn} will not, in general, translate into upper and lower bounds on $|R_n|$, $|T_n|$.

The theory is developed in §6.2 and extended in §6.3 to the case of two identical parallel arrays of periodic breakwaters. Because of the symmetry in this problem it is possible to reduce it to two separate problems, each of which is a straightforward extension of the theory for a single periodic array described in §6.2.

In §6.4 a further generalisation to the two-array scheme is considered in which, whilst retaining the same periodicity in the arrays, the array separation and alignment is allowed to be different, thereby destroying the symmetry. It is conceivable that an approach similar to that used for the unsymmetric double barrier problem considered in chapter 4 and by Morris [55] could be employed here. Instead we choose to develop a wide-spacing approximation, applicable to any number of propagating modes, giving, in matrix form, the reflection and transmission coefficients for all modes in terms of those coefficients previously determined for the single periodic array. Recently, Heckl [31] has also investigated large systems of periodic arrays using a similar multi-modal technique.

The results are presented in §6.5 where first, curves of $|R_n|$, $|T_n|$ against non-dimensional wavenumber are presented for the case of a single periodic array. The results using different formulations turn out to be extremely close, using as little as five terms in the Galerkin expansion, and a comparison suggests that some inaccuracies exist in some cases in previous work on this problem. The corresponding $|R_n|$, $|T_n|$ for the two parallel periodic arrays are then presented and it is shown how total transmission as well as total reflection can occur for certain values of the parameters. This was expected by analogy with the case of two identical surface-piercing barriers considered by Evans & Morris [20], McIver [46] and the results of chapter 4. Results based on the wide-spacing approximation developed in §6.4 are now presented for this case and it is shown to give accurate results for all wavenumbers away from a cut-off provided the ratio of spacing to periodicity is greater than unity. Similar accuracy for the wide-spacing approximation has been reported elsewhere. See for example Martin [44] and Evans & Srokosz [24]. Finally results are presented for the two parallel arrays with unequal spacing using this approximation.

6.2 Formulation and solution

Cartesian co-ordinates are chosen with the barriers occupying $x = 0$, $0 < z < h$ where h is the water depth, in a periodic in-line array, with gaps $2a$ and distance

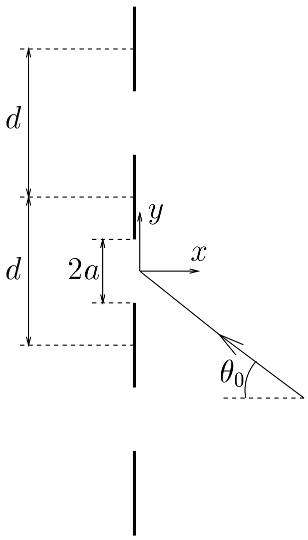

Figure 6.1: Definition sketch of breakwater.

d between their centres. A wave is incident upon the array from $x > 0$ making an angle $\pi - \theta_0 \in [0, \frac{1}{2}\pi)$ with the positive x-direction as illustrated in figure 6.1. Because the barriers extend throughout the depth uniformly the depth dependence can be extracted from the problem and the linearised velocity potential $\Phi(x, y, z, t)$ can be written as

$$\Phi(x, y, z, t) = \mathrm{Re}\{\phi(x, y) \cosh k(h - z) \mathrm{e}^{-i\omega t}\}, \tag{6.2.1}$$

where time-harmonic motion of frequency $\omega/2\pi$ is assumed and k is the real positive root of

$$K = \frac{\omega^2}{g} = k \tanh kh. \tag{6.2.2}$$

Then $\phi(x, y)$ satisfies

$$\frac{\partial^2 \phi}{\partial x^2} + \frac{\partial^2 \phi}{\partial y^2} + k^2 \phi = 0, \quad \text{in the fluid,} \tag{6.2.3}$$

$$\frac{\partial \phi}{\partial x} = 0, \quad \text{on a barrier.} \tag{6.2.4}$$

The incident wave is of the form

$$\phi_{inc}(x, y) = \mathrm{e}^{-ik(x \cos \theta_0 - y \sin \theta_0)}, \tag{6.2.5}$$

having wavelength $\lambda = 2\pi/k$. We write

$$\left.\begin{aligned} \beta_0 &= k \sin \theta_0 \\ \alpha_0 &= k \cos \theta_0 \end{aligned}\right\}, \tag{6.2.6}$$

so that

$$\phi_i(x,y) = \mathrm{e}^{-i(\alpha_0 x - \beta_0 y)}. \tag{6.2.7}$$

Because of the periodicity of the barriers the wave field at a point $y+d$ differs from that at y by a factor $\mathrm{e}^{i\beta_0 d}$, being the change in phase of the incident wave. Thus we may write

$$\phi(x, y+md) = \mathrm{e}^{im\beta_0 d}\phi(x,y), \quad m = 0, \pm 1, \pm 2, \ldots \tag{6.2.8}$$

and we need only consider a typical single strip such as $y \in [-\frac{1}{2}d, \frac{1}{2}d]$, $-\infty < x < \infty$ with (6.2.6) providing the extension of the solution to the whole plane.

It follows from (6.2.8) that we may write

$$\phi(x,y) = \mathrm{e}^{i\beta_0 y}\psi(x,y), \tag{6.2.9}$$

where $\psi(x,y)$ is periodic in y with period d. Hence, the most general form for $\phi(x,y)$ which ensures that (6.2.9) is satisfied is

$$\phi(x,y) = \sum_{n=-\infty}^{\infty} A_n \mathrm{e}^{-i(\alpha_n x - \beta_n y)}, \tag{6.2.10}$$

where

$$\beta_n = \beta_0 + \frac{2n\pi}{d}, \tag{6.2.11}$$

and

$$\alpha_n = (k^2 - \beta_n^2)^{1/2}, \tag{6.2.12}$$

to satisfy (6.2.3). By analogy with (6.2.6) we define

$$\left.\begin{aligned} \beta_n &= k\sin\theta_n \\ \alpha_n &= k\cos\theta_n \end{aligned}\right\}, \tag{6.2.13}$$

whence (6.2.11) becomes

$$\sin\theta_n = \sin\theta_0 + \frac{\lambda n}{d}. \tag{6.2.14}$$

Equation (6.2.14) has real solutions θ_n in pairs, namely θ_n and $\pi - \theta_n$ corresponding to waves travelling in directions symmetric about the line $x = 0$. If

$$\frac{\lambda}{d} > 1 + \sin\theta_0, \tag{6.2.15}$$

then θ_0 , $\pi - \theta_0$ are the only solutions of (6.2.14) corresponding to a single reflected and transmitted wave. This will be the case if the spacing $d < \lambda/2$. In general, the number of real solutions of (6.2.14) depends on the value of λ/d . Thus we have

$$-r \leq n \leq s, \tag{6.2.16}$$

where

$$r = \left[(1 + \sin\theta_0) \frac{d}{\lambda} \right], \tag{6.2.17}$$

$$s = \left[(1 - \sin\theta_0) \frac{d}{\lambda} \right], \tag{6.2.18}$$

and $[x]$ denotes the greatest integer $\leq x$. For $|\beta_n| > k$ we define $\gamma_n = (\beta_n^2 - k^2)^{1/2}$ ($= -i\alpha_n$ for $|\beta_n| < k$) and we introduce the functions

$$\psi_n(y) = \mathrm{e}^{i\beta_n y}, \tag{6.2.19}$$

satisfying

$$\frac{1}{d} \int_{-\frac{1}{2}d}^{\frac{1}{2}d} \psi_m(y) \overline{\psi_n(y)} \, \mathrm{d}y = \delta_{mn}, \tag{6.2.20}$$

where the bar denotes the complex conjugate. (Note that the definition of $\psi_n(y)$ in (6.2.19) is different to that used in the rest of this thesis). We can now write, for $x > 0$

$$\phi(x, y) = \mathrm{e}^{\gamma_0 x} \psi_0(y) + \sum_{n=-\infty}^{\infty} A_n \mathrm{e}^{-\gamma_n x} \psi_n(y), \tag{6.2.21}$$

whilst for $x < 0$

$$\phi(x, y) = \sum_{n=-\infty}^{\infty} B_n \mathrm{e}^{\gamma_n x} \psi_n(y), \tag{6.2.22}$$

and we have assumed $\gamma_n = -i\alpha_n$ for $n = -r, -r+1, \ldots, s-1, s$, $\gamma_n > 0$ otherwise. Now from (6.2.4), ϕ_x is continuous on $x = 0$ for all y so that from (6.2.21), (6.2.22)

$$\phi_x|_{x=0} \equiv U(y) = \gamma_0 \psi_0(y) - \sum_{n=-\infty}^{\infty} \gamma_n A_n \psi_n(y), \tag{6.2.23}$$

$$= \sum_{n=-\infty}^{\infty} \gamma_n B_n \psi_n(y). \tag{6.2.24}$$

We now multiply (6.2.24), (6.2.23) by $\overline{\psi_m(y)}$, integrate over $[-\frac{1}{2}d, \frac{1}{2}d]$, use (6.2.20) and the fact that the velocity $U(y) = 0$ on the interval occupied by the barrier $L_b = [-\frac{1}{2}d, -a] \cup [a, \frac{1}{2}d]$ to obtain

$$-\gamma_n(A_n - \delta_{n0}) = \gamma_n B_n = \frac{1}{d}\int_{L_g} U(y)\overline{\psi_n(y)}\,\mathrm{d}y, \tag{6.2.25}$$

where $L_g = [-a, a]$ is the gap between the barriers. Now

$$\begin{aligned} P(y) &\equiv \phi|_{x=0^+} - \phi|_{x=0^-} \\ &= \sum_{n=-\infty}^{\infty} \{(A_n + \delta_{n0}) - B_n\}\psi_n(y) \\ &= 2\sum_{n=-\infty}^{\infty} A_n\psi_n(y), \end{aligned} \tag{6.2.26}$$

from (6.2.25). The coefficients A_n, B_n for $n = -r, \ldots, s$ are of particular interest being amplitudes of the reflected and transmitted waves. To emphasize this we define $A_n = R_n$ and $B_n = T_n$ for $n = -r, \ldots, s$. Now since $P(y) = 0$ for $y \in L_g$ we obtain

$$\begin{aligned} \sum_{n=-r}^{s} R_n\psi_n(y) &= -\sum_{n=-\infty}^{\infty}{}' A_n\psi_n(y) \\ &= \int_{L_g} U(t)K(y,t)\,\mathrm{d}t, \quad y \in L_g, \end{aligned} \tag{6.2.27}$$

from (6.2.26) and (6.2.25) where

$$K(y,t) = \sum_{n=-\infty}^{\infty}{}'(\gamma_n d)^{-1}\psi_n(y)\overline{\psi_n(t)}, \tag{6.2.28}$$

and the notation $\sum'$ indicates that the values $n = -r, \ldots, s$ are omitted. Let $u_n(y)$ satisfy

$$\int_{L_g} u_n(t)K(y,t)\,\mathrm{d}t = \psi_n(y), \quad y \in L_g, \quad n = -r, \ldots, s. \tag{6.2.29}$$

Then it follows that

$$U(y) = \sum_{n=-r}^{s} R_n u_n(y), \tag{6.2.30}$$

satisfies (6.2.27). Also, from (6.2.25), (6.2.30)

$$\begin{aligned} -\gamma_n d(A_n - \delta_{n0}) &= i\alpha_n d(R_n - \delta_{n0}), \quad \text{for } n = -r, \ldots, s, \\ &= \int_{L_g}\sum_{m=-r}^{s} R_m u_m(y)\overline{\psi_n(y)}\,\mathrm{d}y. \end{aligned} \tag{6.2.31}$$

We define the $(r+s+1)\times(r+s+1)$ matrix $\mathbf{S}$ by

$$S_{nm} = \int_{L_g} u_m(y)\overline{\psi_n(y)}\,\mathrm{d}y \equiv (u_m, \psi_n), \quad n, m = -r, \ldots, s. \tag{6.2.32}$$

Then (6.2.31) may be written

$$i\mathbf{A}(\mathbf{R}-\mathbf{B}) = \mathbf{S}\mathbf{R}, \tag{6.2.33}$$

where

$$\mathbf{R} = (R_{-r}, R_{-r+1}, \ldots, R_{s-1}, R_s)^{\mathrm{T}}, \tag{6.2.34}$$

$$\mathbf{A} = \mathrm{diag}\{\alpha_n d\}_{n=-r,\ldots,s} \tag{6.2.35}$$

$$\mathbf{B} = (0, \ldots, 0, 1, 0, \ldots, 0)^{\mathrm{T}}, \quad \text{with the non-zero entry at } n=0 \text{ position.} \tag{6.2.36}$$

The problem is therefore reduced to solving the integral equations (6.2.29) and computing the matrix $\mathbf{S}$ given by (6.2.32) since then $\mathbf{R}$ is given from (6.2.33) as

$$\mathbf{R} = -i(\mathbf{S}-i\mathbf{A})^{-1}\mathbf{A}\mathbf{B}, \tag{6.2.37}$$

and

$$\mathbf{T} = (T_{-r}, \ldots, T_s)^{\mathrm{T}}, \tag{6.2.38}$$

is given by

$$\mathbf{R}+\mathbf{T} = \mathbf{B}, \tag{6.2.39}$$

which follows from (6.2.25) for $n = -r, \ldots, s$. Hence

$$\mathbf{T} = (\mathbf{S}-i\mathbf{A})^{-1}\mathbf{S}\mathbf{B}. \tag{6.2.40}$$

For the case of $n=0$, corresponding to a single reflected and transmitted wave, (6.2.37) reduces to

$$R_0 = -i\alpha_0 d/(S_{00} - i\alpha_0 d),$$

$$T_0 = S_{00}/(S_{00} - i\alpha_0 d),$$

and $|R_0|^2 + |T_0|^2 = 1$ as required. Thus

$$|R_0| = \alpha_0 d/(S_{00}^2 + \alpha_0^2 d^2)^{1/2}. \tag{6.2.41}$$

An alternative formulation involving $P(y)$ can be derived as follows. We multiply (6.2.26) by $\overline{\psi_m(y)}$, integrate over $[-\frac{1}{2}d, \frac{1}{2}d]$ and use the fact that $P(y) = 0$ for $y \in L_g$ to obtain

$$2A_n = \frac{1}{d} \int_{L_b} P(t) \overline{\psi_n(t)} \, \mathrm{d}t. \tag{6.2.42}$$

From (6.2.24) we have, since $U(y) = 0$ on L_b,

$$0 = \sum_{n=-r}^{s} i\alpha_n d(R_n - \delta_{n0})\psi_0(y) - \sum_{n=-\infty}^{\infty}{}' \gamma_n A_n \psi_n(y), \quad y \in L_b,$$

whence

$$2id \sum_{n=-r}^{s} \alpha_n d(R_n - \delta_{n0})\psi_0(y) = \int_{L_b} P(t) M(y,t) \, \mathrm{d}t, \tag{6.2.43}$$

where

$$M(y,t) = \sum_{n=-\infty}^{\infty}{}' \gamma_n d \psi_n(y) \overline{\psi_n(t)}. \tag{6.2.44}$$

For convenience we have (illegally) assumed the interchange of integration and summation obtaining a divergent infinite series for $M(y,t)$. However it can be shown that our subsequent development carries through with a more rigorous approach to give the same result. Define $p_n(y)$ as the solutions to

$$\int_{L_b} p_n(t) M(y,t) \, \mathrm{d}t = \psi_n(y), \quad y \in L_b, \quad n = -r, \dots, s. \tag{6.2.45}$$

Then it follows that

$$P(y) = 2id \sum_{n=-r}^{s} \alpha_n d(R_n - \delta_{n0}) p_n(y), \tag{6.2.46}$$

satisfies (6.2.43), and from (6.2.42) with $n = -r, \dots, s$,

$$2R_n = 2i \sum_{m=-r}^{s} \alpha_m d(R_m - \delta_{m0}) \int_{L_b} p_m(t) \overline{\psi_n(t)} \, \mathrm{d}t. \tag{6.2.47}$$

We define the $(r+s+1) \times (r+s+1)$ matrix $\mathbf{P}$ by

$$P_{nm} = \int_{L_b} p_m(y) \overline{\psi_n(y)} \, \mathrm{d}y \equiv (p_m, \psi_n), \quad m, n = -r, \dots, s. \tag{6.2.48}$$

Then (6.2.47) may be written

$$\mathbf{R} = i\mathbf{P}\mathbf{A}(\mathbf{R} - \mathbf{B}), \tag{6.2.49}$$

and the comparison of (6.2.33) with (6.2.49) shows that

$$\mathbf{P} = \mathbf{S}^{-1}, \tag{6.2.50}$$

and we have from (6.2.49)

$$\mathbf{R} = -i(\mathbf{I} - i\mathbf{PA})^{-1}\mathbf{PAB}, \tag{6.2.51}$$

and from (6.2.39)

$$\mathbf{T} = (\mathbf{I} - i\mathbf{PA})^{-1}\mathbf{B}. \tag{6.2.52}$$

For a single reflected and transmitted waves

$$|R_0| = \alpha_0 d|P_{00}|/(1 + \alpha_0^2 d^2 P_{00}^2)^{1/2}. \tag{6.2.53}$$

Returning to the velocity formulation we write (6.2.29) and (6.2.32) in operator notation in the form

$$\mathcal{K}u_n = \psi_n, \quad y \in L_g, \tag{6.2.54}$$

$$(u_m, \psi_n) = S_{nm}. \tag{6.2.55}$$

It follows from (6.2.28) that

$$\overline{K(y,t)} = K(t,y), \tag{6.2.56}$$

whence

$$(u, \mathcal{K}v) = (\mathcal{K}u, v), \quad \forall\ u, v \tag{6.2.57}$$

whilst

$$(u, \mathcal{K}u) = \sum_{n=-\infty}^{\infty}{}' (\gamma_n d)^{-1} \left| \int_{L_g} u(y)\overline{\psi_n(y)}\,\mathrm{d}y \right|^2 \geq 0. \tag{6.2.58}$$

Thus

$$S_{nm} = (u_m, \psi_n) = (u_m, \mathcal{K}u_n) = (\mathcal{K}u_m, u_n) = \overline{(u_n, \mathcal{K}u_m)} = \overline{S_{mn}}. \tag{6.2.59}$$

It is clear from (6.2.55), (6.2.58) that S_{nn} is real and $S_{nn} \geq 0$ for all n. Suppose we have a Galerkin approximation $\tilde{u}_n$ to the solution of (6.2.54) such that

$$\begin{aligned}(\tilde{u}_n, \mathcal{K}\tilde{u}_n) &= (\tilde{u}_n, \psi_n) \\ &= \tilde{S}_{nn}, \quad \text{say.}\end{aligned} \tag{6.2.60}$$

Then $\tilde{S}_{nn}$ is real and pursuing the approach given in chapter 2, we find

$$0 \leq \tilde{S}_{nn} \leq S_{nn}. \tag{6.2.61}$$

Using this information we are able prove a similar result for the approximation $\tilde{S}_{nm}$ to $S_{nm} = (u_m, \psi_n)$. Let $\tilde{u}_n \sim u_n$, $\tilde{u}_m \sim u_m$, n, m fixed, then

$$(\tilde{u}_n, \mathcal{K}\tilde{u}_n) \leq (u_n, \mathcal{K}u_n)$$
$$(\tilde{u}_m, \mathcal{K}\tilde{u}_m) \leq (u_m, \mathcal{K}u_m).$$

Now $\tilde{u}_{nm} = \tilde{u}_n + \lambda\tilde{u}_m \sim u_n + \lambda u_m = u_{nm}$, say. Then

$$0 \leq (\tilde{u}_{nm}, \mathcal{K}\tilde{u}_{nm}) \leq (u_{nm}, \mathcal{K}u_{nm}),$$

and expanding both sides, repeating with λ replaced by $-\lambda$, and subtracting, gives

$$|\lambda\tilde{S}_{nm} + \overline{\lambda}\tilde{S}_{mn}| \leq |\lambda S_{nm} + \overline{\lambda}S_{mn}|.$$

Choosing first λ real and then $\lambda = i\mu$, μ real now shows that

$$|\mathrm{Re}\{\tilde{S}_{nm}\}| \leq |\mathrm{Re}\{S_{nm}\}|,$$
$$|\mathrm{Im}\{\tilde{S}_{nm}\}| \leq |\mathrm{Im}\{S_{nm}\}|.$$

Let us now assume an expansion for our unknowns, $u_n(y)$, in the form

$$u_n(y) \simeq \tilde{u}_n(y) = \sum_{k=0}^{N} c_{nk} v_k(y). \tag{6.2.62}$$

and apply Galerkin's method to (6.2.54) with (6.2.59). Thus, substitutng the above approximation into (6.2.54), multiplying through by $\overline{v_n(t)}$ and integrating over L_g we obtain

$$\sum_{k=0}^{N} c_{nk}(\mathcal{K}v_k, v_m) = (\psi_n, v_m), \quad m = 0, \ldots, N, \quad n = -r, \ldots, s, \tag{6.2.63}$$

whilst from (6.2.59)

$$S_{nm} \simeq \tilde{S}_{nm} = \sum_{k=0}^{N} c_{mk}(v_k, \psi_n), \quad n, m = -r, \ldots, s. \tag{6.2.64}$$

In matrix notation, with $\mathbf{K}=\{K_{mn}\}$ where $K_{mn}=(\mathcal{K}v_n, v_m)$, $\mathbf{F}=\{F_{mn}\}$, where $F_{mn}=(\psi_n, v_m)$ and $\mathbf{C}=\{c_{mn}\}$, we have

$$\mathbf{K}\mathbf{C}^{\mathrm{T}}=\mathbf{F}, \tag{6.2.65}$$

and

$$\tilde{\mathbf{S}}=\overline{\mathbf{F}}^{\mathrm{T}}\mathbf{C}^{\mathrm{T}}=\overline{\mathbf{F}}^{\mathrm{T}}\mathbf{K}^{-1}\mathbf{F}. \tag{6.2.66}$$

Using (6.2.28) we obtain

$$K_{mn}=\sum_{r=-\infty}^{\infty}{}'(\gamma_r d)^{-1}F_{mr}\overline{F_{nr}}. \tag{6.2.67}$$

The anticipated square-root singularities at $y=\pm a$, together with resulting simplifications suggest we choose

$$v_n(y)=\frac{1}{\pi}\mathrm{e}^{in\pi/2}\frac{T_n(y/a)}{(a^2-y^2)^{1/2}}, \tag{6.2.68}$$

where $T_n(x)=\cos n\theta$, $x=\cos\theta$ is a Chebychev polynomial, so that

$$\begin{aligned} F_{mn}=(\psi_n, v_m) &= \frac{1}{\pi}\int_{-a}^{a}\frac{\mathrm{e}^{-im\pi/2}T_m(y/a)}{(a^2-y^2)^{1/2}}\mathrm{e}^{i\beta_n y}\,\mathrm{d}y \\ &= \frac{1}{\pi}\mathrm{e}^{-im\pi/2}\int_0^{\pi}\mathrm{e}^{i\beta_n a\cos\theta}\cos m\theta\,\mathrm{d}\theta \\ &= J_m(\beta_n a), \end{aligned} \tag{6.2.69}$$

whilst

$$K_{mn}=\sum_{r=-\infty}^{\infty}{}'(\gamma_r d)^{-1}J_m(\beta_r a)J_n(\beta_r a). \tag{6.2.70}$$

Returning to the pressure difference formulation we have in operator notation

$$\mathcal{M}p_n=\psi_n, \tag{6.2.71}$$

$$(p_m,\psi_n)=P_{nm}, \tag{6.2.72}$$

where again we can show that any approximations to p_n will yield approximations to P_{nm} whose real and imaginary parts are lower bounds. The expansion

$$p_n(y)=\sum_{k=0}^{N}d_{nr}w_k(y), \tag{6.2.73}$$

leads to

$$\mathbf{M}\mathbf{D}^{\mathrm{T}} = \mathbf{G}, \tag{6.2.74}$$

and

$$\tilde{\mathbf{P}} = \overline{\mathbf{G}}^{\mathrm{T}}\mathbf{D}^{\mathrm{T}} = \overline{\mathbf{G}}^{\mathrm{T}}\mathbf{M}^{-1}\mathbf{G}, \tag{6.2.75}$$

where $\mathbf{M} = \{M_{mn}\}$ where $M_{mn} = (\mathcal{M}w_n, w_m)$, $\mathbf{G} = \{G_{mn}\}$ where $G_{mn} = (\psi_n, w_m)$ and $\mathbf{D} = \{d_{mn}\}$. Using (6.2.44) we obtain

$$M_{mn} = \sum_{r=-\infty}^{\infty}{}' \gamma_r d\, G_{mr}\overline{G_{nr}}. \tag{6.2.76}$$

In choosing an appropriate expansion for $p_n(y)$ in the disjoint interval L_b it is convenient to shift the origin of y to the centre of the first barrier so that L_b is $(-\frac{1}{2}d + a, \frac{1}{2}d - a)$. Now the pressure jump across a thin barrier is known to behave like $(c^2 - y^2)^{1/2}$ as $y \to \pm c$ where $c = \frac{1}{2}d - a$. We therefore choose

$$w_n(y) = \frac{-i}{cd(n+1)}(c^2 - y^2)^{1/2}U_n(y/c), \tag{6.2.77}$$

where $U_n(x) = \sin(n+1)\theta/\sin\theta$, $x = \cos\theta$ is a Chebychev polynomial of the second kind. Then

$$\begin{aligned} G_{mn} &= \frac{i}{cd(m+1)}\int_{-c}^{c}(c^2 - y^2)^{1/2}U_m(y/c)\mathrm{e}^{i\beta_n y}\,\mathrm{d}y \\ &= \frac{ic}{d(m+1)}\int_0^{\pi}\sin(m+1)\theta\sin\theta\mathrm{e}^{i\beta_n c\cos\theta}\,\mathrm{d}\theta \\ &= \frac{1}{\beta_n d}\int_0^{\pi}\cos(m+1)\theta\mathrm{e}^{i\beta_n c\cos\theta}\,\mathrm{d}\theta, \end{aligned}$$

after integration by parts

$$= (\beta_n d)^{-1}J_{m+1}(\beta_n c), \tag{6.2.78}$$

and so

$$M_{mn} = \sum_{r=-\infty}^{\infty}{}' \frac{(\gamma_r d)}{(\beta_r d)^2}J_{m+1}(\beta_r c)J_{n+1}(\beta_r c). \tag{6.2.79}$$

A relation expressing conservation of energy can be found using Green's second identity (5.2.26) with the functions ϕ and $\overline{\phi}$ and a contour S consisting of the border of a typical strip of width d and of infinite extent. There is no contribution from the sides y, $y+d$, $-\infty < x < \infty$ due to the periodicity condition (6.2.8) and so energy conservation is simply found to be

$$\sum_{n=-r}^{s} \alpha_n d(R_n\overline{R}_n + T_n\overline{T}_n) = \alpha_0 d. \tag{6.2.80}$$

This is a well-known expression that has been derived in a similar problem by Linton & Evans [43]. In our matrix notation this may be written

$$(\mathbf{AR})^{\mathrm{T}}\overline{\mathbf{R}} + (\mathbf{AT})^{\mathrm{T}}\overline{\mathbf{T}} = \mathbf{B}^{\mathrm{T}}\mathbf{AB}, \tag{6.2.81}$$

which, using $\mathbf{R}+\mathbf{T}=\mathbf{B}$ may be re-written as

$$2\mathbf{R}^{\mathrm{T}}\mathbf{A}\overline{\mathbf{R}} = \mathbf{R}^{\mathrm{T}}\mathbf{AB} + \mathbf{B}^{\mathrm{T}}\mathbf{A}\overline{\mathbf{R}}, \tag{6.2.82}$$

or

$$\mathbf{R}^{\mathrm{T}}\mathbf{A}(\overline{\mathbf{R}} - \mathbf{B}) = (\mathbf{B}^{\mathrm{T}} - \mathbf{R}^{\mathrm{T}})\mathbf{A}\overline{\mathbf{R}}. \tag{6.2.83}$$

But from (6.2.33), we have

$$(\mathbf{B}^{\mathrm{T}} - \mathbf{R}^{\mathrm{T}})\mathbf{A} = i\mathbf{R}^{\mathrm{T}}\mathbf{S}^{\mathrm{T}}, \tag{6.2.84}$$

so that (6.2.83) becomes

$$i\mathbf{R}^{\mathrm{T}}\overline{\mathbf{S}\mathbf{R}} = i\mathbf{R}^{\mathrm{T}}\mathbf{S}^{\mathrm{T}}\overline{\mathbf{R}}, \tag{6.2.85}$$

which is satified since $\overline{\mathbf{S}} = \mathbf{S}^{\mathrm{T}}$ from (6.2.59). A similar argument clearly holds for $\mathbf{P}$ using (6.2.49). Thus our matrix formulation ensures that the energy conservation equation is satisfied identically.

6.3 Two parallel arrays of breakwaters

It is possible to extend the method to consider a further parallel identical array of breakwaters a distance $2b$ from the first. From symmetry the problem can be expressed in terms of two separate problems. Thus if the arrays occupy $x = \pm b$, $-\infty < y < \infty$ we can express $\phi(x,y)$ as

$$\phi(x,y) = \tfrac{1}{2}\{\phi^s(x,y) + \phi^a(x,y)\}, \tag{6.3.1}$$

where

$$\phi^s(x,y) = \phi^s(-x,y) \quad \text{with} \quad \frac{\partial \phi^s}{\partial x} = 0 \quad \text{on } x = 0, \tag{6.3.2}$$

whilst

$$\phi^a(x,y) = -\phi^a(-x,y) \quad \text{with} \quad \phi^a = 0 \quad \text{on } x = 0. \tag{6.3.3}$$

In this way we need only restrict attention to $x \geq 0$ since (6.3.2) and (6.3.3) provide the extension into $x \leq 0$ and (6.3.1) provides the full potential.

We consider first $\phi^s(x,y)$ and write, for $x > b$

$$\phi^s(x,y) = \mathrm{e}^{\gamma_0(x-b)}\psi_0(y) + \sum_{n=-\infty}^{\infty} A_n^s \mathrm{e}^{-\gamma_n(x-b)}\psi_n(y), \tag{6.3.4}$$

whilst for $0 < x < b$,

$$\phi^s(x,y) = \sum_{n=-\infty}^{\infty} B_n^s \cosh \gamma_n x \psi_n(y), \tag{6.3.5}$$

satisfying (6.3.2).

The form for ϕ^a is the same in $x > b$ as (6.3.4) with A_n^s replaced A_n^a, whilst in $0 \leq x \leq b$ we need to replace $B_n^s \cosh \gamma_n x$ by $B_n^a \sinh \gamma_n x$.

Following the procedure as for the single line of barriers from equations (6.2.21) up to (6.2.33) now leads to

$$\int_{L_g} u_n^s(t) K^s(y,t)\,\mathrm{d}t = \psi_n(y), \quad y \in L_g, \tag{6.3.6}$$

where

$$K^s(y,t) = {\sum_{n=-\infty}^{\infty}}' (\gamma_n d)^{-1}(1 + \coth \gamma_n b)\psi_n(y)\overline{\psi_n(t)}, \tag{6.3.7}$$

where we have written

$$U^s(y) = \sum_{n=-r}^{s} \left\{ R_n^s(1 + i \cot \alpha_n b) + \delta_{n0}(1 - i \cot \alpha_n b) \right\} u_n^s(y), \tag{6.3.8}$$

and

$$i\alpha_n d(R_n^s - \delta_{n0}) = \sum_{m=-r}^{s} \left\{ R_m^s(1 + i \cot \alpha_m b) + \delta_{m0}(1 - i \cot \alpha_m b) \right\} S_{nm}^s, \tag{6.3.9}$$

where the $(r+s+1) \times (r+s+1)$ matrix $\mathbf{S}_s$ has elements given by

$$S_{nm}^s = \int_{L_g} u_m^s(y)\overline{\psi_n(y)}\,\mathrm{d}y, \quad m,n = -r,\ldots,s. \tag{6.3.10}$$

In matrix notation this may be written

$$i\mathbf{A}(\mathbf{R}_s - \mathbf{B}) = \mathbf{S}_s\{(\mathbf{I} + i\mathbf{C}_s)\mathbf{R}_s + (\mathbf{I} - i\mathbf{C}_s)\mathbf{B}\}, \tag{6.3.11}$$

with $\mathbf{A}$, $\mathbf{B}$ defined as before,

$$\mathbf{R}_s = (R^s_{-r}, \ldots, R^s_s)^{\mathrm{T}}, \tag{6.3.12}$$

and

$$\mathbf{C}_s = \mathrm{diag}\{\cot \alpha_n b\}_{n=-r,\ldots,s}. \tag{6.3.13}$$

A similar procedure for $\phi^a(x, y)$ leads to

$$i\mathbf{A}(\mathbf{R}_a - \mathbf{B}) = \mathbf{S}_a\{(\mathbf{I} - i\mathbf{C}_a)\mathbf{R}_a + (\mathbf{I} + i\mathbf{C}_a)\mathbf{B}\}, \tag{6.3.14}$$

where $\mathbf{C}_a = \mathrm{diag}\{\tan \alpha_n b\}_{n=-r,\ldots,s}$ and in (6.3.7), (6.3.10), K^s, u^s, S^s_{nm} become K^a, u^a_n, S^a_{nm} and the $\coth \gamma_n b$ in $K^s(y,t)$ becomes $\tanh \gamma_n b$ in $K^a(y,t)$. It follows from (6.3.11) that

$$\mathbf{R}_s = -\left[\mathbf{S}_s + i(\mathbf{S}_s\mathbf{C}_s - \mathbf{A})\right]^{-1}\left[\mathbf{S}_s - i(\mathbf{S}_s\mathbf{C}_s - \mathbf{A})\right]\mathbf{B}, \tag{6.3.15}$$

whilst from (6.3.14)

$$\mathbf{R}_a = -\left[\mathbf{S}_a - i(\mathbf{S}_a\mathbf{C}_a + \mathbf{A})\right]^{-1}\left[\mathbf{S}_a + i(\mathbf{S}_a\mathbf{C}_a + \mathbf{A})\right]\mathbf{B}. \tag{6.3.16}$$

Now the energy conservation condition for $\mathbf{R}_s$ or $\mathbf{R}_a$ is

$$\sum_{n=-r}^{s} \alpha_n d R^{s,a}_n \overline{R}^{s,a}_n = \alpha_0 d, \tag{6.3.17}$$

or in matrix notation (for R^s)

$$\mathbf{R}_s^{\mathrm{T}}\mathbf{A}\overline{\mathbf{R}}_s = \mathbf{B}^{\mathrm{T}}\mathbf{A}\mathbf{B}. \tag{6.3.18}$$

To show that this is indeed satisfied we note that (6.3.15) may be written

$$\mathbf{R}_s = -(\mathbf{H}^{\mathrm{T}} + i\mathbf{A})^{-1}(\mathbf{H}^{\mathrm{T}} - i\mathbf{A})\mathbf{B}, \tag{6.3.19}$$

where

$$\mathbf{H}^{\mathrm{T}} = (\mathbf{C}_s\mathbf{A}^{-1} - \mathbf{S}_s^{-1})^{-1} = \overline{\mathbf{H}}. \tag{6.3.20}$$

Then it can be shown by elementary manipulations that (6.3.18) is satisfied. The same argument can be used for $\mathbf{R}_a$

Returning to (6.3.1) – (6.3.4) we see that as $x \to +\infty$

$$\phi(x,y) \sim \mathrm{e}^{-i\alpha_0(x-b)}\psi_0(y) + \frac{1}{2}\sum_{n=-r}^{s}(R_n^s + R_n^a)\mathrm{e}^{i\alpha_n(x-b)}\psi_n(y), \tag{6.3.21}$$

whilst as $x \to -\infty$,

$$\phi(x,y) \sim \frac{1}{2}\sum_{n=-r}^{s}(R_n^s - R_n^a)\mathrm{e}^{-i\alpha_n(x+b)}\psi_n(y), \tag{6.3.22}$$

so that the overall reflection and transmission coefficents are given by

$$\left.\begin{aligned} R_n &= \tfrac{1}{2}(R_n^s + R_n^a)\mathrm{e}^{-2i\alpha_n b} \\ T_n &= \tfrac{1}{2}(R_n^s - R_n^a)\mathrm{e}^{-2i\alpha_n b} \end{aligned}\right\}, \quad n = -r, \ldots, s. \tag{6.3.23}$$

Repeating the Galerkin approximation as before leads to

$$\tilde{\mathbf{S}}_s = \overline{\mathbf{F}}^{\mathrm{T}}\mathbf{K}_s^{-1}\mathbf{F} \tag{6.3.24}$$

with $\mathbf{F}$ defined as before, and $\mathbf{K}_s = \{K_{mn}^s\}$ where

$$K_{mn}^s = \sum_{r=-\infty}^{\infty}{}'(\gamma_r d)^{-1}(1 + \coth\gamma_r b)J_m(\beta_r a)J_n(\beta_r a), \tag{6.3.25}$$

whilst

$$\tilde{\mathbf{S}}_a = \overline{\mathbf{F}}^{\mathrm{T}}\mathbf{K}_a^{-1}\mathbf{F}, \tag{6.3.26}$$

where $\mathbf{K}_a = \{K_{mn}^a\}$ and

$$K_{mn}^a = \sum_{r=-\infty}^{\infty}{}'(\gamma_r d)^{-1}(1 + \tanh\gamma_r b)J_m(\beta_r a)J_n(\beta_r a). \tag{6.3.27}$$

A pressure-difference formulation can be obtained by proceeding in exactly the same manner as for the single line of barriers and gives

$$\mathbf{R}_s = -\left[\mathbf{I} + i(\mathbf{C}_s - \mathbf{P}_s\mathbf{A})\right]^{-1}\left[\mathbf{I} - i(\mathbf{C}_s - \mathbf{P}_s\mathbf{A})\right]\mathbf{B}, \tag{6.3.28}$$

and

$$\mathbf{R}_a = -\left[\mathbf{I} - i(\mathbf{C}_a + \mathbf{P}_a\mathbf{A})\right]^{-1}\left[\mathbf{I} + i(\mathbf{C}_a + \mathbf{P}_a\mathbf{A})\right]\mathbf{B}, \tag{6.3.29}$$

where a repeat of the Galerkin approximation gives

$$\tilde{\mathbf{P}}_s = \overline{\mathbf{G}}^{\mathrm{T}} \mathbf{M}_s^{-1} \mathbf{G}, \tag{6.3.30}$$

with $\mathbf{G}$ defined as before and $\mathbf{M}_s = \{M_{mn}^s\}$ where

$$M_{mn}^s = \sum_{r=-\infty}^{\infty}{}' \frac{(\gamma_r d)}{(\beta_r d)^2} (1 + \coth \gamma_r b)^{-1} J_{m+1}(\beta_r c) J_{n+1}(\beta_r c), \tag{6.3.31}$$

whilst

$$\tilde{\mathbf{P}}_a = \overline{\mathbf{G}}^{\mathrm{T}} \mathbf{M}_a^{-1} \mathbf{G}, \tag{6.3.32}$$

where $\mathbf{M}_a = \{M_{mn}^a\}$ and where

$$M_{mn}^a = \sum_{r=-\infty}^{\infty}{}' \frac{(\gamma_r d)}{(\beta_r d)^2} (1 + \tanh \gamma_r b)^{-1} J_{m+1}(\beta_r c) J_{n+1}(\beta_r c), \tag{6.3.33}$$

and $c = \frac{1}{2}d - a$ as before.

6.4 Wide-spacing approximation

In §6.3 we were able to take advantage of symmetry arguments in order to separate the problem of two identical periodic arrays into two simple problems, each being a straightforward extension of the single periodic array. If we consider a second array having different periodicity d and different spacing ratio a/d, the problem becomes much more complicated, not least since the number of radiated modes at each array will, in general, be different for a given incident wave. However, if we require that the periodicity be the same for each array, but allow a/d to be different for the second array, then a relatively simple solution for the reflection and transmission coefficients can be derived using the wide-spacing approximation. The basis of this approximation is the assumption that the two sets of barriers are far enough apart that the effect on an array of the decaying modes radiated from the other array is negligible.

We shall use a matrix formulation to obtain the reflection and transmission coefficients for a pair of periodic barriers positioned on the lines $x = \pm b$, each having period d. The array on $x = b$ has spacing ratio a_1/d, whilst on $x = -b$, the spacing is a_2/d. Having obtained our approximation we shall test its accuracy using the accurate numerical results derived in §6.3 for the case $a_1 = a_2 = a$ thus giving us an estimate of the region of validity for results obtained when $a_1 \neq a_2$.

The essential result of §6.2 was (6.2.37) and (6.2.40), which related the reflection and transmission coefficients to the matrix $\mathbf{S}$. The simple form for $\mathbf{B}$ in (6.2.37) stems from the incident wave. It is straightforward to show that the reflection and transmission coefficients resulting from an incident wave given by

$$\sum_{n=-r}^{s} D_n \mathrm{e}^{\mp i\alpha_n x}\psi_n(y), \quad \text{from } x = \pm\infty, \tag{6.4.1}$$

is

$$\mathbf{R}^{(i)}(\mathbf{D}) = -i(\mathbf{S}^{(i)} - i\mathbf{A})^{-1}\mathbf{A}\mathbf{D} \equiv \mathcal{R}^{(i)}\mathbf{D} \tag{6.4.2}$$

$$\mathbf{T}^{(i)}(\mathbf{D}) = (\mathbf{S}^{(i)} - i\mathbf{A})^{-1}\mathbf{S}^{(i)}\mathbf{D} \equiv \mathcal{T}^{(i)}\mathbf{D}, \tag{6.4.3}$$

for $i = 1, 2$, where $\mathcal{R}^{(i)}$, $\mathcal{T}^{(i)}$ are reflection and transmission *matrices* and

$$\mathbf{D} = (D_{-r}, \ldots, D_s)^{\mathrm{T}}, \tag{6.4.4}$$

and the superscript i refers to a spacing a_i/d leading to a corresponding matrix $\mathbf{S}^{(i)}$. Thus the matrices $\mathcal{R}^{(i)}$, $\mathcal{T}^{(i)}$ contain the essential information for the array in that they convert a set of incident waves described by the vector $\mathbf{D}$ into a set of reflection and transmission coefficients described by $\mathbf{R}^{(i)}(\mathbf{D})$ and $\mathbf{T}^{(i)}(\mathbf{D})$ respectively. Notice from symmetry that the results (6.4.2), (6.4.3) are independent of the sign in (6.4.1).

We are now in a position to apply the wide-spacing approximation. In $x > b$ we assume

$$\phi(x,y) \sim \mathrm{e}^{-i\alpha_0 x}\psi_0(y) + \sum_{n=-r}^{s} R_n^{(w)} \mathrm{e}^{i\alpha_n x}\psi_n(y), \tag{6.4.5}$$

or an incident wave field described by $\mathbf{B}$ and a vector reflection coefficient $\mathbf{R}^{(w)}$. For $x < -b$ we assume

$$\phi(x,y) \sim \sum_{n=-r}^{s} T_n^{(w)} \mathrm{e}^{-i\alpha_n x}\psi_n(y), \tag{6.4.6}$$

or a vector transmission coefficient $\mathbf{T}^{(w)}$. For $|x| < b$ away from $x = \pm b$ we assume

$$\phi(x, y) \sim \sum_{n=-r}^{s} (U_n \mathrm{e}^{i\alpha_n x} + V_n \mathrm{e}^{-i\alpha_n x}) \psi_n(y), \tag{6.4.7}$$

described by the vectors $\mathbf{U}$, $\mathbf{V}$. We now consider the wave interactions occuring at the array at $x = b$, using an origin shift of $X = x - b$ so that we can use the reflection and transmission matrices defined by (6.4.2), (6.4.3) with $i = 1$. Then the reflected waves described by $\mathbf{R}^{(w)}$ are manifested through the reflection of $\mathbf{B}$ and by the transmission of $\mathbf{U}$ giving

$$\mathbf{\Delta R}^{(w)} = \mathcal{R}^{(1)} \mathbf{\Delta}^{-1} \mathbf{B} + \mathcal{T}^{(1)} \mathbf{\Delta U}, \tag{6.4.8}$$

where

$$\mathbf{\Delta} = \mathrm{diag}\{\mathrm{e}^{i\alpha_n b}\}_{n=-r,\ldots,s} \tag{6.4.9}$$

has been introduced to account for the phase shift associated with the shift in origin. In the same way, the waves travelling away from the array in $x < b$, and described by $\mathbf{V}$ are due partly to the waves transmitted from $\mathbf{B}$ and the waves reflected from $\mathbf{U}$. Thus

$$\mathbf{\Delta}^{-1} \mathbf{V} = \mathcal{T}^{(1)} \mathbf{\Delta}^{-1} \mathbf{B} + \mathcal{R}^{(1)} \mathbf{\Delta U}. \tag{6.4.10}$$

In the same manner, we can consider the wave interactions at the array $x = -b$ after a change of coordinates $X = x + b$ allowing the use of our reflection and transmission matrices. This yields

$$\mathbf{\Delta T}^{(w)} = \mathcal{T}^{(2)} \mathbf{\Delta V}, \tag{6.4.11}$$

and

$$\mathbf{\Delta}^{-1} \mathbf{U} = \mathcal{R}^{(2)} \mathbf{\Delta V}, \tag{6.4.12}$$

Using (6.4.10) and (6.4.12) we obtain

$$\mathbf{U} = \mathbf{\Delta} \left[\mathbf{I} - \mathcal{R}^{(2)} \mathbf{\Delta}^2 \mathcal{R}^{(1)} \mathbf{\Delta}^2 \right]^{-1} \mathcal{R}^{(2)} \mathbf{\Delta}^2 \mathcal{T}^{(1)} \mathbf{\Delta}^{-1} \mathbf{B}, \tag{6.4.13}$$

$$\mathbf{V} = \mathbf{\Delta} \left[\mathbf{I} - \mathcal{R}^{(1)} \mathbf{\Delta}^2 \mathcal{R}^{(2)} \mathbf{\Delta}^2 \right]^{-1} \mathcal{T}^{(1)} \mathbf{\Delta}^{-1} \mathbf{B}, \tag{6.4.14}$$

whence the reflection and transmission coefficients are found from (6.4.8), (6.4.11) to be

$$\mathbf{R}^{(w)} = \mathbf{\Delta}^{-1} \left\{ \mathcal{R}^{(1)} + \mathcal{T}^{(1)}\mathbf{\Delta}^2 \left[\mathbf{I} - \mathcal{R}^{(2)}\mathbf{\Delta}^2\mathcal{R}^{(1)}\mathbf{\Delta}^2 \right]^{-1} \mathcal{R}^{(2)}\mathbf{\Delta}^2\mathcal{T}^{(1)} \right\} \mathbf{\Delta}^{-1}\mathbf{B}, \quad (6.4.15)$$

and

$$\mathbf{T}^{(w)} = \mathbf{\Delta}^{-1}\mathcal{T}^{(2)}\mathbf{\Delta}^2 \left[\mathbf{I} - \mathcal{R}^{(1)}\mathbf{\Delta}^2\mathcal{R}^{(2)}\mathbf{\Delta}^2 \right]^{-1} \mathcal{T}^{(1)}\mathbf{\Delta}^{-1}\mathbf{B}. \quad (6.4.16)$$

A similar approach has been used by Heckl [31] in considering the multi-mode problem of more than one periodic array of circular cylinders. If the parameters of the problem are chosen such that there is only one reflected and transmitted wave from an array of screens, the matrices above reduce to scalar quantities and (6.4.15), (6.4.16) become

$$R_0^{(1,2)} = R_0^{(1)}\mathrm{e}^{-2i\alpha_0 b} + \frac{T_0^{(1)}R_0^{(2)}T_0^{(1)}\mathrm{e}^{2i\alpha_0 b}}{1 - R_0^{(1)}R_0^{(2)}\mathrm{e}^{4i\alpha_0 b}}, \quad (6.4.17)$$

and

$$T_0^{(1,2)} = \frac{T_0^{(1)}T_0^{(2)}}{1 - R_0^{(1)}R_0^{(2)}\mathrm{e}^{4i\alpha_0 b}}, \quad (6.4.18)$$

which are well-known wide-spacing expressions occuring in many approximations to two-body scattering problems.

6.5 Results

In sections §6.2 and §6.3 we have derived expressions for all the reflection and transmission coefficients arising at a particular incident wavelength and given incident angle and array periodicity, firstly in the case of a single array and then for two parallel arrays of breakwaters. These coefficients rely upon the matrices $\mathbf{S}$ using the velocity formulation or $\mathbf{P}$ using the pressure difference formulation (include subscripts a, s for the antisymmetric and symmetric problems in the case of the double array.) The accuracy with which these matrices can be estimated determines how good the approximations to the reflection and transmission coefficients are. For sufficiently large wavelengths there exists just one reflected and transmitted wave

N	$\|R_0\|$(velocity)	$\geq$	$\|R_0\|$(pressure)
0	0.8608729		0.8114980
1	0.8193251		0.8192764
2	0.8192860		0.8192860
Exact	0.8192860		

Table 6.1: Convergence of upper and lower bounds to the exact solution when $\theta_0 = 0$ and $a/c = 1$. Here $ka = 3$, $M = 1000$.

N	$\tilde{S}_{0,0}$	$\tilde{S}_{0,-1} = \tilde{S}_{-1,0}$	$\tilde{S}_{-1,-1}$	$\tilde{P}_{0,0}$	$\tilde{P}_{0,-1} = \tilde{P}_{-1,0}$	$\tilde{P}_{-1,-1}$
0	4.043751	4.012717	4.212316	0.921356	1.096094	1.303971
1	4.407085	4.017003	4.245722	1.191195	1.132021	1.308755
2	4.419828	4.025257	4.251068	1.629835	1.549062	1.705261
3	4.419840	4.025272	4.251086	1.644088	1.556824	1.709488
4	4.419842	4.025273	4.251087	1.644537	1.557205	1.709810
5	4.419842	4.025273	4.251087	1.644543	1.557204	1.709810

Table 6.2: Convergence of the elements of the matrices $\tilde{\mathbf{S}}$ and $\tilde{\mathbf{P}}$ where $\theta_0 = 0^{\circ}$, $a/c = 0.2$, $kd = 5$ gives two modes, $M = 2000$.

and it follows from (6.2.41), (6.2.53) and (6.2.63) that the two formulations provide upper and lower bounds to the true value of $|R_0|$, $|T_0|$ in the case of a single line of barriers. Table 6.1 illustrates a particular example of this. Here, we have chosen the special case of normal incidence and equal screen to gap ratio for which an exact expression for the reflection coefficient exists due to Baldwin & Heins [4] namely

$$\left.\begin{array}{l} |R| = \sin\theta \\ |T| = \cos\theta \end{array}\right\}, \quad \text{where} \quad \theta = \sum_{n=1}^{\infty} \left\{ \sin^{-1}\left(\frac{ka}{(n-\frac{1}{2})\pi}\right) - \sin^{-1}\left(\frac{ka}{n\pi}\right) \right\}.$$

The accuracy obtained in this case gives us an indication of the accuracy we can expect when bounds no longer exist. Here, conservation of energy is automatically ensured due to the matrix structure that is employed and cannot be use as a check for accuracy as in Williams & Crull [74].

We find that, in nearly all cases, results from the two formulations agree to within at least three significant figures with just six terms ($N = 5$) in the Galerkin approximation. The exceptions occur when the two arrays of breakwaters are placed extremely close together (e.g. $b/d = 0.01$), where the strength of the singularity at the tip of a barrier becomes large and more terms are required not just in the

Galerkin approximation, but also in the evaluation of the elements of the matrices $\mathbf{K}_{s,a}$, $\mathbf{M}_{s,a}$. These elements require the evaluation of an infinite series which must be truncated to a size M say. For a single line of barriers K_{mn} and M_{mn}, the elements of $\mathbf{K}$ and $\mathbf{M}$, also require the same treatment and in both cases it is vital that the entries of these matrices are accurate enough to ensure sufficient accuracy for $|R_n|$ and $|T_n|$. It is trivial to show that terms in each of the infinite series arising in this chapter decay like $O(n^{-2})$. An asymptotic correction to account for the truncation of the infinite series in the manner described in §3.4 is more difficult to compute for this problem due to the way in which the angle of incidence manifests itself in the terms of the series. For normal incidence this difficulty is avoided, but for general θ_0 we do not use any asymptotic correction. As a result, we need to take a larger value of M for the same degree of accuracy enjoyed in other problems in this thesis. It was found that taking $M = 1000$ was sufficient for three significant figures accuracy in $|R_n|$ and $|T_n|$ in most cases, and for extreme cases a value of $M = 2000$ was used. Table 6.2 illustrates the convergence of elements of $\tilde{\mathbf{S}}$ and $\tilde{\mathbf{P}}$ for a typical set of parameters for which there are two modes, 0 and -1.

Agreement between results derived from the two formulations was also sometimes found to diminish as the non-dimensional wavenumber kd increased (to beyond a value of $kd = 15$). Here again, small inaccuracies in computing the infinite sums may have a larger effect on the coefficients of reflection and transmission since they are themselves the solution of a matrix equation of increased size due to the introduction of higher propagating wave modes. Nevertheless, agreement between the two formulations was always good enough to claim at least two significant figures accuracy even in most extreme cases. As was observed in §3.4 for the single barrier in finite depth, we note that the velocity formulation gives highly accurate results for small N when the gap is small whilst if the gap is large and the barrier is small, it is the pressure difference formulation that performs well.

Figures 6.2 and 6.3 show the behaviour of the reflection coefficients, $|R_n|$, as the wavenumber, kd, varies for a single periodic array of breakwaters. The first of

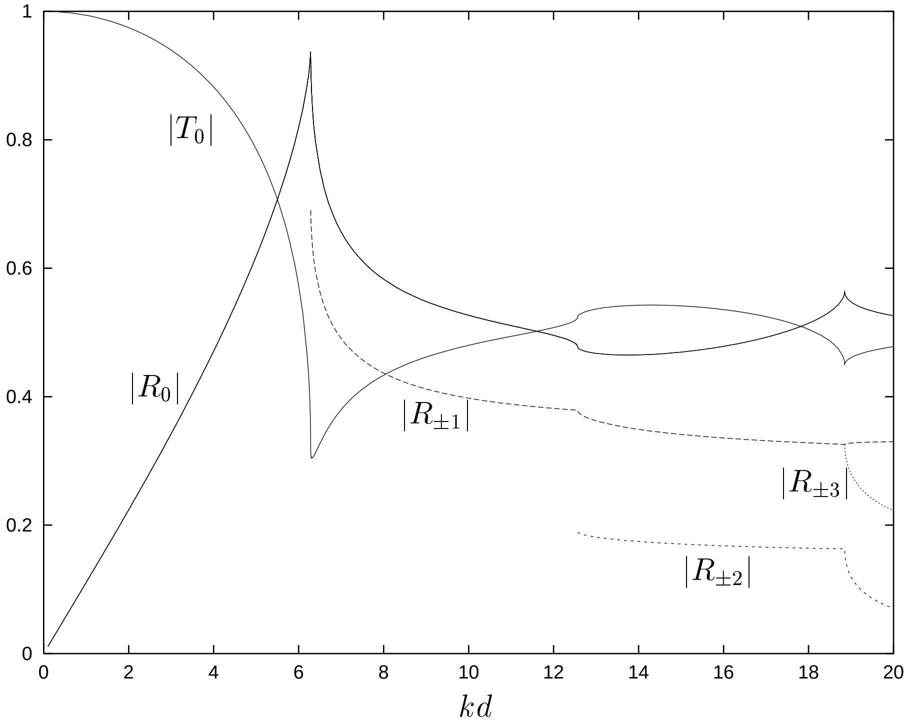

Figure 6.2: $|R_n|$ against non-dimensionalised wavenumber kd for a single line of barriers; $a/c = 0.5$, $\theta_0 = 0^{\text{o}}$.

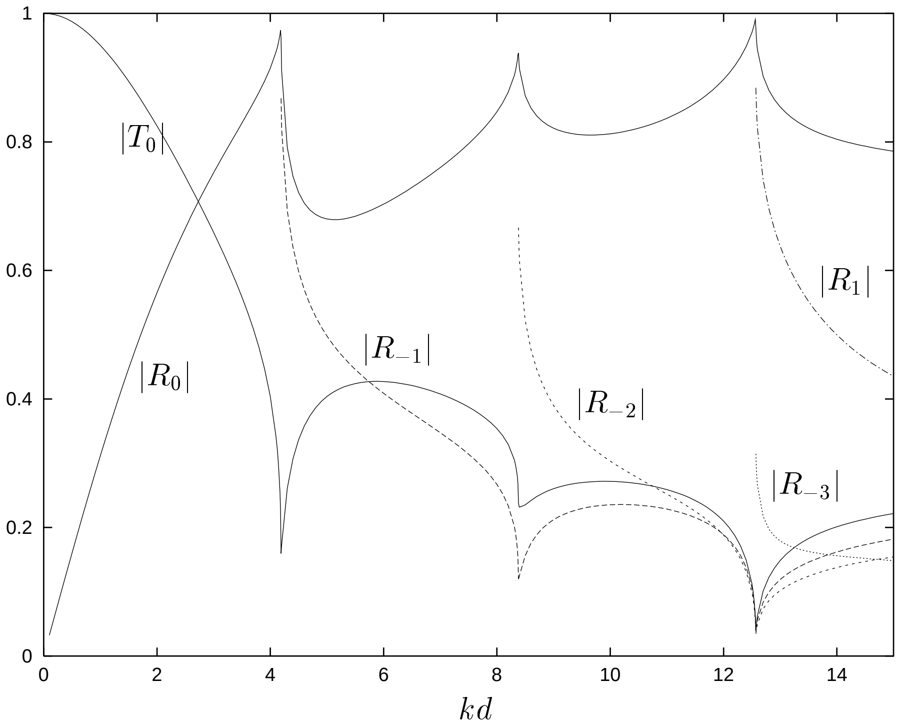

Figure 6.3: $|R_n|$ against non-dimensionalised wavenumber kd for a single line of barriers; $a/c = 0.2$, $\theta_0 = 30^{\text{o}}$.

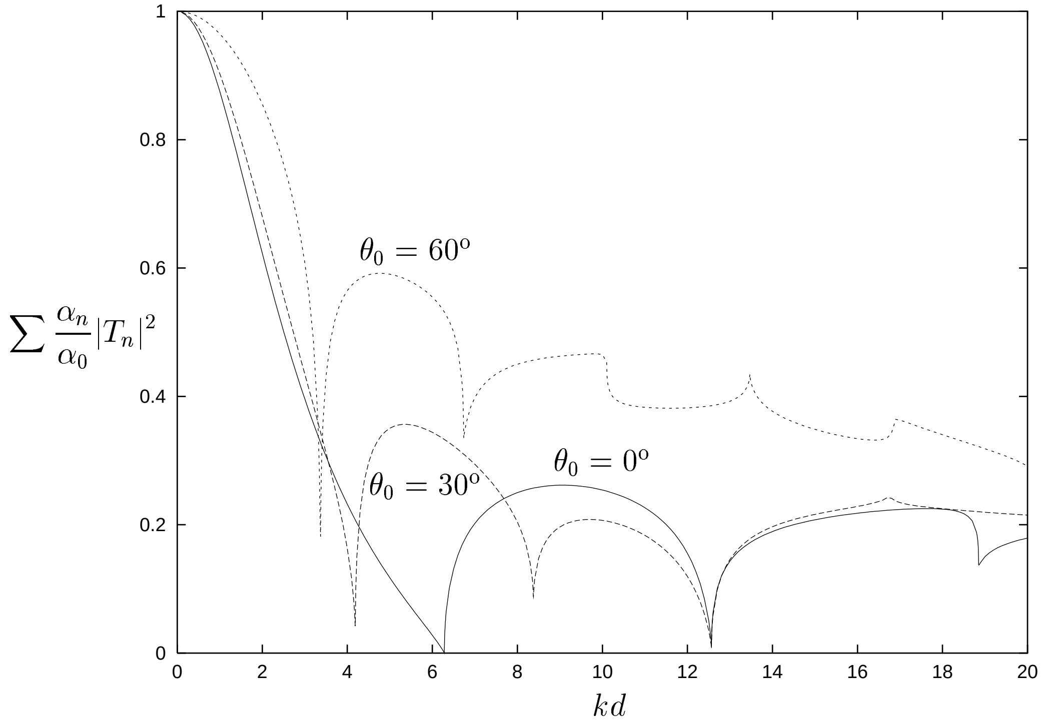

Figure 6.4: Proportion of incident wave energy transmitted through a single line of screens as θ_0 varies vs. kd with $a/c = 0.2$.

these two graphs shows the effect of a normally-incident wave with $a/c = 0.5$ (equal screen and gap size) and compares favourably with graphs shown by Dalrymple & Martin [7] and Williams & Crull [74] who present curves of $|R_0|$ and $|T_0|$ only. The first of these authors used a matched eigenfunction approach to determine their results, but did not solve for the higher reflected and transmitted modes. Williams & Crull [74] used a Green's function method and derived expressions for the higher wave modes occuring at wavelengths beyond the first cut-off but did not present any curves associated with $|R_n|$, $|T_n|$ for $n \geq 0$. Figure 6.2 shows the introduction of the higher propagating modes as kd passes through the cut-off frequencies located for this arrangement at $kd = 2m\pi$ from (6.2.16). Here $kd = 20$ corresponds to $\lambda/d \simeq 1/3$. Note that we do not show curves of $|T_n|$, because from (6.2.39) we have $|T_n| = |R_n|$ for $n \neq 0$ and $|T_0| = |1 - R_0|$.

In figure 6.3 we show the effect on the reflection coefficients of an incident wave making an angle $\theta_0 = 30^{\mathrm{o}}$ to the normal and with a spacing ratio given by $a/c = 0.2$. Comparison with the same arrangement presented in Williams & Crull [74, figure

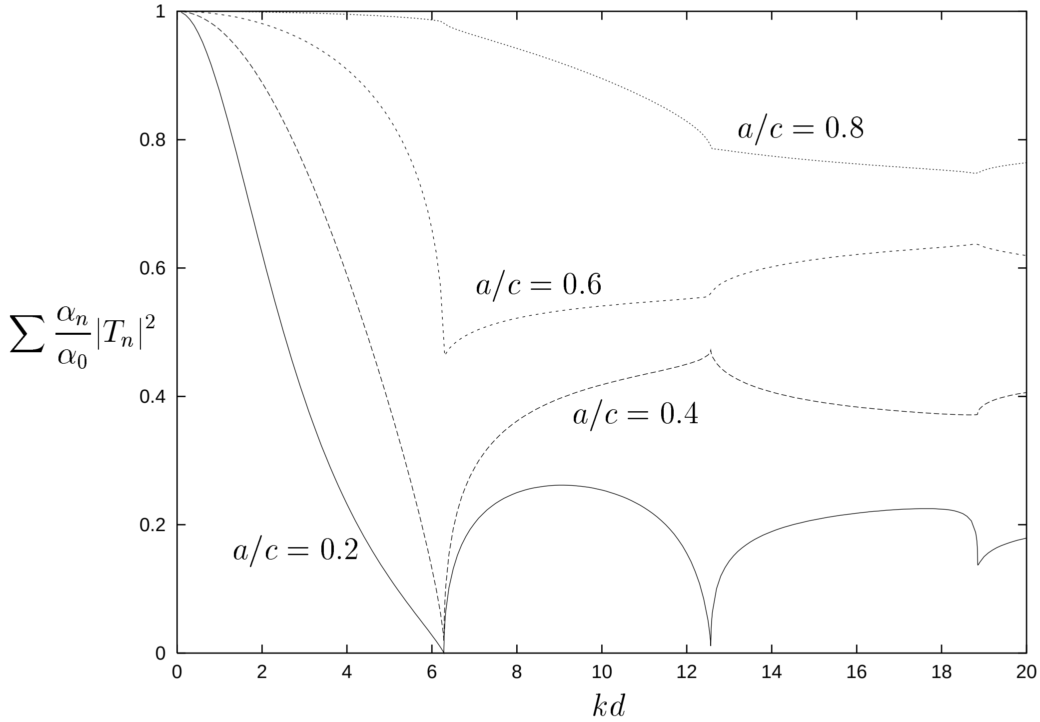

Figure 6.5: Proportion of incident wave energy transmitted through a single line of screens as a/c varies vs. kd with $\theta_0 = 0^{\circ}$.

5] shows a marked discrepancy in the curves of $|R_0|$ in between the first two cut-offs. Other computations to compare the results of Williams & Crull [74] with those given by this method suggests that some of their curves may be in error especially in the case of oblique wave incidence. It is noted from figure 6.3 that the reflection coefficient for the fundamental mode is the dominant reflected wave and that other modes at higher wavenumbers, although large near the cut-off at which they occur, soon become less prominent as kd is increased. Again, we find no reason to present curves of $|T_n|$ since they are evident from the form of the curves for $|R_n|$.

One way of measuring the effectiveness of a breakwater over a range of parameters is to consider the total transmitted wave energy through the array as a proportion of the incident wave energy. This quantity is obtained by computing

$$T_{total} = \sum_{n=-r}^{s} \frac{\alpha_n}{\alpha_0}|T_n|^2 \tag{6.5.1}$$

which comes from (6.2.81). In figure 6.4 the effect of varying the angle of incidence, θ_0, on T_{total} as kd increases is shown. It can be seen that maximum reflection occurs for normally-incident waves where for $kd > 4$, or $\lambda/d < 1.5$, the proportion of incident wave energy passing through the breakwater is always less than 25% for the case of a gap to screen ratio of 0.2. Increasing the angle of incidence has the effect of increasing the total transmitted energy, a result that has been observed in other barrier problems, see for example Evans & Morris [20] or chapter 3. Figure 6.5 shows the effect of gap size on T_{total} for normally-incident waves. As expected, increasing the ratio of gap size to barrier size, a/c, increases the total transmitted energy and it is interesting to note that for large kd, or very short wavelengths $T_{total} \simeq a/c$. This can be explained as follows. For high frequency waves, the barriers will effectively block the waves incident on the portion of the array occupied by the barriers whereas the waves incident upon the gaps will not feel the presence of the barriers and so this part of the incident wave energy can pass through uninhibited. Thus we expect the relation $T_{total} \to a/c$ as $kd \to \infty$ to hold. This limit is clearly independent of the angle which the incident wave makes with the array and so it is not surprising to see this asymptotic behaviour also occuring in figure 6.4 where $a/c = 0.2$ and θ_0 varies.

Results for two identical parallel arrays of screens are presented in figures 6.6–6.11. In general, the curves for the reflection and transmission coefficients are complicated due to the interactions between the two arrays but there are certain features that stand out. We no longer have the condition $\mathbf{R} + \mathbf{T} = \mathbf{B}$, and so it is useful to show moduli of both reflection and transmission coefficients. In all graphs shown we restrict the range of kd for no other reason but to avoid unnecessary confusion.

In general it can be seen that the addition of an extra array, as expected, reduces the overall transmitted wave energy. For example, comparison of figures 6.9 and 6.5 shows that over a large range of kd, for an array spacing given by $b/d = 0.25$, the transmitted energy is considerably lower for all values of a/c. This is especially true in the range of $4 < kd < 8$ or $0.75 < \lambda/d < 1.5$. Note that an undesirable feature of a double array set-up is that very often there exists a value of kd, usually well below the first cut-off, at which *total* transmission occurs.

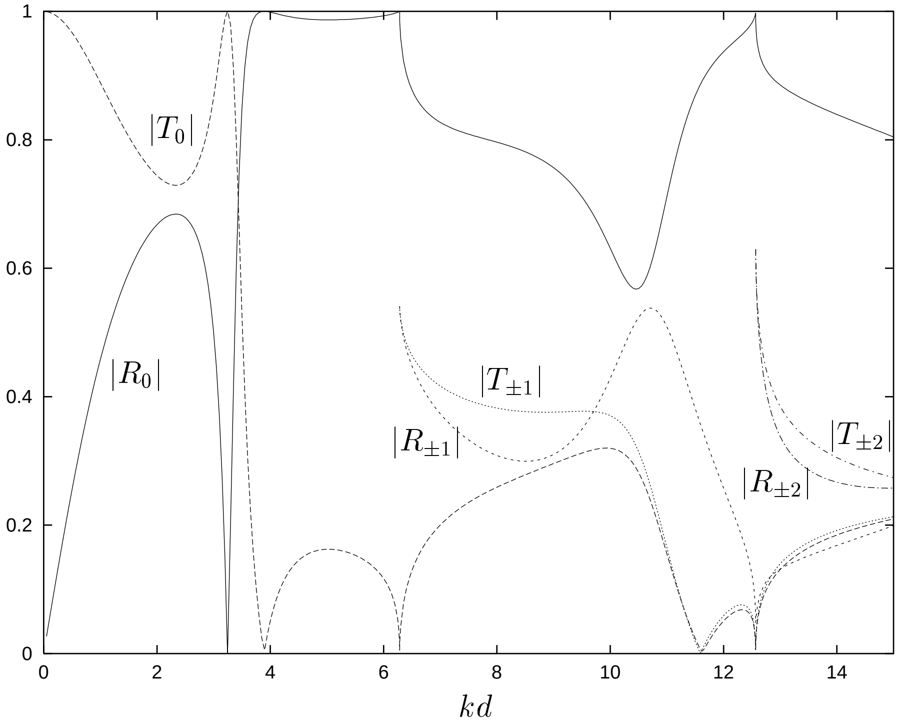

Figure 6.6: $|R_n|$, $|T_n|$ against non-dimensionalised wavenumber kd for a double array of screens; $a/c = 0.2$, $b/d = 0.05$, $\theta_0 = 0^{\text{o}}$

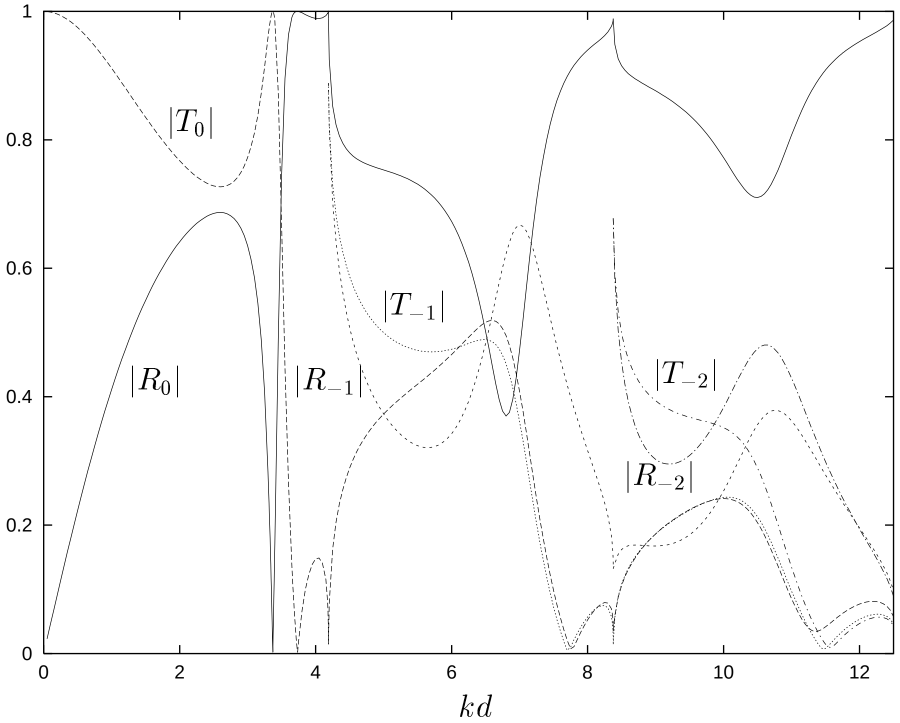

Figure 6.7: $|R_n|$, $|T_n|$ against non-dimensionalised wavenumber kd for a double array of screens; $a/c = 0.2$, $b/d = 0.05$, $\theta_0 = 30^{\text{o}}$.

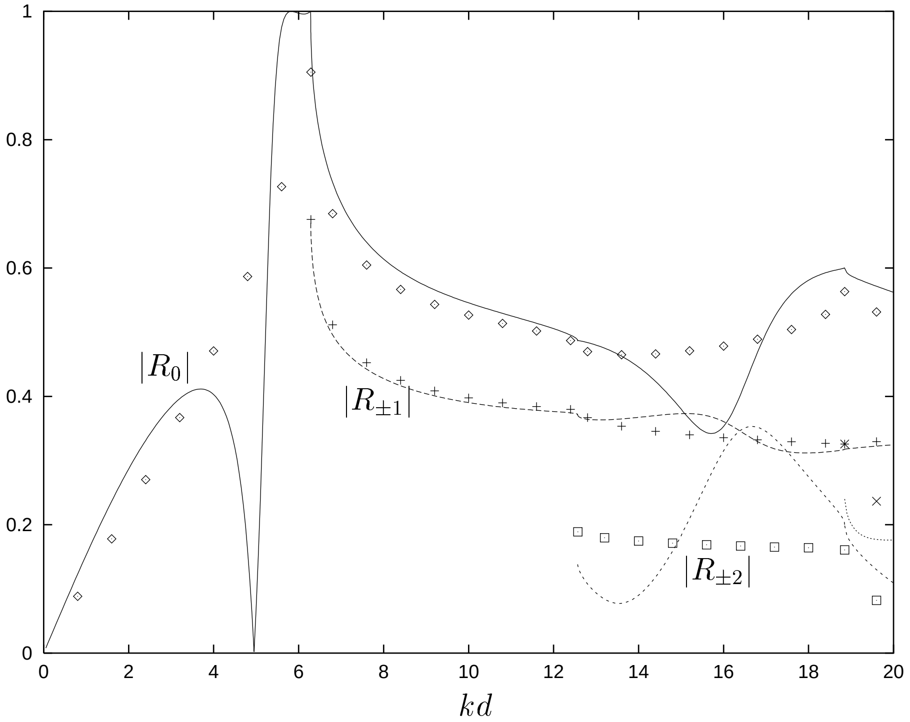

Figure 6.8: A comparison between $|R_n|$ for a closely spaced double array (lines) and a single array (points) with $a/c = 0.5$, $\theta_0 = 0^{\text{o}}$ and $b/d = 0.05$.

Figure 6.6 shows the effect of a normally-incident wave on a closely-spaced double array ($b/d = 0.05$) with $a/c = 0.2$. It can be seen that there exists both zeros of reflection *and* transmission for such an arrangement. This phenomenon is not surprising by analogy with the problem of scattering of two identical vertical surface-piercing barriers considered in chapter 4, where zeros of reflection and transmission exist at any barrier size to spacing ratio. Here, however, it appears that zeros of transmission exist for only certain arrangements. Thus, increasing the spacing between the two sets of arrays moves the wavenumber at which the zero exists nearer to the first cut-off frequency and it will eventually be lost. Likewise, it appears that increasing the angle of incidence has a similar effect, since the wavenumber at which the first cut-off occurs is reduced.

It is noted from (6.3.26) that the condition for no transmitted waves is that $\mathbf{R}_s = \mathbf{R}_a$ and it can easily be shown that this translates into the following condition on $\mathbf{S}_s$ and $\mathbf{S}_a$:

$$\|(\mathbf{S}_s^{-1} - \mathbf{S}_a^{-1})\mathbf{A} - (\mathbf{C}_s + \mathbf{C}_a)\| = 0 \qquad (6.5.2)$$

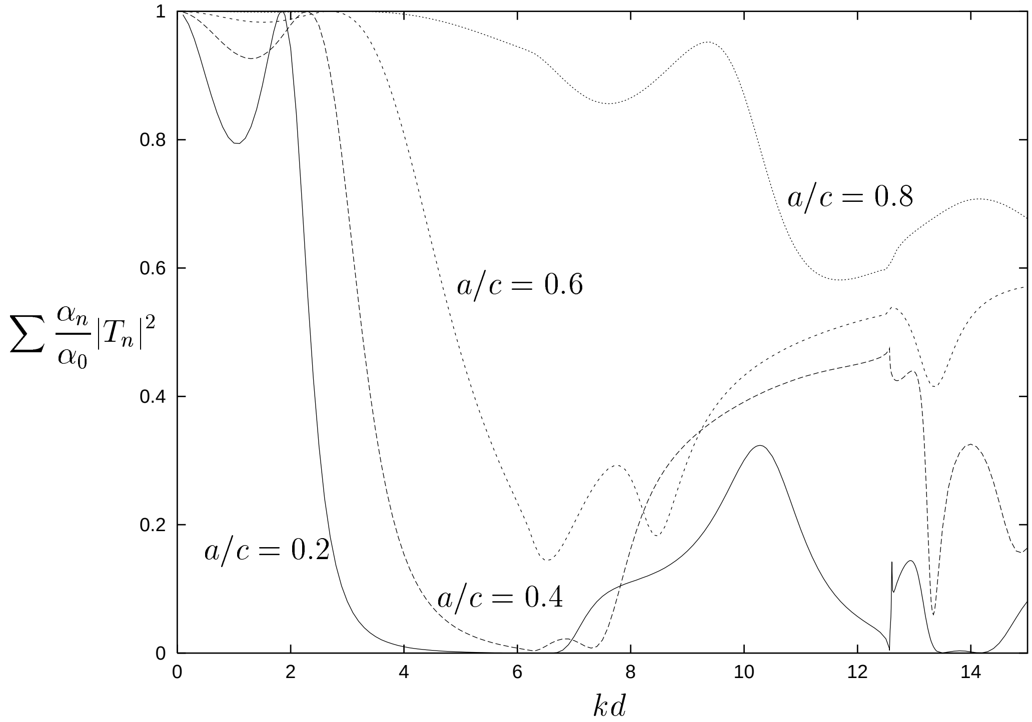

Figure 6.9: Proportion of incident wave energy transmitted through a double array of breakwaters as a/c varies vs. kd with $b/d = 0.25$, $\theta_0 = 0^{\circ}$.

from (6.3.11), (6.3.14). If there is only one reflected and transmitted wave the condition for no transmission is reduced to finding the roots of

$$f(kd, \theta_0, a/d, b/d) = \alpha_0 d \left((S^s_{00})^{-1} - (S^a_{00})^{-1} \right) - 2 \operatorname{cosec} 2\alpha_0 b = 0. \qquad (6.5.3)$$

Thus we can verify that only one zero of transmission exists for the arrangement in figure 6.6 at $kd = 3.890$. Although from figure 6.6 there appears to be zeros of transmission at higher wavenumbers, our accurate computations of (6.5.3) show that there are no others. We do not expect there to be zeros of total transmitted wave energy for values beyond the first cut-off as this requires that the rather strict condition (6.5.2) be satisfied.

Figure 6.7 again shows the zeros of reflection and transmission for the same geometry, but with incident waves making an angle $\theta_0 = 30^{\circ}$ to the normal. Here, $|T_0| = 0$ for $kd = 3.733$ and it can be seen that the zeros of reflection and transmission along with the first cut-off now occur over a smaller range of kd. Increasing θ_0 still further has the effect of losing the zeros of first transmission and then reflection.

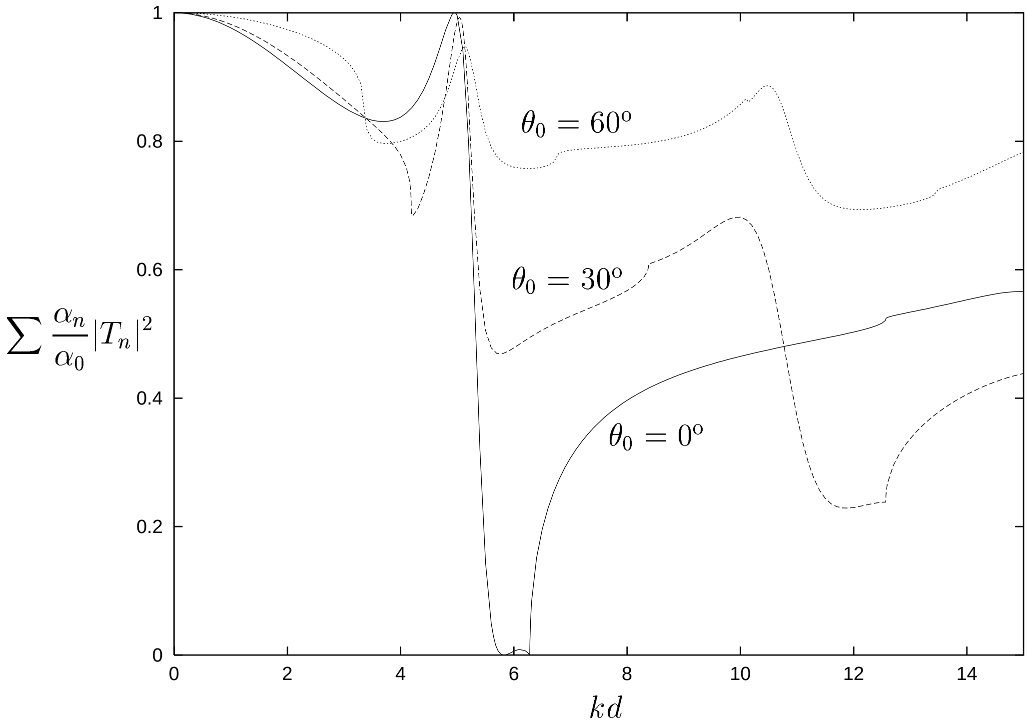

Figure 6.10: Proportion of incident wave energy transmitted through a double array of breakwaters as θ_0 varies vs. kd with $a/c = 0.5$, $b/d = 0.05$.

In order to show the effect of the introduction of a second identical array on the wave field, we compare, in figure 6.8, curves of $|R_n|$ occuring in the case of a single array with those for a closely-spaced double array. It shows that the results for the two closely-spaced arrays have the underlying features of the single array, but exhibit sizeable differences at certain wavenumbers where the wave interaction between the two arrays is important and leads to zeros of reflection and transmission as can be seen in figure 6.8. Similar effects have been observed in the problems of scattering by one or two surface-piercing barriers; see for example McIver [46].

Figures 6.9, 6.10 and 6.11 show the variation of total transmitted energy, T_{total}, with changing a/c, θ_0 and b/d respectively. Thus we see that increasing θ_0 from normal incidence loses zeros of $|R_0|$ and $|T_0|$, whilst separation of the array by too much ($b/d = 0.5$ in figure 6.11) has the result of causing two zeros of reflection to occur before the first cut-off.

Finally, we present results using the wide-spacing approximation developed in §4. Figures 6.12 and 6.13 make the comparison of the wide-spacing results to those

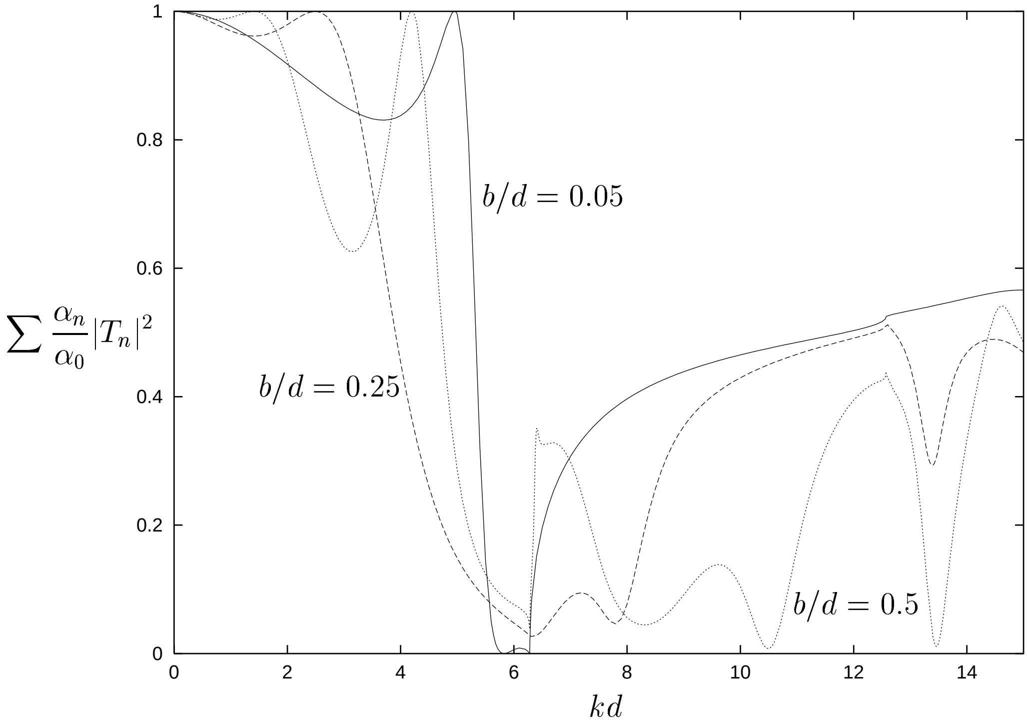

Figure 6.11: Proportion of incident wave energy transmitted through a double array of breakwaters as b/d varies vs. kd with $a/c = 0.5$, $\theta_0 = 0^{\circ}$.

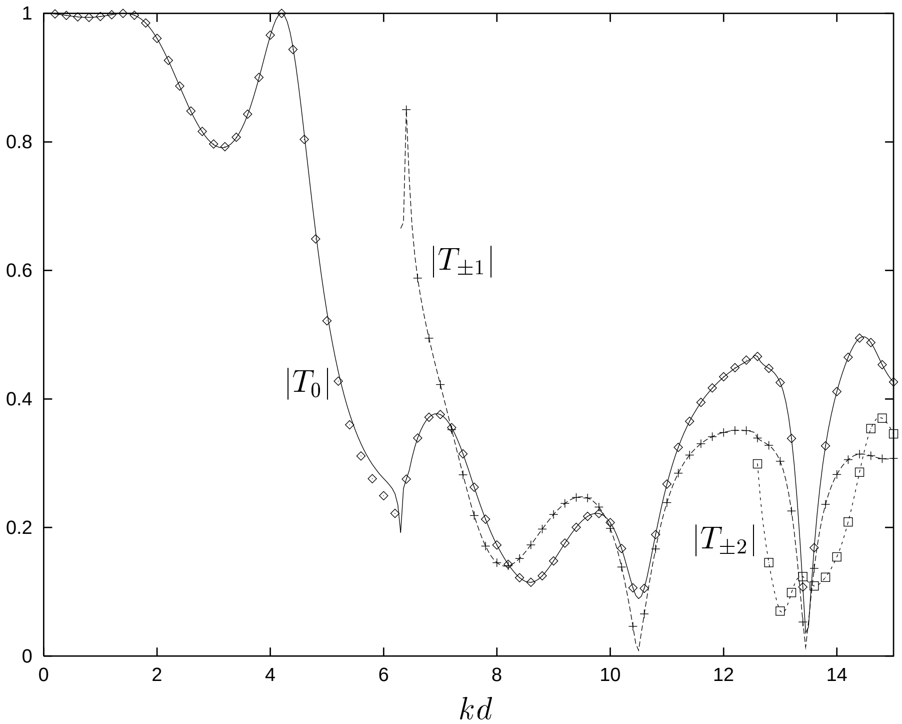

Figure 6.12: A comparison of $|T_n|$ between a double array (lines) and a wide-spacing approximation (points) with $a/c = 0.5$, $b/d = 0.5$, $\theta_0 = 0^{\circ}$.

derived from the full solution of the problem of two identical parallel arrays. The former of these two graphs is for $b/d = 0.5$, corresponding to a ratio of array separation to periodicity of 1:1, and where we have choosen $a/c = 0.5$ and $\theta_0 = 0^o$. For this fairly large array separation, agreement is excellent for both low wavenumbers (long waves) and high wavenumbers (short waves) for all $|T_n|$, the only discrepancies arising just before the first cut-off frequency, located for this arrangement at $kd = 2\pi$. This disagreement is more evident in figure 6.13, the only difference to the previous example being that the array separation has been halved ($b/d = 0.25$). We expect the results to be poorer for closer spacings, but it is also possible to explain the breakdown of agreement close to the first cut-off quite simply. The wide-spacing approximation relies on the assumption that the evanescent or decaying modes can be ignored. However, as kd approaches a cut-off from below, we will have $k \to \beta_m$ for some m, or equivalently, $\gamma_m \to 0$. So, in for example (6.3.4), the effect of one of the evanescent modes, having coefficient A_m^s, becomes important and hence the full solution and the wide-spacing approximation will not to be in good agreement. Of course, just beyond this cut-off, the γ_m becomes an α_m corresponding to a propagating mode which is accounted for and there is no longer a problem with a large contribution from an evanescent term. It is also noted that the wide-spacing approximation is good for large or small kd away from a cut-off where the influence from γ_n's are exponentially small as b/d increases.

It is expected that the wide-spacing approach will not provide a good approximation to the exact results when the regime of zeros of transmission is entered, since it is clear from (6.4.18) and the knowledge that zeros of transmission do not occur in the case of a single array, that $|T_0|$ computed this way can never be zero.

We now use the accuracy observed in figure 6.13 to examine the case of two arrays which are not identical, but have the same periodicity. In fact, since we have not specified anything about the position of the second array relative to the first in our analysis in §4, it is clear that the results for the reflection and transmission coefficients are independent of the orientation of the second array for large-enough

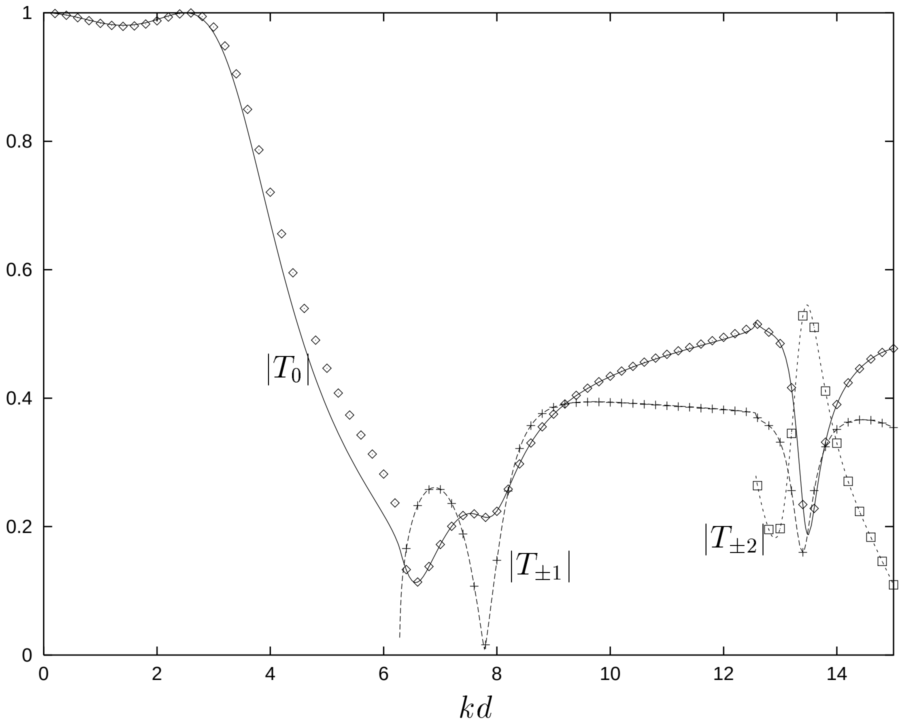

Figure 6.13: A comparison of $|T_n|$ between a double array (lines) and a wide-spacing approximation (points) with $a/c = 0.5$, $b/d = 0.25$, $\theta_0 = 0^{\mathrm{o}}$.

array separations. In other words, arranging the second array so that the barriers 'cover' the gaps of the first array leads to the same $|R_n|$ and $|T_n|$ as for a set-up where the gaps are aligned with one another under the wide-spacing approximation.

It can be seen from figure 6.14 that, although two sets of arrays consisting of large barriers and small gaps produces less transmitted energy in general it can still cause a large amount of transmitted energy for some values of kd.

It is not difficult to use the wide-spacing approximation used in §6.4 for two arrays of breakwaters to investigate a full multi-modal wave propagation through N such arrays each having the same periodicity. The separation between any two arrays and the barrier to gap ratio in each array would be arbitrary and the solution would require only the characteristics of each array in isolation. These sort of ideas have been used recently by Heckl [31].

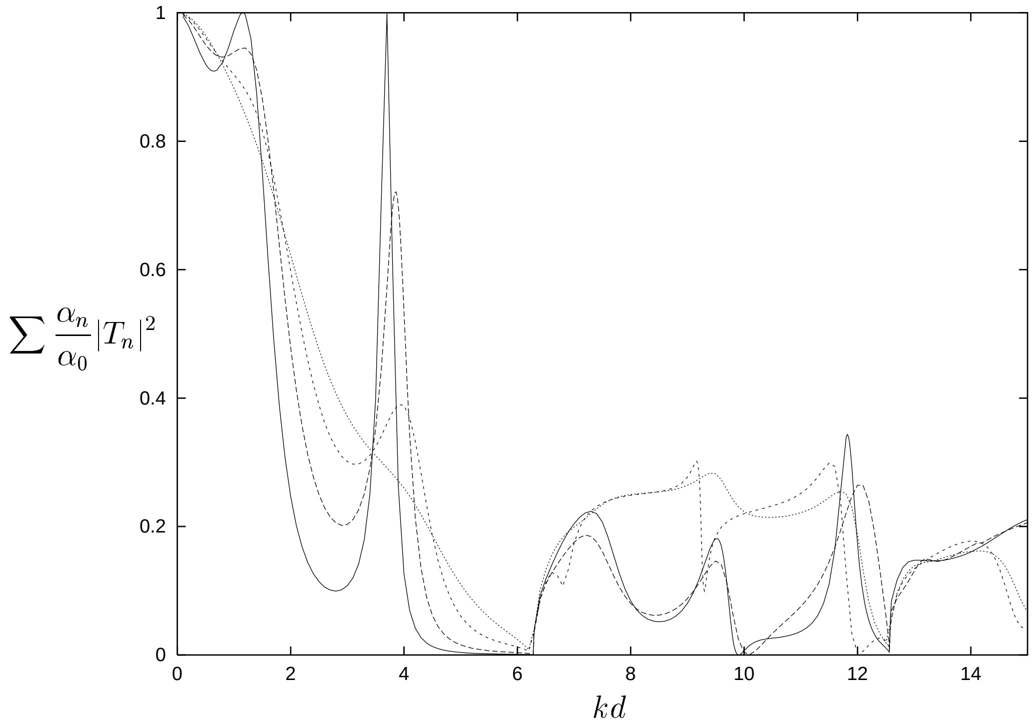

Figure 6.14: A wide-spacing approximation for two different arrays with $a_1/c = 0.2$, $b/d = 0.5$, $\theta_0 = 0^{\text{o}}$. $a_2/c = 0.2$ (——), 0.4 (– – –), 0.6 (- - - -), 0.8 (······).

Chapter 7

Scattering by a step in the sea bed

7.1 Introduction

In this chapter we consider the effect upon an obliquely-incident plane wave as it progresses from one constant depth to another over a long rectangular step in the ocean floor, a problem previously considered by Miles [52] in 1967 in the case of normally-incident waves. Using potential flow theory close to the corner of the step reveals an inverse cube-root singularity in the velocity at the corner, not as strong as for a thin barrier but nevertheless significant.

This problem is chosen as perhaps the simplest of its type involving a rectangular geometry, the challenge being to adapt the methods presented in the previous chapters for thin barriers to geometries involving right-angled corners. Our task is initially made easier due to the formulation adopted by Miles [52]. He sets up the problem in terms of a scattering matrix relating the outgoing to the incoming wave amplitudes. This scattering matrix involves weighted integral of functions related to the velocity above the corner of the step which satisfy a pair of integral equations with the same symmetric positive-definite kernel. The solution is approximated using the Schwinger variational principle (equivalent to a one-term Galerkin method) with a crude choice of trial function which nevertheless gave results which were in good agreement with those obtained for the infinite step due to Newman [57] a few years earlier. This latter problem, in which waves pass from a region of finite water depth over a rectangular step into infinite depth, was also formulated in terms of an unknown velocity above the step and solved using what is in effect a Galerkin method with an expansion for the unknown velocity in terms of the complete set of vertical eigenfunctions applicable to the region of finite water depth. Despite not having taken account of the singularity at the corner of the step, the Galerkin approximation has been shown throughout this thesis to be very powerful and it is therefore not surprising that Newman [56] reports accuracy of 3 decimal places for the reflection and transmission coefficients with only ten terms in the expansion.

In the long-wave limit to the step problem we have explicit expressions for the reflection and transmission coefficients, originally due to Lamb [40, §176]. For a similar analysis in the case of oblique incidence, see Mei [51].

There are numerous references in the literature to geometries involving blocks in finite depth to which the following method may be employed. For example, Mei & Black [49] consider the scattering by a rectangular block protruding from the sea-bed as well as a fixed surface-piercing rectangular block using a variational principle to find reflection and transmission coefficients. In the case of oblique wave scattering by an indentation, or a trench, in the sea floor, Kirby & Dalrymple [37] match eigenfunction expansions to form an infinite system of equations which gives approximations to reflection and transmission coefficients after truncation.

In §7.2 we follow the approach of Miles [52] and derive a pair of integral equations in terms of unknown functions related to the velocity above the corner of the step. The reflection and transmission coefficients are found from a scattering matrix which relies on knowledge of a 2×2 matrix $\mathbf{S}$ whose elements are simple weighted integrals of the velocity-related unknown functions. An N-term Galerkin method is used to approximate the solution to the integral equations using test functions which possess the correct singular behaviour at the corner of the step. The only substantial difference in the numerical procedure between this and barrier problems of previous chapters is in the calculation of Bessel functions of fractional order rather than integer order.

The problems encountered in the previous chapters all involved thin-walled structures which permit the derivation of a complementary method of solution based on the pressure difference across a barrier. There is no obvious way of extending this in the case of a block. Assigning an artificial value to the potential on the inside of the block is a possible way of getting round the problem, but this approach runs into difficulties at an early stage. Instead it proves possible to formulate the problem alternatively in terms of an unknown pressure throughout the depth at the discontinuity rather than the usual pressure jump. This function consists of the pressure across the gap above the step and the pressure on the vertical face of the step. There are, however, some features of this formulation yet to be resolved and as a result it is not considered further here.

In §7.3 we show the accuracy of the method by showing the covergence of the approximation to the elements of $\mathbf{S}$ with increasing N. These are shown to be bounded above by their true values by virtue of the use of Galerkin's method. Also included is a comparison with results obtained from a matched eigenfunction method which requires the solution of a large system of equations. Some typical curves are presented showing reflection and transmission coefficients.

7.2 Formulation and solution

Cartesian co-ordinates are chosen with the mean free surface at $y = 0$ and y measured vertically downwards. The step in the ocean floor occurs at $x = 0$, $-\infty < z < \infty$ and in $-\infty < x < 0$ the water depth is h_1 whilst in $0 > x > \infty$ it is h_2 and we assume without loss of generality that $h_2 < h_1$. The set up is shown in figure 7.1.

We allow waves to be incident upon the step from either $x = -\infty$ or from $x = +\infty$ having frequency $\omega/2\pi$. It follows from classical linear water-wave theory that there exists a complex velocity potential $\phi(x, y, z, t)$ which we may write as

$$\Phi(x, y, z, t) = \mathrm{Re}\{\phi(x, y)\mathrm{e}^{ilz}\mathrm{e}^{-i\omega t}\}, \tag{7.2.1}$$

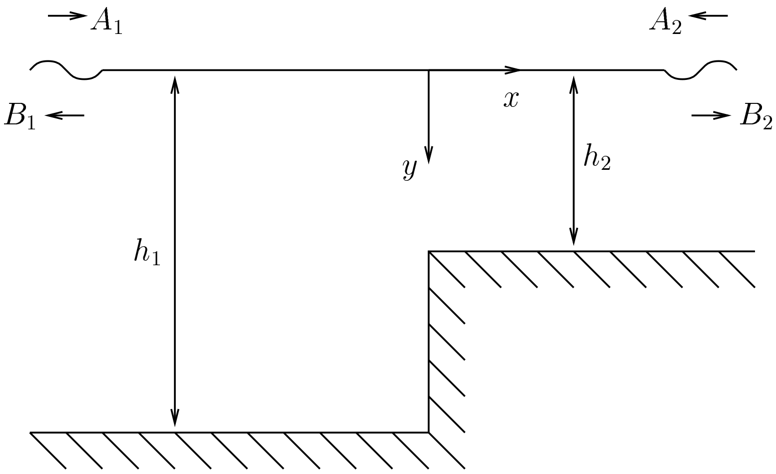

Figure 7.1: Step in the ocean floor.

where l is the wavenumber in the z-direction. Then $\phi(x,y)$ satisfies

$$\phi_{xx} + \phi_{yy} - l^2\phi = 0, \quad \text{in the fluid} \tag{7.2.2}$$

$$\phi_y = 0, \quad \begin{cases} y = h_1, & x < 0 \\ y = h_2, & x > 0 \end{cases} \tag{7.2.3}$$

$$\phi_x = 0, \quad x = 0,\ h_2 < y < h_1 \tag{7.2.4}$$

$$K\phi + \phi_y = 0, \quad y = 0,\ -\infty < x < \infty, \tag{7.2.5}$$

where $K = \omega^2/g$ whilst

$$\phi,\ \phi_x \text{ are continuous for } x = 0,\ 0 < y < h_2\,. \tag{7.2.6}$$

We construct two sets of vertical eigenfunctions corresponding to the two regions $x < 0$ and $x > 0$ which are orthogonal over $[0, h_1]$ and $[0, h_2]$ respectively. Thus

$$\psi_{i,n}(y) = N_{i,n}^{-1/2} \cos k_{i,n}(h_i - y), \quad i = 1, 2, \quad n = 0, 1, 2, \ldots, \tag{7.2.7}$$

where

$$N_{i,n} = \frac{1}{2}\left(1 + \frac{\sin 2k_{i,n}h_i}{2k_{i,n}h_i}\right), \quad i = 1, 2, \quad n = 0, 1, 2, \ldots, \tag{7.2.8}$$

where $i = 1, 2$ denotes the eigenfunctions appropriate to $x < 0$ and $x > 0$ respectively. Here, $k_{i,n}$ are the real positive roots of

$$K + k_{i,n} \tan k_{i,n}h_i = 0, \quad i = 1, 2, \quad n = 1, 2, \ldots \tag{7.2.9}$$

and we define $k_{i,0} = -ik_i$ where k_i are the wavenumbers associated with the waves in the two depths and satisfies

$$K = k_i \tanh k_i h_i, \quad i = 1, 2. \tag{7.2.10}$$

The $\psi_{i,n}$ now satisfy the following orthogonality relations

$$\frac{1}{h_i}\int_0^{h_i} \psi_{i,n}(y)\psi_{i,m}(y)\,\mathrm{d}y = \delta_{mn}, \quad i = 1, 2. \tag{7.2.11}$$

We can now write a general solution to the problem satisfying (7.2.2), (7.2.3), (7.2.5) which has the correct behaviour as $x \to \pm\infty$. Thus in $x \leq 0$

$$\phi(x,y) = -\{A_1 \mathrm{e}^{i\alpha_1 x} + B_1 \mathrm{e}^{-i\alpha_1 x}\}\psi_{1,0}(y) - \sum_{n=1}^{\infty} U_{1,n}\mathrm{e}^{\alpha_{1,n}x}\psi_{1,n}(y), \tag{7.2.12}$$

and in $x \geq 0$,

$$\phi(x,y) = \{A_2 \mathrm{e}^{-i\alpha_2 x} + B_2 \mathrm{e}^{i\alpha_2 x}\}\psi_{2,0}(y) + \sum_{n=1}^{\infty} U_{2,n}\mathrm{e}^{-\alpha_{2,n}x}\psi_{2,n}(y), \tag{7.2.13}$$

where the α_i are given by

$$\alpha_i = (k_i^2 - l^2)^{1/2} = k_i \cos\theta_i, \quad l = k_i \sin\theta_i, \tag{7.2.14}$$

and

$$\alpha_{i,n} = (k_{i,n}^2 + l^2)^{1/2}. \tag{7.2.15}$$

At this stage we allow an arbitrary description of the far-field wave amplitudes. If waves are to be incident only from $x = -\infty$ then setting $A_2 = 0$ gives $R_- = B_1/A_1$, $T_- = -B_2/A_1$ for the reflection and transmission coefficients for waves travelling from deeper to shallower water. Similarly, for waves travelling from shallower to deeper water (from $x = +\infty$), setting $A_1 = 0$ gives $R_+ = B_2/A_2$, $T_+ = -B_1/A_2$. We may express this information in terms of a scattering matrix by writing

$$\begin{pmatrix} B_1 \\ B_2 \end{pmatrix} = \mathbf{X}\begin{pmatrix} A_1 \\ A_2 \end{pmatrix}, \quad \text{with } \mathbf{X} = \begin{pmatrix} R_- & -T_+ \\ -T_- & R_+ \end{pmatrix}. \tag{7.2.16}$$

Then it may be shown (Porter & Chamberlain [64]) that the well-known relations (see Kreisel [39]) between the various reflection and transmission coefficients may be satisfied identically by this formulation.

It is noted from (7.2.14) that as a wave passes over the step it changes direction. Moreover, if $l > k_i$ then there will be no wave propagation beyond the step. In fact total reflection can only occur for waves travelling into deeper water and not vice versa. The reason for this is as follows. For a wave incident from $x = -\infty$ a choice of k_1 and θ_1 gives $l = k_1 \sin\theta_1 < k_1 < k_2$, where this last step comes from $h_1 > h_2$ and an examination of the dispersion relation. Thus total reflection cannot occur in this case. However, for waves travelling from $x = +\infty$ into deeper water it can be shown using (7.2.14) that no transmission will occur if $k_1/k_2 < \sin\theta_2 < 1$ and so for any choice of k_2 there will always exists a critical incident angle beyond which no transmission will occur.

The property of total reflection provides the motivation for constructing edge waves above a long uniform rectangular shelf protruding from the sea bed, as in Evans & McIver [18]. Edge waves exist in many problems in water waves where there is uniformity or periodicity in one of the dimensions. They are solutions of the problem in which no waves are radiated out to infinity but instead travel along the direction of uniformity. By considering the shelf wide enough, it can be seen that under the conditions metioned above waves are able to be reflected back from each edge of the protrusion and travel along the top of the block.

Returning to the problem considered here, we define $\phi_x|_{x=0} \equiv U(y)$. Then

$$U(y) = -i\alpha_1(A_1 - B_1)\psi_{1,0}(y) - \sum_{n=1}^{\infty} \alpha_{1,n} U_{1,n} \psi_{1,n}(y) \tag{7.2.17}$$

$$= -i\alpha_2(A_2 - B_2)\psi_{2,0}(y) - \sum_{n=1}^{\infty} \alpha_{2,n} U_{2,n} \psi_{2,n}(y). \tag{7.2.18}$$

Using the orthogonality of $\psi_{i,n}$, $i = 1,2$ in (7.2.17) and (7.2.18) we obtain

$$-i\alpha_i h_i (A_i - B_i) = \int_{L_g} U(y)\psi_{i,0}(y)\,\mathrm{d}y, \quad i = 1,2 \tag{7.2.19}$$

$$-\alpha_{i,n} h_i U_{i,n} = \int_{L_g} U(y)\psi_{i,n}(y)\,\mathrm{d}y, \quad i = 1,2, \quad n \geq 1, \tag{7.2.20}$$

where $L_g = [0, h_2]$. Here we have used the fact that $U(y) = 0$ for $y \in L_s = [h_2, h_1]$.

Applying continuity of pressure across $x = 0$, $y \in L_g$ yields

$$0 = (A_1 + B_1)\psi_{1,0}(y) + (A_2 + B_2)\psi_{2,0}(y) + \sum_{n=1}^{\infty} U_{1,n}(y)\psi_{1,n}(y) + \sum_{n=1}^{\infty} U_{2,n}(y)\psi_{2,n}(y). \tag{7.2.21}$$

Substituting (7.2.20) into (7.2.21) gives

$$\int_{L_g} U(t)K(y,t)\,\mathrm{d}t = (A_1 + B_1)\psi_{1,0}(y) + (A_2 + B_2)\psi_{2,0}(y), \quad y \in L_g, \tag{7.2.22}$$

where

$$K(y,t) = \sum_{n=1}^{\infty} \left\{ \frac{\psi_{1,n}(y)\psi_{1,n}(t)}{\alpha_{1,n}h_1} + \frac{\psi_{2,n}(y)\psi_{2,n}(t)}{\alpha_{2,n}h_2} \right\}. \tag{7.2.23}$$

Introducing the the following vector and matrix definitions

$$\mathbf{A} = \begin{pmatrix} A_1 \\ A_2 \end{pmatrix}, \quad \mathbf{B} = \begin{pmatrix} B_1 \\ B_2 \end{pmatrix}, \quad \mathbf{\Psi}(y) = \begin{pmatrix} \psi_{1,0}(y) \\ \psi_{2,0}(y) \end{pmatrix}, \quad \mathbf{K} = \begin{pmatrix} \alpha_1 h_1 & 0 \\ 0 & \alpha_2 h_2 \end{pmatrix}, \tag{7.2.24}$$

allows us to re-write (7.2.19) thus

$$-i\mathbf{K}(\mathbf{A} - \mathbf{B}) = \int_{L_g} U(y)\mathbf{\Psi}(y)\,\mathrm{d}y, \quad y \in L_g, \tag{7.2.25}$$

and (7.2.22) becomes

$$\mathbf{\Psi}^{\mathrm{T}}(y)(\mathbf{A} + \mathbf{B}) = \int_{L_g} U(t)K(y,t)\,\mathrm{d}t, \quad y \in L_g. \tag{7.2.26}$$

Following Miles [52], we introduce the vector function $\mathbf{U}(t) = (u_1(t), u_2(t))^{\mathrm{T}}$ related to the scalar function $U(t)$ by

$$U(t) = \mathbf{U}^{\mathrm{T}}(\mathbf{A} + \mathbf{B}). \tag{7.2.27}$$

Then if $\mathbf{U}(t)$ satisfies

$$\int_{L_g} K(y,t)\mathbf{U}(t)\,\mathrm{d}t = \mathbf{\Psi}(y), \quad y \in L_g, \tag{7.2.28}$$

then $U(t)$ defined by (7.2.27) will satisfy (7.2.26). Using the definition (7.2.27) for $U(t)$ in (7.2.25) gives

$$-i\mathbf{K}(\mathbf{A} - \mathbf{B}) = \int_{L_g} \mathbf{\Psi}(y)\mathbf{U}^{\mathrm{T}}(y)(\mathbf{A} + \mathbf{B})\,\mathrm{d}y. \tag{7.2.29}$$

If we define the 2×2 matrix $\mathbf{S}$ by

$$\mathbf{S} = \int_{L_g} \mathbf{\Psi}(y)\mathbf{U}^{\mathrm{T}}(y),\ \mathrm{d}y, \tag{7.2.30}$$

which in component form is

$$S_{ij} = \int_{L_g} u_j(y)\psi_{i,0}(y)\,\mathrm{d}y, \tag{7.2.31}$$

then (7.2.29) becomes

$$-i\mathbf{K}(\mathbf{A} - \mathbf{B}) = \mathbf{S}(\mathbf{A} + \mathbf{B}). \tag{7.2.32}$$

Rearrangement of the above equation gives the relation between the input and output wave amplitudes in the form

$$\mathbf{B} = \mathbf{X}\mathbf{A}, \tag{7.2.33}$$

as in (7.2.16) where

$$\mathbf{X} = (\mathbf{K} + i\mathbf{S})^{-1}(\mathbf{K} - i\mathbf{S}). \tag{7.2.34}$$

Using the two harmonic functions ϕ and $\overline{\phi}$ in Green's second identity, (5.2.26) leads to an equation expressing conservation of energy, namely

$$\beta|B_1|^2 + |B_2|^2 = \beta|A_1|^2 + |A_2|^2, \tag{7.2.35}$$

where $\beta = \alpha_1 h_1/\alpha_2 h_2$. This expression is satisfied identically by virtue of the scattering matrix formulation, (7.2.33), that has been invoked. See, for example, the discussion surrounding equation (4.2.8).

The reflection and transmission coefficients due to incident waves from either infinity, $R_\pm$, $T_\pm$ are just the elements of $\mathbf{X}$ given in (7.2.16). Because of the change in depth into which the transmitted wave progresses, a scaling factor of

$$\tilde{T}_- = T_- \frac{\psi_{2,0}(0)}{\psi_{1,0}(0)}. \tag{7.2.36}$$

and

$$\tilde{T}_+ = T_+ \frac{\psi_{1,0}(0)}{\psi_{2,0}(0)}. \tag{7.2.37}$$

recovers the transmission coefficients for the free-surface displacement.

In operator notation, (7.2.28) may be written

$$\mathcal{K}u_i = \psi_{i,0}, \quad y \in L_g, \quad i = 1, 2, \tag{7.2.38}$$

with (7.2.31) as

$$(u_j, \psi_{i,0}) = S_{ij}, \quad i, j = 1, 2, \tag{7.2.39}$$

where $(\cdot, \cdot)$ denotes the inner product over L_g. Once u_i are known from (7.2.38) then (7.2.39) gives all the information needed to find the transmission and reflection coefficients from (7.2.33) with (7.2.34).

We now write

$$u_i(y) = \sum_{n=0}^{N} a_n^{(i)} v_n(y), \quad i = 1, 2, \tag{7.2.40}$$

where $a_n^{(i)}$ are unknown coefficients and $v_n(y)$ are as yet undefined expansion functions. Substituting into (7.2.38) multiplying through by $v_m(t)$ and integrating over $[0, h_2]$ gives

$$\sum_{n=0}^{N} a_n^{(i)} (\mathcal{K}v_n, v_m) = (\psi_{i,0}, v_m), \quad m = 0, \ldots, N, \tag{7.2.41}$$

or

$$\sum_{n=0}^{N} a_n^{(i)} K_{mn} = F_{m0}^{(i)}, \quad i = 1, 2, \tag{7.2.42}$$

where

$$K_{mn} = (\mathcal{K}v_n, v_m) = \sum_{i=1,2} \sum_{r=1}^{\infty} \frac{F_{mr}^{(i)} F_{nr}^{(i)}}{\alpha_{i,r} h_i}, \tag{7.2.43}$$

and

$$F_{mn}^{(i)} = (v_m, \psi_{i,n}). \tag{7.2.44}$$

Using (7.2.40) in (7.2.39) gives the approximation to the elements S_{ij} as

$$S_{ij} \simeq \tilde{S}_{ij} = \sum_{n=0}^{N} a_n^{(j)} F_{n0}^{(i)}, \quad i, j = 1, 2, \tag{7.2.45}$$

and (7.2.42), (7.2.45) can be combined to give a matrix form for $\tilde{\mathbf{S}} = \{S_{ij}\}$, namely

$$\tilde{\mathbf{S}} = \mathbf{L}^{\mathrm{T}} \mathbf{K}^{-1} \mathbf{L}, \tag{7.2.46}$$

where we define the $(N+1)\times(N+1)$ matrix $\mathbf{K}=\{K_{mn}\}$ and the $(N+1)\times 2$ matrix $\mathbf{L}=\{L_{mn}\}$ with $L_{mn}=F^{(n)}_{m0}$. Now

$$\begin{aligned} F^{(i)}_{mn}=(v_m,\psi_{i,n}) &= \int_0^{h_2} v_m(t)\psi_{i,n}(t)\,\mathrm{d}t, \quad i=1,2 \\ &= N_{i,n}^{-1/2}\int_0^{h_2} v_m(t)\cos k_{i,n}(h_i-t)\,\mathrm{d}t \\ &= N_{i,n}^{-1/2}\cos k_{i,n}h_i\int_0^{h_2}\hat{v}_m(t)\cos k_{i,n}t\,\mathrm{d}t, \end{aligned} \tag{7.2.47}$$

where we have introduced the reduced function

$$\hat{v}_m(t)=v_m(t)-K\int_y^{h_2} v_m(t)\,\mathrm{d}t, \tag{7.2.48}$$

which therefore satisfies

$$\hat{v}'_m(y)=0, \quad \text{on } y=0\,. \tag{7.2.49}$$

It remains to choose the set of functions $\hat{v}_n(y)$ so as to reflect the anticipated singularity in the velocity at the corner of the step and also to provide a simple form for K_{mn} . Simple analysis of the potential flow at a right angled corner in an unbounded fluid gives $u_i(y)\propto(h_2-y)^{-1/3}$ as $y\to h_2$. Thus, in order to preserve a simple form for K_{mn} , we choose

$$\hat{v}_m(t)=\left[(-1)^m\frac{2^{1/6}(2m)!\Gamma(\frac{1}{6})}{\pi\Gamma(2m+1/3)h_2^{1/3}}\right](h_2^2-t^2)^{-1/3}C^{1/6}_{2m}\left(\frac{t}{h_2}\right), \quad t\in[0,h_2] \tag{7.2.50}$$

where

$$C^{\nu}_n(\cos\theta)=\sum_{m=0}^{n}\frac{\Gamma(\nu+m)\Gamma(\nu+n-m)}{m!(n-m)!\,[\Gamma(\nu)]^2}\cos(n-2m)\theta \tag{7.2.51}$$

are orthogonal ultraspherical Gegenbauer polynomials satisfying $C^{\nu}_n(-x)=(-1)^n$ $C^{\nu}_n(x)$. The motivation for the choice these polynomials comes from the desire to use an orthogonal polynomial with an inverse cube-root term as its natural weighting function. We see that the choice for $\hat{v}_m(t)$ in (7.2.50) has the required singular behaviour at $t=h_2$ and satisfies (7.2.49) by virtue of the fact that $C^{\nu}_{2m}(x)$ is an even function of x . We also note from (7.2.40) that we have expanded the regular part of the unknown functions $u_i(y)$ in terms of (weighted) orthogonal polynomials and so we can expect that increasing N , the truncation size, will ensure an increasingly

N	$h_2/h_1 = 0.1$			$h_2/h_1 = 0.5$		
	$\tilde{S}_{11}$	$\tilde{S}_{12} = \tilde{S}_{21}$	$\tilde{S}_{22}$	$\tilde{S}_{11}$	$\tilde{S}_{12} = \tilde{S}_{21}$	$\tilde{S}_{22}$
0	1.525872	1.137133	0.847431	6.909465	6.085486	5.359770
1	1.528752	1.138253	0.847866	6.916521	6.086853	5.360035
2	1.528808	1.138285	0.847885	6.919964	6.089609	5.362240
3	1.528812	1.138287	0.847886	6.920186	6.089788	5.362385
4	1.528813	1.138287	0.847886	6.920221	6.089816	5.362408
5	1.528813	1.138287	0.847886	6.920229	6.089823	5.362413
6	1.528813	1.138287	0.847886	6.920231	6.089825	5.362415
7	1.528813	1.138287	0.847886	6.920231	6.089825	5.362415

Table 7.1: Convergence of the elements of $\tilde{\mathbf{S}}$ with increasing N in the case $Kh_2 = 1$, $h_2/h_1 = 0.1,\ 0.5$

accurate representation of the functions being modelled. Using this choice of $\hat{v}_m(y)$ in (7.2.47) gives

$$F^{(i)}_{mn} = N^{-1/2}_{i,n} \frac{\cos k_{i,n}h_i}{(k_{i,n}h_2)^{1/6}} J_{2m+1/6}(k_{i,n}h_2) \tag{7.2.52}$$

for $n \geq 1$ (see Erdélyi *et al.* [9, §1.12, eqn. 10]) and for $n = 0$ we use $k_{i,0} = -ik_i$ which yields

$$F^{(i)}_{m0} = (-1)^m N^{-1/2}_{i,0} \frac{\cosh k_i h_i}{(k_i h_2)^{1/6}} I_{2m+1/6}(k_i h_2). \tag{7.2.53}$$

Thus from (7.2.43)

$$K_{mn} = \sum_{i=1,2} \sum_{r=1}^{\infty} \frac{\cos^2 k_{i,r}h_i}{N_{i,r}(\alpha_{i,r}h_i)(k_{i,r}h_2)^{1/3}} J_{2n+1/6}(k_{i,r}h_2) J_{2m+1/6}(k_{i,r}h_2). \tag{7.2.54}$$

Notice that the approximations $|\tilde{S}_{ij}|$ are bounded above by their true values, an identity which follows from the use of a Galerkin approximation in (7.2.38), (7.2.39). See the discussion surrounding equations (5.3.77)–(5.3.79) for a proof of this.

7.3 Results

The problem has been expressed in terms of a scattering matrix, $\mathbf{X}$ relating incoming and outgoing wave amplitudes at either infinity. The reflection and transmission coefficients arising due to an incident wave from $x = \pm\infty$ are elements of $\mathbf{X}$ given by (7.2.16), with the factors (7.2.36), (7.2.37) included to account for the change in depth. We denote by $R_\pm$, $\tilde{T}_\pm$ the reflection and transmission coefficients due to

	$kh_1 = 1,\ h_2/h_1 = 0.1$		$kh_1 = 1,\ h_2/h_1 = 0.5$	
Eigenfunction, $N =$	$\lvert R_-\rvert = \lvert R_+\rvert$	$\lvert\tilde{T}_-\rvert$	$\lvert R_-\rvert = \lvert R_+\rvert$	$\lvert\tilde{T}_-\rvert$
100	0.11135	1.03988	0.41327	1.28607
200	0.11138	1.03988	0.41341	1.28607
300	0.11138	1.03988	0.41345	1.28607
Miles's Variational	0.12047	1.03877	0.41964	1.28195
Step approximation	0.1223	1.0385	0.4192	1.2823
Our results	0.12257	1.03850	0.41887	1.28245

Table 7.2: Comparison of Eigenfunction, Variational and Step approximation methods with our results.

waves coming from $x = \pm\infty$ and we have assumed without loss of generality that $h_1 > h_2$ (i.e. deeper water in $x < 0$). Unlike the problems in previous chapters, the behaviour of the modulus of the reflected and transmitted wave depends on the direction of the incident wave due to the change in depth.

In order to estimate $\mathbf{X}$ and hence $R_\pm$, $\tilde{T}_\pm$, we must compute the 2×2 matrix $\tilde{\mathbf{S}}$, arising from the Galerkin approximation, in (7.2.34). This requires the evaluation of the elements of the matrix $\mathbf{K}$ which are defined by infinite series in (7.2.43). These are truncated at a value of M, say. It is noted that the terms in the series (7.2.43) decay like $O(r^{-7/3})$ as $r\to\infty$, which is not particularly rapid and so to improve the accuracy of the elements we use a method described in §3.4 of chapter 3. This involves numerically summing the leading order asymptotic behaviour of the terms neglected due to truncation, which, as it happens, is a relatively quick and straightforward task. This allows us to take a value of M as low as 500 to gain accuracy of five decimal places in $|R_\pm|$, $|\tilde{T}_\pm|$

Table 7.1 shows the convergence of the elements of $\tilde{\mathbf{S}}$ with increasing truncation parameter, N, for two typical cases where the height of the step is $h_2/h_1 = 0.1$ and 0.5. Here we have chosen $M = 2000$. For the case $h_2/h_1 = 0.1$, where the face of the step occupies $\frac{9}{10}$ths of the depth, seven-figure accuracy appears to have been reached for $N = 4$, whilst for a step occupying half the depth ($h_2/h_1 = 0.5$), $N = 7$ achieves similar accuracy. This is consistent with the observation made in §3.4, in which convergence improved in the velocity formulation the smaller gap

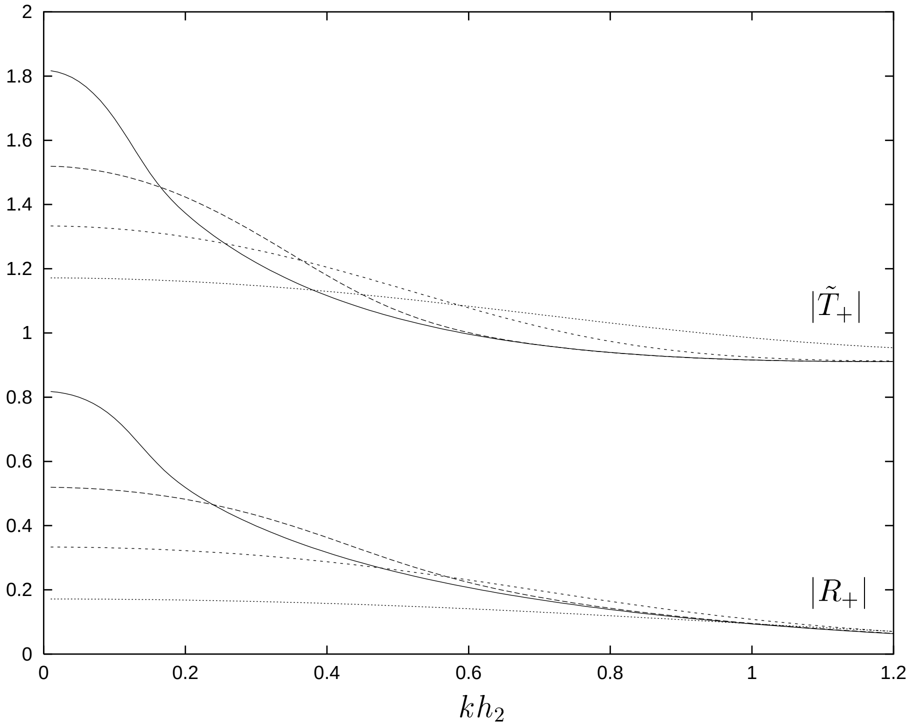

Figure 7.2: Reflection and transmission for normally-incident waves travelling into deeper water: $h_2/h_1 = 0.01\,(\text{———}),\ 0.1\,(-\,-\,-),\ 0.25\,(\text{-}\quad\text{-}\quad\text{-}),\ 0.5\,(\cdots\cdots)$.

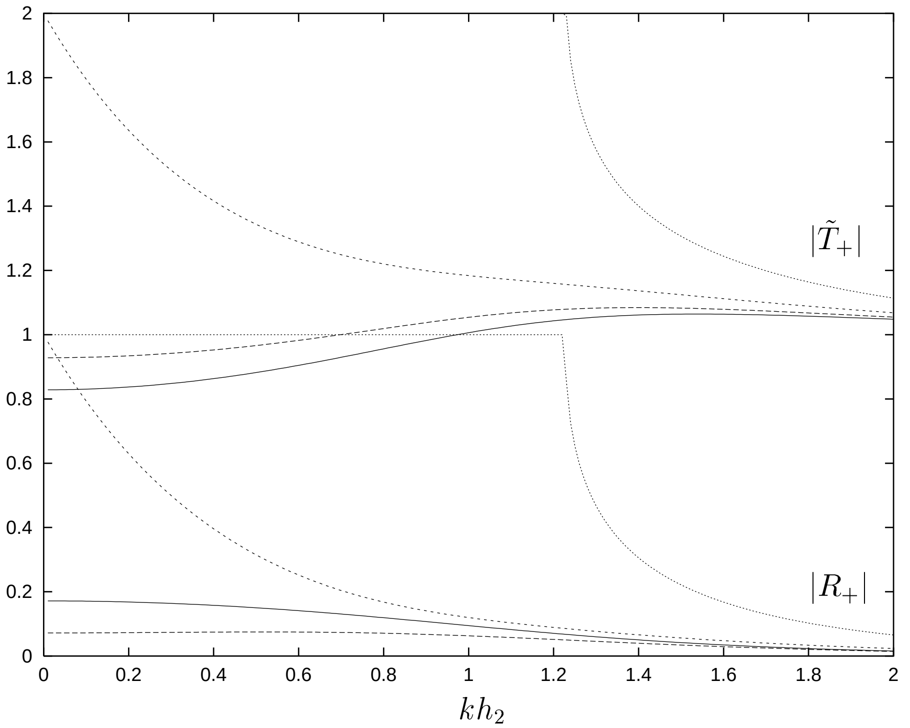

Figure 7.3: Reflection and transmission for oblique waves travelling into deeper water with $h_2/h_1 = 0.5\,,\ \theta_2 = 0^{\rm o}\,(\text{———}),\ 30^{\rm o}\,(-\,-\,-),\ 45^{\rm o}\,(\text{-}\quad\text{-}\quad\text{-}),\ 60^{\rm o}\,(\cdots\cdots)$.

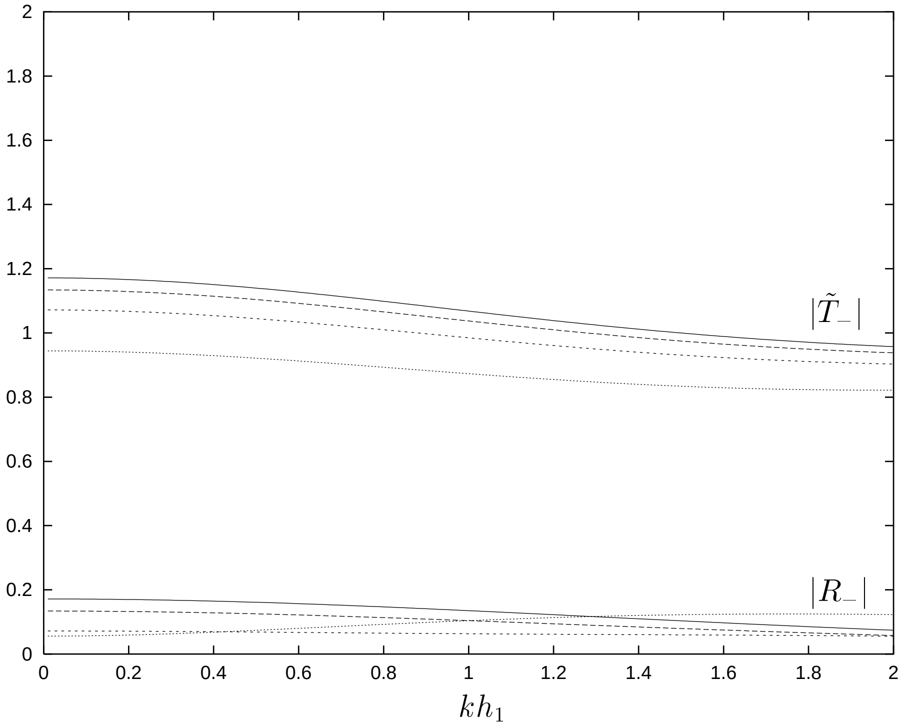

Figure 7.4: Reflection and transmission for oblique waves travelling into shallow water with $h_2/h_1 = 0.5$, $\theta_1 = 0^o$ (———), 30^o (– – –), 45^o (- - -), 60^o (······).

was made above a bottom-mounted vertical barrier. For small steps in the sea bed ($0 \ll h_2/h_1 < 1$), convergence is similar to that found in this latter example. A complementary formulation based on the pressure at the step has not been presented due to some minor difficulties that have yet to be resolved. Had we been able to do so, the agreement between the results from the two formulations would give an even stronger indication of their accuracy.

Our results are compared with a number of existing methods for approximating the wave field due to a step in table 7.2. Firstly, we have the method of matching eigenfunction expansions such that an infinite system of equations arises which is truncated at a value N (say) and solved. We have taken values of $N = 100,\ 200$, and 300 and used a program written by C.M. Linton to compute the values shown. Despite the apparent convergence of the results for reflection and transmission coefficients, they are quite a way from our values. Miles's [52] variational (or, equivalently, one-term Galerkin) approximation to the step involved him using a simple choice of trial function for the velocity above the step with no consideration of the singularity

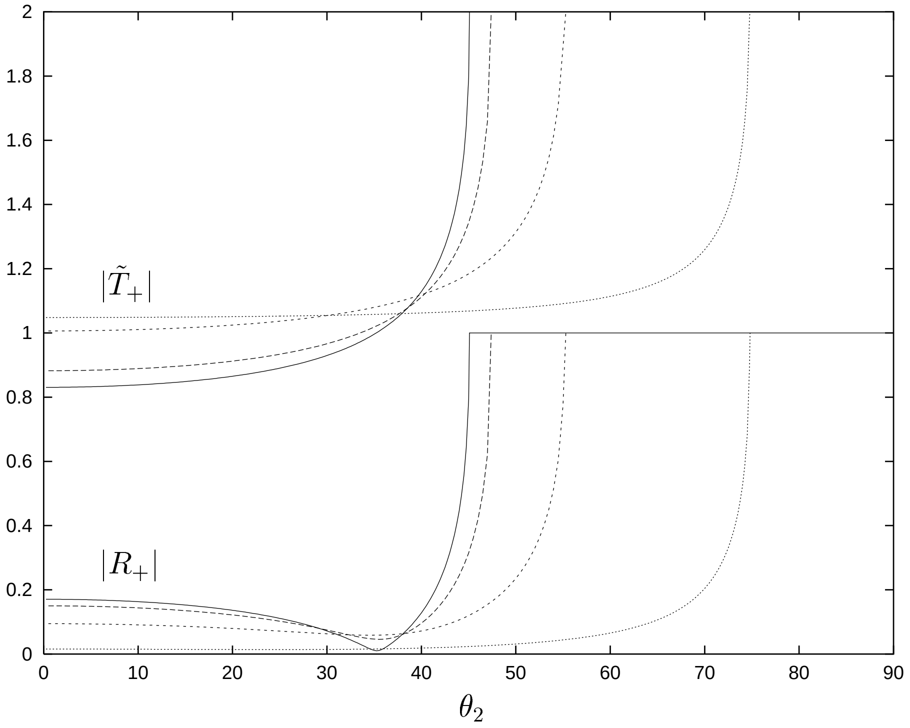

Figure 7.5: Variation of $|R_+|$, $|\tilde{T}_+|$ with incident angle as waves pass into deeper water: $h_2/h_1 = 0.5$ $kh_2 = 0.1$ (———), 0.5 (– – –), 1.0 (- - -), 2.0 (· · · · · ·).

at the corner. These results are in agreement to two decimal places with those of our method. It can be seen in table 7.1 that the one-term Galerkin method ($N = 0$) is also accurate to nearly three decimal places with our choice of trial function.

Finally, we compare with the step approximation method due to Evans & Linton [17]. In this, the fluid region is conformally mapped into a strip of uniform width such that this new problem resembles the scattering of waves in constant depth fluid due a variable impedance, $K(x)$, on the free surface instead of the usual constant K. By discretising the free surface into intervals of constant impedance they were able to express the reflection and transmission coefficients in terms of a transition matrix involving the properties of the solution to a simpler problem for which an exact solution was obtained. the method has been shown to agree very well with solutions to a variety of bottom profiles including the bottom-mounted vertical barrier and so its agreement with our results, which are believed to be accurate to all five decimal places shown, is not surprising.

In figure 7.2 the reflection and transmission coefficients due to a normally-incident wave moving into deeper water is plotted against non-dimensional wavenumber kh_2. As the step becomes more pronounced, the results begin to resemble the curves given by Newman [57] for the infinite step. However, we know from Lamb [40, §176] that in the long wave limit, the reflection coefficient is given by $|R_+| = (1 - \sqrt{h_2/h_1})/(1 + \sqrt{h_2/h_1})$, which can be confirmed from the figure.

Figures 7.3 and 7.4 show the variation of reflection and transmission coefficients with dimensionless wavenumber for a variety of angles of wave incidence, figure 7.3 being shallow to deep water propagation and figure 7.4 showing deep to shallow. For the first of these total reflection is possible beyond a critical wavenumber, as discussed earlier in §7.2. In both figures 7.3 and 7.4 it can be seen that as the critical angle for total reflection is approached then $|\tilde{T}_+| \to 2$ consistent with explicit results of Mei [51, pp.127–130] based on the linear shallow-water wave theory.

Chapter 8

Conclusion

In this thesis we have considered a number of problems concerned with the interaction of water waves with obstacles in finite depth using the classical theory of linear waves. We have concentrated primarily on a variety of situations involving thin vertical barriers with a view to approximating important quantities such as reflected and transmitted wave fields accurately and efficiently. The particular problems covered have been investigated to varying degrees by a number of authors. However, the methods previously employed for solving such problems have encountered difficulties in convergence of the approximation arising primarily from the presence of a singularity at the edge of a thin plate. Those approaches that have attempted to incorporate the singularity have, in general, been limited to the accuracy that could be achieved.

We have developed an approach which combines the ideas of achieving arbitrary accuracy whilst taking explicit account of the singularity. Chapter 3 describes in detail the principles behind this approach, which is subsequently adapted to the particular problem being considered. Crucial to the method is the derivation of singular intergal equations in terms of functions related *either* to the velocity of the fluid across a vertical boundary *or* to the pressure-difference across a barrier (termed as complemetary formulations). It also proves beneficial to express the desired hydrodynamic quantities such as reflection and transmission coefficients in terms of weighted integrals, or functionals, of these functions. A Galerkin method is used to approximate the unknown function by a truncated expansion in terms of a set of test functions. It is known that if the approximation differs by a term of $O(\epsilon)$ from the true value, the resulting approximation to the global hydrodynamic quantities will differ from their true values by a term of $O(\epsilon^2)$. In addition, bounds on certain quantities of the solution can be established when the kernel of the integral operator is positive-definite and self-adjoint. The one-term Galerkin method is equivalent to the variational approximation which has been used widely in the context of linear water waves. By using a truncated series of test functions which correctly model the behaviour at the edge of the barrier, results show how, in most cases, only a few terms are needed in the Galerkin expansion to gain very high accuracy.

In the final chapter, we have considered the problem of the scattering of surface waves by a vertical step on the sea bed. Here, the singularity at the corner of the step is different to that due to a thin barrier, and functions correctly modelling this singularity are introduced into the Galerkin approximation once again giving good accuracy with few terms in the expansion. It is not difficult, therefore, to apply these ideas to other wave scattering problems involving geometries with right-angled corners. Indeed, the problems of chapters 3, 4, 5 and 6 can all, in principle, be reworked with thin barriers replaced by barriers having finite thickness. In fact, the scattering of waves by a periodic array of rectangular blocks has recently been considered by Fernyhough & Evans [27] to predict all possible travelling wave modes using a fusion of the ideas of chapter 6 for the scattering of waves by a periodic array of thin barriers with an adaptation of the functions introduced for the step in chapter 7. Also considered recently are the determination of edge wave frequencies along a coastline consisting of a periodic array of rectangular protusions (see Evans & Fernyhough [16]). A formulation, complementary to the velocity formulation has yet to be fully developed.

Returning to thin barriers, the approach used in §3.2 for the barrier with a single gap or for a barrier with gaps above and below, can be extended to considering multiple barriers with gaps in finite depth. It would also be possible to use the methods of this thesis to rework Miles's [53] problem of the diffraction of waves by a barrier reef, in which his two-dimensional model consists of a submerged rectangular step protruding from a vertical coastline with a thin submerged vertical barrier placed on the corner of the step. However for a thin surface-piercing barrier extending to a point vertically above the step corner, the presence of two singularites of different strengths would require a new set of functions in the Galerkin expansion.

Whilst this thesis has concentrated on scattering problems, but it is believed that these methods can be applied with equal success to problems in approximating the radiation of surface waves due to small amplitude motion of thin barriers or blocks.

In summary, we have developed an accurate and efficient approach to approximating various aspects of the solution of a variety of problems in linear water waves and shown by the examples covered how it may be applied to many other problems involving similar geometries.

Appendix A

In order to obtain the behaviour of G as the source point is approached, we note that we may write (4.5.13) as

$$G(x,y;0,a_i) = -\frac{i}{2kh}\psi_0(a_i)\psi_0(y)\mathrm{e}^{ik|x|} - \sum_{n=1}^{\infty}\left\{\frac{1}{2k_n h}\psi_n(a_i)\psi_n(y)\mathrm{e}^{-k_n|x|} - S_n(a_i)\right\} - G_i, \tag{A.1}$$

where

$$S_n(a_i) = \frac{1}{n\pi}\cos\frac{n\pi}{h}(h-a_i)\cos\frac{n\pi}{h}(h-y)\mathrm{e}^{-n\pi|x|/h}, \tag{A.2}$$

and we have subtracted the leading order asymptotic behaviour for large n from each term in the sum in (A.1), so that the resulting series in brackets in (A.1) converegs for all x, y, and then added it back on as the term G_i, given by

$$G_i = \sum_{n=1}^{\infty} S_n(a_i) = \sum_{n=1}^{\infty}\frac{1}{2n\pi}\left\{\cos\frac{n\pi}{h}(a_i+y) + \cos\frac{n\pi}{h}(a_i-y)\right\}\mathrm{e}^{-n\pi|x|/h}. \tag{A.3}$$

If we let

$$z = |x| + i(y-a_i), \quad \text{and} \quad z' = |x| + i(y+a_i) = z + 2ia_i, \tag{A.4}$$

then we are able to write (A.3) as

$$G_i = \sum_{n=1}^{\infty}\frac{1}{4n\pi}\left\{\mathrm{e}^{-n\pi\overline{z}'/h} + \mathrm{e}^{-n\pi z'/h} + \mathrm{e}^{-n\pi z/h} + \mathrm{e}^{-n\pi\overline{z}/h}\right\}, \tag{A.5}$$

and using the identity

$$\sum_{n=1}^{\infty}\frac{\mathrm{e}^{-ns}}{n} = -\log(1-\mathrm{e}^{-s}), \tag{A.6}$$

gives

$$G_i = -\frac{1}{4\pi}\log\left\{|1-\mathrm{e}^{-\pi z/h}|^2|1-\mathrm{e}^{-\pi z'/h}|^2\right\}. \tag{A.7}$$

Now

$$|1-\mathrm{e}^{-\pi z/h}| = \frac{\pi r_i}{h}|1+O(\pi r_i/h)|, \tag{A.8}$$

with $r_i^2 = x^2+(y-a_i)^2$ whilst from (A.4)

$$\begin{aligned}|1-\mathrm{e}^{-\pi z'/h}| &= |1-\mathrm{e}^{-2i\pi a_i/h}\mathrm{e}^{-\pi z/h}| \\ &= 2\sin(\pi a_i/h)+O(\pi r_i/h).\end{aligned} \tag{A.9}$$

Finally, using (A.8), (A.9) in (A.7) gives

$$G_i = -\frac{1}{2\pi}\log\left\{\frac{2\pi r_i}{h}\sin\left(\frac{\pi a_i}{h}\right)\right\}, \tag{A.10}$$

as the leading order behaviour as $r_i \to 0$. The remainder of the Green function can be evaluated to give the asymptotic limit for the full source potential at the source point. Hence

$$G(x,y;0,a_i) = R(a_i) - G_i, \quad \text{as } r_i \to 0, \tag{A.11}$$

where

$$R(a_i) = -\frac{i}{2N_0kh}\cosh^2 k(h-a_i) - \sum_{n=1}^{\infty}\left\{\frac{\cos^2 k_n(h-a_i)}{2N_nk_nh} - \frac{\cos^2 n\pi(1-a_i/h)}{n\pi}\right\}, \tag{A.12}$$

and the series above is convergent.

To obtain the far-field behaviour of the Green function, we note from (4.5.13) that

$$G(x,y;0,a_i) \simeq -\frac{i}{2kh}N_0^{-1/2}\cosh k(h-a_i)\mathrm{e}^{ik|x|}\psi_0(y), \quad \text{as } |x| \to \pm\infty. \tag{A.13}$$

Bibliography

[1] Abramowitz, M.A. & Stegun, I 1964 *Handbook of mathematical functions*, Dover.

[2] Abul-Azm, A.G. 1993 Wave diffraction through submerged breakwaters. *J. Waterway, Port, Coastal & Oc. Eng.* **119**(6), 587–605.

[3] Achenbach, J.D. & Li, Z.L. 1986 Reflection and transmission of scalar waves by a periodic array of screens. *Wave Motion* **8**, 225–234.

[4] Baldwin, G.L. & Heins, A.E. 1954 On the diffraction of a plnae wave by an infinite plane grating. *Math. Scand.* **2**, 103–118.

[5] Budal, K. & Falnes, J. 1977 Optimum operation of improved wave-power convertors. *Marine Sciences Comm.* **3**, 133–150.

[6] Chambers, G. LL. 1967 A comparison of two variational methods. *J. Inst. Maths. Applics.* **3**, 166–168.

[7] Dalrymple, R.A. & Martin, P.A. 1990 Wave diffraction through offshore breakwaters. *J. Waterway, Port, Coastal & Oc. Eng.* **116**, 727–741.

[8] Dean, W.R. 1945 On the reflexion of surface waves by a flat plate floating vertically. *Proc. Camb. Phil. Soc.* **41**, 231–238.

[9] Erdélyi *et al.* 1954 *Tables of Integral Transforms.* McGraw-Hill.

[10] Evans, D.V. 1970 Diffraction of surface waves by a submerged vertical plate. *J. Fluid. Mech.* **40**, 433–451.

[11] Evans, D.V. 1975 A note on the total reflexion or transmission of surface waves in the presence of parallel obstacles. *J.Fluid Mech.* **67**, 465–472.

[12] Evans, D.V. 1976 A theory for wave power absorption by oscillating bodies. *J. Fluid Mech.* **77**, 1–25.

[13] Evans, D.V. 1975 Water wave transmission through barriers with small gaps. *J. Engng. Maths.* **11**, 1–10.

[14] Evans, D.V. 1978 The oscillating water column wave energy device. *J. Inst. Maths. Applics.* **22**, 423–433.

[15] Evans, D.V. 1982 Wave-power absorption by systems of oscillating surface pressure distributions. *J. Fluid. Mech.* **114**, 481–499.

[16] Evans, D.V. & Fernyhough, M. 1995 Edge waves along periodic coastlines - II. *J. Fluid Mech.* **296**, 307–325.

[17] Evans, D.V. & Linton, C.M. 1994 On step approximations for water-wave problems. *J. Fluid Mech.* **278** 229–249.

[18] Evans, D.V. & McIver, P. 1984 Edge waves over a shelf: A full linear theory. *J. Fluid Mech.* **142**, 79–95.

[19] Evans, D.V. & McIver, P. 1987 Resonant frequencies in a container with a vertical baffle. *J. Fluid Mech.* **175**, 295–307.

[20] Evans, D.V. & Morris, C.A.N. 1972 The effect of a fixed vertical barrier on obliquely incident surface waves in deep water. *J. Inst. Appl. Maths Applics* **9**, 198–204.

[21] Evans, D.V. & Morris, C.A.N. 1974 Complementary approximations to the solution of a problem in water waves. *J. Inst. Appl. Maths Applics* **10**, 1–9.

[22] Evans, D.V. & Porter, R. 1995 Hydrodynamic characteristics of an oscillating water column device. *To be published in Appl. Ocean Res.*

[23] Evans, D.V. & Porter, R. 1995 Complementary methods for scattering by thin barriers In Advances in Fluid Mechanics: *Mathematical Techniques in water waves.* (Ed. B.N Mandal), Comp. Mech.

[24] Evans, D.V. & Srokosz, M. 1979 A theory for wave power absorption by two independently oscillating bodies. *J. Fluid Mech.* **90**, 337–362.

[25] Falnes, J. & McIver, P. 1985 Surface wave interactions with systems of oscillating bodies and pressure distributions. *Appl. Ocean Res.* **7**(4), 225–234.

[26] Falcão, J. & Sarmento, A.J.N.A. 1980 Wave generation by a periodic surface pressure and its application in wave-energy extraction. *15th Int. Cong. Theor. Appl. Mech., Toronto.*

[27] Fernyhough, M. & Evans, D.V. 1995 Scattering by a periodic array of rectangular blocks. *J. Fluid Mech. to appear.*

[28] Garrett, C.J.R. 1970 Bottomless harbours. *J. Fluid Mech.* **43**, 433–449.

[29] Gradshteyn, I.S. & Ryzhik, I.M. 1981 *Tables of Integrals, Series and Products.* New York: Academic Press.

[30] Guiney, D.C., Noye, B.J. and Tuck, E.O. 1972 Transmission of water waves through small apertures. *J. Fluid Mech.* **55**, 149–167.

[31] Heckl, M.A. 1992 Sound propagation in bundles of periodically arranged cylindrical tubes. *Acustica* **77**, 143–152.

[32] Jarvis, R.J. 1971 The scattering of surface waves by two vertical plane barriers. *J. Inst. Appl. Maths Applics* **7**, 207–215.

[33] Jeyakumaran, M. & McIver, P. 1995 Approximations to sloshing frequencies for rectangular tanks with internal structures. *J. Eng. Math.* **29**, 537–556.

[34] John, F. 1948 Waves in the presence of an inclined barrier. *Comm. Pure. Appl. Math.* **1**, 149–200.

[35] Jones, D.S. 1964 *The theory of electromagnetism.* Oxford: Pergamon Press.

[36] Karp, S.N. & Williams, W.E. 1957 Equivalence relations in diffraction theory. *Proc. Camb. Phil. Soc.* **53**, 683–690.

[37] Kirby, J.T. & Dalrymple, R.A. 1983 Propagation of obliquely incident water waves over a trench. *J. Fluid Mech.* **133**, 47–63.

[38] Kober, H. 1957 *Dictionary of Conformal Representations.* Dover, New York.

[39] Kreisel, G. 1949 Surface waves. *Q. Appl. Maths.* **7**, 21.

[40] Lamb, H. 1932 *Hydrodynamics*, Cambridge University Press.

[41] Levine, H. & Rodemich, E. 1958 Scattering of surface waves on an ideal fluid. *Math. and Stat. Lab. Tech. Report No.78* , Stanford University.

[42] Lewin, M. 1963 The effect of vertical barriers on progressive waves. *J. Math. Phys.* **42**, 287–300.

[43] Linton, C.M. & Evans, D.V. 1993 Hydrodynamic characteristics of bodies in channels. *J. Fluid Mech.* **252**, 647–666.

[44] Martin, P.A. 1985 Multiple scattering of surface water waves and the null-field method. *Proc. 15th Symp. Naval Hydrodynamics, Hamburg*, pp. 119–132, National Academy Press.

[45] Mandal, B.N. & Dolai, D.P. 1994 Oblique water wave diffraction by thin vertical barriers in water of uniform finite depth. *Appl. Ocean Res.* **16**, 195–203.

[46] McIver, P. 1985 Scattering of surface waves by two surface-piercing vertical barriers. *IMA J. Appl Math.* **35**, 1–17.

[47] McIver, M.P. 1985 The interaction of water waves with submerged bodies. PhD thesis, University of Bristol.

[48] Mei, C.C. 1966 Radiation and scattering of transient gravity waves by vertical plates. *Quart. J. Mech. Appl. Math.* **19**, 417–440.

[49] Mei, C.C. & Black, J.L. 1969 Scattering of surface waves by rectangular obstacles in waters of finite depth. *J. Fluid Mech.* **38**, 499–511.

[50] Mei, C.C. 1976 Power extraction from water waves. *J. Ship. Res.* **20**(2), 63–66.

[51] Mei, C.C. 1983 *The applied dynamics of ocean surface waves*, Wiley Interscience.

[52] Miles, J.W. 1967 Surface-wave scattering matrix for a shelf. *J. Fluid. Mech.* **28**, 755-767.

[53] Miles, J.W. 1981 Diffraction of gravity waves by a barrier reef. *J. Fluid. Mech.* **109**, 115–123.

[54] Miles, J.W. & Gilbert, J.F. 1968 Scattering of surface waves by a circular dock. *J. Fluid. Mech.* **34**, 783–793.

[55] Morris, C.A.N. 1975 A variational approach to an unsymmetric water-wave scattering problem. *J. Engng. Math.* **9**, 291–300.

[56] Newman, J.N. 1965 Propagation of water waves past long two-dimensional obstacles. *J. Fluid Mech.* **23**, 23–29.

[57] Newman, J.N. 1965 Propagation of water waves over an infinite step. *J. Fluid Mech.* **23**, 399–415.

[58] Newman, J.N. 1974 Interaction of water waves with two closely spaced barriers. *J. Fluid Mech.* **66**, 97–106.

[59] Newman, J.N. 1976 The interaction of stationary vessels with regular waves. *Proc. 11th Symp. Naval Hydrodynamics*, 451–501.

[60] Packham, B.A. & Williams, W.E. 1972 A note on the transmission of water waves through small apertures. *J. Inst. Maths. Applics.* **10**, 176–184.

[61] Parsons, N. & Martin P. 1993 Scattering of water waves by submerged curved plates and by surface-piercing plates. *Appl. Ocean Res.* **16**,129–139

[62] Porter, D. 1972 The transmission of surface waves through a gap in a vertical barrier. *Proc. Camb. Phil. Soc.* **71**, 411–440.

[63] Porter, D. 1974 The radiation and scattering of surface waves by vertical barriers. *J. Fluid Mech.* **63**, 625–634.

[64] Porter, D. & Chamberlain, P.G. 1995 Linear Wave Scattering by Two-dimensional Topography. In Advances in Fluid Mechanics: *Gravity Waves in Water of Finite Depth.* (Ed. J.N. Hunt), Comp. Mech.

[65] Porter, R & Evans, D.V. 1995 Complementary approximations to wave scattering by vertical barriers. *J. Fluid Mech.* **294**, 155–180.

[66] Porter, R. & Evans, D.V. 1995 Wave scattering by periodic arrays of breakwaters. *To be published in Wave Motion.*

[67] Simon, M.J. 1981 Wave-energy extraction by a submerged cylindrical resonant duct. *J. Fluid Mech.* **104**, 159–187.

[68] Smith, C.M. 1983 Some problems in linear water wave theory. PhD thesis, University of Bristol.

[69] Thomas, J.R. 1982 The hydrodynamics of certain wave energy absorbers. PhD thesis, University of Bristol.

[70] Tuck, E.O. 1971 Transmission of water waves through small holes. *J. Fluid Mech.* **49**, 65–73.

[71] Tuck, E.O. 1975 Matching problems involving flow through small holes. *Adv. Appl. Maths.* **15**, 90–158.

[72] Ursell, F. 1947 The effect of a fixed vertical barrier on surface waves in deep water. *Proc. Camb. Phil. Soc.* **43**, 374–382.

[73] Wehausen, J.N. & Laitone, E.V. 1960 *Surface waves.* Handbuch der Physik. Springer.

[74] Williams, A.N. & Crull, W.W. 1993 Wave diffraction by thin screen breakwaters, *J. Waterway, Port, Coastal & Oc. Eng.* **119**, 606–617.

[75] Wu, C.P. 1973 Variational and iterative methods for waveguides and arrays. In *Computational Techniques for Electromagnetics* (ed. R. Mittra), pp. 266–304. Pergamon